N(T)

GRAVITY GRADIENT MOMENTUM DUMPING AND DYNAMICS ANALYSIS

Augmentation Task No. 25

LMSC-A842319 5 September 1967

GRAVITY GRADIENT MOMENTUM DUMPING AND DYNAMICS ANALYSIS

Augmentation Task No. 25

LMSC-A842319 5 September 1967

Prepared Under Contract No. NAS8-21003 by

LOCKHEED MISSILES & SPACE COMPANY
A Group Division of Lockheed Aircraft Corporation
Sunnyvale, California

for

NATIONAL AERONAUTICS AND SPACE ADMINISTRATION
GEORGE C. MARSHALL SPACE FLIGHT CENTER
Huntsville, Alabama

Prepared by: B. J. Lehman for D. R. Ingwerson

Approved by: [signature]

ACKNOWLEDGEMENTS

Dr. Dale Ingwerson was responsible for directing the analysis in subsections II.1 through II.5. Dr. Gabriel Margulies and Dr. Lee Hooker developed the flexible cluster mathematical model. The ATOMS simulation work was completed by Mr. Lou Reinkens. Dr. Jim Pope performed the bending mode analysis. The momentum dumping loops and control laws were finalized by Mr. Hal Rearick and Mr. Don Hitzl.

Dr. Dale Ingwerson was responsible for directing the analysis in subsections II.1 through II.5. Dr. Gabriel Margulies and R. Lee Hooker developed the flexible cluster mathematical model. The ATOMS simulation work was completed by Mr. Lou Reinkens. Dr. Jim Pope performed the lending mode analysis. The momentum dumping loops and control laws were finalized by Mr. Hal Rearick and Mr. Don Hitzl. Dr. R. L. Martindale was responsible for subsection II-6 with the analysis provided by Dr. P. B. Chin, the facilities survey and computer requirements provided by F. Barnes, and the simulation system conceptual design and integration provided by D. J. Horowitz.

CONTENTS

ILLUSTRATIONS

TABLES

Section 1
GRAVITY-GRADIENT MOMENTUM DUMPING

1.1 ALTERNATE IMPLEMENTATIONS

Several control loops and control laws have been considered for dumping CMG momentum by gravitational torques. The various methods analyzed, as well as their relative merits, are discussed below.

1.1.1 Continuous

This method considers attitude deviation $\bar{\alpha}$ a continuous function of stored angular momentum during each quarter of the dark side passage. The method is presented in Ref. 1-1, the control loop shown in Fig. 1-1 and the control law matrix $\bar{G}$ in Table 1-3. The feedback gains a, b, c, and d must have precise values for the method to perform satisfactorily. A digital computer simulation showed that the attitude deviations required were quite large (as high as 30 deg) immediately after sunset. For these reasons, this method is not recommended.

1.1.2 Discrete (Maximum and Minimum H Sampling)

This method is defined as one in which the vehicle attitude deviation $\bar{\alpha}$ for each quarter of each dark side passage is a discrete variable. This may be an advantage for some experiments in that the vehicle attitude is constant over each quarter of the dark side of the orbit.

Reference 1-2 describes a maximum and minimum $\bar{H}$ sampling form of the method in which $\bar{H}$ is assumed to vary sinusoidally. This gives an approximation to a true integration which would determine the average value of H for any kind of variation.

The method is not recommended because it would give a false indication of the average for other than sinusoidal variations since it responds to maximum and minimum values only.

1.1.3 Discrete (Averaged $\bar{H}$ Sampling)

If the angular momentum $\bar{H}$ is integrated over each orbit period and the integrator is sampled and reset to zero at each sundown so as to obtain the true average angular momentum for each orbit, then this value might be used. This implementation is somewhat complex, however, requiring three digital integrators and three registers to store the average value of $\bar{H}$.

1.1.4 Discrete (H Sampling at Sunset)

If the angular momentum is sampled and held at each sunset as shown in Fig. 1-1, the angular momentum may be dumped satisfactorily. $\bar{H}_2$ is sampled at each sundown at which time $\bar{H}_2 = \bar{H}_1 = \bar{H}_0$ since $\bar{\alpha} = \bar{0}$ during the light side passage. The sampler and zero-order hold consist of three registers reset once each orbit. A bias vector $\bar{H}_b$ is added to the output of the hold to make all three components of the angular momentum approach zero.

In terms of the notation of Ref. 1-2, Table 1-1, the differential equations for the accumulation of angular momentum, assuming that the principal axes coincide with the geometric axes $(\delta = 0)$, are

$$\bar{H}_1' = \bar{u} \qquad \text{for light side of orbit and}$$

$$\bar{H}_1' = \bar{B}\bar{G}(\bar{H}_o + \bar{H}_b) + \bar{u} \qquad \text{for dark side of orbit}$$

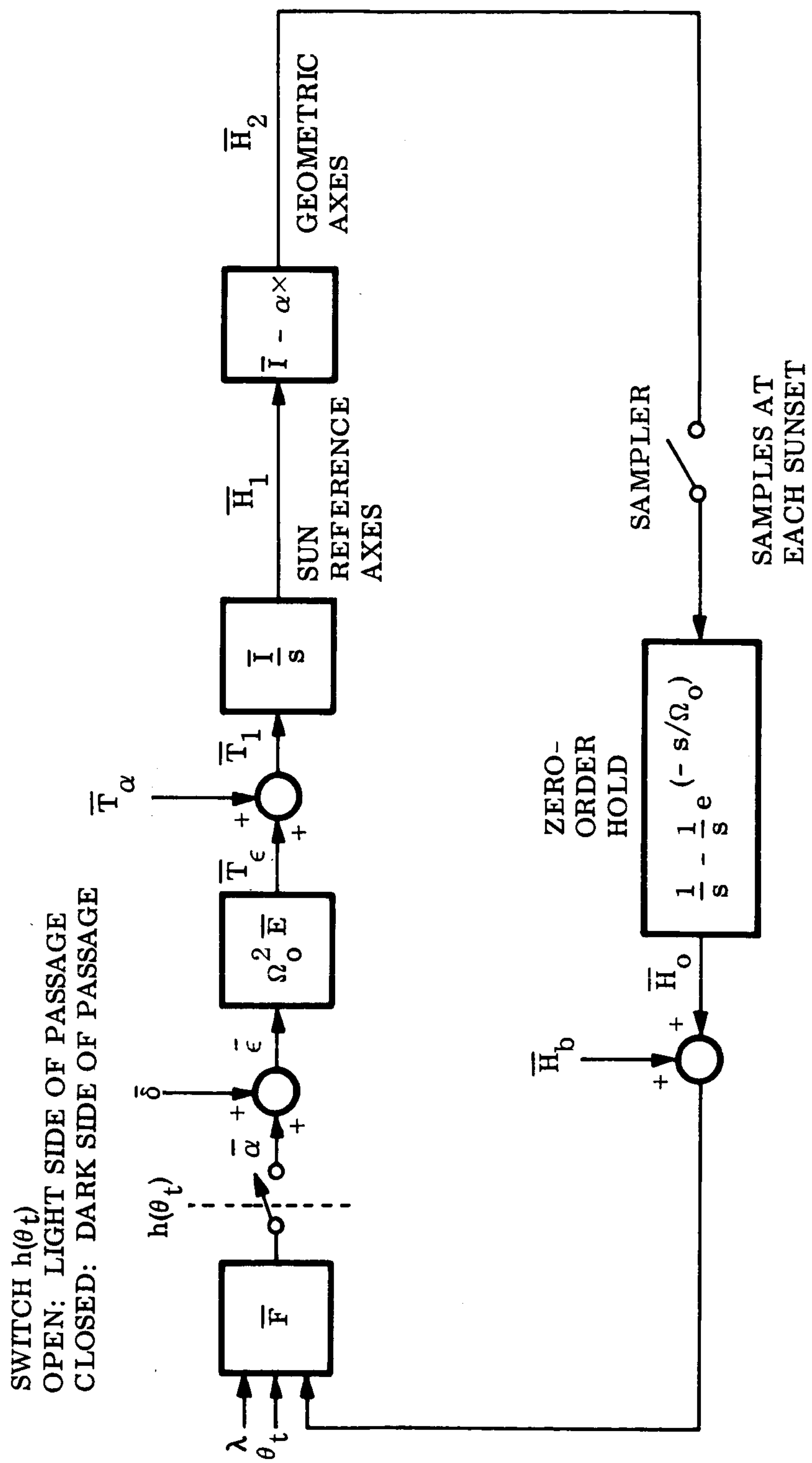

Fig. 1-1 Angular Momentum Sampled and Held at Each Sunset

Choose a $\bar{G}$ such that

$$\int_{2\pi}^{4\pi} \bar{B}\bar{G}\,dt = \begin{bmatrix} a & 0 & 0 \\ 0 & b & 0 \\ 0 & 0 & c \end{bmatrix} \triangleq \bar{M}$$

One such $\bar{G}$ is given in Ref. 1-2, Eq. (1.7). Another is given in the following section.

Define $\bar{H}_{1(n)}$ as $\bar{H}_1\left[(2n+1)\,2\pi\right]$ which is $\bar{H}_1(t)$ at sundown of the nth orbit, $n = 0, 1, 2, \ldots$.

Then

$$\bar{H}_{1(n)} = (\bar{M} + \bar{I})^n\,\bar{H}_{1(o)} + \bar{M}^{-1}\,(\bar{M} + \bar{I})^n\,\bar{U} - \bar{M}^{-1}\,\bar{U}$$

$$+ (\bar{M} + \bar{I})^n\,\bar{H}_b - \bar{H}_b \qquad n = 0, 1, 2, \ldots$$

where

$$\bar{U} \triangleq \int_0^{4\pi} \bar{u}\,dt\ .$$

For convergence of $\bar{H}_{1(n)}$, $-2 < a < 0$, $-2 < b < 0$, and $-2 < c < 0$. $\bar{H}_{1(n)}$ then converges to

$$\bar{H}_1(\infty) = -\begin{bmatrix} \dfrac{U_1}{a} + H_{b1} \\ \dfrac{U_2}{b} + H_{b2} \\ \dfrac{U_3}{c} + H_{b3} \end{bmatrix}$$

The components of $\overline{H}_1(\infty)$ may be made equal to zero by setting

$$H_{b1} = -\frac{U_1}{a}$$

$$H_{b2} = -\frac{U_2}{b}$$

$$H_{b3} = -\frac{U_3}{c}$$

Of the several considered, this method is the easiest to implement, the easiest to analyze, does not require an assumption as to the form of the disturbance torques, and is stable. It is therefore recommended for the automatic mode of operation.

This method is also recommended for the manual backup mode because of its simplicity. If it is used for both automatic and manual modes, the astronauts should become accustomed to its operating characteristics and be better able to use it manually.

1.2 DISCRETE IMPLEMENTATION DUMPING CONTROL LAWS

The purpose of this analysis is to derive general control laws similar in form to (1.7) in Ref. 1-2. Several simplifying assumptions are relaxed and the appropriate control laws are established.

Basically, we are interested in solutions to the following differential equation:

$$\dot{\overline{H}}_1 = h(\theta_t)\,\Omega_o^2\,\overline{E}\,\overline{F}\,\overline{H}_o + \overline{T}_d \qquad (1.1)$$

where $h(\theta_t)$ is a switch governing the operation of the momentum dumping:

$$h(\theta_t) = \frac{1}{2}\left[1 - \text{sgn}\,(\sin\rho + \sin\theta_t)\right]$$

and

$\overline{H}_1$ = components of stored angular momentum in sun-referenced axes

θ_t = true anomaly of the orbit

Ω_o = mean orbital rate

$\overline{E}$ = matrix derivable from the gravity gradient torque

$\overline{F}$ = control law

$\overline{T}_d$ = disturbance torques

$\overline{H}_o$ = sampled components of stored angular momentum

Making the change of variable $\tau = 2\,\theta_t$, we obtain

$$\overline{H}_1' = h(\theta_t)\,\overline{E}_1\,\overline{F}\,\overline{H}_0 + \overline{u} \qquad (1.2)$$

where

$$\overline{E}_1 = \frac{1}{2}\,\Omega_o\,\overline{E}$$

$$\overline{u} = \frac{1}{2\Omega_o}\,\overline{T}_d$$

The control law matrix $\overline{F}$ is to be chosen such that the solution of Eq. (1.2) over a complete orbit is

$$\Delta\overline{H}_1 = -\begin{bmatrix} a & 0 & 0 \\ 0 & b & 0 \\ 0 & 0 & c \end{bmatrix} \overline{H}_o + \text{secular disturbances} \qquad (1.3)$$

1.2.1 Pitch and Roll in Arbitrary Axes

In order to proceed, the matrix $\overline{E}$ and the column vector $\overline{u}$ must be established. The gravity gradient torques on a vehicle in circular orbit are given approximately by

$$\overline{T}_g = 3\Omega_o^2 (\hat{R} \times \overline{J}_1 \hat{R}) \tag{1.4}$$

where $\hat{R}$ is the normalized radius vector and $\overline{J}_1$ is the inertia matrix of the cluster expressed in sun-referenced axes. As before,

$$\overline{J}_p = \begin{bmatrix} J_1 & 0 & 0 \\ 0 & J_2 & 0 \\ 0 & 0 & J_3 \end{bmatrix} \tag{1.5}$$

is the inertia matrix in principal axes and

$$\overline{J}_1 = \overline{J}_2 + (\overline{\alpha} \times \overline{J}_2) + (\alpha \times J_2)' + 0\,(\alpha^2) \tag{1.6}$$

is the matrix transformation from geometric axes (sub 1), to sun-referenced axes, (sub 2). Here the three angles of α_i, $i = 1, 2, 3$, are assumed small. However, the principal axes of the cluster are assumed to be displaced from the geometric axes by three angles of ν_i, $i = 1, 2, 3$, which are not necessarily small. Here ν_i is a rotation about x_2, ν_2 is a rotation about the rotated y_2, and ν_3 is a rotation about the twice rotated z_2 axis. So, with

$$\overline{J}_2 = \overline{L}\,\overline{J}_p\,\overline{L}' \tag{1.7}$$

and

$$\bar{L} = \begin{bmatrix} c_2c_3 & -c_2s_3 & s_2 \\ c_1s_3 + s_1s_2c_3 & c_1c_3 - s_1s_2s_3 & -s_1c_2 \\ s_1s_3 - c_1s_2c_3 & s_1c_3 + c_1s_2s_3 & c_1c_2 \end{bmatrix}$$

where $s_j = \sin \nu_j$ and $c_j = \cos \nu_j$

the result of carrying out the computation specified by Eqs. (1.6) and (1.7) is

$$J_1 = \begin{bmatrix} 2(\alpha_2K_4-\alpha_3K_5)+K_0 & -\alpha_1K_4+\alpha_2K_3+\alpha_3K_2+K_5 & \alpha_1K_5+\alpha_2K_1-\alpha_3K_3+K_4 \\ -\alpha_1K_4+\alpha_2K_3+\alpha_3K_2+K_5 & 2(-\alpha_1K_3+\alpha_3K_5)+(K_0-K_2) & -\alpha_1(K_1+K_2)-\alpha_2K_5+\alpha_3K_4+K_3 \\ \alpha_1K_5+\alpha_2K_1-\alpha_3K_3+K_4 & -\alpha_1(K_1+K_2)-\alpha_2K_5+\alpha_3K_4+K_3 & 2(\alpha_1K_3-\alpha_2K_4)+(K_1+K_0) \end{bmatrix}$$

where the following definitions are used:

$$K_0 = \left(J_1c_3^2 + J_2s_3^2\right) c_2^2 + J_3\, s_2^2$$

$$K_1 = \left(J_1s_3^2 + J_2c_3^2\right) s_1^2 + \left(J_1c_3^2 + J_2s_3^2\right)\left(c_1^2s_2^2 - c_2^2\right) + J_3\left(c_1^2c_2^2 - s_2^2\right)$$
$$- 2(J_1 - J_2)\, s_1c_1s_2s_3c_3$$

$$K_2 = -\left(J_1s_3^2 + J_2c_3^2\right) c_1^2 - \left(J_1c_3^2 + J_2s_3^2\right)\left(s_1^2s_2^2 - c_2^2\right) - J_3\left(s_1^2c_2^2 - s_2^2\right)$$
$$- 2(J_1 - J_2)\, s_1c_1s_2s_3c_3$$

$$K_3 = s_1c_1\left[J_1s_3^2 + J_2c_3^2 - \left(J_1c_3^2 + J_2s_3^2\right) s_2^2 - J_3c_2^2\right]$$
$$- (J_1 - J_2) \cos 2\nu_1\, s_2s_3c_3$$

$$K_4 = (J_1 - J_2)s_1c_2s_3c_3 - \left(J_1c_3^2 + J_2s_3^2 - J_3\right) c_1s_2c_2$$

$$K_5 = (J_1 - J_2)c_1c_2s_3c_3 + \left(J_1c_3^2 + J_2s_3^2 - J_3\right) s_1s_2c_2$$

Now the gravity gradient torque $\overline{T}g$ must be computed; for this

$$\hat{R}' = (\cos \theta_t ,\ \sin \theta_t \sin \lambda ,\ \sin \theta_t \cos \lambda) \tag{1.9}$$

and $\overline{T}_g = \overline{T}_c + \overline{T}_d$ = controllable torque + disturbing torque.

This is a natural division since the terms containing α_i i = 1, 2, 3, in $\overline{J}_1$ [Eq. (1.8)] are grouped into $\overline{T}_c$ and the remaining terms contribute to $\overline{T}_d$. Thus, by controlling the cluster attitude on the dark side of the orbit through the three (small) angles α_i , control of the accrual of angular momentum can be established.

Then

$$\overline{T}_g = 2\Omega_0 \overline{E}_1 \begin{bmatrix} \alpha_1 \\ \alpha_2 \\ \alpha_3 \end{bmatrix} + \overline{T}_d = 2\Omega_0 \overline{E}_1 \alpha + 2\Omega_0 \overline{u} \tag{1.10}$$

a straightforward computation utilizing Eqs. (1.8), (1.9), and (1.4) yields the matrix $\overline{E}_1$ and the vector $\overline{u}$. They are

$$\overline{E}_1 = \frac{3}{4}\Omega_0 \overline{B} \begin{bmatrix} -(K_1 + K_2) & -K_5 & K_4 \\ K_5 & K_1 & -K_3 \\ -K_4 & K_3 & K_2 \end{bmatrix} + \frac{3}{4}\Omega_0 \overline{C} \begin{bmatrix} 2 & -1 & -1 \\ -2 & 4 & -2 \\ -1 & -2 & 4 \end{bmatrix} \begin{bmatrix} K_3 & 0 & 0 \\ 0 & K_4 & 0 \\ 0 & 0 & K_5 \end{bmatrix}$$

where $\bar{B}$ is defined in Ref. 1-2 on page 1-3 and

$$\bar{C} = \begin{bmatrix} (1 - c_\tau)\, s_{2\lambda} & 0 & 0 \\ 0 & s_\tau c_\lambda & 0 \\ 0 & 0 & s_\tau s_\lambda \end{bmatrix}$$

where $c_\beta = \cos_\beta$ and $s_\beta = \sin_\beta$

and

$$\bar{u} = \begin{bmatrix} m_1 \\ m_2 \\ m_3 \end{bmatrix} - c_\tau \begin{bmatrix} m_1 \\ m_4 \\ m_5 \end{bmatrix} + s_\tau \begin{bmatrix} m_6 \\ m_7 \\ m_8 \end{bmatrix}$$

where the following definitions are used:

$$m_1 = \frac{3}{4}\, \Omega_0 \left[(K_1 + K_2) \frac{1}{2}\, s_{2\lambda} - K_3 c_{2\lambda} \right]$$

$$m_2 = \frac{3}{4}\, \Omega_0 \left[- K_4 s_\lambda^2 + K_5 \frac{1}{2}\, s_{2\lambda} \right]$$

$$m_3 = \frac{3}{4}\, \Omega_0 \left[- K_4 \frac{1}{2}\, s_{2\lambda} + K_5\, c_\lambda^2 \right]$$

$$m_4 = \frac{3}{4}\, \Omega_0 \left[K_4 (1 + c_\lambda^2) + K_5 \frac{1}{2}\, s_{2\lambda} \right]$$

$$m_5 = \frac{3}{4}\, \Omega_0 \left[- K_4 \frac{1}{2}\, s_{2\lambda} - K_5 (1 + s_\lambda^2) \right]$$

$$m_6 = \frac{3}{4}\, \Omega_0 \left[K_4\, s_\lambda - K_5\, c_\lambda \right]$$

$$m_7 = \frac{3}{4}\, \Omega_0 \left[- K_1\, c_\lambda - K_3\, s_\lambda \right]$$

$$m_8 = \frac{3}{4}\, \Omega_0 \left[- K_2\, s_\lambda + K_3\, c_\lambda \right]$$

Thus, with $\overline{E}_1$ and $\overline{u}$ defined, we are in a position to determine the control law matrix $\overline{F}$. The control law matrix is to be determined such that

$$\Delta \overline{H}_1 = - \begin{bmatrix} a & 0 & 0 \\ 0 & b & 0 \\ 0 & 0 & c \end{bmatrix} \begin{bmatrix} h_{10} \\ h_{20} \\ h_{30} \end{bmatrix} + \begin{bmatrix} 4\pi m_1 \\ 4\pi m_2 \\ 4\pi m_3 \end{bmatrix} \tag{1.11}$$

is the solution of the matrix differential equation over a complete orbit.

In analogy to previous control laws given in Ref. 1-2, the most general form for the control law $\overline{F}$ is

$$\overline{F} = \frac{4}{3\Omega_o} \begin{bmatrix} 0 & 0 & 0 \\ f_1 & f_2 & f_3 \\ f_4 & f_5 & f_6 \end{bmatrix} \tag{1.12}$$

where

$$f_i = p_i + q_i S_s + r_i S_c$$

$$S_s = \text{sgn}(\sin \tau)$$

$$S_c = \text{sgn}(\cos \tau)$$

The p_i , q_i , r_i which comprise a set of 18 unknown functions of λ and the K_i ($i = 1, 2, \ldots, 5$) are to be determined. A complete solution for $\overline{F}$ in the following form was computed.

$$\overline{F} = \frac{4}{3\Omega_o} \begin{bmatrix} 0 & 0 & 0 \\ p_1 + q_1 S_s & r_2 S_c & p_3 + r_3 S_c \\ q_4 S_s & p_5 + r_5 S_c & r_6 S_c \end{bmatrix} \tag{1.13}$$

However, the functions p , q , and r are so lengthy and complicated that this solution is not presented here.

Instead, various simplifications are introduced and the corresponding control laws derived. First, all ν_i i = 1, 2, 3 are assumed zero; this corresponds to alignment of the cluster principal axes with the geometric axes. Then

$$K_0 = J_1 , \quad K_1 = -J_1 + J_3 , \quad K_2 = -J_2 + J_1 , \quad K_3 = K_4 = K_5 = 0$$

and

$$\overline{F} = \frac{4}{3\Omega_o} \begin{bmatrix} 0 & 0 & 0 \\ -\frac{a}{4K_1} s_\lambda S_s & \frac{b}{8K_1}\left(1 + s_\lambda^2\right) S_c & \frac{c}{16K_1} s_{2\lambda} S_c \\ \frac{a}{4K_2} c_\lambda S_s & -\frac{b}{16K_2} s_{2\lambda} S_c & -\frac{c}{8K_2}\left(1 + c_\lambda^2\right) S_c \end{bmatrix} \qquad (1.14)$$

yielding

$$\overline{G} = \begin{bmatrix} 0 & 0 & 0 \\ -\frac{a}{4} s_\lambda S_s & \frac{b}{8}\left(1 + s_\lambda^2\right) S_c & \frac{c}{16} s_{2\lambda} S_c \\ \frac{a}{4} c_\lambda S_s & -\frac{b}{16} s_{2\lambda} S_c & -\frac{c}{8}\left(1 + c_\lambda^2\right) S_c \end{bmatrix} \qquad (1.15)$$

This should be compared with Eq. (1.7) in Ref. 1-2; both are control laws for discrete implementations but this one contains no constant terms.

1.2.2 Yaw Along a Principal Axis

If a single large rotation ν_1 of the principal axes about the x_2 axis is made and with the definition

$$\Delta = 16\left(K_1 K_2 + K_3^2\right)$$

where, now

$$K_1 = J_2 s_1^2 + J_3 c_1^2 - J_1$$

$$K_2 = -J_2 c_1^2 - J_3 s_1^2 + J_1$$

$$K_3 = (J_2 - J_3) s_1 c_1$$

the control law matrix is:

$$\bar{F} = \frac{4}{3\Omega_o}\begin{bmatrix} 0 & 0 & 0 \\ \dfrac{-aS_s}{8(K_1 s_\lambda - K_3 c_\lambda)} & \dfrac{2K_2\left(1 + s_\lambda^2\right) - K_3 s_{2\lambda}}{\Delta} bS_c & \dfrac{-2K_3\left(1 + c_\lambda^2\right) + K_2 s_{2\lambda}}{\Delta} cS_c \\ \dfrac{aS_s}{8(K_2 c_\lambda + K_3 s_\lambda)} & \dfrac{-2K_3\left(1 + s_\lambda^2\right) - K_1 s_{2\lambda}}{\Delta} bS_c & \dfrac{-2K_1\left(1 + c_\lambda^2\right) - K_3 s_{2\lambda}}{\Delta} cS_c \end{bmatrix}$$

(1.16)

1.2.3 Arbitrary Intervals of Daylight and Darkness

Throughout the previous analysis it has been assumed that momentum dumping will be performed during precisely one half of the orbit, i.e., on the dark side. A more realistic model would account for the asymmetrical light and dark sides of the orbit. Consider the following sketch:

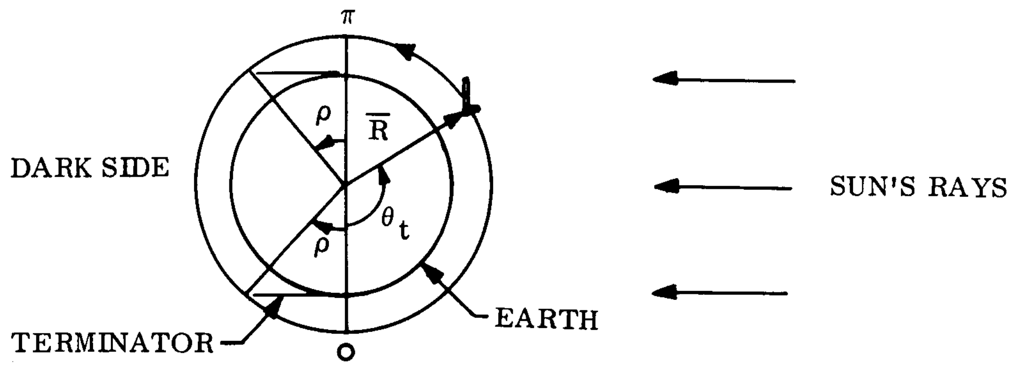

Typically, $\rho = 15$ deg. Thus the light side of the orbit would consist of $-\rho < \theta_t < \pi + \rho$ and the dark side from $\pi + \rho \leq \theta_t \leq 2\pi - \rho$. With this asymmetry introduced, the control law corresponding to Eq. (1.15) was derived. Defining

$$C_1 = \frac{2}{1 + \cos 2\rho}, \quad C_2 = \frac{2}{2 - \sin 2\rho}, \quad \Delta_o = 2(\sin 2\rho - \pi + 2\rho)$$

$$\epsilon_1 = \frac{-s_\lambda^2 \rho}{\Delta_o} \qquad \epsilon_2 = \frac{s_\lambda c_\lambda \rho}{\Delta_o}$$

$$\epsilon_3 = \frac{-s_\lambda c_\lambda \rho}{\Delta_o} \qquad \epsilon_4 = \frac{c_\lambda^2 \rho}{\Delta_o}$$

we have

$$\overline{G} = \begin{bmatrix} 0 & 0 & 0 \\ \dfrac{-aC_1}{4} s_\lambda S_s & bC_2\left[\dfrac{1 + s_\lambda^2}{8} S_c + \epsilon_1\right] & cC_2\left[\dfrac{s_\lambda c_\lambda}{8} S_c + \epsilon_3\right] \\ \dfrac{aC_1}{4} c_\lambda S_s & bC_2\left[\dfrac{-s_\lambda c_\lambda}{8} S_c + \epsilon_2\right] & cC_2\left[-\dfrac{1 + c_\lambda^2}{8} S_c + \epsilon_4\right] \end{bmatrix} \qquad (1.17)$$

It is noted that Eq. (1.17) reduces to Eq. (1.15) when $\rho = o$.

Similarly, the control law corresponding to Eq. (1.16) can be established. If additionally we define

$$\delta_1 = \frac{-8\left(2K_2 s_\lambda^2 - K_3 s_{2\lambda}\right)\rho}{\Delta_o} \qquad \delta_3 = \frac{-8\left(K_2 s_{2\lambda} - 2K_3 c_\lambda^2\right)\rho}{\Delta_o}$$

$$\delta_2 = \frac{8\left(K_1 s_{2\lambda} + 2K_3 s_\lambda^2\right)\rho}{\Delta_o} \qquad \delta_4 = \frac{8\left(2K_1 c_\lambda^2 + K_3 s_{2\lambda}\right)\rho}{\Delta_o}$$

the appropriate control law is:

$$\bar{F} = \frac{4}{3\Omega_o}\begin{bmatrix} 0 & 0 & 0 \\ \frac{-aC_1S_s}{8(K_1 s_\lambda - K_3 c_\lambda)} & \frac{bC_2}{\Delta}\left\{\left|2K_2\left(1 + s_\lambda^2\right) - K_3 s_{2\lambda}\right| S_c + \delta_1\right\} & \frac{cC_2}{\Delta}\left\{\left|-2K_3\left(1 + c_\lambda^2\right) + K_2 s_{2\lambda}\right| S_c + \delta_3\right\} \\ \frac{aC_1S_s}{8(K_2 c_\lambda + K_3 s_\lambda)} & \frac{bC_2}{\Delta}\left\{\left|-2K_3\left(1 + s_\lambda^2\right) - K_1 s_{2\lambda}\right| S_c + \delta_2\right\} & \frac{cC_2}{\Delta}\left\{\left|-2K_1\left(1 + c_\lambda^2\right) - K_3 s_{2\lambda}\right| S_c + \delta_4\right\} \end{bmatrix} \qquad (1.18)$$

Note again that Eq. (1.18) reduces to Eq. (1.16) if $\rho = 0$.

1.3 SUNSET $\bar{H}$ SAMPLING SYSTEM SIMULATION

The vehicle will be required to maneuver through angles as large as 15 deg to make use of the gravity-gradient momentum-dumping laws derived in subsection 1.2. The derivation assumes the vehicle can follow four consecutive step commands with zero error. Clearly, the control system will lag behind the momentum-dumping commands. To demonstrate the sensitivity of the momentum dumping to these maneuver errors, the discrete ($\bar{H}$ sampling at sunset) momentum-dumping control law was incorporated in a simulation program. The simulation program showed that the vehicle will not follow the required step command changes without intolerably large errors. This result was obtained with both the Langley attitude control law and the cross-product $\overline{H}$ feedback attitude control law. It is concluded that while the momentum dumping law is practical, the attitude control laws (which provide acceptable null attitude control) will require modification to make vehicle maneuvers feasible.

These modifications would be the subject of further studies. The recommended studies would consist of evaluating the following considerations: (1) filtering the step commands to reduce the required gimbal angle rates, (2) inclusion of the cos φ_i division in the commanded value of $\dot{\lambda}_i$ to increase the loop gain at large values of φ_i (cross-product law) (3) modification of the Langley control law to agree with Eq. (5.6) of Ref. 1-1, and (4) implementation of more complex control laws to eliminate or minimize the cross-coupling which appears to restrict maneuvering capability.

1.4 REFERENCES

1-1. Lockheed Missiles & Space Company, Conceptual Design and Analysis of Control System for Apollo Telescope Mount, by Dr. D.R. Ingwerson et al., LMSC-A842157, Sunnyvale, Calif., 17 Mar 1967

1-2. -----, Final Report for ATM and Cluster System Analyses, Augmentation Task Nos. 1 and 19, LMSC-A842251, 7 Jul 1967

1-3. -----, User's Manual: Apollo Telescope Mount Simulation (ATOMS), by L.M. Reinkens and W.L. Wong, LMSC-A842251-1, Jun 1967

Section 2
EXPERIMENT POINTING SYSTEM SIMULATION

This section summarizes the simulation results for MSFC's version of the Experiment Pointing System (EPS). The simulation, ATOMS, was extended to include (1) a more elaborate sensor model, (2) constraints on the inner gimbal angles and inner and outer gimbal angle rates, (3) the cross-product control law with H-vector feedback, and (4) continuous and discrete momentum dumping control laws.

2.1 MATHEMATICAL MODEL

The following equations are consistent with the ATOMS user's manual (Ref. 2-1) and have been implemented in ATOMS.

2.1.1 Cross-Product Attitude Control Law

$$\begin{bmatrix} \dot{\lambda}_1 \\ \dot{\lambda}_2 \\ \dot{\lambda}_3 \\ \dot{\phi}_1 \\ \dot{\phi}_2 \\ \dot{\phi}_3 \end{bmatrix} = \begin{bmatrix} -\sin\lambda_1 & 0 & -\cos\lambda_1 \\ -\cos\lambda_2 & -\sin\lambda_2 & 0 \\ 0 & -\cos\lambda_3 & -\sin\lambda_3 \\ -\sin\phi_1\cos\lambda_1 & \cos\phi_1 & \sin\phi_1\sin\lambda_1 \\ \sin\phi_2\sin\lambda_2 & -\sin\phi_2\cos\lambda_2 & \cos\phi_2 \\ \cos\phi_3 & \sin\phi_3\sin\lambda_3 & -\sin\phi_3\cos\lambda_3 \end{bmatrix} \begin{bmatrix} \epsilon_1 \\ \epsilon_2 \\ \epsilon_3 \end{bmatrix}$$

Without H-vector feedback:

$$\begin{bmatrix} \epsilon_1 \\ \epsilon_2 \\ \epsilon_3 \end{bmatrix} = \begin{bmatrix} \Gamma_{11} \mathring{A}_{23} + \Gamma_{21} \omega_1 \\ \Gamma_{12}\left(-\mathring{A}_{13}\right) + \Gamma_{22}\omega_2 \\ \Gamma_{13} \tan^{-1}\left(\mathring{A}_{12}/\mathring{A}_{22}\right) + \Gamma_{23} \omega_3 \end{bmatrix}$$

With H-vector feedback:

$$\begin{bmatrix} \epsilon_1 \\ \epsilon_2 \\ \epsilon_3 \end{bmatrix} = \begin{bmatrix} KS_1 & 0 & 0 \\ 0 & KS_2 & 0 \\ 0 & 0 & KS_3 \end{bmatrix} \begin{bmatrix} \bar{H}_{21} - \dfrac{H_2(1)}{H_{MAG}} \\ \bar{H}_{22} - \dfrac{H_2(2)}{H_{MAG}} \\ \bar{H}_{23} - \dfrac{H_2(3)}{H_{MAG}} \end{bmatrix}$$

where

$$\dot{\bar{H}}_{21} = \Gamma_{11} \mathring{A}_{23} + \Gamma_{21} \omega_1$$

$$\dot{\bar{H}}_{22} = \Gamma_{12}\left(-\mathring{A}_{13}\right) + \Gamma_{22} \omega_2$$

$$\dot{\bar{H}}_{23} = \Gamma_{13} \tan^{-1}\left(\mathring{A}_{12}/\mathring{A}_{22}\right) + \Gamma_{23} \omega_3$$

and

$H_2(I)$ ≡ stored total CMG angular momentum vector

H_{MAG} ≡ magnitude of the CMG angular momentum

$\dot{\lambda}_i$ ≡ outer gimbal rates

$\dot{\phi}_i$ ≡ inner gimbal rates

λ_i ≡ outer gimbal angles

ϕ_i ≡ inner gimbal angles

$\mathring{A}_{ij}$ ≡ inertial position

ω_i ≡ body (1) rates

Saturation:

$$\dot{\lambda}_i = \begin{cases} 4.54 \text{ deg/sec} & \dot{\lambda}_i > 4.54 \text{ deg/sec} \\ \dot{\lambda}_i & \dot{\lambda}_i \leq 4.54 \text{ deg/sec} \end{cases}$$

$$\dot{\phi}_i = \begin{cases} 4.54 \text{ deg/sec} & \dot{\phi}_i > 4.54 \text{ deg/sec} \\ \dot{\phi}_i & \dot{\phi}_i \leq 4.54 \text{ deg/sec} \end{cases}$$

$$\phi_i = \begin{cases} 70 \text{ deg}, \ \dot{\phi}_i = 0 & \phi_i > 70 \text{ deg} \\ \phi_i & \phi_i \leq 70 \text{ deg} \end{cases}$$

2.1.2 Experiment Pointing System

$$T_\alpha = \begin{cases} W_3 & |W_3| \leq K_3 \\ K_3 \operatorname{sgn} W_3 & |W_3| > K_3 \end{cases}$$

$$T_\beta = \begin{cases} W_4 & |W_4| \leq K_4 \\ K_4 \operatorname{sgn} W_4 & |W_4| > K_4 \end{cases}$$

$$\begin{bmatrix} W_1 \\ W_2 \end{bmatrix} = \begin{bmatrix} K_{11} & K_{12} \\ K_{21} & K_{22} \end{bmatrix} \begin{bmatrix} V_3 \\ V_4 \end{bmatrix} + \begin{bmatrix} K_{14} & U_1 \\ K_{25} & U_3 \end{bmatrix}$$

$$V_3 = \begin{cases} V_1 & |V_1| \leq K_1 \\ K_1 \operatorname{sgn} V_1 & |V_1| > K_1 \end{cases}$$

$$V_4 = \begin{cases} V_2 & |V_2| \leq K_2 \\ K_2 \operatorname{sgn} V_2 & |V_2| > K_2 \end{cases}$$

where for position sensors:

$$\dot{V}_1 = -\frac{1}{\tau_1}\left[C\mathring{A}\right]_{13} - \frac{1}{\tau_1} V_1$$

$$\dot{V}_2 = \frac{1}{\tau_2}\left[C\mathring{A}\right]_{23} - \frac{1}{\tau_2} V_2$$

for rate sensor:

$$\begin{cases} \dot{U}_1 = U_2 \\ \dot{U}_2 = -\omega_{n_1}^2 U_1 - 2\zeta_1 \omega_{n_1} U_2 + \omega_{n_1}^2 \omega_4 \end{cases}$$

$$\begin{cases} \dot{U}_3 = U_4 \\ \dot{U}_4 = -\omega_{n_2}^2 U_3 - 2\zeta_2 \omega_{n_2} U_4 + \omega_{n_2}^2 \omega_5 \end{cases}$$

for torquer:

$$\dot{W}_3 = \frac{1}{\tau_3} W_1 - \frac{1}{\tau_3} W_3$$

$$\dot{W}_4 = \frac{1}{\tau_4} W_2 - \frac{1}{\tau_4} W_4$$

and

K_i ≡ saturation levels

T_α, T_β ≡ EPS gimbal torques

ω_{ni} ≡ gyro natural frequency

ζ_i ≡ gyro damping ratio

$\left[C\mathring{A}\right]_{ij}$ ≡ position measurement

ω_i ≡ body 2 rate measurement

2.1.3 Continuous Momentum Dumping

$$F1 = \begin{bmatrix} 0 & 0 & 0 \\ -KM(1)\,\mathrm{sgn}(\sin 2P) & KM(3)\,\mathrm{sgn}(\cos 2P) & KM(5)\,\mathrm{sgn}(\cos 2P) \\ KM(2)\,\mathrm{sgn}(\sin 2P) & -KM(4) & -KM(6) \end{bmatrix}$$

$$\underline{CM} = (F1)\,\underline{H2}$$

$$Y = \begin{bmatrix} \mathring{A}_{23} + CM(1) \\ -\mathring{A}_{13} + CM(2) \\ \tan^{-1}\left(\frac{\mathring{A}_{12}}{A_{22}}\right) + CM(3) \end{bmatrix}$$

For either CMG control law, replace in CMG model

$$\begin{cases} \mathring{A}_{23} = Y(1) \\ -\mathring{A}_{13} = Y(2) \\ \tan^{-1}\left(\frac{\mathring{A}_{12}}{A_{22}}\right) = Y(3) \end{cases}$$

where

P	≡	true anomaly measured from sunrise
KM(i)	≡	input gains
$\underline{H2}$	≡	current total stored angular momentum
$\underline{CM}$	≡	momentum dump control signal

2.1.4 Discrete Momentum Dumping

$$F1 = \begin{bmatrix} 0 & 0 & 0 \\ -KM(1)\ \mathrm{sgn}(\sin 2P) & KM(3)\ \mathrm{sgn}(\cos 2P) & KM(5)\ \mathrm{sgn}(\sin 2P) \\ KM(2)\ \mathrm{sgn}(\sin 2P) & -KM(4)\ \mathrm{sgn}(\cos 2P) & -KM(6)\ \mathrm{sgn}(\cos 2P) \end{bmatrix}$$

$\underline{H2}$ ≡ sampled at sunset only

$$\underline{CM} = (F1)\ \underline{H2}$$

Proceed as in continuous case

2.1.5 Initial Conditions

In order to investigate the MSFC cases, the data presented in Tables 2-1 and 2-2 were used. The three cases were initialized with telescope offsets as follows:

Case 1: β = 2.5 arc sec

$\alpha = 0$

Case 2: $\alpha = \beta$ = 100 arc sec

Case 3: $\alpha = 0$

$\beta = 0$

where α and β are telescope gimbal angles.

Table 2-1

INERTIA PROPERTIES, MASSES, AND HINGE LOCATIONS

Carrier:

J_{11} = 819, 147 kg-m^2

J_{22} = 4,412,603 kg-m^2

J_{33} = 4,383,947 kg-m^2

J_{12} = - 191,285 kg-m^2

J_{13} = 45,809 kg-m^2

J_{23} = - 15,172 kg-m^2

Mass (M_c): 52,026 kg

Hinge Vector:

H_1 = 106.3 m

H_2 = 11.8 m

H_3 = 237.1 m

Spar:

J_{44} = 954 kg-m^2

J_{55} = 2111 kg-m^2

J_{66} = 2309 kg-m^2

$J_{45} = J_{46} = J_{56} = 0$

Mass (M_s): 2000 kg

Hinge Vector:

$H_4 = H_5 = H_6 = 0$

Table 2-2

CONTROL DATA FOR MSFC CASES

Item	Values
Control Moment Gyros	
Inner Gimbal Orientation (Initial)	$\varphi_1 = \varphi_2 = \varphi_3 = 0$
Outer Gimbal Orientation (Initial)	$\lambda_1 = \lambda_2 = \lambda_3 = 45$ deg
Angular Momentum	$H^{CMG} = 2720$ N-m-sec
Control Gains	
Position Gains	$\Gamma_{11} = 66.6$; $\Gamma_{12} = \Gamma_{13} = 358$ rad/sec
Rate Gains	$\Gamma_{21} = 212$; $\Gamma_{22} = \Gamma_{23} = 1140$
Langley law without saturation is used.	
Telescope	
Position Sensor Saturation	$\lvert K_1 \rvert = \lvert K_2 \rvert = 0.00038$ rad
Torquer Saturation	$\lvert K_3 \rvert = \lvert K_4 \rvert = 20.07$ N-m
Position Gains	$K_{12} = K_{21} = 2,419,220$ rad/sec
Rate Gains	$K_{14} = K_{25} = 208,850$
Flexure Pivot Constants	$K^f_\alpha = K^f_\beta = 70$ N-m/rad
Back EMF Constants	$C_\alpha = C_\beta = 0$
Position Time Constants	$\tau_1 = \tau_2 = 0.016$ sec
Torquer Time Constants	$\tau_3 = \tau_4 = 0.003$ sec
Gyro Damping Ratios	$\zeta_1 = \zeta_2 = 0.707$
Gyro Natural Frequency	$\omega_n(1) = \omega_n(2) = 188.4$ rad/sec

For case (3) the disturbance torque about carrier e_1 axis

$$T_1 = A \sin 4\pi t$$

$$A = \text{Amplitude} = 158{,}000 \text{ N-m}$$

For these data, this vehicle was placed in a circular orbit at 463 km altitude in the ecliptic plane at the vernal equinox. The carrier offsets are nulled.

2.2 RESULTS

The transient response of the ATM control system is presented in Figs. 2-1 through 2-3 for the three MSFC cases. The nomenclature associated with the automatic plots is presented in Table 2-3.

The first MSFC case is depicted in Figs. 2-1a through 2-1l. An initial offset (β) was introduced on the telescope of 2.5 arc sec. It is of particular interest to observe the Euler angle history of the telescope (TH 4, TH 5, TH 6) on Fig. 2-1i. From these results it appears that system gains are sized to yield a highly damped system. There is no overshoot and the 10- to 90-percent rise time is about 0.14 sec. Thus the swiftness of the response is quite high. The minor oscillations in this response are due to the sensor characteristics.

The second MSFC case illustrates the response of the EPS to an initial offset of 100 arc sec on both the α and β EPS gimbal axes. Since the EPS control system has a very fast response, the method used in atoms to simulate the saturation of the EPS nonlinear control elements is inadequate. As a result, the time-response characteristics presented in Figs. 2-2a through 2-2l do not illustrate any nonlinear control elements. Figure 2-2i illustrates the EPS Euler angle history (TH 4, TH 5, TH 6) and shows a highly damped system.

For the MSFC case 3, a sinusoidal disturbance torque was introduced about the e_1-axis of the carrier. The corresponding transient response of the system is shown in Figs. 2-3a through 2-3l. Figure 2-3g illustrates torque history. TCA and TCB are the EPS control torques about the α and β gimbal axes. TP1, TP2, TP3 are the CMG control torques combined with the sinusoidal disturbance torque. Since this disturbance torque is applied only about the e_1-axis of the vehicle it appears only on the TP1 time history, combined with the applied CMG control torque along that axis.

The effect of this disturbance torque on the EPS is illustrated by the Euler angle histories (Fig. 2-3i) of the telescope or EPS. In particular, the TH4 Euler angle illustrates the major pointing error of the EPS. This error appears nearly as a ramp, which may not be satisfactory for the EPS, although there is insufficient data to say conclusively that it is an unstable condition.

2.3 REFERENCES

2.1 Lockheed Missiles & Space Co., User's Manual: Apollo Telescope Mount Simulation (Atoms), LMSC-A842251-1, Sunnyvale, Calif., Jun 1967

Table 2-3

LABELS USED IN PLOTS

Label	Explanation
TIME	Time (sec)
W1, W2, W3	Cartesian components of angular velocity for Body 1 (deg/sec)
W4, W5, W6	Same as above for Body 2 (deg/sec)
Q1, Q2, Q3, Q4	Euler parameters for Body 1
ALPHA, BETA	Euler angles of Body 2 relative to Body 1 (deg)
ALPHAD, BETAD	Rates of Euler angles (deg/sec)
LAMDA1, LAMDA2, LAMDA3	Outer gimbal angles for the three CMG's (deg)
PHI1, PHI2, PHI3	Inner gimbal angles (deg)
TCA, TCB	Total torques applied to Body 2 (for β and B respectively) (N-m)
TP1, TP2, TP3	Torques resulting from CMG control (N-m)
TH1, TH2, TH3	Euler angles for roll, pitch, and yaw of Body 1 (deg)
THD1, THD2, THD3	Rates of above quantities (deg/sec)
TH4, TH5, TH6	Euler angles for roll, pitch, and yaw of Body 2 (deg)
THD4, THD5, THD6	Rates of above quantities (deg/sec)
H21, H22, H23	Components of total CMG angular momentum (N-m-sec)
H2	Magnitude of CMG angular momentum (N-m-sec)
PSI	True anomaly of orbit (deg)

PRECEDING PAGE BLANK NOT FILMED

APOLLO TELESCOPE MOUNT SIMULATION

CASE NUMBER 0
MSFC CASE 1, EPS 2.5 ASEC

DATE
22 AUG 67

NAME - L M REINKENS
DEPT - 5534
BLD - 538
EXT - 28912

TABLE OF CONTENTS

APOLLO TELESCOPE MOUNT SIMULATION

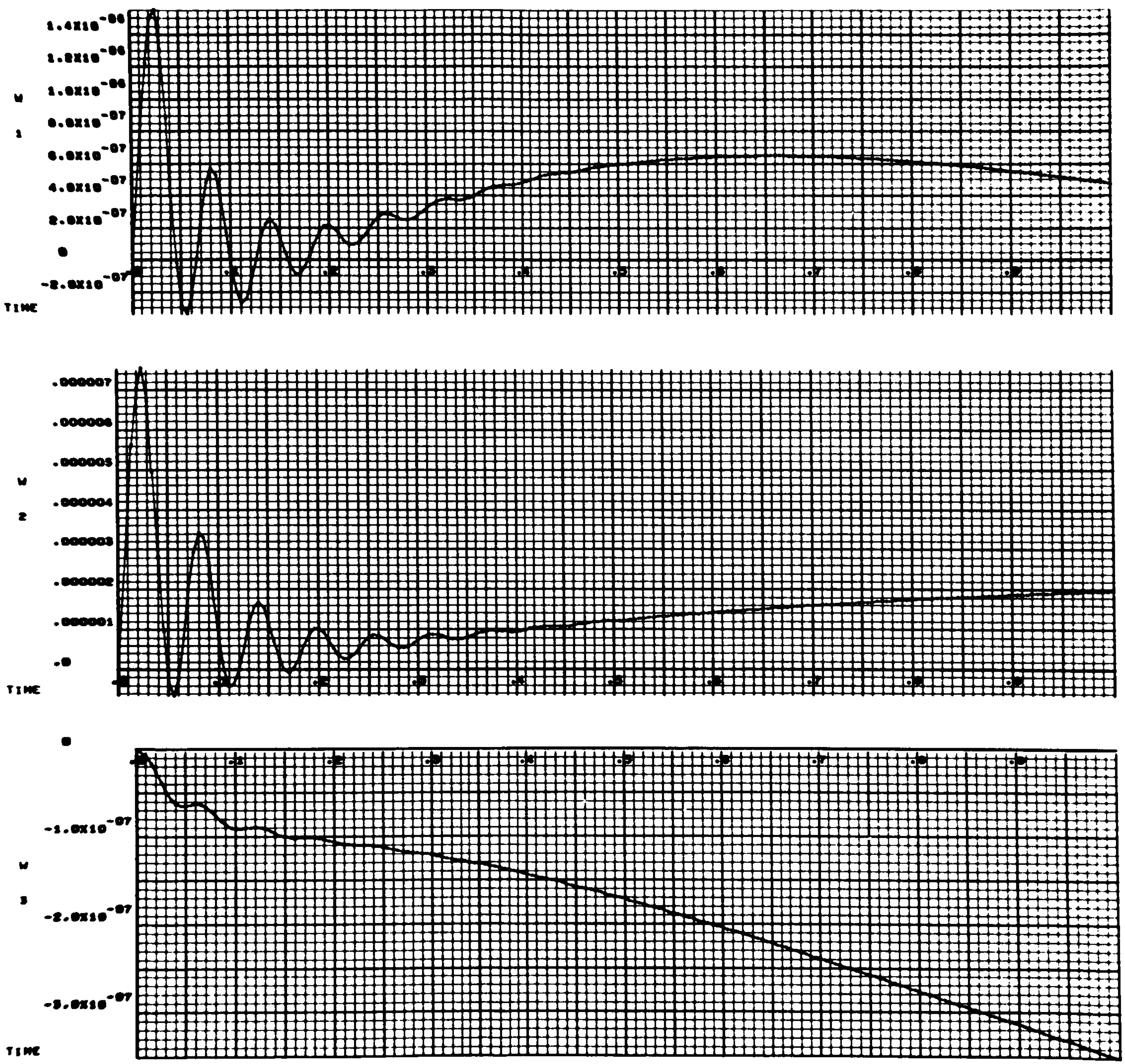

Fig. 2-1a MSFC Case 1

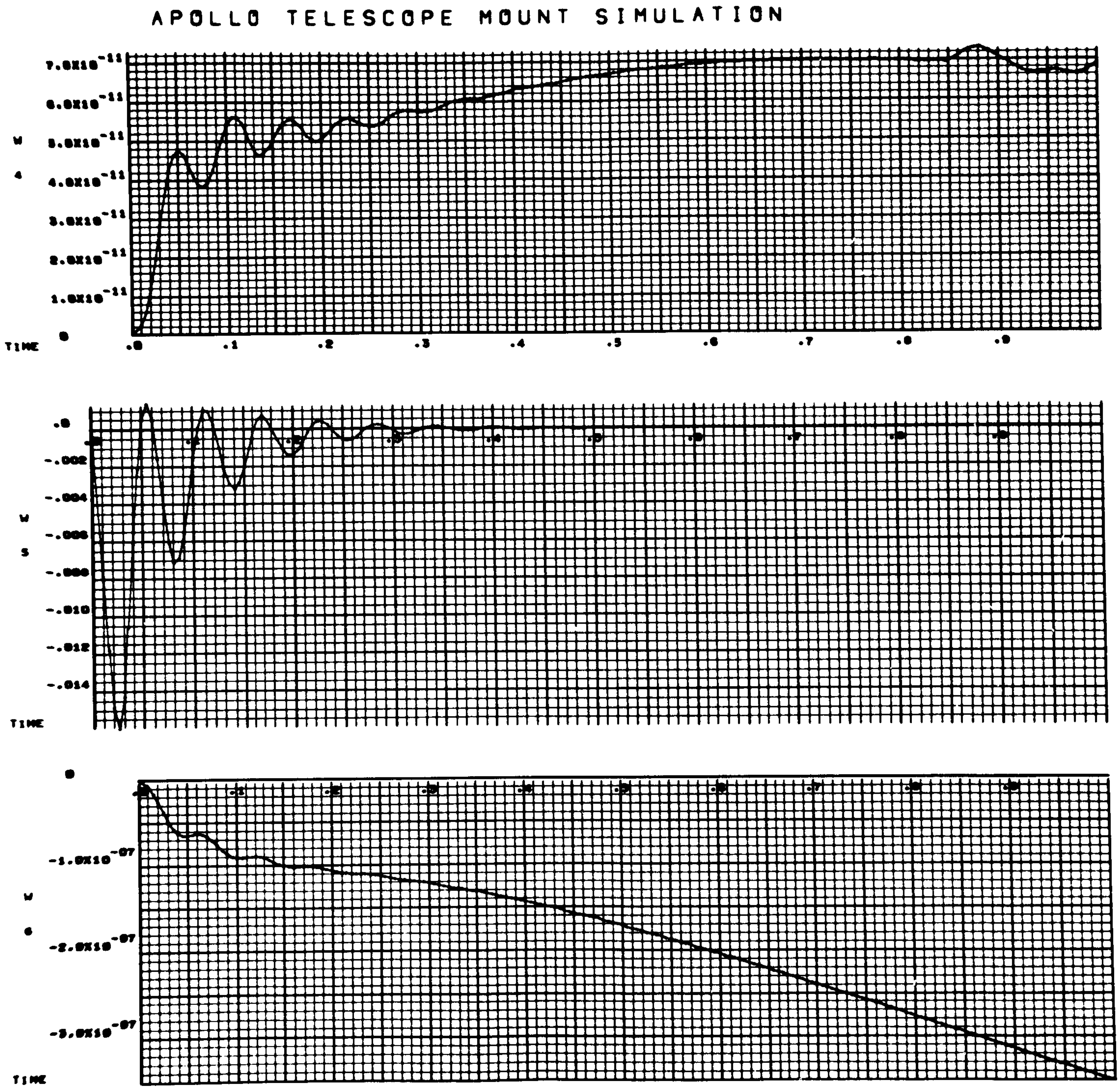

Fig. 2-1b MSFC Case 1 (Cont.)

APOLLO TELESCOPE MOUNT SIMULATION

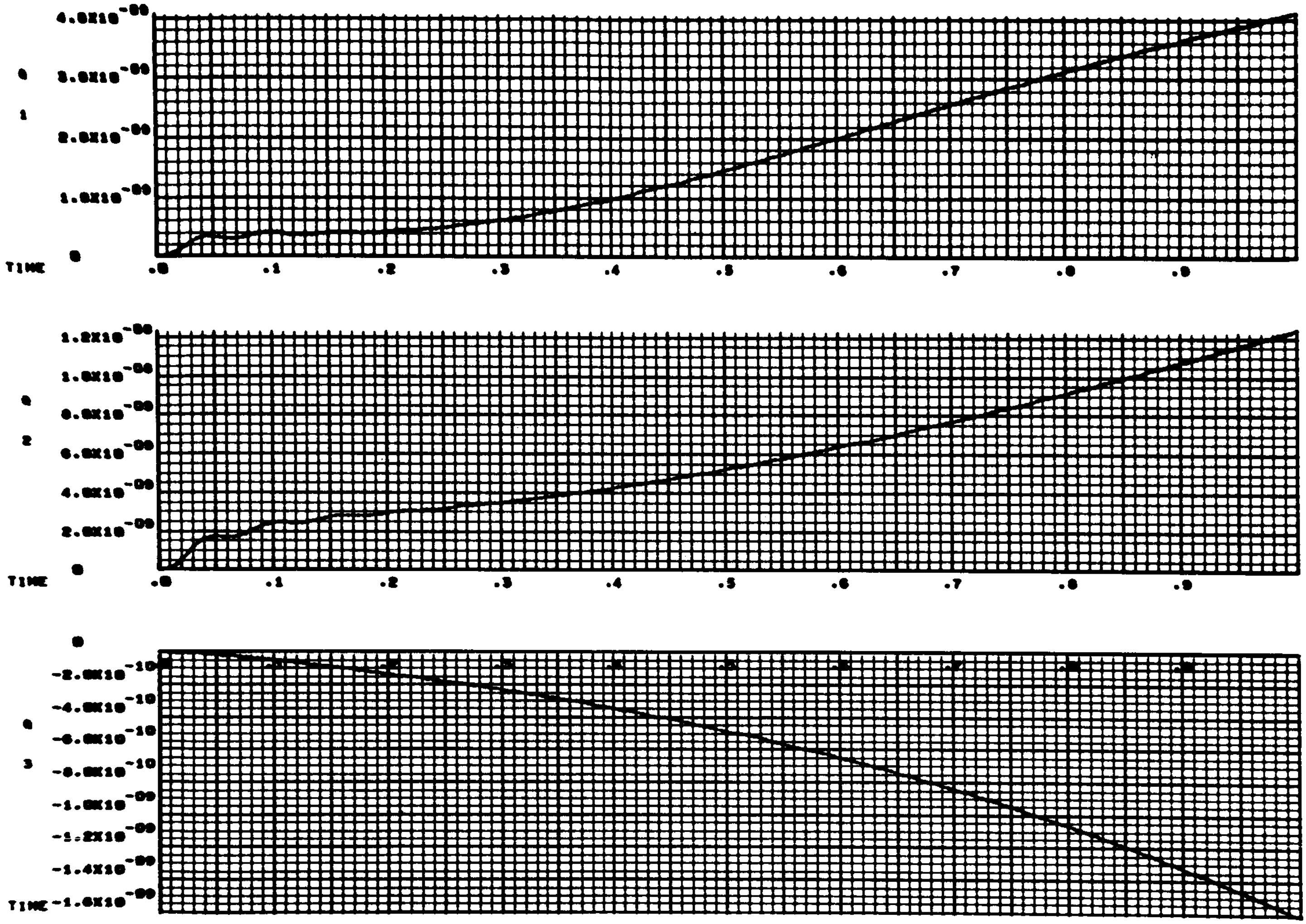

Fig. 2-1c MSFC Case 1 (Cont.)

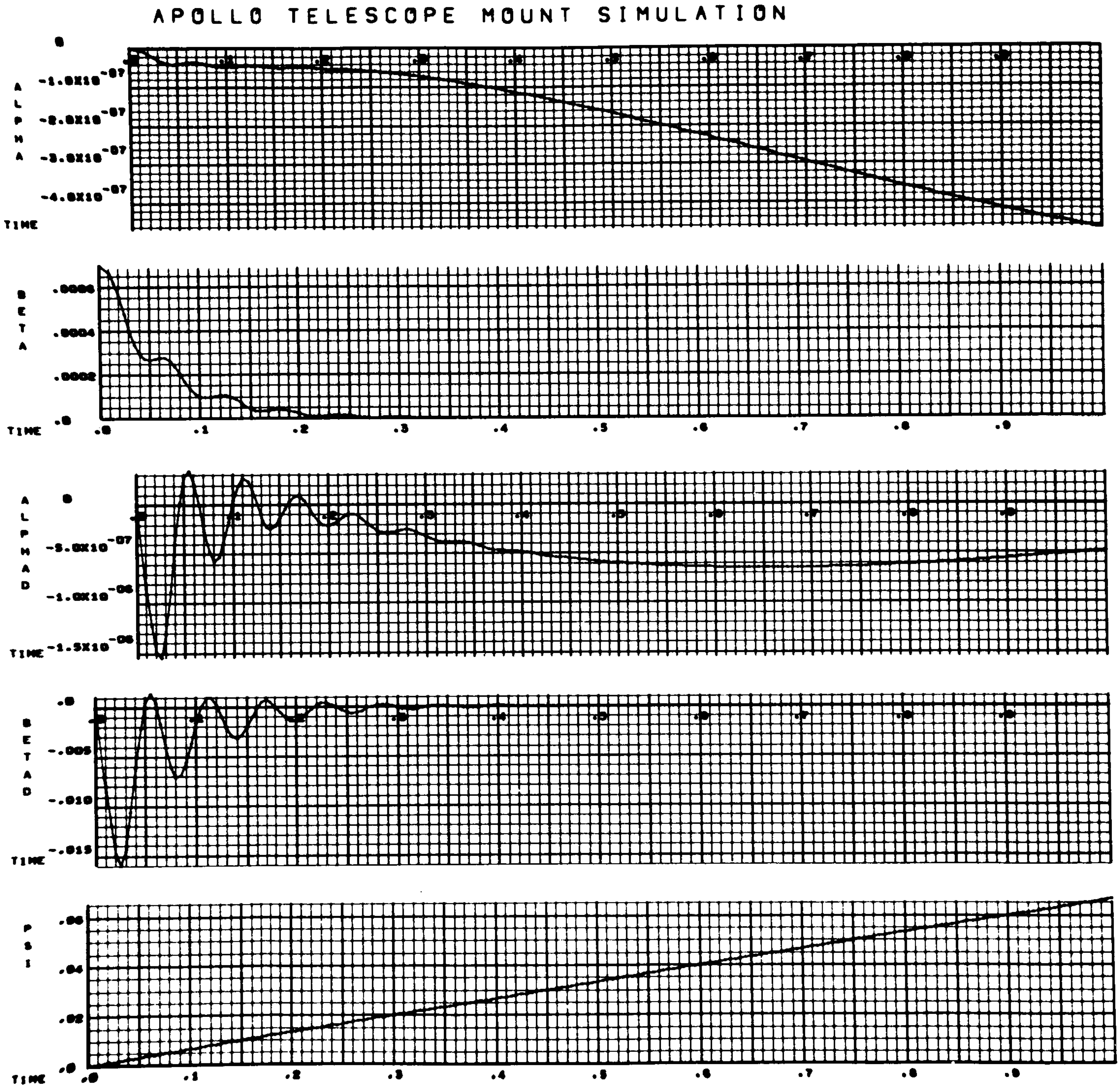

Fig. 2-1d MSFC Case 1 (Cont.)

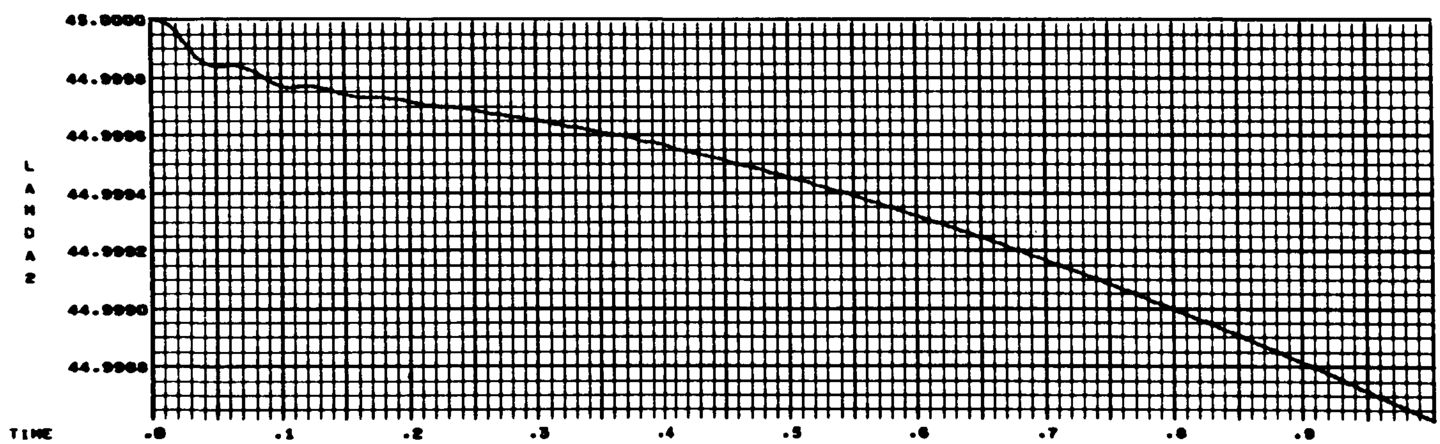

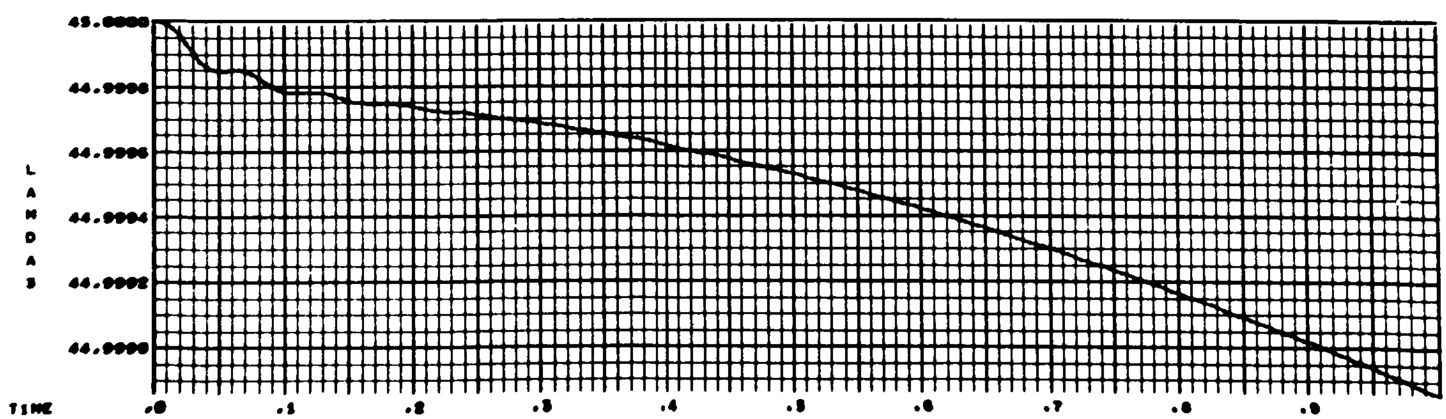

Fig. 2-1e. MSFC Case 1 (Cont.)

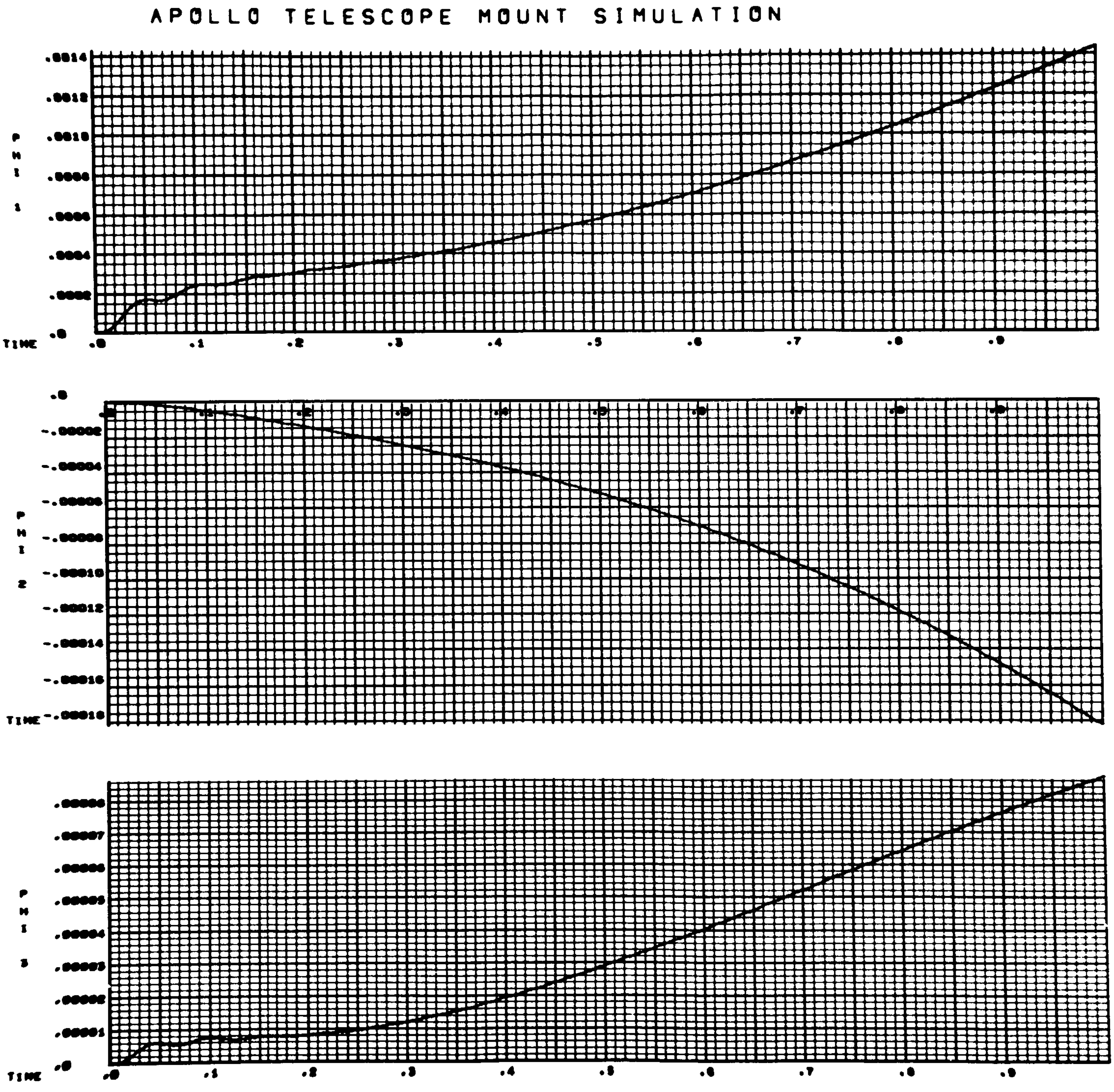

Fig. 2-1f MSFC Case 1 (Cont.)

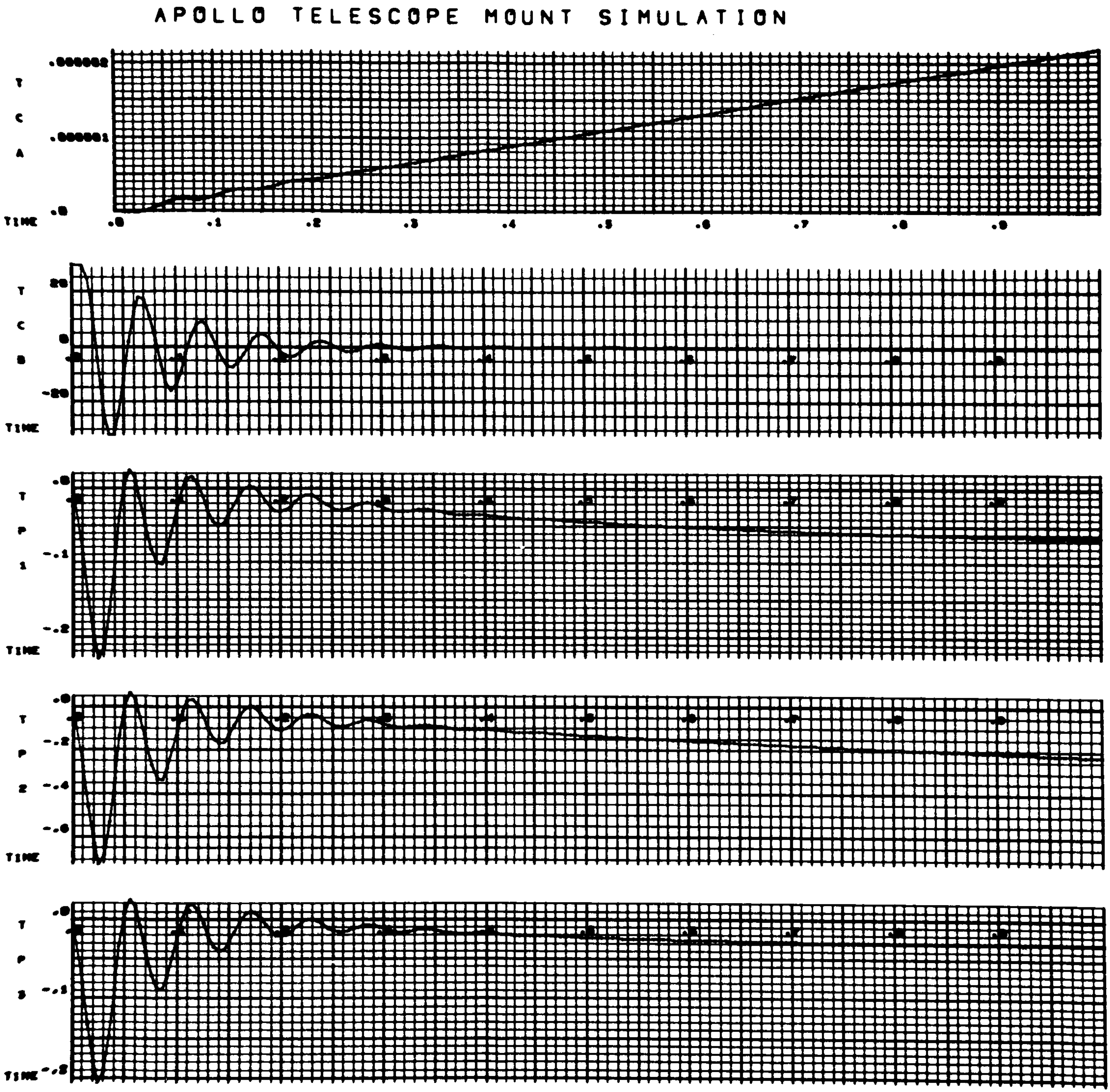

Fig. 2-1g MSFC Case 1 (Cont.)

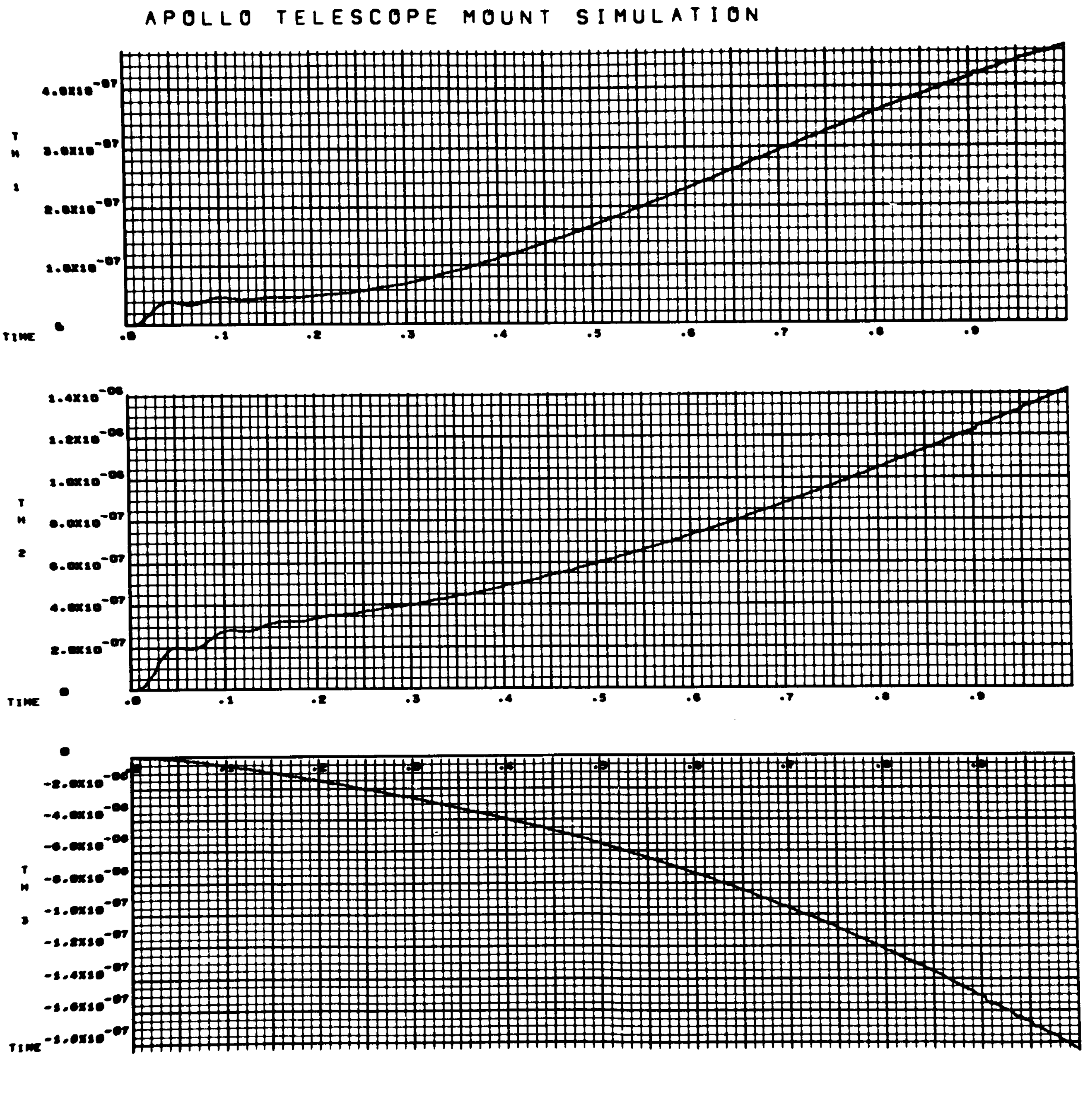

Fig. 2-1h MSFC Case 1 (Cont.)

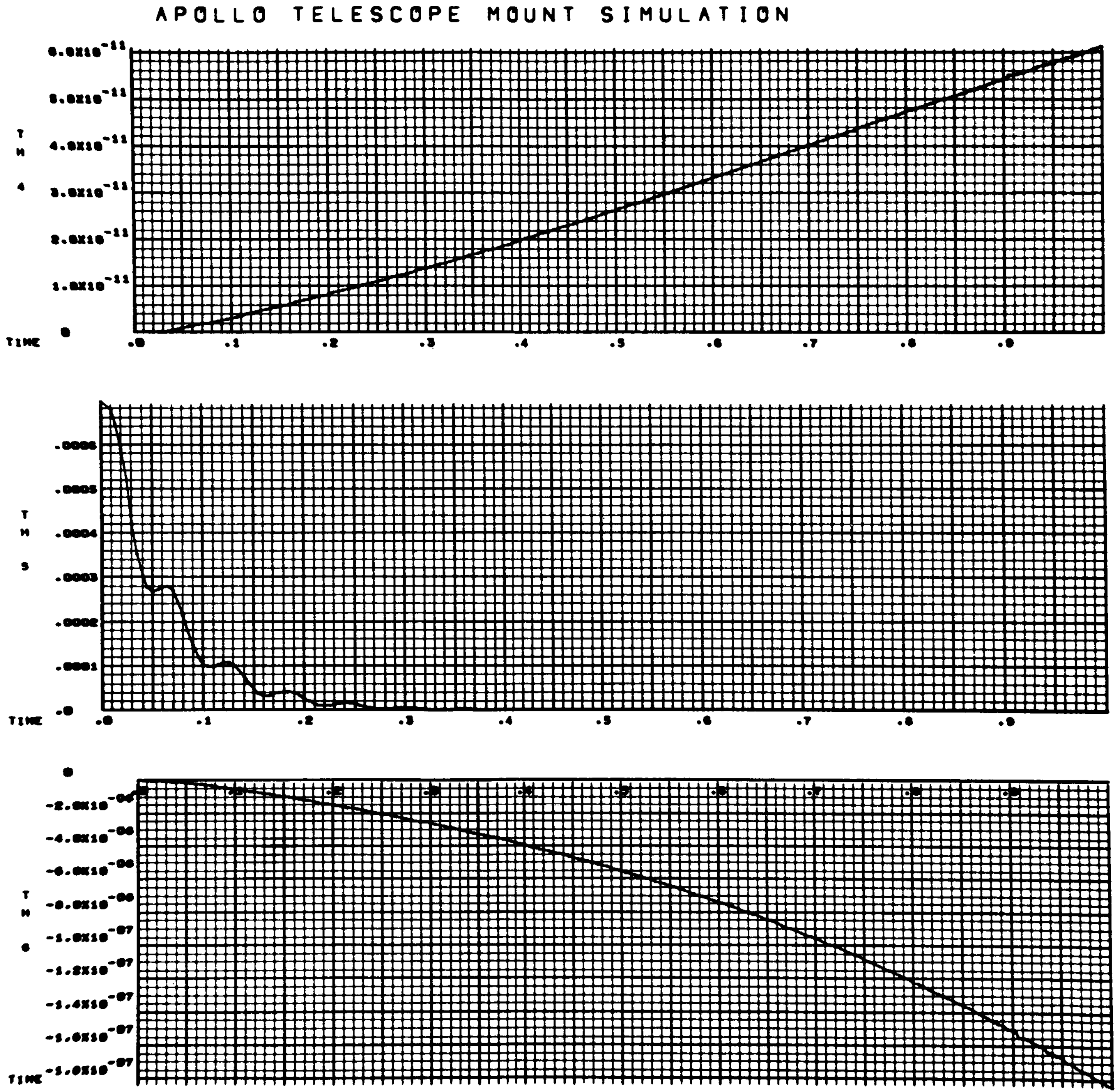

Fig. 2-1i MSFC Case 1 (Cont.)

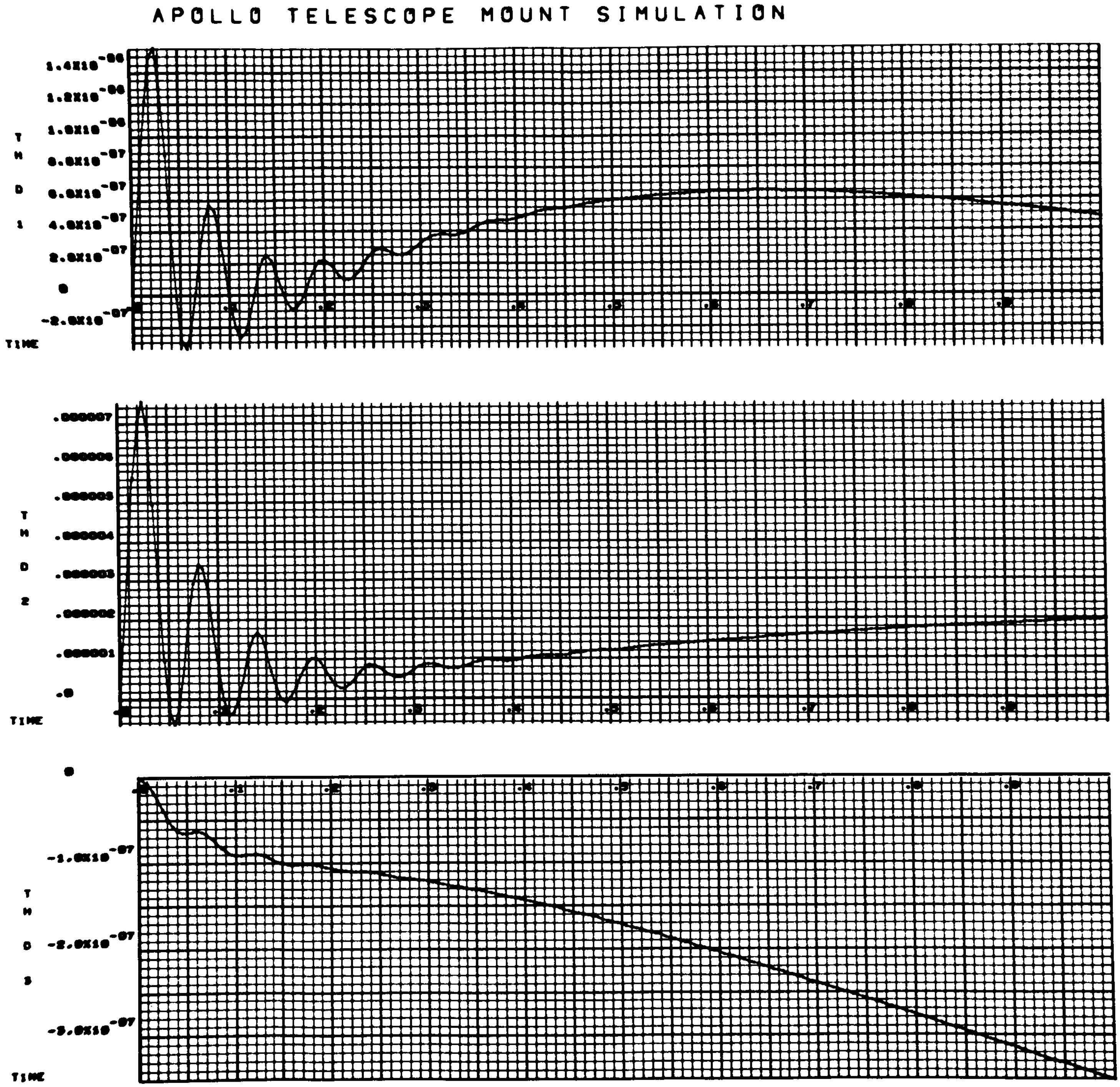

Fig. 2-1j MSFC Case 1 (Cont.)

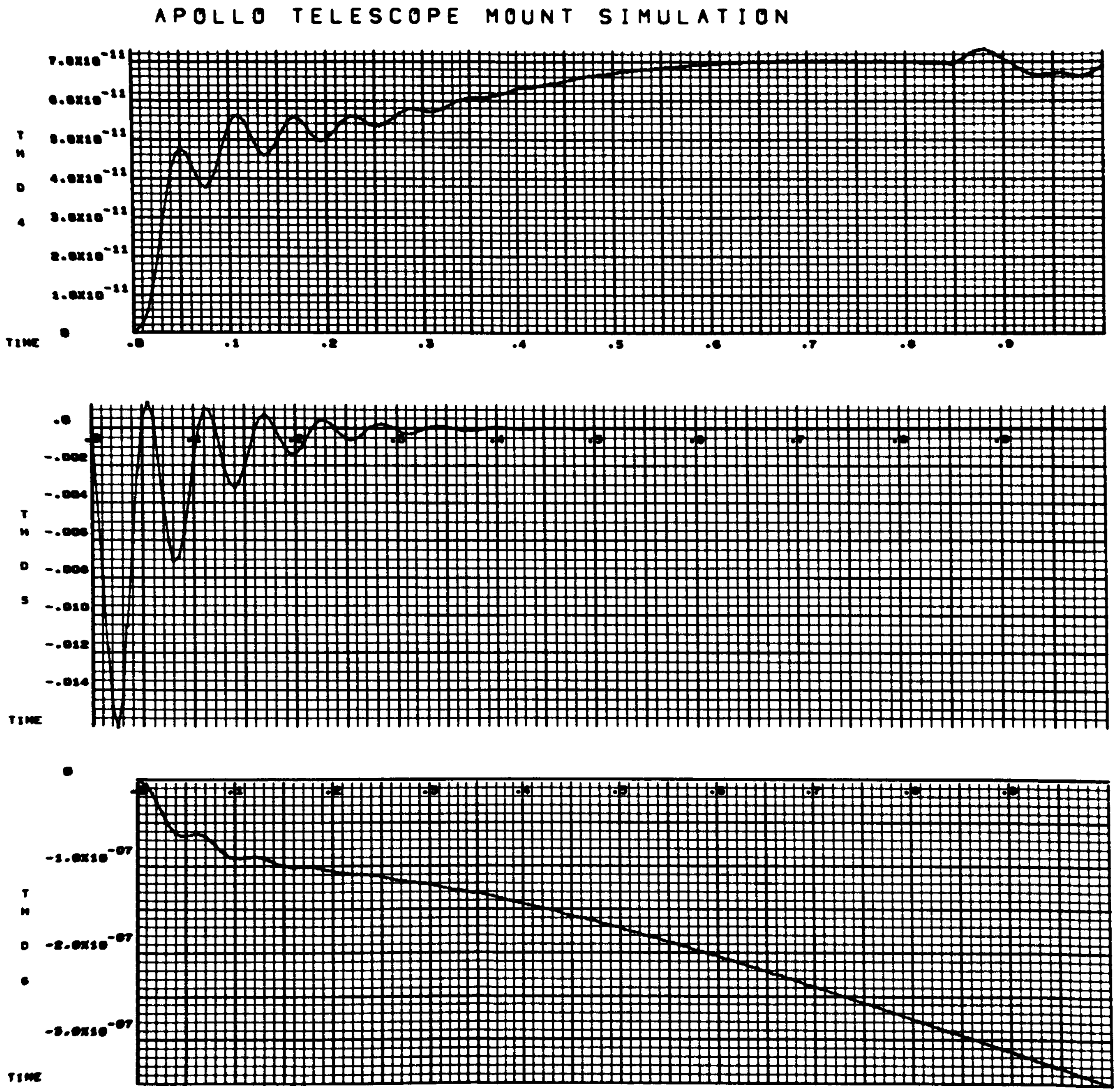

Fig. 2-1k MSFC Case 1 (Cont.)

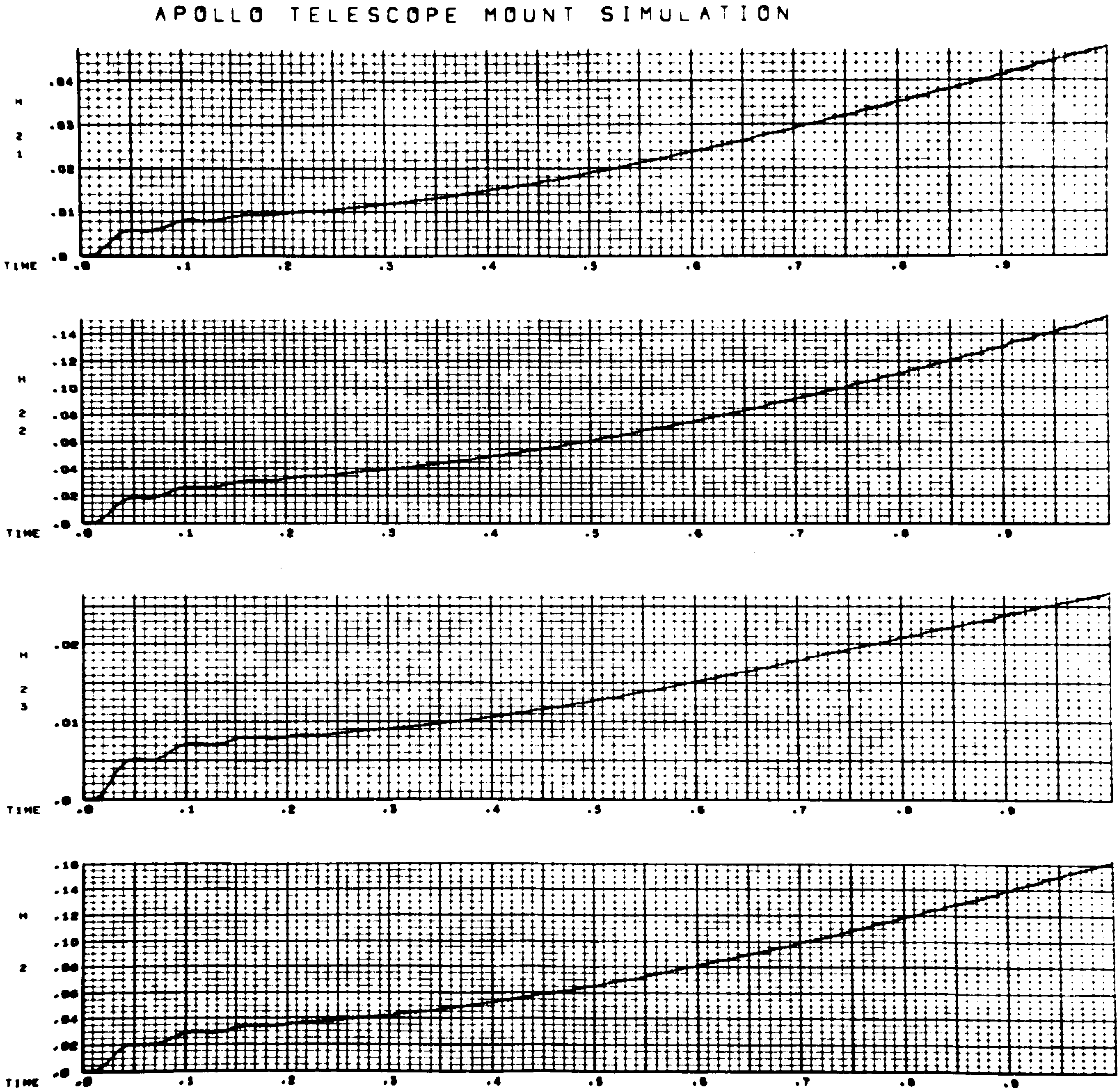

Fig. 2-11 MSFC Case 1 (Cont.)

APOLLO TELESCOPE MOUNT SIMULATION

CASE NUMBER 0
MSFC CASE 2, EPS 100 ASEC

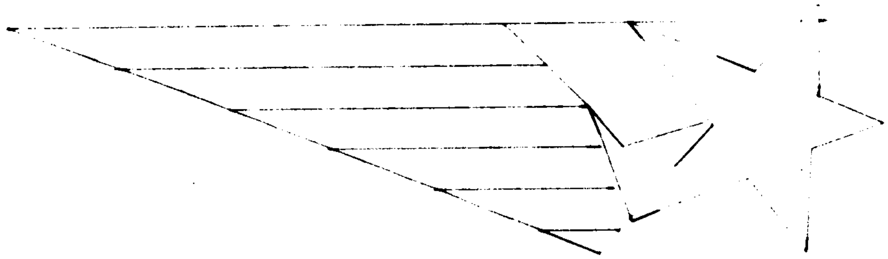

DATE
24 AUG 67

NAME - L M REINKENS
DEPT - 5534
BLD - 538
EXT - 28912

TABLE OF CONTENTS

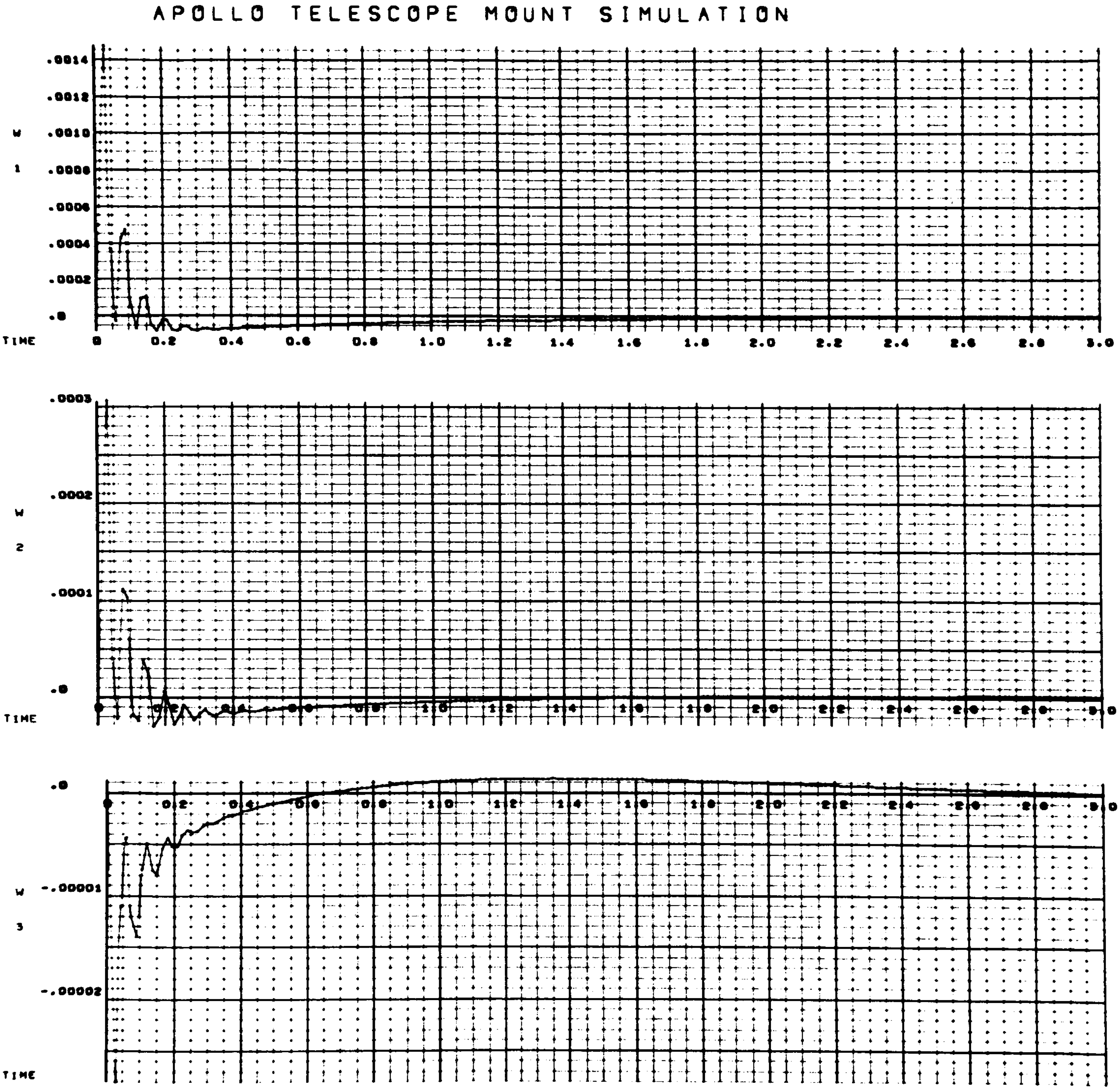

Fig. 2-2a MSFC Case 2

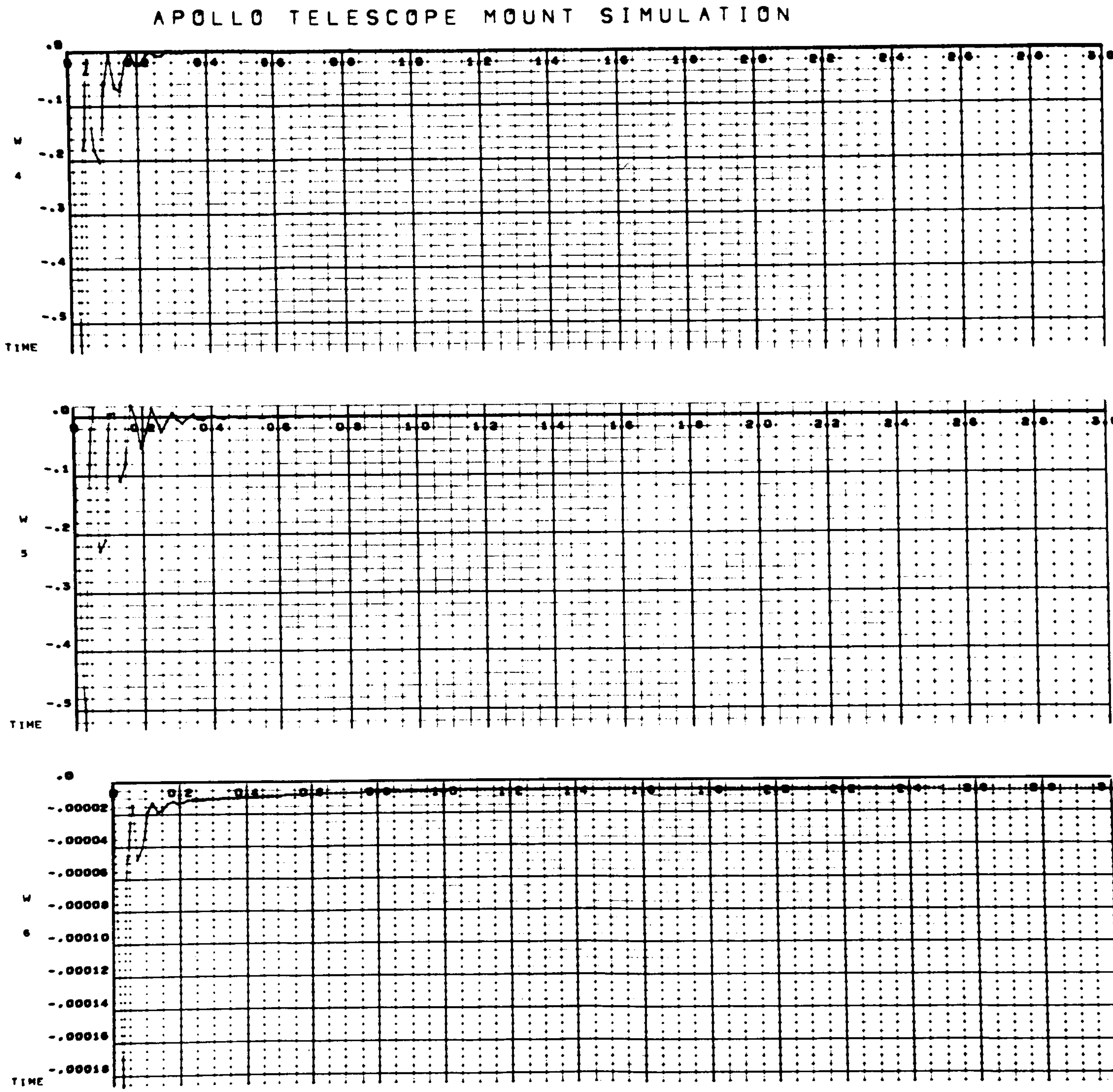

Fig. 2-2b MSFC Case 2 (Cont.)

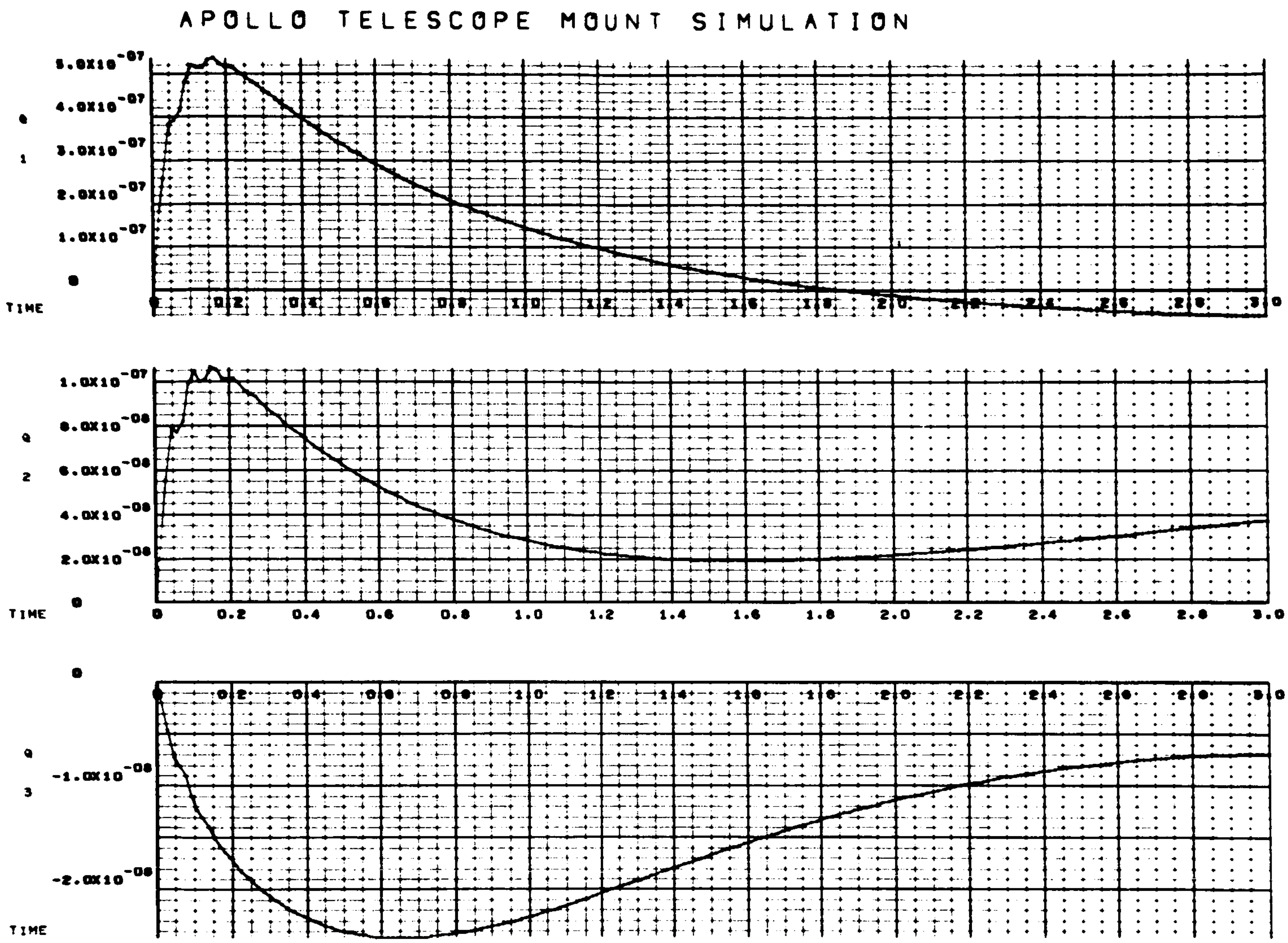

Fig. 2-2c MSFC Case 2 (Cont.)

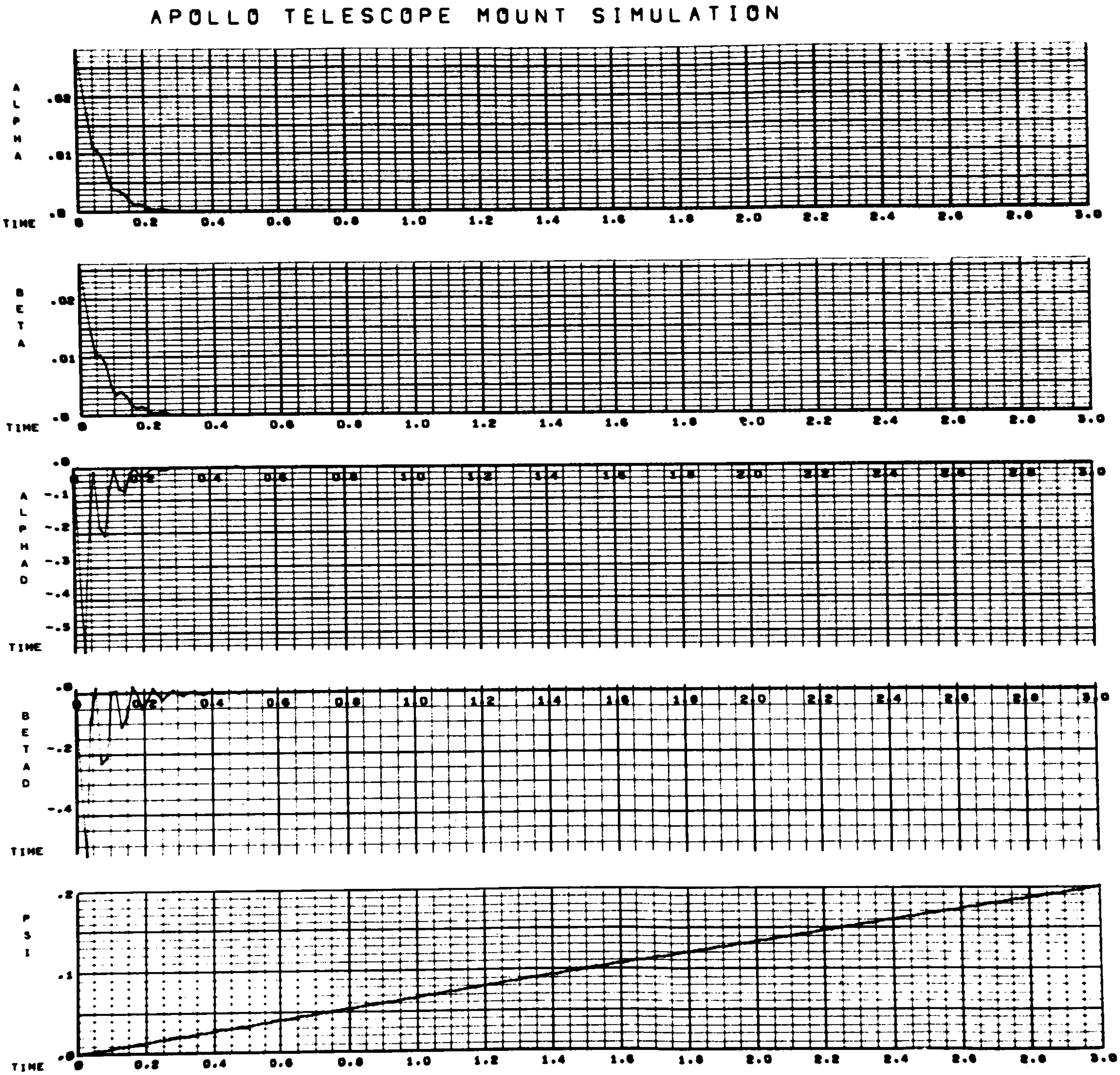

Fig. 2-2d MSFC Case 2 (Cont.)

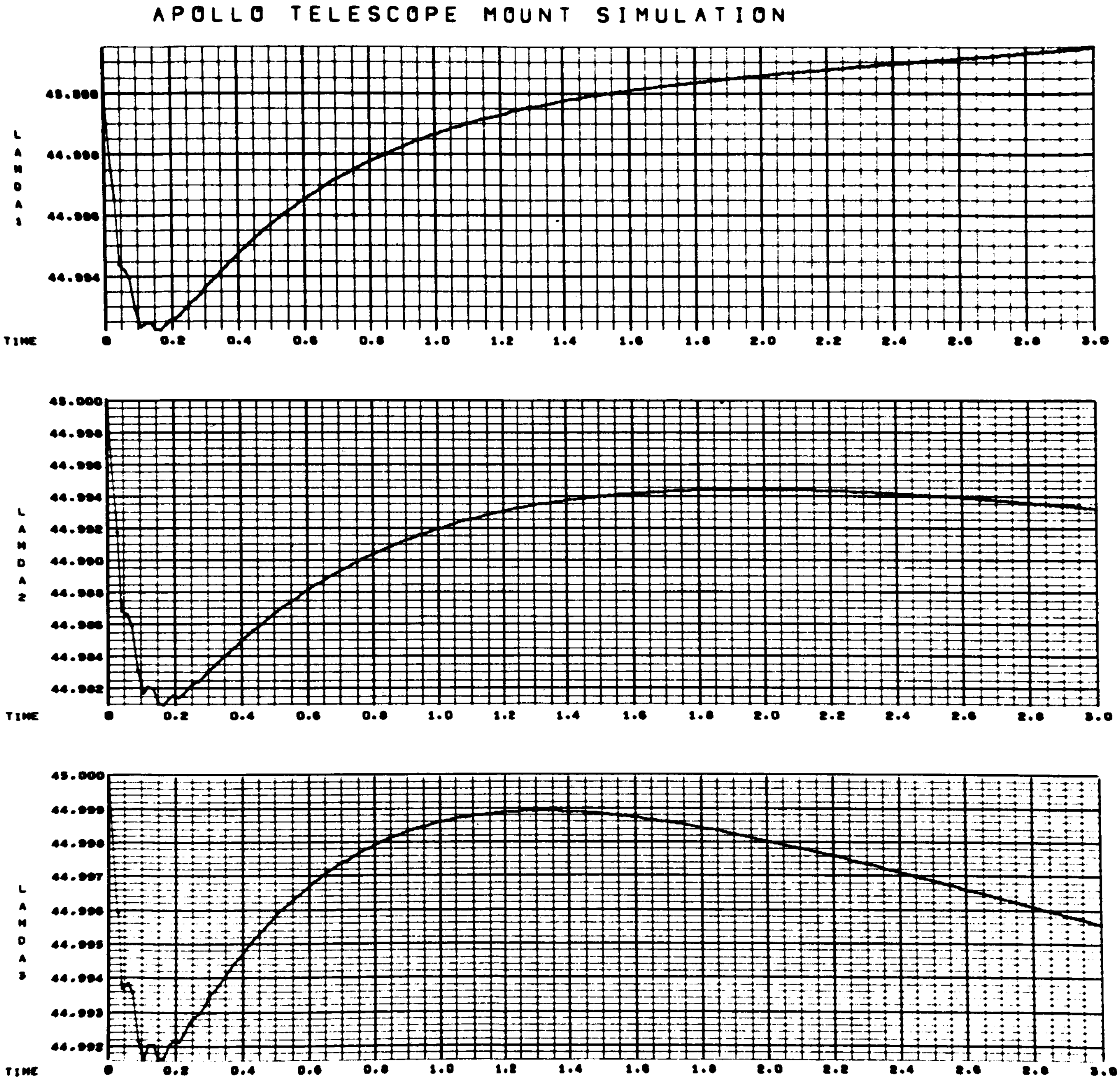

Fig. 2-2e MSFC Case 2 (Cont.)

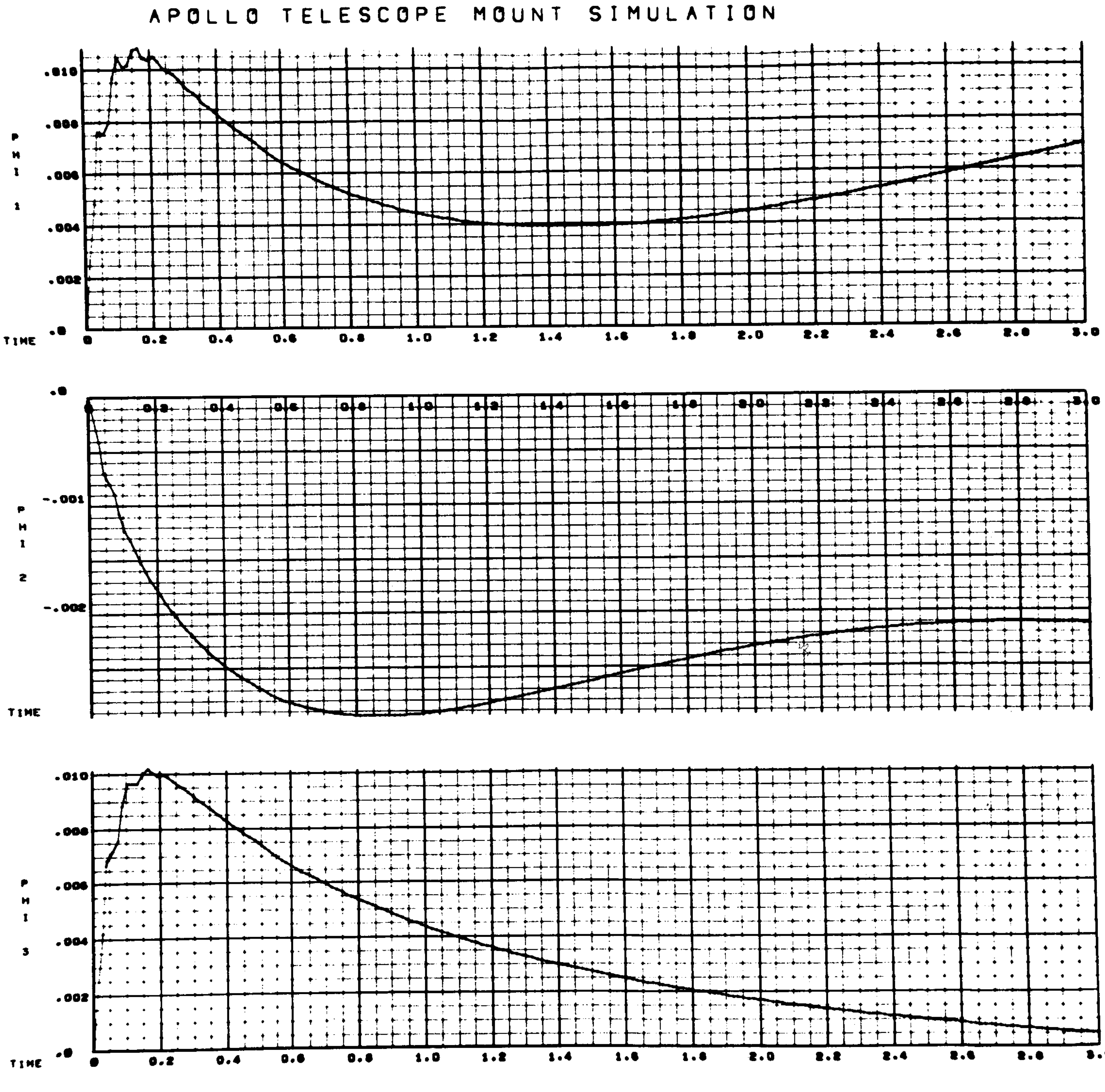

Fig. 22f MSFC Case 2 (Cont.)

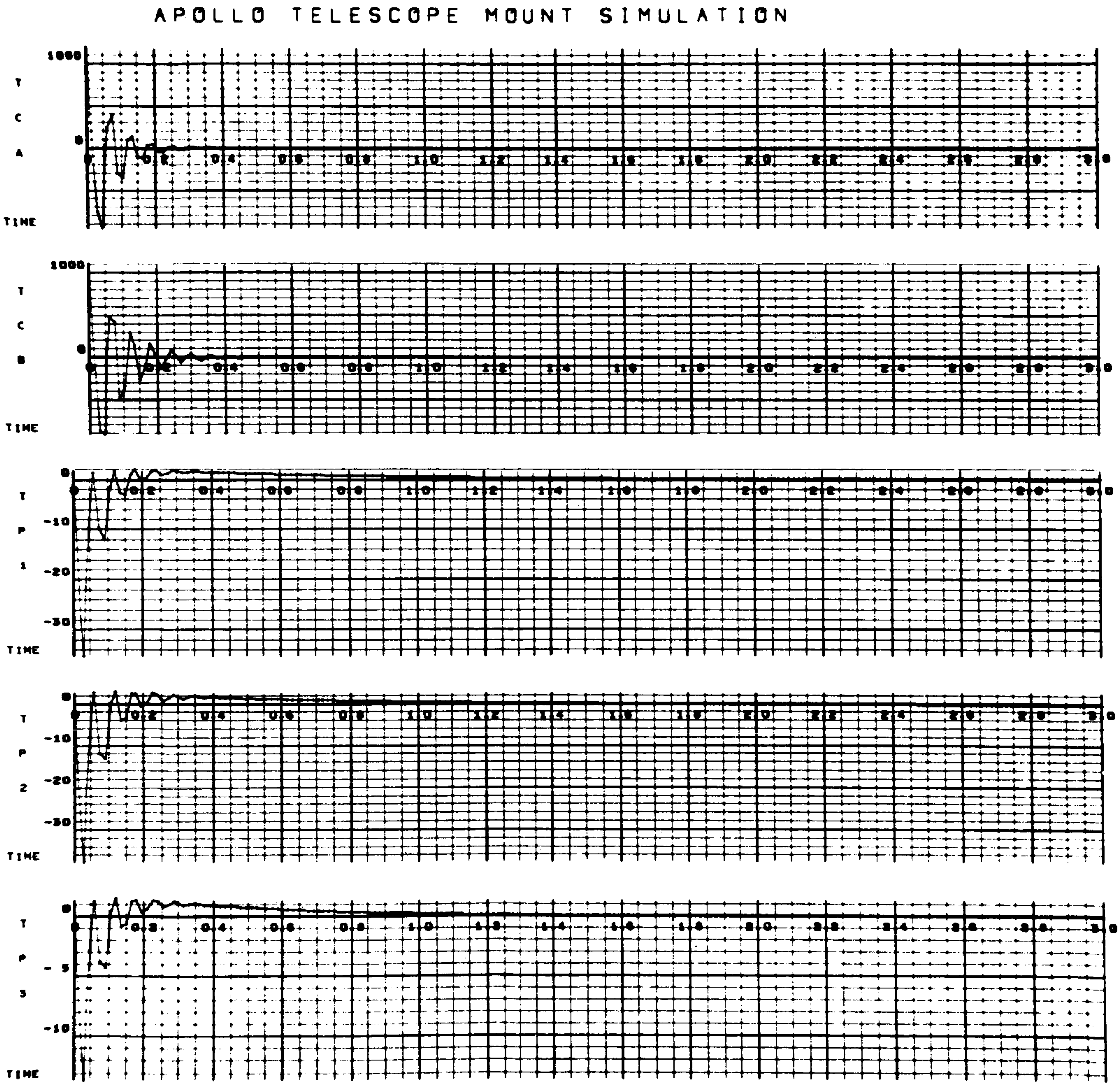

Fig. 22g MSFC Case 2 (Cont.)

APOLLO TELESCOPE MOUNT SIMULATION

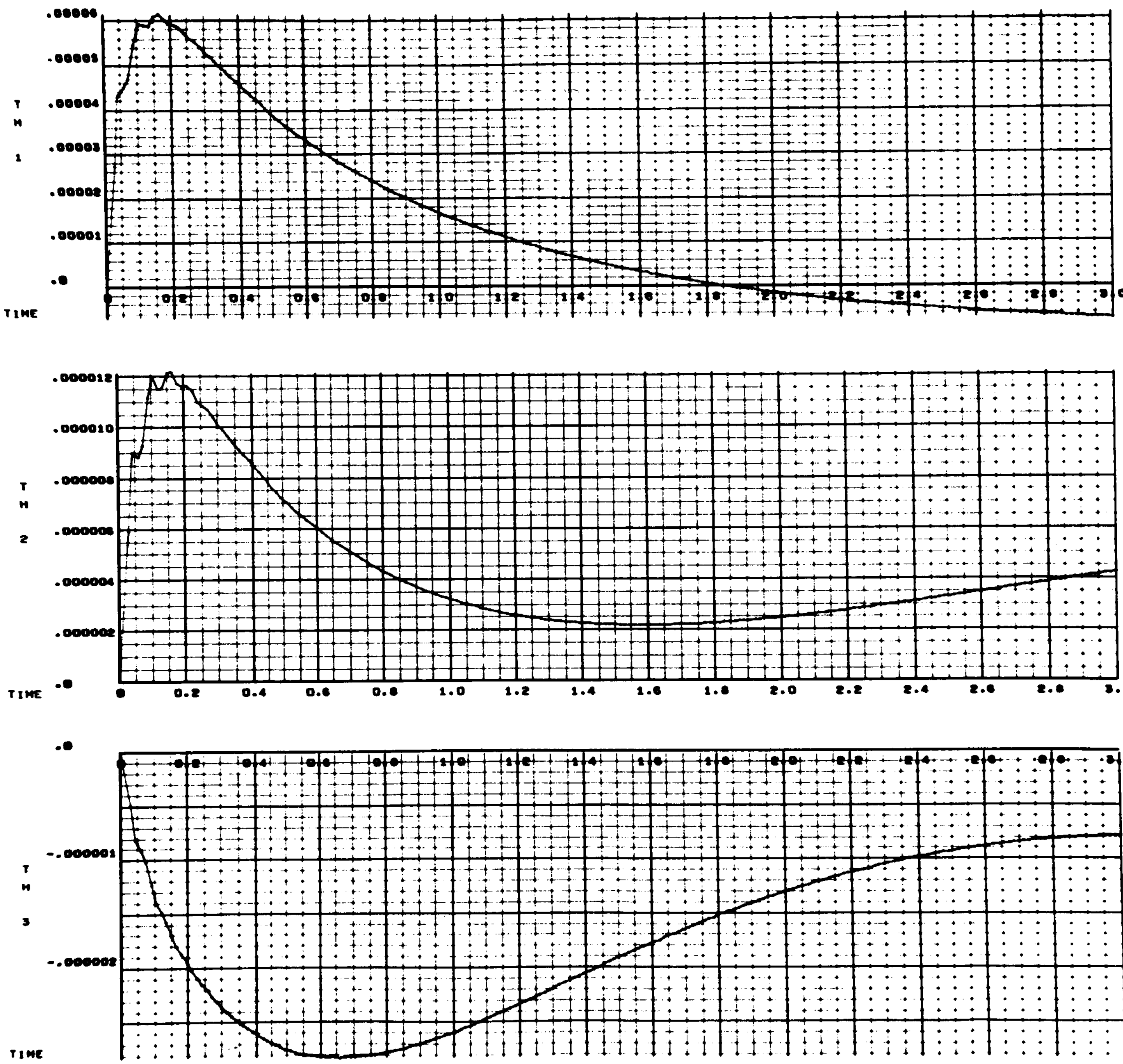

Fig. 2-2h MSFC Case 2 (Cont.)

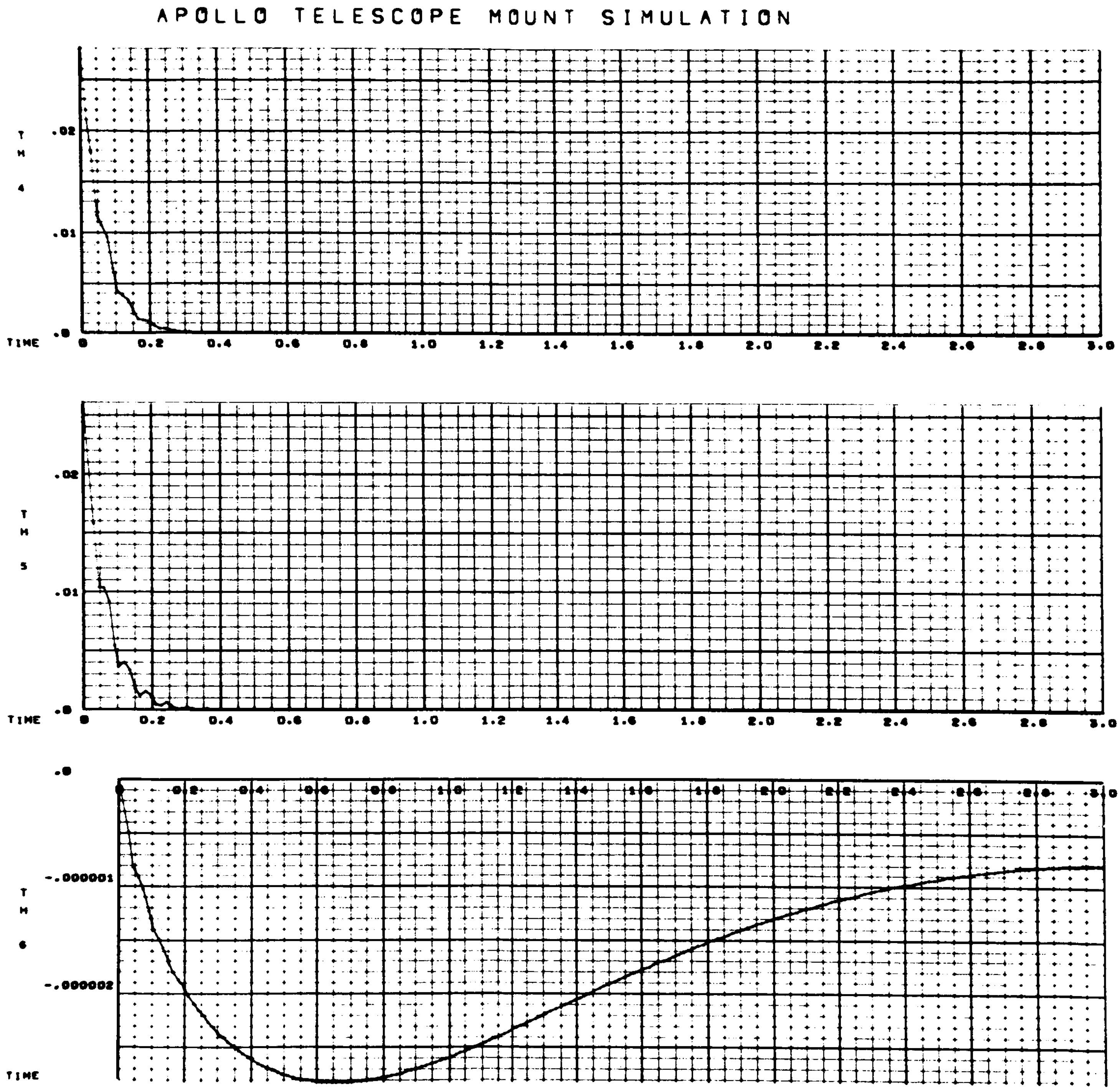

Fig. 2-2i MSFC Case 2 (Cont.)

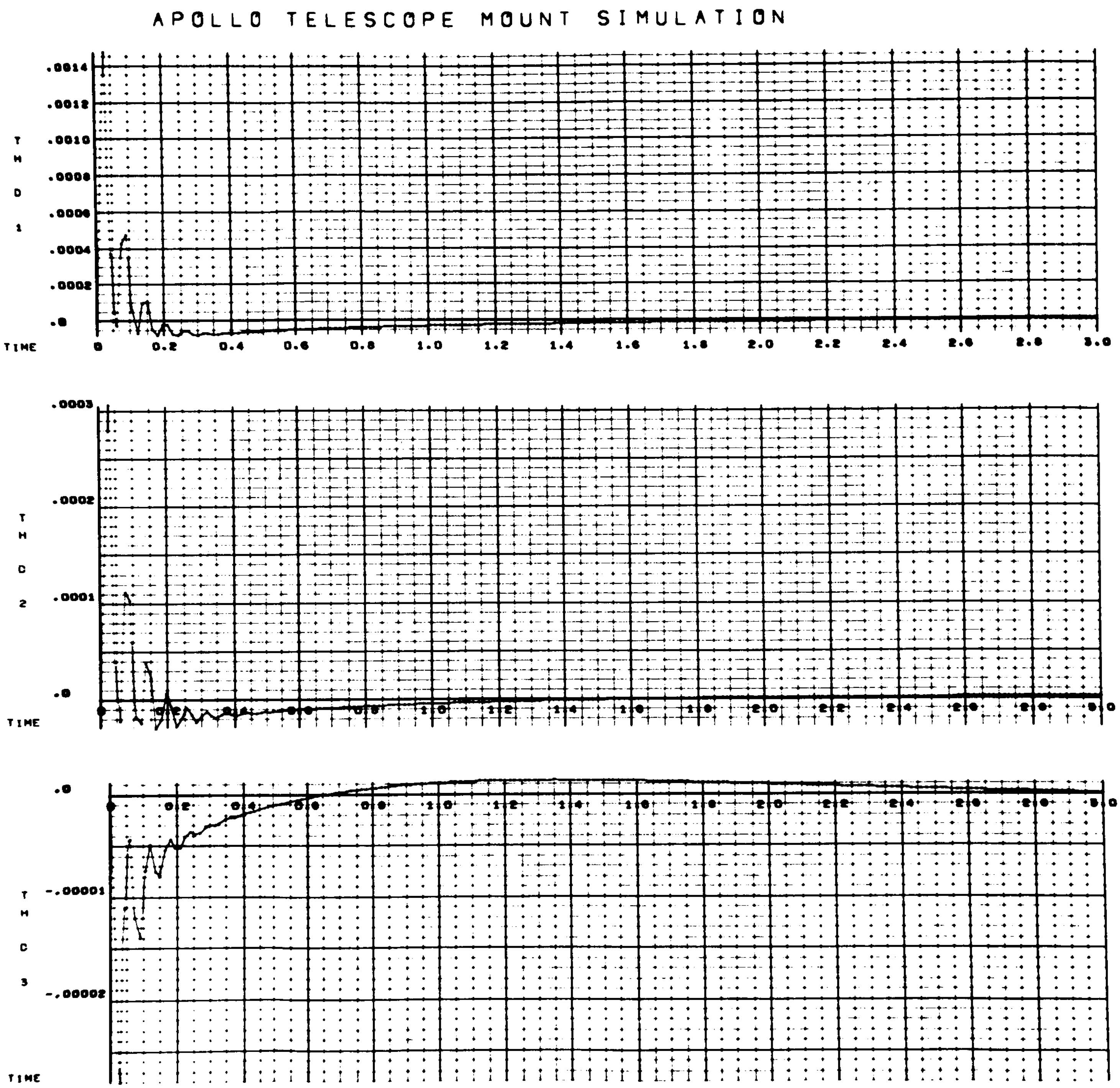

Fig. 22j MSFC Case 2 (Cont.)

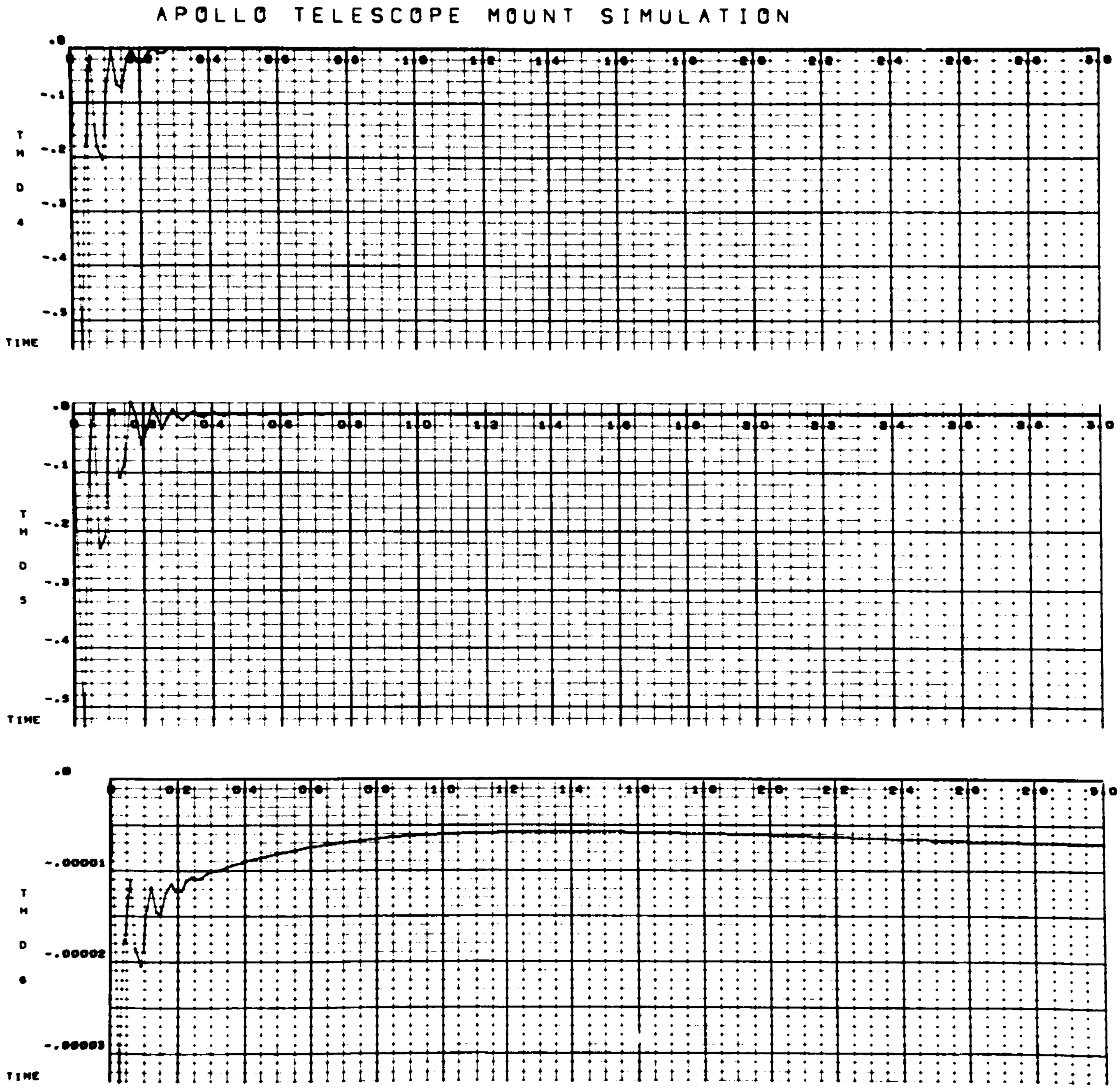

Fig. 2-2k MSFC Case 2 (Cont.)

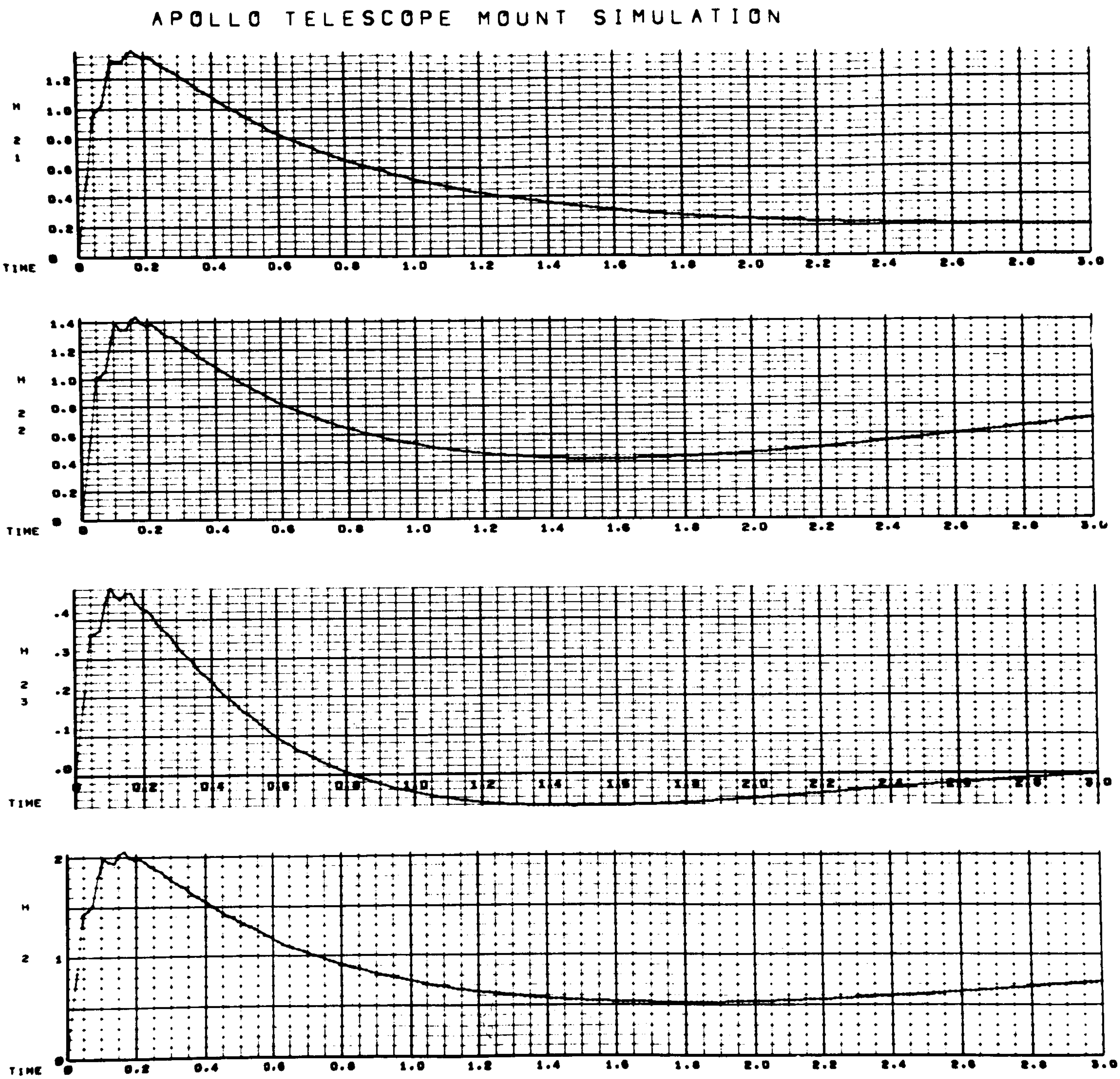

Fig. 2-21 MSFC Case 2 (Cont.)

APOLLO TELESCOPE MOUNT SIMULATION

• • • • • •

CASE NUMBER 0
MSFC CASE 3, EPS CREW TORQUE

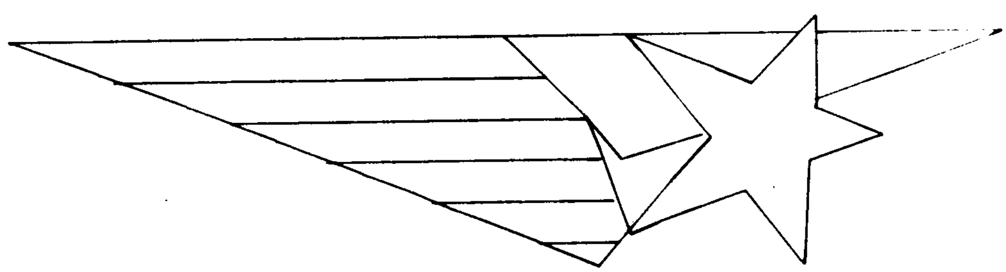

DATE
22 AUG 67

NAME - L M REINKENS
DEPT - 5534
BLD - 538
EXT - 28912

TABLE OF CONTENTS

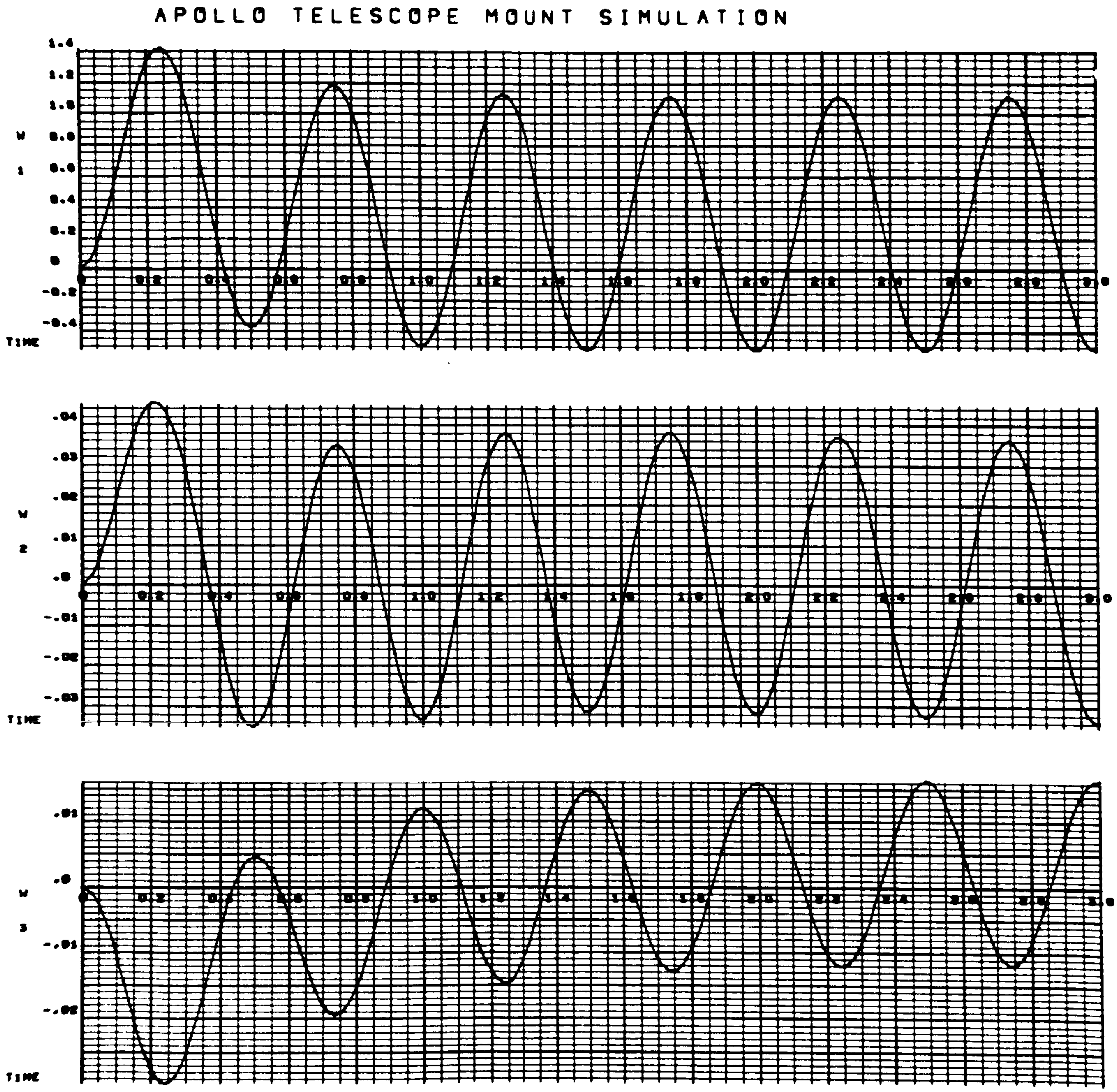

Fig. 2-3a MSFC Case 3

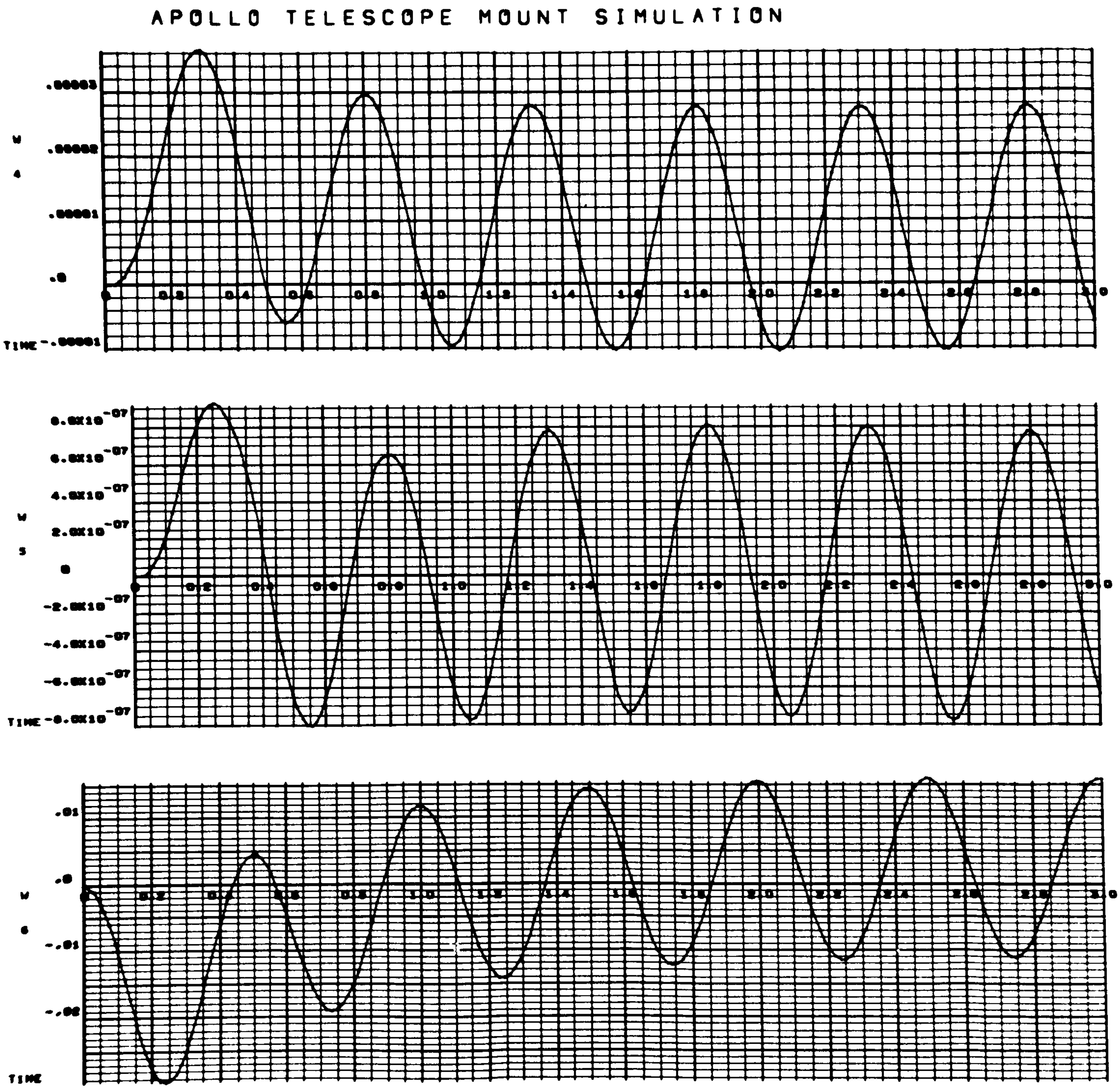

Fig. 2-3b MSFC Case 3 (Cont.)

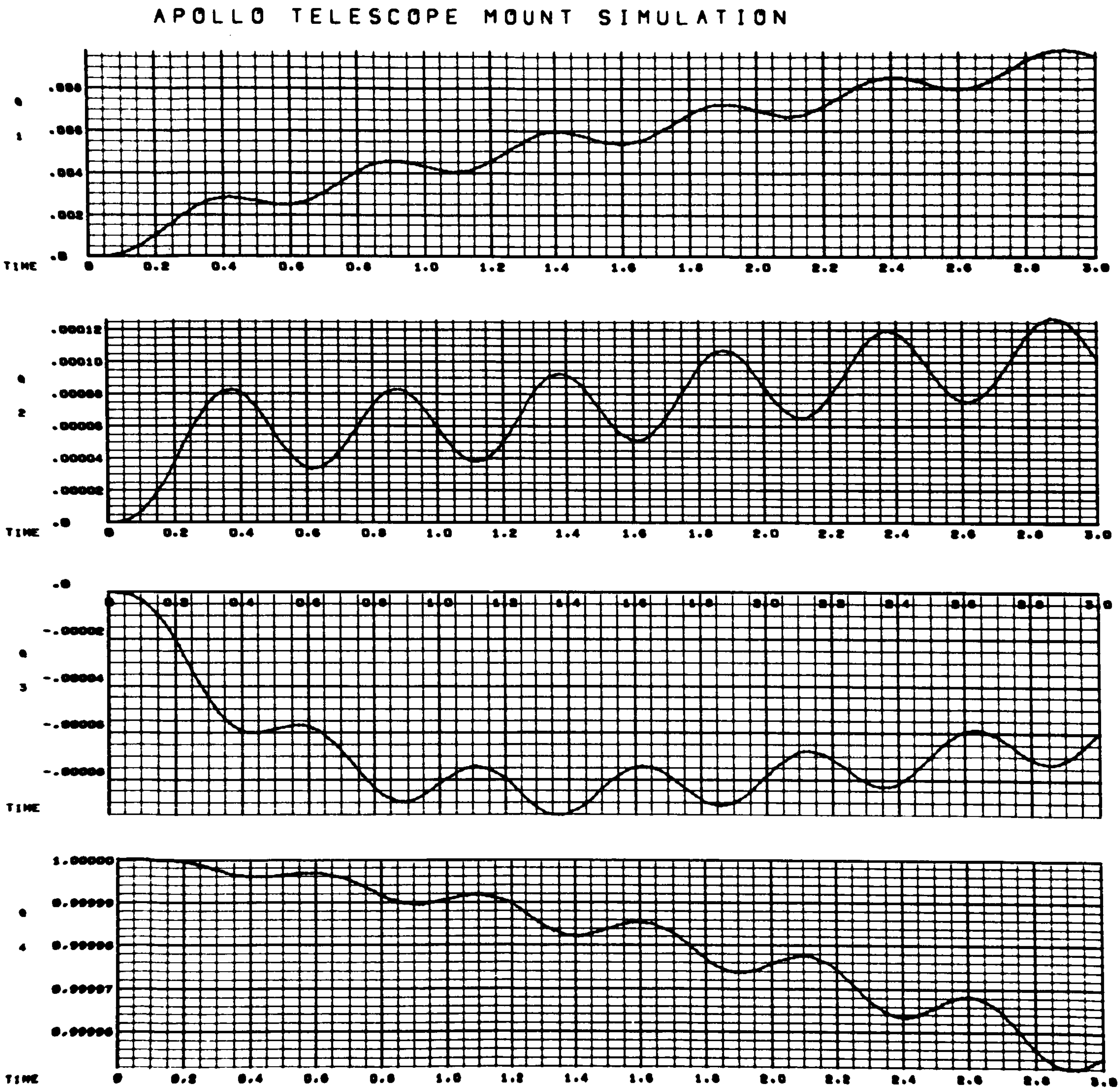

Fig. 2-3c MSFC Case 3 (Cont.)

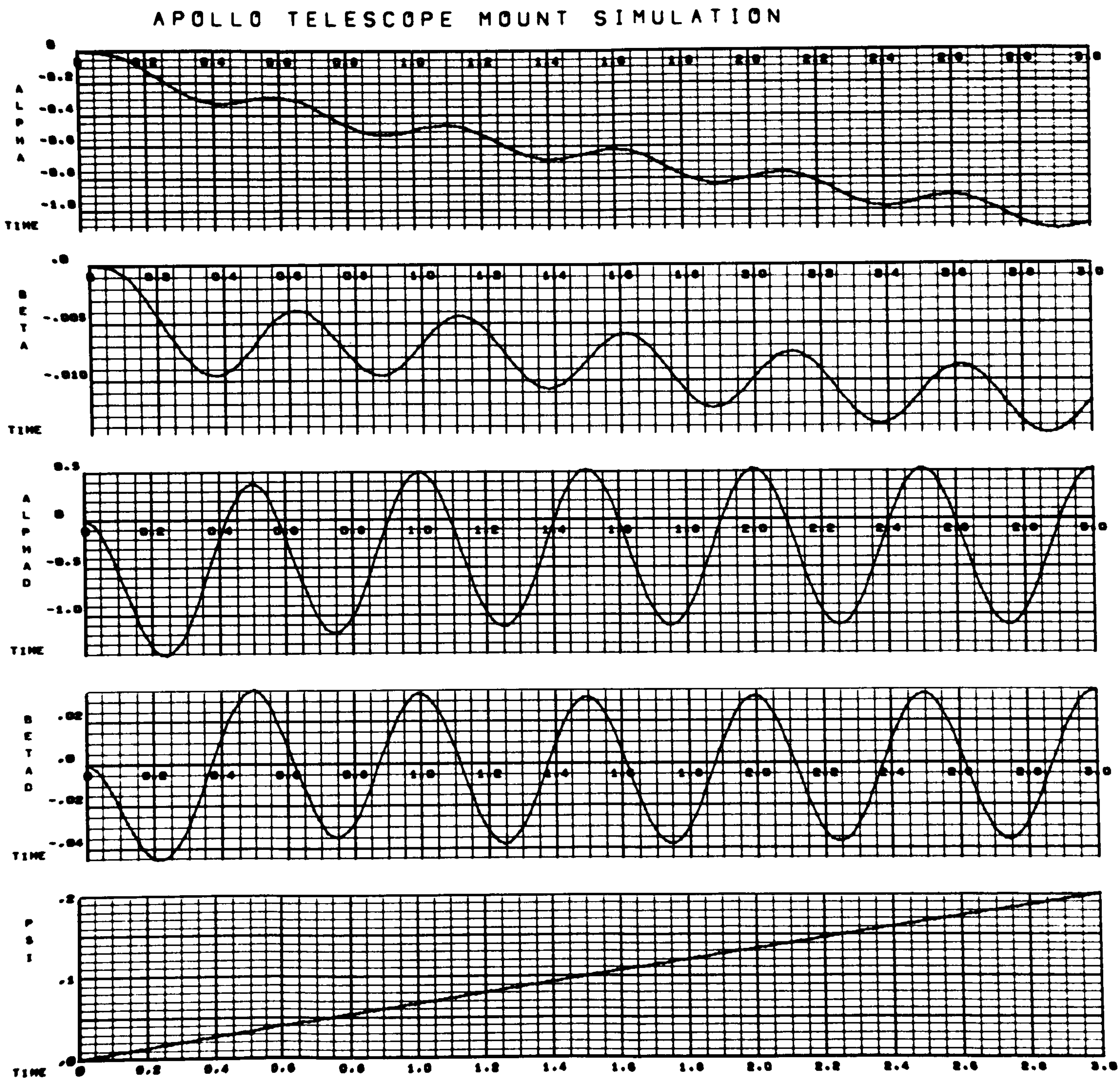

Fig. 2-3d MSFC Case 3 (Cont.)

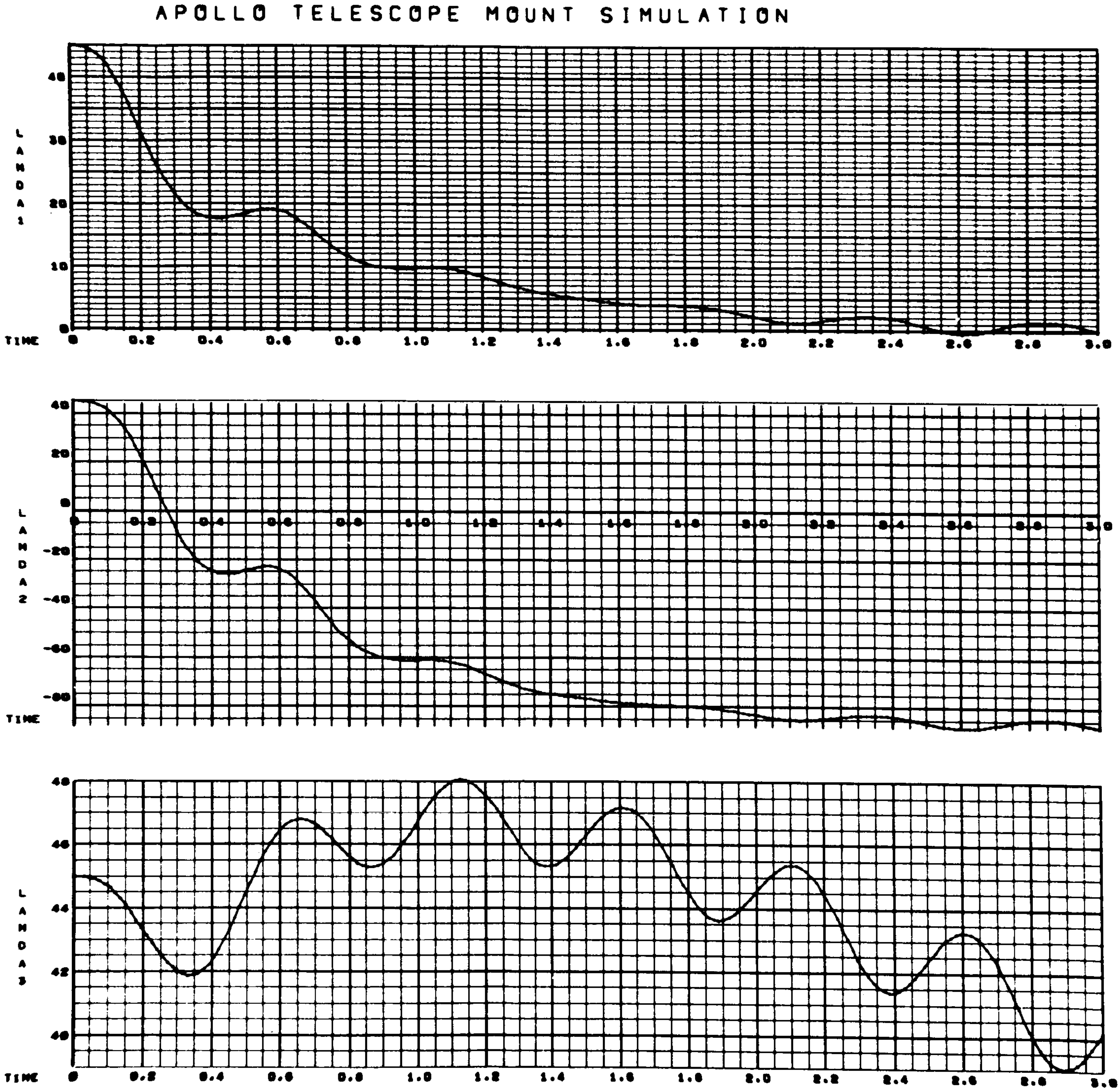

Fig. 2-3e MSFC Case 3 (Cont.)

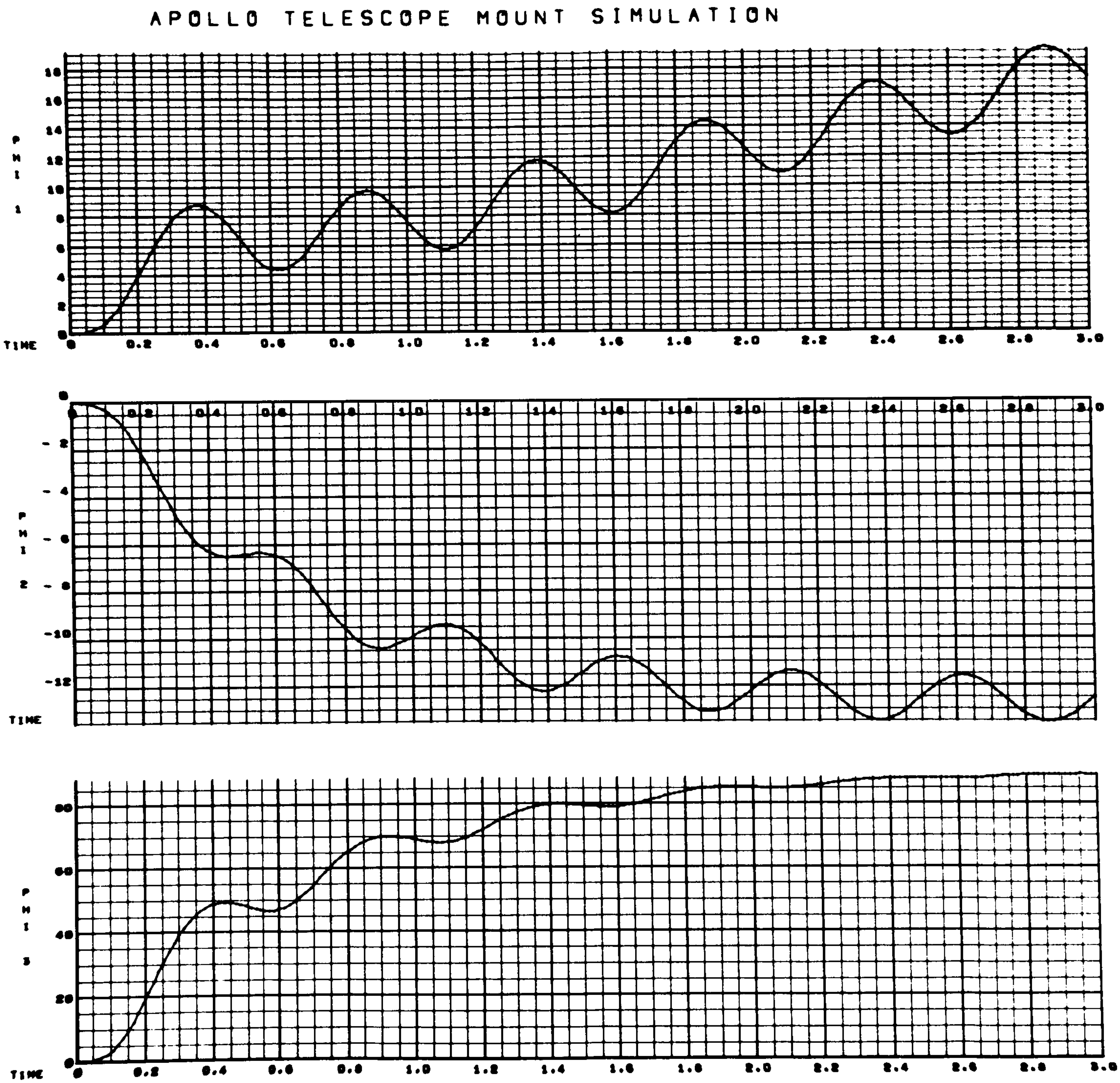

Fig. 2-3f MSFC Case 3 (Cont.)

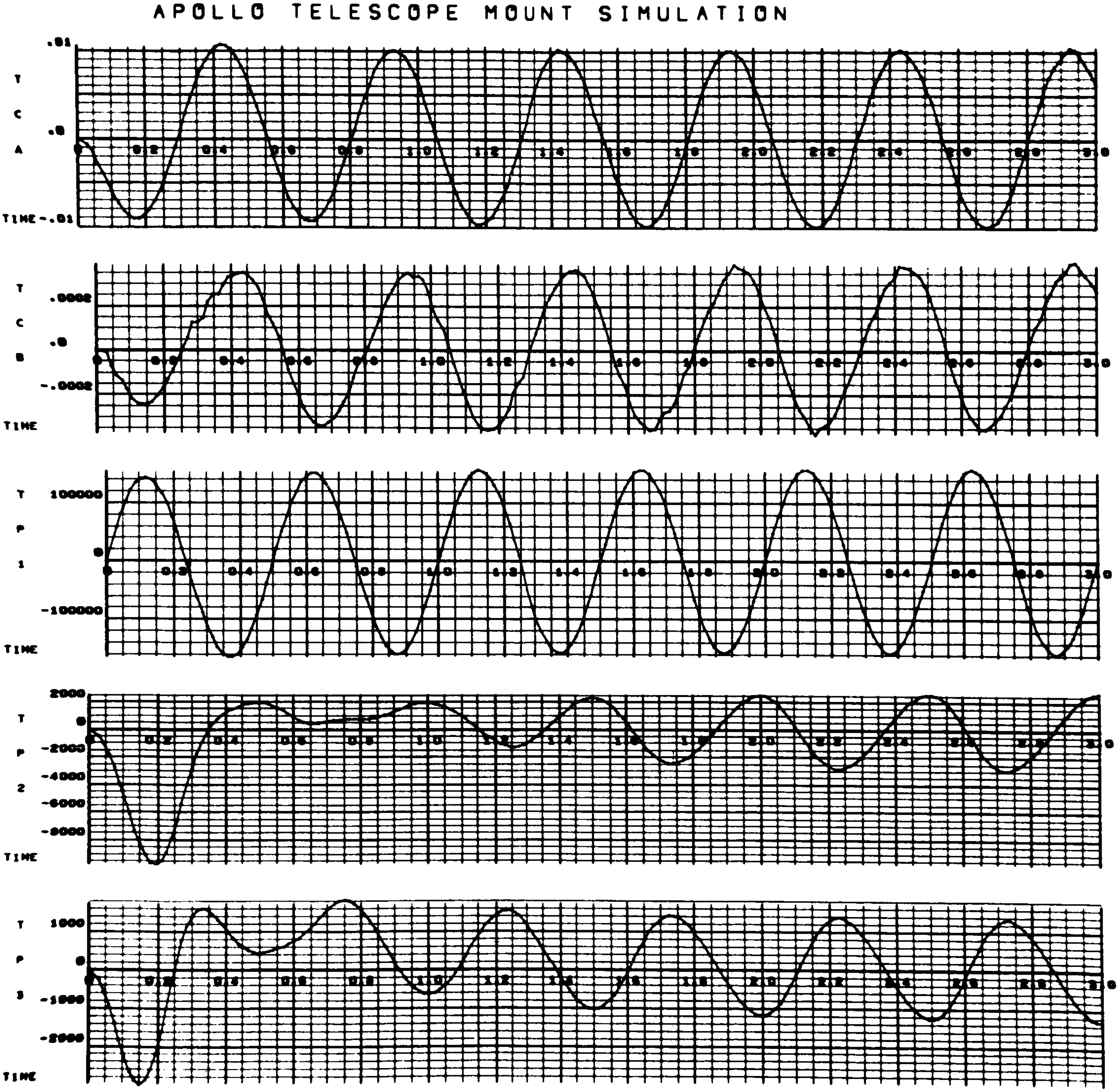

Fig. 2-3g MSFC Case 3 (Cont.)

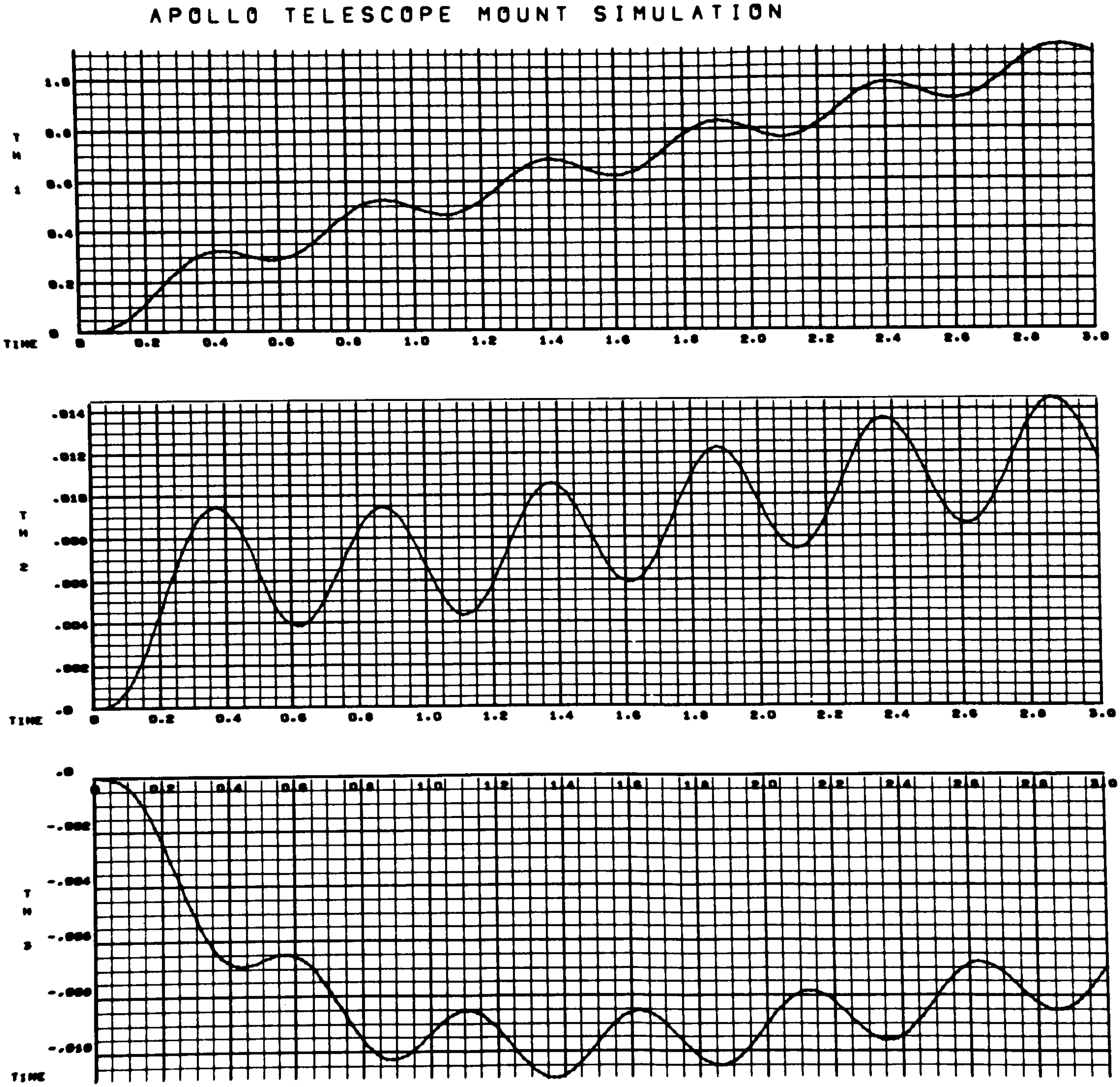

Fig. 2-3h MSFC Case 3 (Cont.)

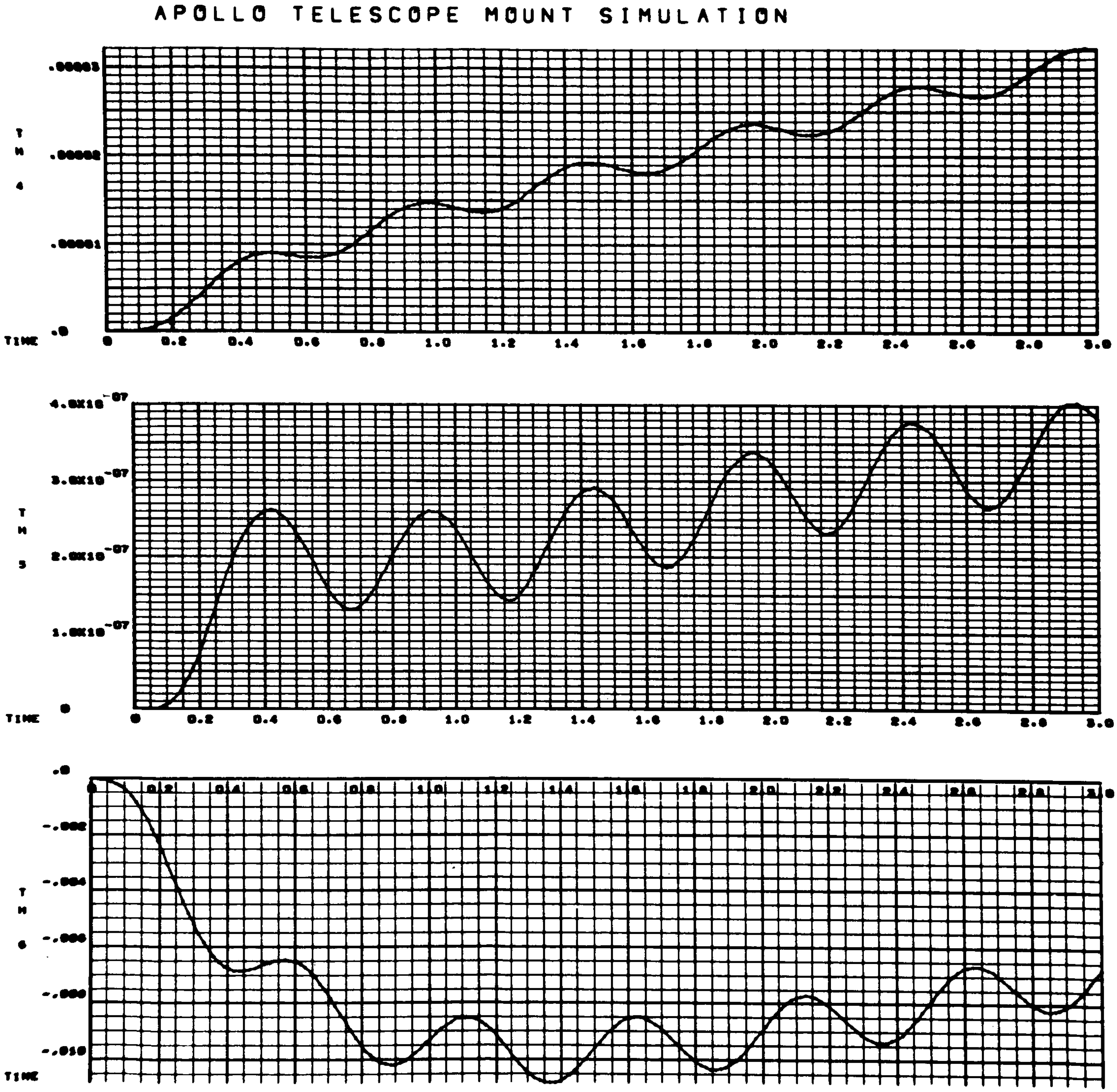

Fig. 2-3i MSFC Case 3 (Cont.)

APOLLO TELESCOPE MOUNT SIMULATION

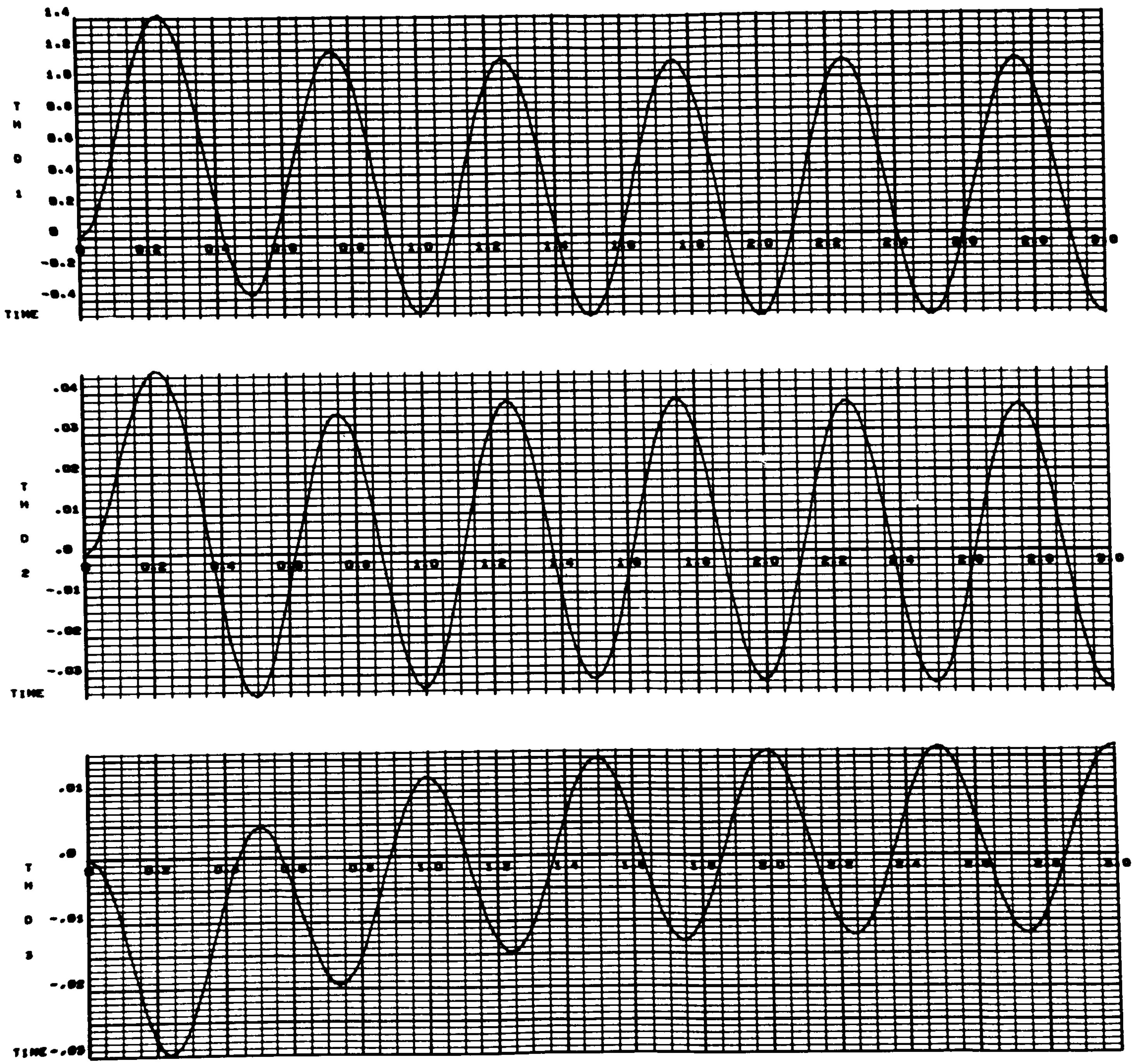

Fig. 2-3j MSFC Case 3 (Cont.)

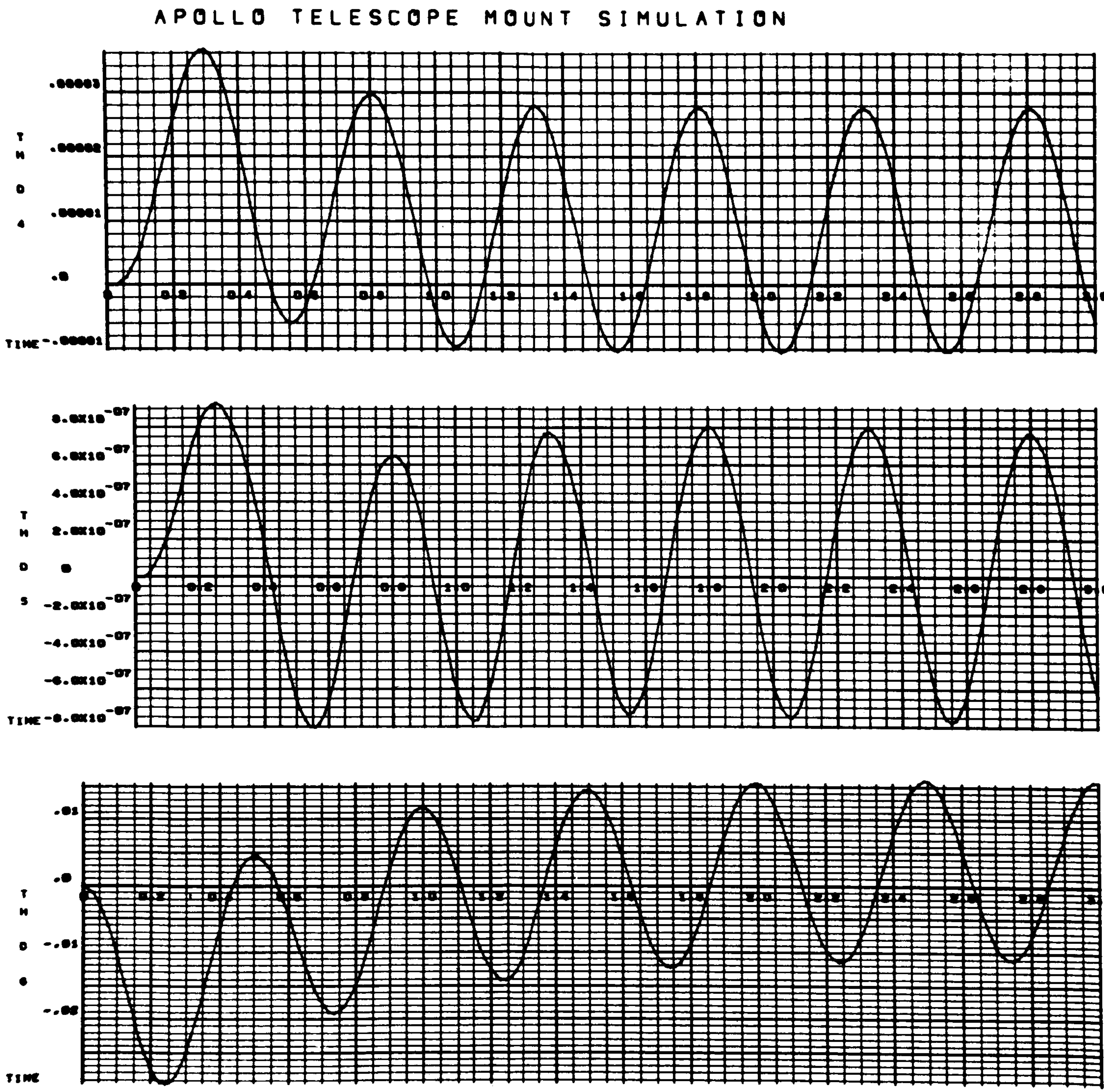

Fig. 2-3k MSFC Case 3 (Cont.)

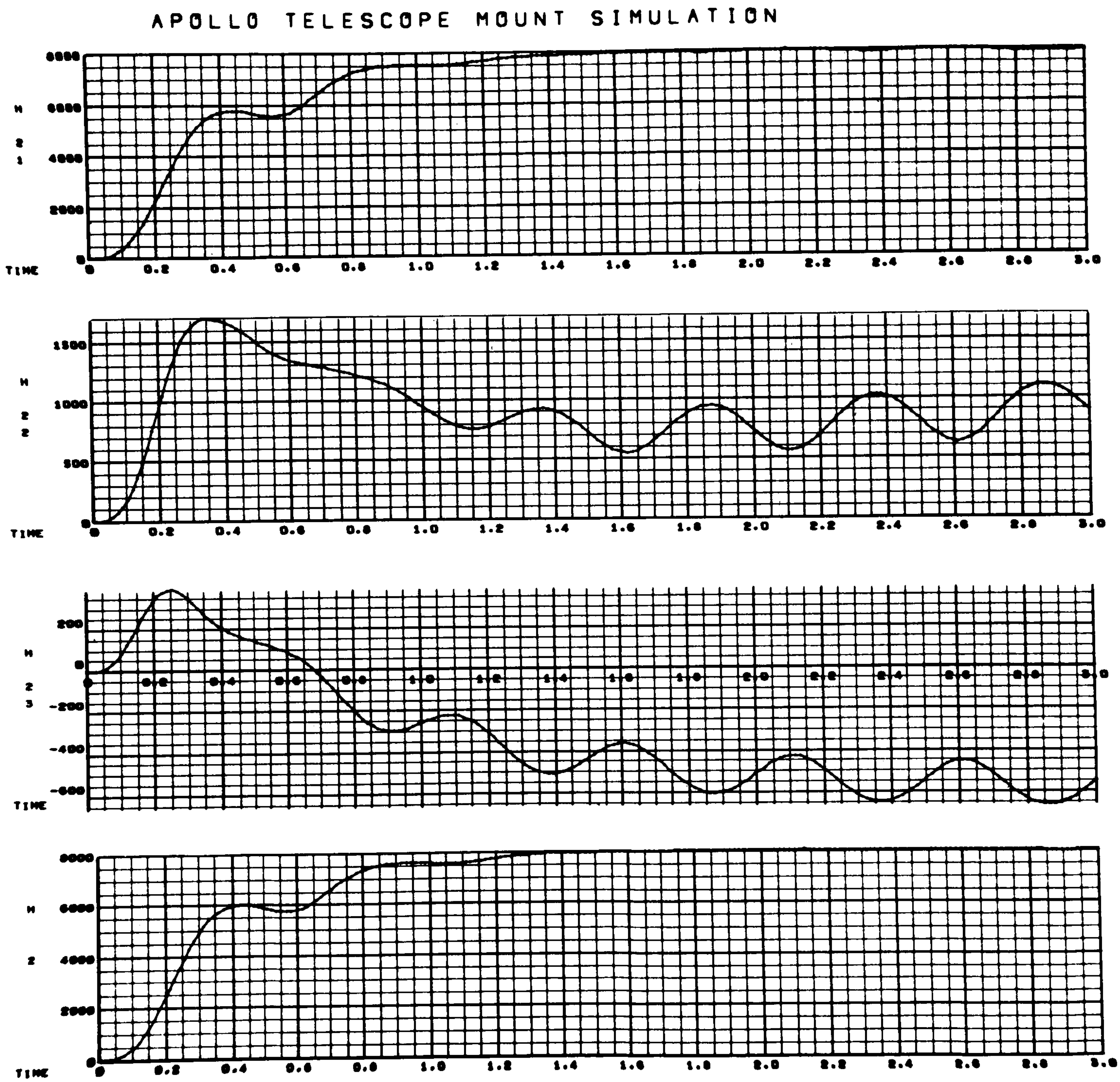

Fig. 2-31 MSFC Case 3 (Cont.)

Section 3
VIBRATION STABILITY ANALYSIS

Vibration of the AAP Cluster introduces serious limitations on the speed of response obtainable. The control system must not only produce satisfactory rigid-body motion, it must at the same time avoid introducing unstable vibratory motion.

The modes of free vibration are of two distinct types: those in which the motion occurs wholly within the x-y plane and those in which out-of-plane displacements occur. For small angular displacements, the three-axis control problem can therefore be broken into two separate problems. Motion within the x-y plane produces rotations only about the z-axis so that control about the z-axis can be treated as a single-axis problem. Out-of-plane motion, on the other hand, produces rotations about both the x and y axes and consequently the analysis must include the effects of cross-coupling between these two axes.

3.1 Z-AXIS CONTROL

The block diagram for z-axis control is shown in Fig. 3-1, where the vehicle dynamics are composed of the rigid-body inertia plus the seven in-plane bending modes given in Ref. 3.1. The natural frequencies of each mode are given in this reference; all were assumed to have damping ratios of 0.01. The gain factor associated with the i th mode is given by the expression

$$K_i = \frac{\phi_i'(a)\ \phi_i'(b)}{M_i}$$

where $\phi_i'(a)$ is the slope of the normalized mode function at the CMG location, $\phi_i'(b)$ is the slope at the sensor location, and M_i is the generalized mass for the i th

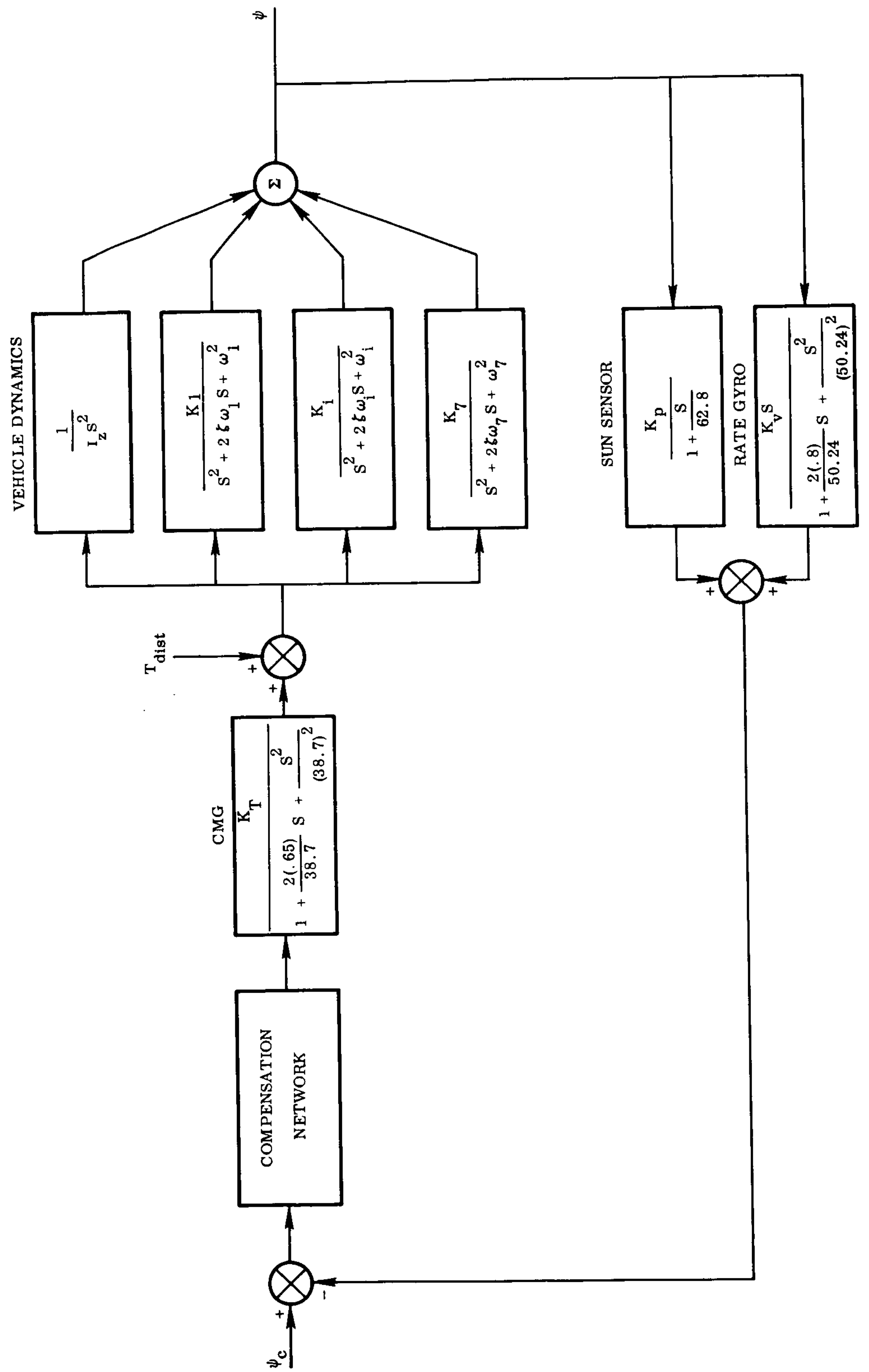

Fig. 3-1 Block Diagram for Z-Axis Control

mode. These quantities are tabulated in the reference. In the analysis the CMG's and sensors are all assumed to be mounted on the Rack at a point equivalent to node 15 (in the reference). It is apparent that the system performance will depend upon the placement of the CMG's and sensors and that the total angular displacement shown in Fig. 3-1 represents the displacement at the sensor. It is also apparent that the disturbance torque shown in Fig. 3-1 represents a torque at the CMG location. In general, disturbance torques must be added in through gain factors dependent upon their points of application.

For the assumed CMG and sensor location, the vehicle dynamics can be represented by the pole-zero locations shown in Fig. 3-2. Considering only rigid-body motion, satisfactory control can be achieved by using a control torque proportional to position plus rate. Figure 3-3 shows the open-loop frequency response using such a control torque when the effects of the bending modes are included. To improve the low-frequency response, the gain should be increased from the value indicated on the figure. The gain cannot be increased appreciably, however, without causing instability at a frequency near that of the lowest frequency bending mode (12 rad/sec). This problem can be avoided by eliminating the rate gyro and adding a compensation network that attenuates all the bending mode frequencies. This approach was used by both Marshall and LMSC. The transfer function of the compensation network recommended by Marshall is

$$\frac{(1 + S)\ (1 + 2S)}{\left[1 + \frac{2\ (0.7)}{2}\ S + \frac{S^2}{(2)^2}\right]\left[1 + \frac{2\ (0.7)}{2.8}\ S + \frac{S^2}{(2.8)^2}\right]}$$

The open-loop frequency response using this network is shown in Fig. 3-4.

The network used by LMSC is given by the transfer function

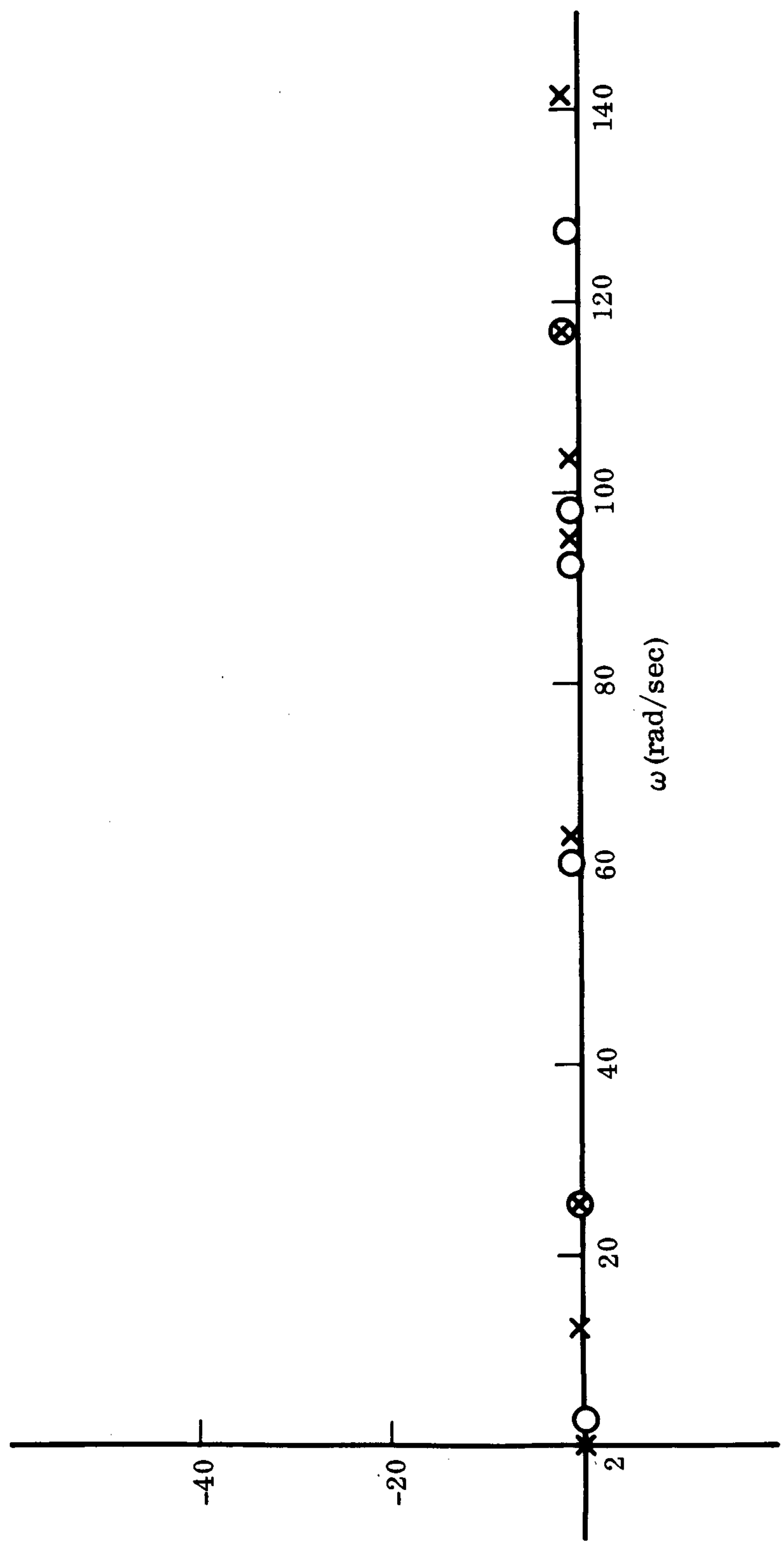

Fig. 3-2 Pole-Zero Locations Corresponding to In-Plane Bending Modes, Vehicle Dynamics Only

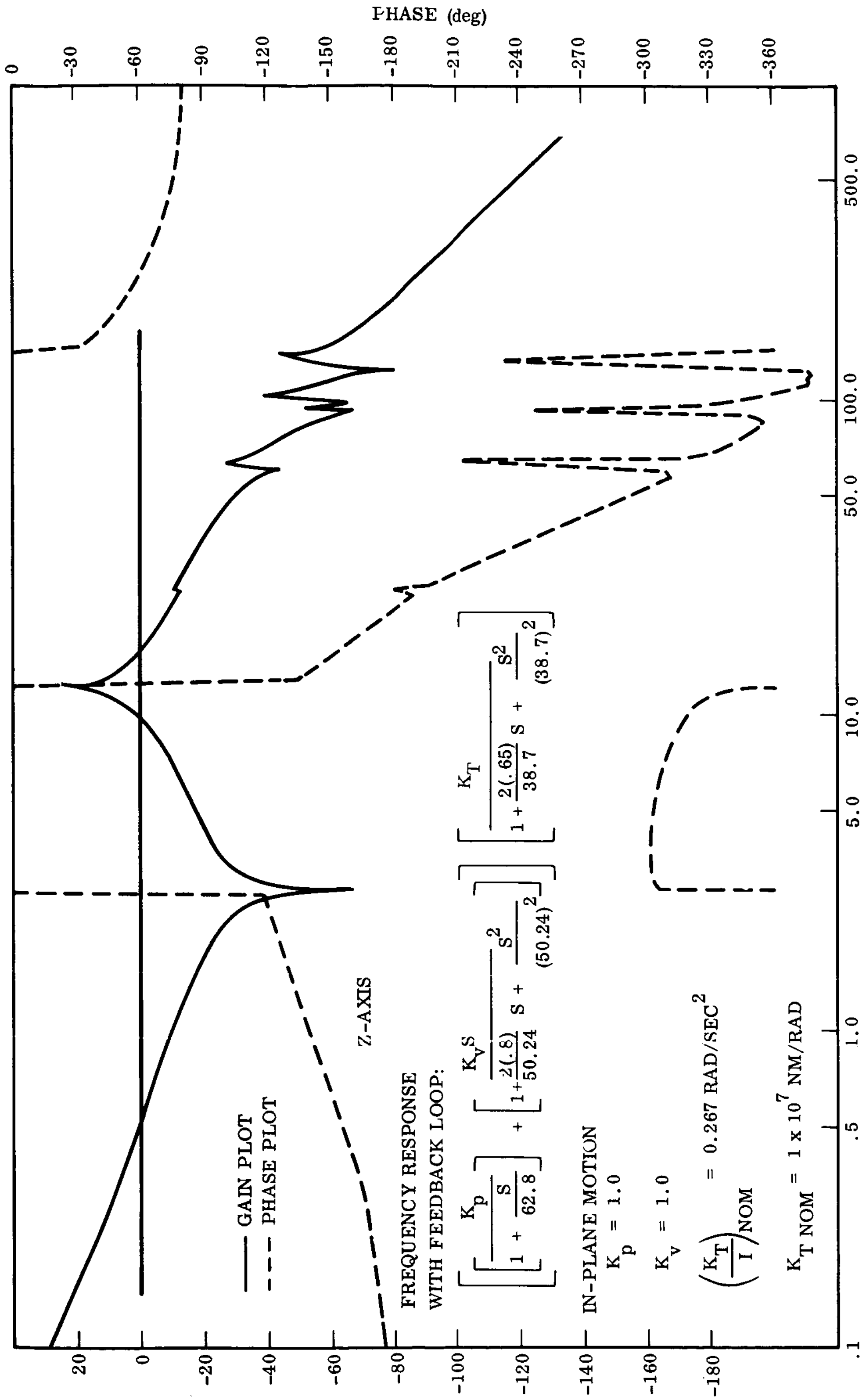

Fig. 3-3 Open-Loop Frequency Response With Control Torque Proportional to Position Plus Rate

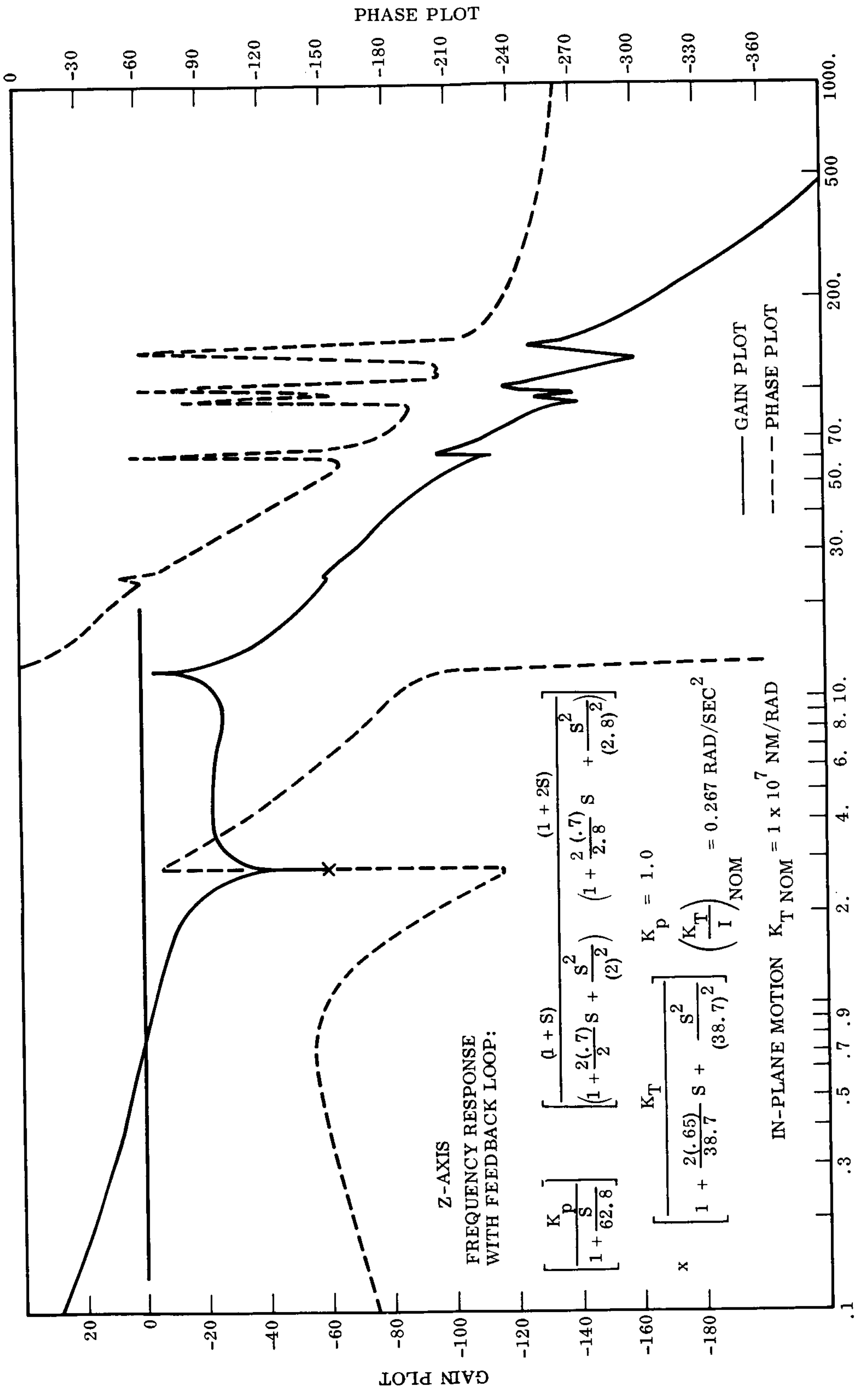

Fig. 3-4 Open-Loop Frequency Response Using MSFC-Recommended Transfer Function

$$\frac{1 + 4S}{\left[1 + \frac{2(0.6)}{2.8} S + \frac{S^2}{(2.8)^2}\right]\left[1 + \frac{2(0.4)}{5.0} S + \frac{S^2}{(5.0)^2}\right]\left[1 + \frac{2(0.25)}{7.0} S + \frac{S^2}{(7.0)^2}\right]}$$

The open-loop frequency response for this network is shown in Fig. 3-5.

The Marshall and LMSC networks produce comparable performance, each having a bandwidth of about 1 rad/sec.

3.2 X AND Y AXIS CONTROL

Control about the x and y axes is considerably more difficult to analyze because of the crosscoupling between the two axes. Both control loops contribute to the characteristic equation. With the 11 modes of vibration and compensation networks of the form used for the z-axis, a system having up to 36 poles results. The block diagram for this case is that shown in Fig. 3-6. Analogous to the case of z-axis control, the K_{xi}, K_{yi} and M_i are obtained from the reference for the 11 out-of-plane modes of vibration. Trial runs used the same control schemes for both the x and y axes as were used for the z axis except that the gains were adjusted so that the ratio of gain to rigid body inertia were the same as those for the z axis. Open-loop frequency responses were obtained by opening the x-axis control loop while leaving the y-axis loop closed. Figure 3-7 shows the frequency response when using a position sensor plus rate gyro without any other compensation network. It is apparent that this leads to an unstable system. Figures 3-8 and 3-9 show the frequency responses using the Marshall and LMSC networks, respectively, with the rate gyros eliminated. The responses are similar throughout the frequency range of interest and represent stable systems. For the gain shown, the bandwidth is rather narrow and can be improved by increasing gain. Since the shape of the x-axis open-loop response depends upon the y-axis gain, it is not readily apparent what effect increasing both gains would have. If the y-axis gain is left unchanged, then the figures show that increasing the x-axis gain by about 20 db will improve the x-axis bandwidth. Adjustment of the y-axis gain would require further study but it seems likely that it should be increased by the same factor. It is expected that a bandwidth of about 1 rad/sec for each axis can be achieved.

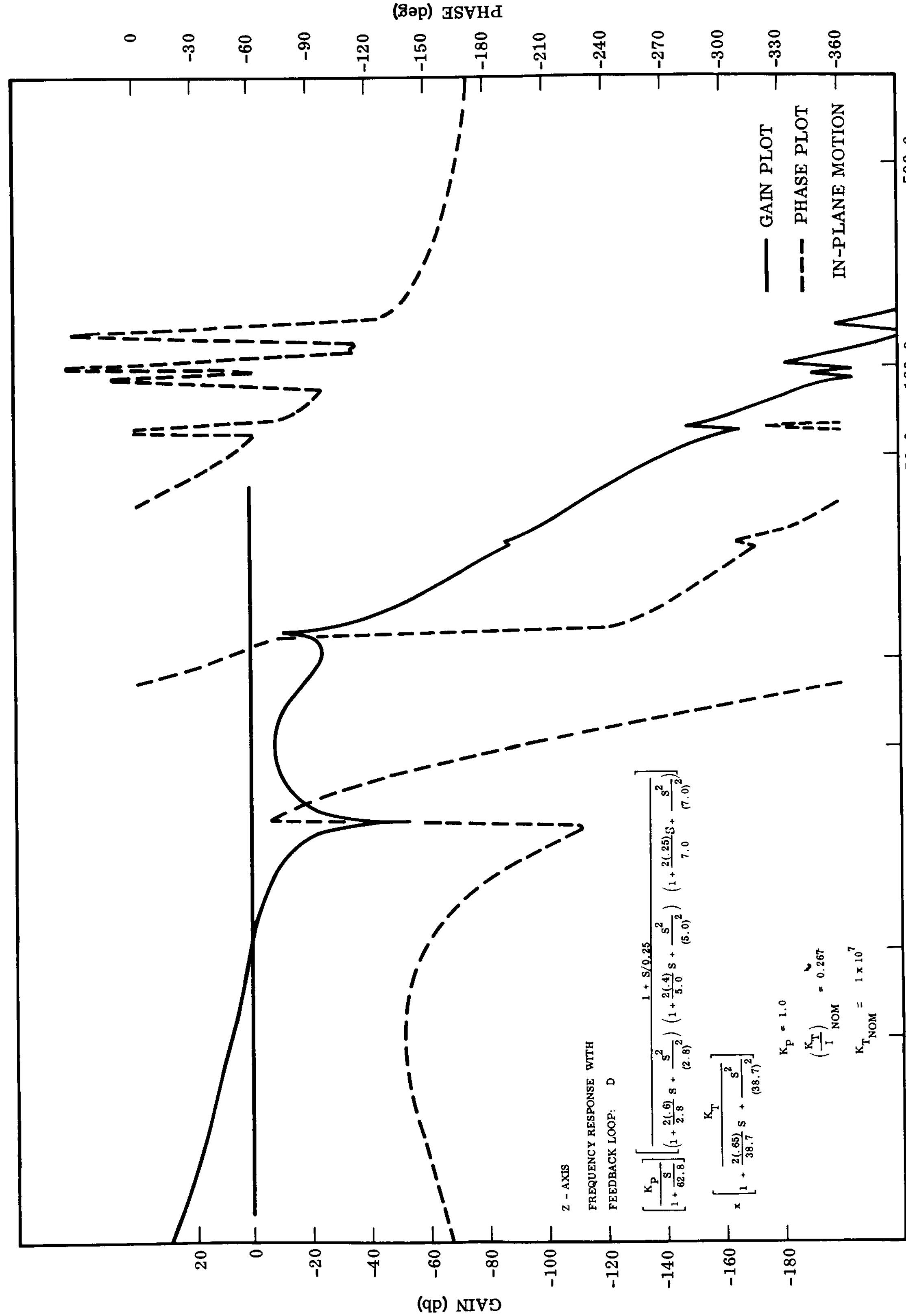

Fig. 3-5 Open-Loop Frequency Response Using LMSC-Recommended Transfer Function

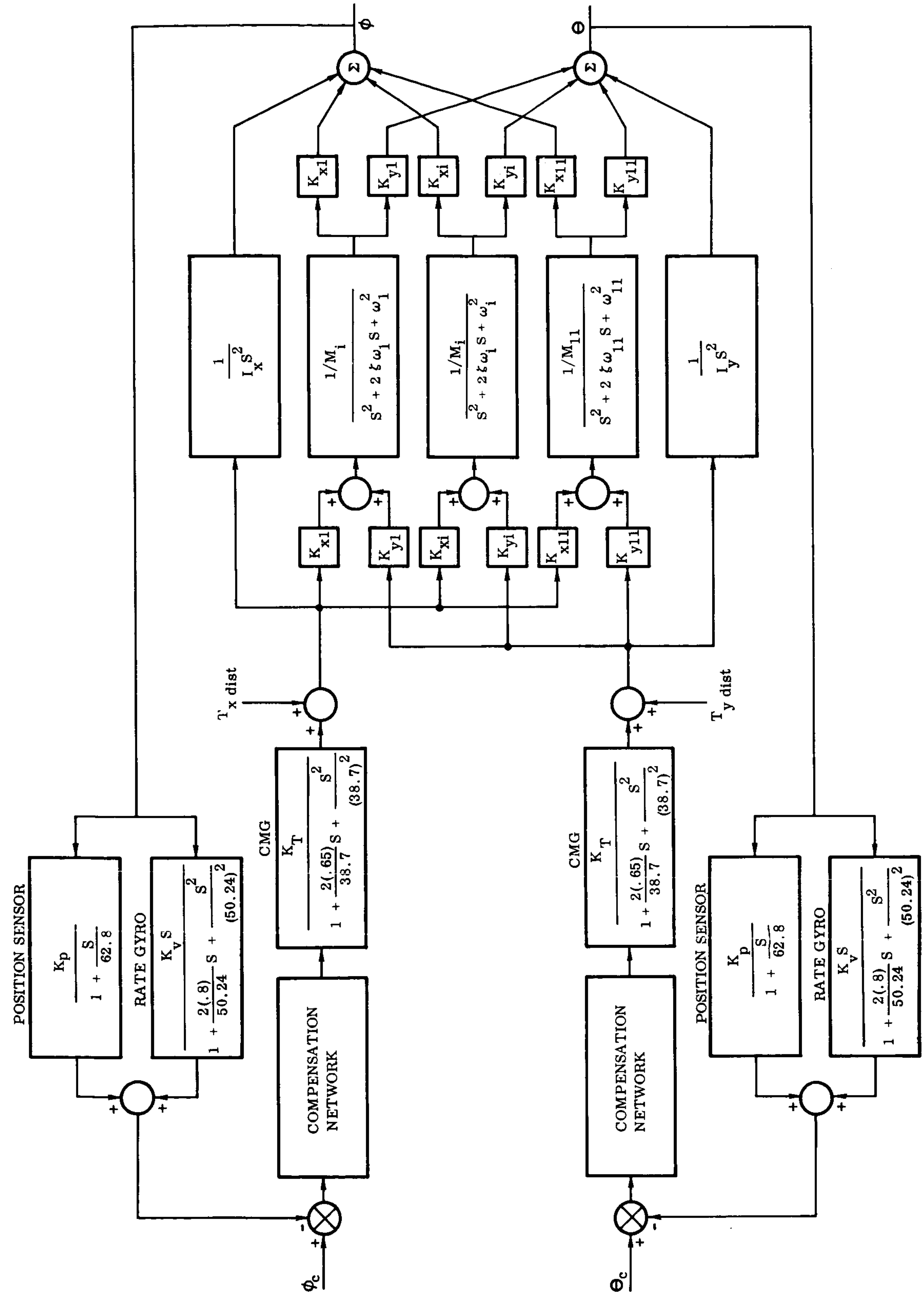

Fig. 3-6 Block Diagram for Control of X and Y Axes

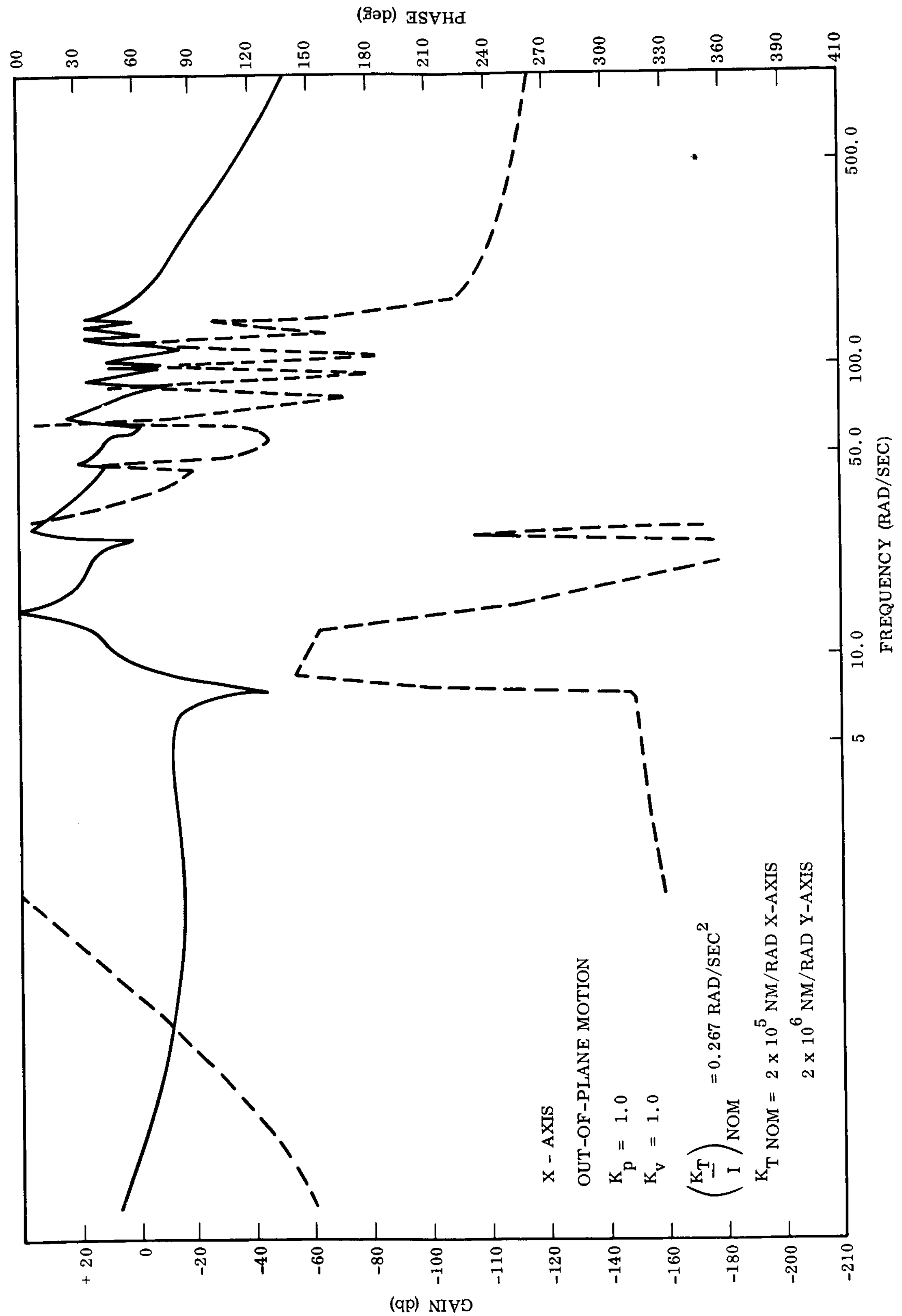

Fig. 3-7 Open-Loop Frequency Response Using a Position Sensor Plus Rate Gyro

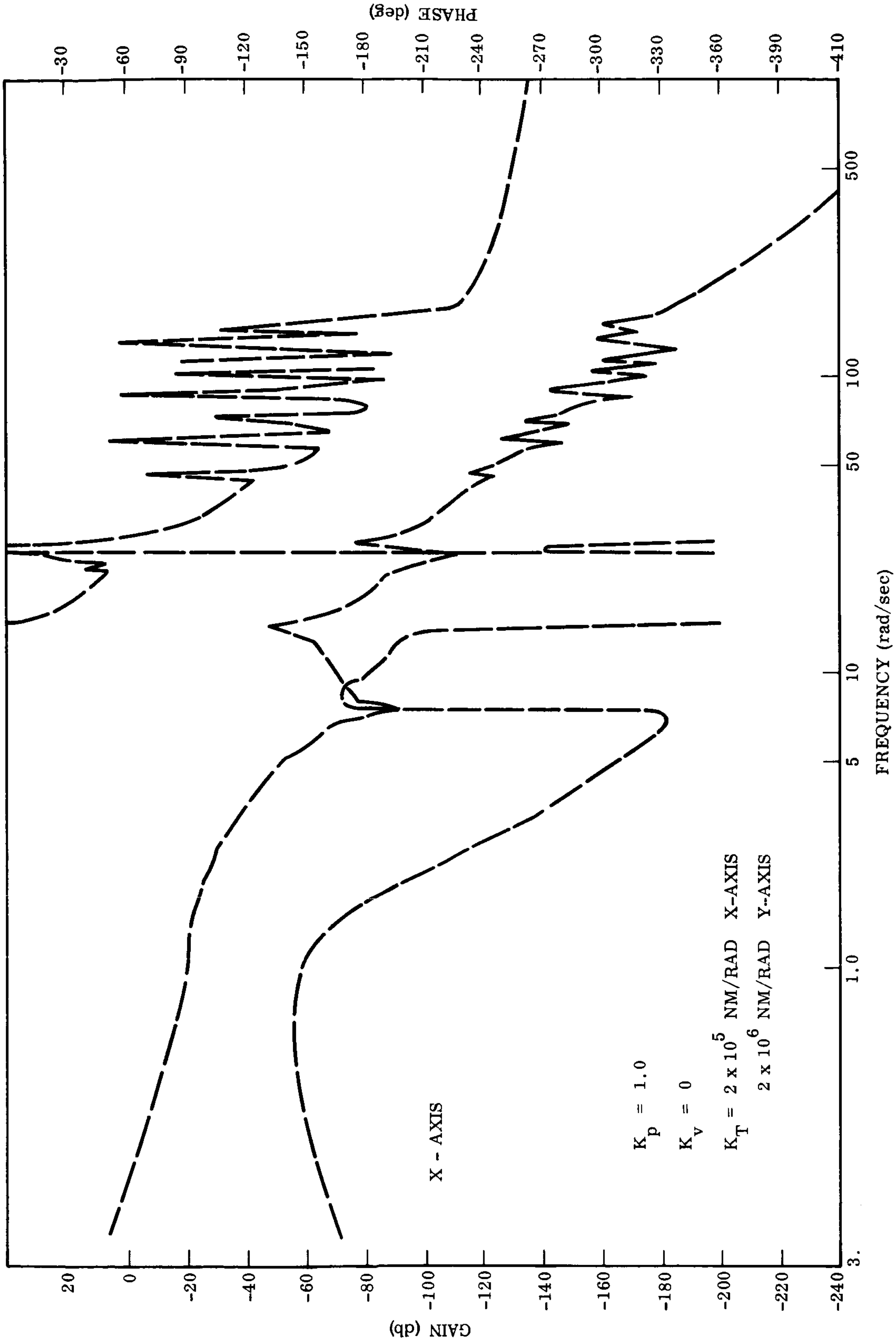

Fig. 3-8 Open-Loop Frequency Response Using MSFC Network and no Rate Gyro

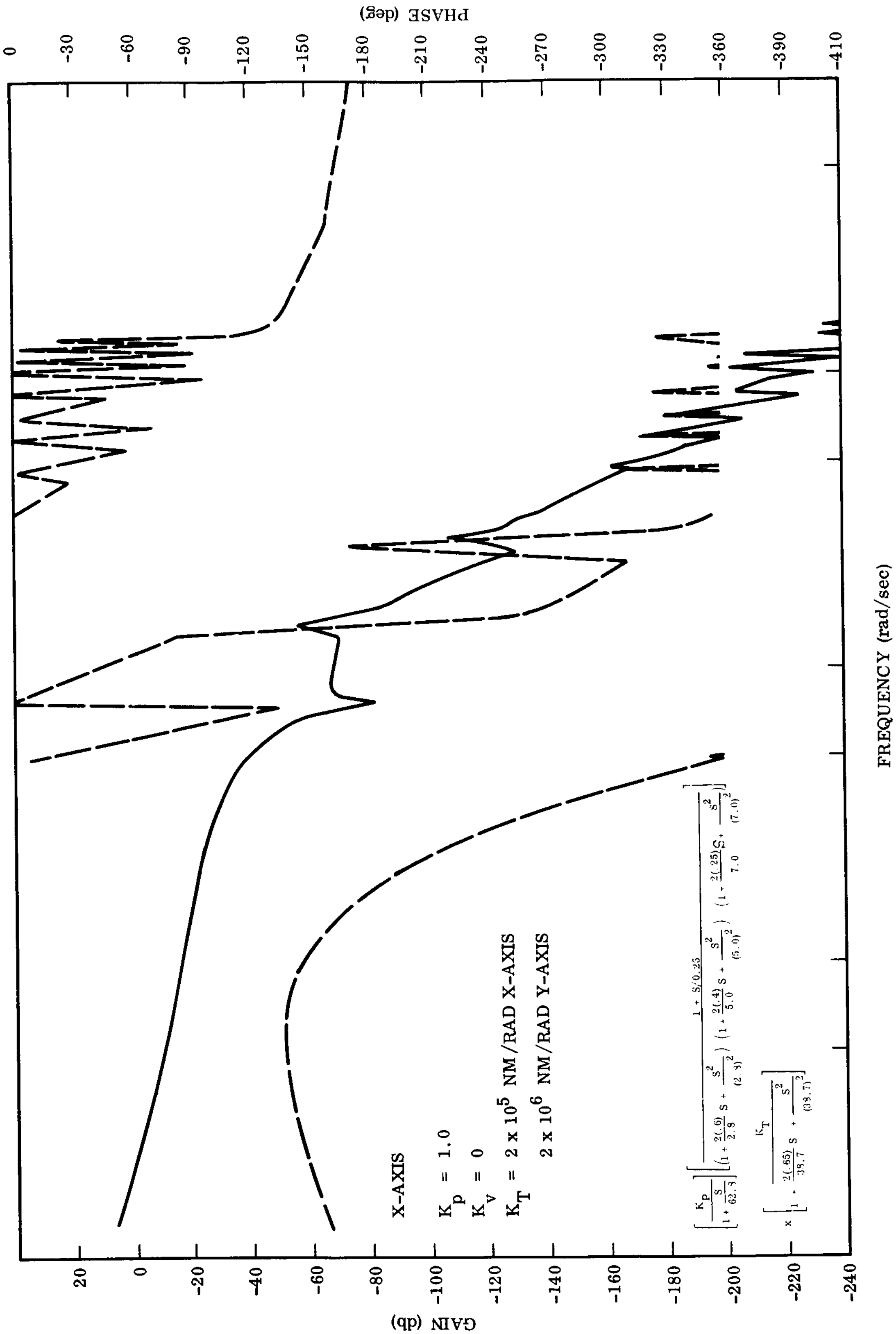

Fig. 3-9 Open-Loop Frequency Response Using LMSC Network and no Rate Gyro

3.3 REFERENCES

3.1 Brown Engineering Company, Vibration Analysis of the S-IVB Workshop with Cluster in the AAP-3/4 Configuration, T.D. Cl-SLS-3-009, 5 May 1967

Section 4
MATHEMATICAL MODEL OF THE FLEXIBLE ATM CLUSTER

4.1 INTRODUCTION

The model derived in this section is an extensive generalization of the one previously described in Section 6 of LMSC-A842157, dated 17 March 1967. While the equations describing the telescope, the control moment gyros, and the corresponding control laws retain the same form and are not repeated here, the total system of equations within which these former equations are now to be coupled has been completely revised to account for the flexible modes of attitude motion of the ATM cluster.

The basic point of view adopted in the derivation of the present model is that the flexible ATM cluster is not a homogeneous deformable continuum, but rather a network of interconnected rigid bodies subjected to continuous rotational deflections about these interconnections. The structural "topology" of the cluster provides an excellent physical motivation for this assumption, with the possible exception of the solar panels, which may perhaps be better described as continuously deformable media. However, from the point of view of a subsequent computer simulation program, the enormous complexity of combining the partial differential equations of continuum mechanics with the ordinary differential equations of rigid body mechanics seemed to preclude any possibility of arriving at a numerically tractable scheme in terms of realistic computer time. Indeed, such a mixed formulation requires, in general, that several boundary value problems be solved between each pair of successive integration points in the time domain. The assumption that the panels may also be treated as rigid bodies bending about their attachment points therefore appeared as a very reasonable compromise.

While it can be expected, on physical grounds, that the rotational bending about the various idealized hinge-points will indeed be small, no such assumption was made in the derivation of the dynamical equations. The equations derived are complete and fully nonlinear, the intention being that they constitute an exact formulation from which subsequent linearizations may be made; to have proceeded with the standard linearized normal-mode vibration analysis would be begging the question insofar as determining the effects of nonlinear dynamical couplings is concerned.

As in the previous formulation given in LMSC-A842157, the Eulerian form of the equations of motion was adopted rather than the Lagrangian form. In this way it was possible to derive the dynamical equations without fixing a priori the number of rigid bodies in the network decomposition of the ATM cluster, even though the specific derivation given refers to a ten-body decomposition. At the same time, the total number of degrees of freedom of the system may be increased or decreased by decreasing or increasing (respectively) the number of corresponding "locked-mode" constraint torque equations. This is particularly useful in allowing one to adjust the model easily to possible subsequent design changes, especially in view of the fact that in the Eulerian formulation scalar components of torques and moments of forces are along body axes rather than along generalized axes corresponding to generalized coordinates of a Lagrangian formulation.

The notation employed in this model is analogous to but more complex than the one used in LMSC-A842157. Because ten bodies and nine hinge points will be involved, it will be necessary to introduce doubly-indexed physical vectors and summation sets in order to achieve a systematic and consistent derivation of the system equations. This revised notation is defined in this section.

4.2 ASSUMPTIONS AND NOTATION

In an exact sense, the entire ATM vehicle can be represented as a continuously deformable system with a very inhomogeneous distribution of bending characteristics. That is to say, if we regard the ATM vehicle as a cluster of interconnected parts, the flexibility across the interconnections is in general much greater than the intrinsic flexibility of each component part. Consequently, it is physically realistic to consider the system as a network of rigid bodies interconnected by elastic dissipative joints or "hinges". This network decomposition of the ATM vehicle into a system of interconnected rigid bodies can be made as large as necessary; for example, the S-IVB, which in one sense represents one body of the system, could be broken down dynamically into several interconnected rigid parts.

For the present mathematical model we have assumed a ten-body decomposition of the ATM vehicle as shown in Fig. 4-1. The ten bodies are interconnected by nine junction (nodal) points located as shown in Fig. 4-2. These nodes act as generalized "hinges" about which relative rotational motion can occur between the corresponding adjacent bodies. Of these nine junction points, only the one labeled 2 (i.e., the geometric point at the intersection of the telescope's gimbal axes, providing these gimbals do not bend) has a set of physical gimbals associated with it. The remaining eight junctions are conceptual hinge-points, i.e., centers of relative rotation between adjacent bodies. If large relative rotational motion were to be considered about any of these conceptual hinges, any specific parametrization of this motion (e.g., in terms of some set of Euler angles) would imply a definite sequence of single-axis finite rotations in the presence of physically nonexistent gimbals. For small motions, however, the commutativity of small-angle rotations guarantees consistency between the actual physical process of rotational bending and whatever angle-parameterization is chosen to describe it mathematically.

It is worth emphasis that, for the purpose of deriving the dynamical model, an exact mathematical description of the relative rotational motions about the various hinges is not needed; the complete mathematical formulation becomes necessary only for the kinematical equations and for the component-scalarization of the vector dynamical equations. It suffices to observe that for each such hinge about which the rotational motion has less than three degrees of freedom there will arise equal and opposite constraint torques on the adjacent bodies connected by that hinge. The occurrence of such "locked-modes" of rotation (whose axes are the supports of the associated constraint torques) can arise quite naturally when one chooses to approximate the actual rotational bending taking place about a given hinge. If we consider, for example, the possible attitude deflections of the CSM (body 9 in Fig. 4-1) relative to the MDS (body 10) to which it is docked – the docking being described mathematically by hinge 9 – it can be expected that the axial elastic restoring moment about the CSM's long axis is much larger than the ones about transversal axes orthogonal to the

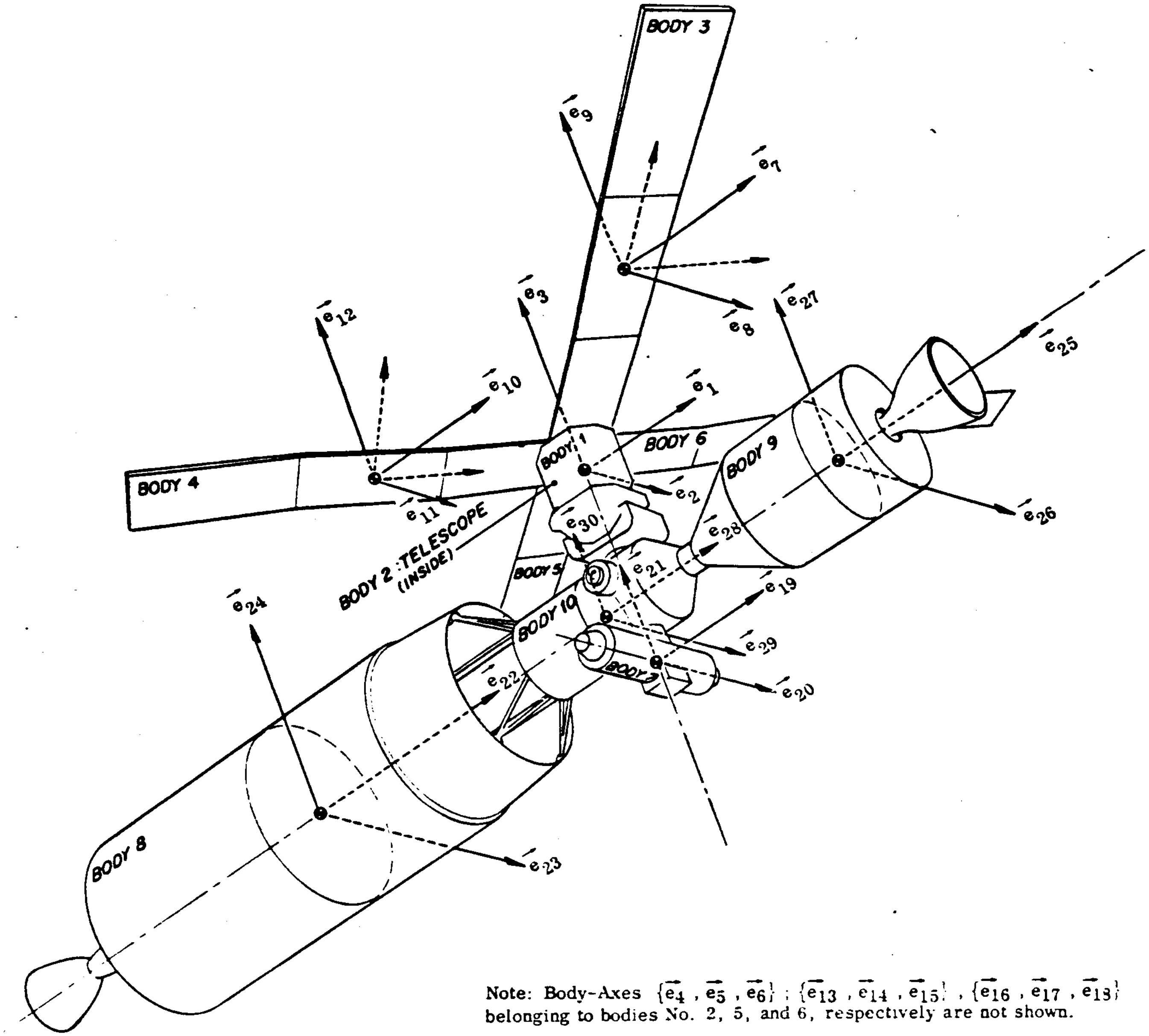

Note: Body-Axes $\{\vec{e}_4, \vec{e}_5, \vec{e}_6\}$; $\{\vec{e}_{13}, \vec{e}_{14}, \vec{e}_{15}\}$, $\{\vec{e}_{16}, \vec{e}_{17}, \vec{e}_{13}\}$ belonging to bodies No. 2, 5, and 6, respectively are not shown.

Fig. 4-1 Decomposition of the ATM Vehicle into a Network of Ten Interconnected Rigid Bodies

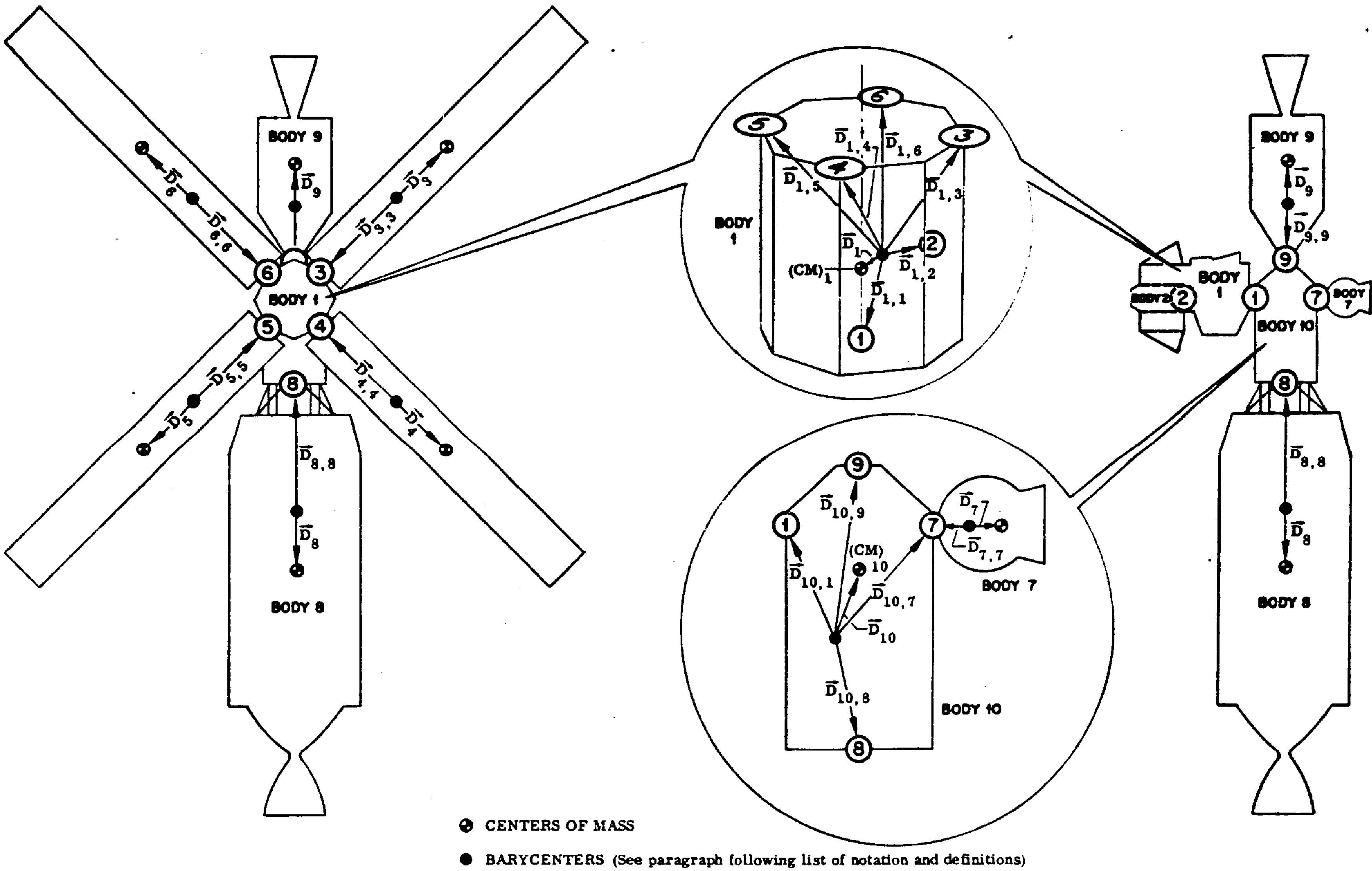

Fig. 4-2 Top and Side Views of the ATM Vehicle Showing Location of the Hinge Points and Corresponding Barycentric Vectors Which Appear in the Final Equation of Motion

long axis. It may be desirable, therefore, to disallow rotational motion about the CSM's long axis and to consider only transversal motion across that axis. That is to say, the rotational bending about hinge 9 would have only two degrees of freedom and would give rise to a constraint torque about an axis identifiable with the CSM's long axis for small deflections.

It is clear that approximations such as discussed above are useful primarily in narrowing the dynamic range of natural frequencies that will occur in the digital simulation program, but the decision to introduce them into the model must be based on detailed tradeoff studies between the numerical tractability of the model on the one hand and the ignorability of high-frequency dynamical effects on the other.

Referring now to Figs. 4-1 and 4-2 (and keeping in mind that an additional breakdown into more bodies and hinges may be required for a subsequent analysis) we define the following summation sets:

$S = \{1,2,3,4,5,6,7,8,9,10\}$	set of (labels of) the ten bodies
$\lambda, \mu, \nu, \ldots\ldots$	lower case Greek letters, used as indices denoting typical elements of S; e.g., $\lambda \epsilon S$
$J = \{1,2,3,4,5,6,7,8,9\}$	set of (labels of) the nine junction points or hinges interconnecting the ten bodies.
$j, k, \ldots\ldots$	lower case Latin letters, used as indices, denoting typical elements of J; e.g., $j \epsilon J$
J_λ (for each $\lambda \epsilon S$)	set of (labels of) those hinges on body λ; e.g., $J_{10} = \{1,7,8,9\}$, $J_8 = \{8\}$, etc.
$S_{\lambda,j}$ (for each $\lambda \epsilon S$, $j \epsilon J_\lambda$)	set of bodies connected to body λ at hinge j, possibly by a chain of intermediate bodies
$k_\lambda(\mu)$ (for $\lambda \neq \mu$)	that particular hinge on body λ which leads to body μ; thus, $k_\lambda(\mu) \epsilon J_\lambda$
$S_{\lambda\mu} \equiv S_{\lambda k_\lambda(\mu)}$	abbreviated notation for the connected set of bodies attached to that hinge of body λ which leads to body μ (includes body μ as well as others "in that direction")

$C_{\mu\nu} \equiv \{\kappa \mid k_\kappa(\mu) \neq k_\kappa(\nu)\}$ — chain of bodies directly connecting body μ to body ν (body μ and body ν not included)

$R_\lambda \equiv S - \{\lambda\}$

$R_{\lambda\mu} \equiv S - \{\lambda\} - S_{\lambda\mu}$

— abbreviated notation for residual sets whose definitions, as indicated, are self-explanatory

For $\lambda \epsilon S$ and $j \epsilon J_\lambda$, let

m_λ = mass of body λ

$m = \sum_\nu m_\nu$ = total mass (the sum $\sum_\nu$ is understood to range over all $\nu \epsilon S$)

$m_{\lambda\mu} = \Sigma_{\nu \epsilon S_{\lambda\mu}} m_\nu$ (total mass of bodies in set $S_{\lambda\mu}$ previously defined)

$\bar{\bar{\Phi}}_\lambda$ = inertia dyadic of body λ about its center of mass

$\vec{\omega}_\lambda$ = angular velocity vector of body λ

$\vec{F}_\lambda$ = external force on body λ

$\vec{T}_\lambda$ = external torque on body λ

$\vec{\rho}_\lambda$ = vector from an inertial origin to the center of mass of body λ

$\vec{\rho}$ = vector from inertial origin to system's composite center of mass

$\vec{F}^H_{\lambda j}$ = interaction force on body λ, transmitted through hinge j

$\vec{T}^H_{\lambda j}$ = torque on body λ, transmitted through hinge j (due to springs, dampers, and "gimbal" constraints, if any)

$\vec{H}_{\lambda,j}$ = vector from center of mass of body λ to hinge j
$\equiv \vec{H}_{\lambda\mu}$ for any $\mu \epsilon S_{\lambda,j}$

$$\vec{D}_\lambda \equiv - \sum_{j \epsilon J_\lambda} \sum_{\mu \epsilon S_{\lambda,j}} m_\mu m^{-1} \vec{H}_{\lambda,j} = - \sum_{\mu \neq \lambda} m_\mu m^{-1} \vec{H}_{\lambda\mu}$$

(by above convention for $\vec{H}_{\lambda\mu}$)

$$\begin{cases} \vec{D}_{\lambda,j} \equiv \vec{D}_\lambda + \vec{H}_{\lambda,j} \\ \vec{D}_{\lambda\mu} \equiv \vec{D}_\lambda + \vec{H}_{\lambda\mu} \end{cases} ,$$

(Thus $\vec{D}_{\lambda,j} = \vec{D}_{\lambda\mu}$ for any $\mu \epsilon S_{\lambda,j}$)

$$\bar{\bar{X}}_\lambda \equiv (m_\lambda D_\lambda^2 + \Sigma_{\mu \neq \lambda} m_\mu D_{\lambda\mu}^2)\bar{\bar{1}} - (m_\lambda \vec{D}_\lambda \vec{D}_\lambda + \Sigma_{\mu \neq \lambda} m_\mu \vec{D}_{\lambda\mu} \vec{D}_{\lambda\mu})$$

($\bar{\bar{1}}$: identity dyadic)

$$\bar{\bar{\Phi}}_\lambda{}^* \equiv \bar{\bar{\Phi}}_\lambda + \bar{\bar{X}}_\lambda \equiv \bar{\bar{\Phi}}_{\lambda\lambda} \text{ and } \bar{\bar{\Phi}}_{\lambda\mu} \equiv m(\vec{D}_{\mu\lambda}\vec{D}_{\lambda\mu} - \vec{D}_{\mu\lambda} \cdot \vec{D}_{\lambda\mu}\bar{\bar{1}}) \text{ for } \mu \neq \lambda$$

This completes the list of notation and definitions.

The physical interpretation of the various $\vec{D}$ vectors and the dyadic $\bar{\bar{\Phi}}*$ defined above is quite straightforward. If for each $j \epsilon J_\lambda$ we augment the mass distribution of body λ by point masses $\Sigma_{\nu \epsilon S_{\lambda j}} m_\nu$ located at the hinges j respectively, we obtain a new center of mass for the augmented body λ. In Fig. 4-2, this new center of mass, which we call barycenter, is denoted by a full black dot. Then in body λ, $\vec{D}_\lambda$ is the vector from the barycenter to the original center of mass, while $\vec{D}_{\lambda,j}$ is the vector from the barycenter to hinge j, for $j \epsilon J_\lambda$. (Equivalently, for $\mu \epsilon S_{\lambda,j}$, $\vec{D}_{\lambda\mu}$ is the vector from the barycenter to hinge j; these are different notations for the same vector, and in Fig. 4-2 the notation $\vec{D}_{\lambda,j}$ is used. The symmetric notation $\vec{H}_{\lambda\mu}$, $\vec{D}_{\lambda\mu}$ is quite useful, as seen in the definition of $\vec{D}_\lambda$, in allowing one to replace double sums by simple single sums.) Finally, $\bar{\bar{\Phi}}*$ is the inertia dyadic of the augmented body λ about its barycenter. From the definition of the barycentric vectors $\vec{D}_\lambda$ and $\vec{D}_{\lambda\mu}$, we have the identity

$$m_\lambda \vec{D}_\lambda + \sum_{\mu \neq \lambda} m_\mu \vec{D}_{\lambda\mu} = \vec{0}. \tag{4.1}$$

4.3 DYNAMICAL EQUATIONS (PRELIMINARY FORM)

Newton's and Euler's equations for body λ are

$$\vec{F}_\lambda + \sum_{j \epsilon J_\lambda} \vec{F}_{\lambda j}^H = m_\lambda \ddot{\vec{\rho}}_\lambda \tag{4.2}$$

$$\bar{\bar{\Phi}}_\lambda \cdot \dot{\vec{\omega}}_\lambda + \vec{\omega}_\lambda \times \bar{\bar{\Phi}}_\lambda \cdot \vec{\omega}_\lambda = \vec{T}_\lambda + \sum_{j \epsilon J_\lambda} \vec{T}_{\lambda j}^H + \sum_{j \epsilon J_\lambda} \vec{H}_{\lambda,j} \times \vec{F}_{\lambda j}^H \tag{4.3}$$

We shall use Newton's equations to eliminate the unknown hinge into action forces $\vec{F}^H_{\lambda j}$ from the Euler equations

From the definition of the hinge vectors $\vec{H}$ we have

$$\vec{\rho}_\mu - \vec{\rho}_\nu = -\vec{H}_{\mu\nu} + \Sigma_{\kappa\epsilon C_{\mu\nu}} (\vec{H}_{\kappa\mu} - \vec{H}_{\kappa\nu}) + \vec{H}_{\nu\mu}$$

and hence

$$m(\vec{\rho}_\mu - \vec{\rho}) = \Sigma_{\nu\neq\mu} m_\nu (\vec{\rho}_\mu - \vec{\rho}_\nu)$$

$$= \Sigma_{\nu\neq\mu} [(-m_\nu)\vec{H}_{\mu\nu} + \Sigma_{\kappa\epsilon C_{\mu\nu}} m_\nu (\vec{H}_{\kappa\mu} - \vec{H}_{\kappa\nu}) + m_\nu \vec{H}_{\nu\mu}]$$

Renaming the summation index in the last term in brackets and using the definition for $\vec{D}_\mu$ in the first term in brackets, the above becomes

$$m(\vec{\rho}_\mu - \vec{\rho}) = m\vec{D}_\mu + \Sigma_{\nu\neq\mu} \Sigma_{\kappa\epsilon C_{\mu\nu}} m_\nu (\vec{H}_{\kappa\mu} - \vec{H}_{\kappa\nu}) + \Sigma_{\kappa\neq\mu} m_\kappa \vec{H}_{\kappa\mu} \quad (4.4)$$

In the double sum appearing in Eq. (4.4), the maximal range for the inner summation index κ is the set R_μ - T, where T is the collection of terminal bodies in S, i.e., bodies having only one hinge. On the other hand, for a fixed κ, the corresponding range of summation for ν is the set $R_{\kappa\mu}$ which is empty whenever ϵ T. Hence the maximal range R_μ - T for the index κ can be trivially augmented to R_μ when we interchange the order of summation in the double sum of Eq. (4.4) (observe that $R_{\kappa\mu} = R_\kappa - S_{\kappa\mu}$ and $\vec{H}_{\kappa\nu} \equiv \vec{H}_{\kappa\mu}$ whenever $\nu \epsilon S_{\kappa\mu}$)

$$\Sigma_{\nu \neq \mu} \Sigma_{\kappa \in C_{\mu\nu}} m_\nu (\vec{H}_{\kappa\mu} - \vec{H}_{\kappa\nu})$$

$$= \Sigma_{\kappa \neq \mu} \Sigma_{\nu \in R_{\kappa\mu}} m_\nu (\vec{H}_{\kappa\mu} - \vec{H}_{\kappa\nu})$$

$$= \Sigma_{\kappa \neq \mu} [(m - m_\kappa - m_{\kappa\mu}) \vec{H}_{\kappa\mu} - \Sigma_{\nu \in R_\kappa - S_{\kappa\mu}} m_\nu \vec{H}_{\kappa\nu}]$$

$$= \Sigma_{\kappa \neq \mu} [(m - m_\kappa - m_{\kappa\mu}) \vec{H}_{\kappa\mu} - \Sigma_{\nu \neq \kappa} m_\nu \vec{H}_{\kappa\nu} + m_{\kappa\mu} \vec{H}_{\kappa\mu}]$$

$$= \Sigma_{\kappa \neq \mu} [(m - m\ ) \vec{H}_{\kappa\mu} - \Sigma_{\nu \neq \kappa} m_\nu \vec{H}_{\kappa\nu}]$$

$$= \Sigma_{\kappa \neq \mu} [(m - m_\kappa) \vec{H}_{\kappa\mu} + m\vec{D}_\kappa]$$

$$= \Sigma_{\kappa \neq \mu} (m\vec{D}_{\kappa\mu} - m_\kappa \vec{H}_{\kappa\mu}) . \qquad (4.5)$$

in which we have used again the definitions of the barycentric vectors $\vec{D}$. Substituting Eq. (4.5) into Eq. (4.4) and dividing both sides by m, we obtain

$$\vec{\rho}_\mu - \vec{\rho} = \vec{D}_\mu + \Sigma_{\kappa \neq \mu} \vec{D}_{\kappa\mu} \qquad (4.6)$$

Next, by summing Newton's equations (4.2) (written for μ instead of λ) over all $\mu \in S_{\lambda,j}$, we can isolate the hinge interaction force $\vec{F}^H_{\lambda j}$ at hinge j on body λ:

$$X\vec{F}^H_{\lambda j} = \sum_{\mu \in S_{\lambda,j}} (\vec{F}_\mu - m_\mu \ddot{\vec{\rho}}_\mu)$$

$$= \sum_{\mu \in S_{\lambda,j}} \left[\vec{F}_\mu - m_\mu (m^{-1} \sum_\nu \vec{F}_\nu) - m_\mu (\ddot{\vec{\rho}}_\mu - \ddot{\vec{\rho}}) \right] \qquad (4.7)$$

since $\ddot{\vec{\rho}} = m^{-1} \sum_\nu \vec{F}_\nu$ by Newton's law. Thus the last term in the Euler (4.3) i.e., the moment of the interaction forces on body λ, is given by

$$\sum_{j \in J_\lambda} \vec{H}_{\lambda,j} \times \vec{F}^H_{\lambda j} = \sum_{\mu \neq \lambda} \vec{H}_{\lambda\mu} \times \left[\vec{F}_\mu - m_\mu (m^{-1} \sum_\nu \vec{F}_\nu) - m_\mu (\ddot{\vec{\rho}}_\mu - \ddot{\vec{\rho}}) \right]$$

$$= \vec{D}_\lambda \times \vec{F}_\lambda + \sum_{\mu \neq \lambda} \vec{D}_{\lambda\mu} \times \vec{F}_\mu - \sum_{\mu \neq \lambda} m_\mu \vec{H}_{\lambda\mu} \times (\ddot{\vec{\rho}}_\mu - \ddot{\vec{\rho}}) \quad (4.8)$$

Now we substitute Eq. (4.6) into the last term of Eq. (4.8) and obtain

$$- \sum_{\mu \neq \lambda} m_\mu \vec{H}_{\lambda\mu} \times (\ddot{\vec{\rho}}_\mu - \ddot{\vec{\rho}}) = - \sum_{\mu \neq \lambda} m_\mu \vec{H}_{\lambda\mu} \times \ddot{\vec{D}}_{\lambda\mu} + m \sum_{\mu \neq \lambda} \vec{D}_{\lambda\mu} \times \ddot{\vec{D}}_{\mu\lambda} \quad (4.9)$$

The intermediate steps required to establish Eq. (4.9) are nontrivial and constitute the main difficulty in the derivation of the dynamical equation. These steps are outlined below; however, the reader who is primarily interested in the final equations of motion may proceed directly to Eq. (4.10).

The first step in substituting Eq. (4.6) into the last term of Eq. (4.8) leads to

$$- \Sigma_{\mu \neq \lambda} m_\mu \vec{H}_{\lambda\mu} \times (\ddot{\vec{\rho}}_\mu - \ddot{\vec{\rho}}) = - \Sigma_{\mu \neq \lambda} m_\mu \vec{H}_{\lambda\mu} \times (\ddot{\vec{D}}_\mu + \Sigma_{\nu \neq \mu} \ddot{\vec{D}}_{\nu\mu}). \quad (4.9a)$$

The terms on the right corresponding to $\nu = \lambda$ are $- \Sigma_{\mu \neq \lambda} m_\mu \vec{H}_{\lambda\mu} \times \ddot{\vec{D}}_{\lambda\mu}$ and are the desired first term on the right of Eq. (4.9). For the remaining terms in Eq. (4.9a) (corresponding to $\nu \neq \lambda$), we eliminate $\ddot{\vec{D}}_\mu$ by use of identity (4.1) and have left (denoting explicitly the summation ranges in terms of the residual sets R)

$$\sum_{\mu \in R_\lambda} \sum_{\nu \in R_\mu} m_\nu (\vec{H}_{\lambda\mu} \times \ddot{\vec{D}}_{\mu\nu}) - \sum_{\mu \in R_\lambda} \sum_{\nu \in R_\mu - \{\lambda\}} m_\mu (\vec{H}_{\lambda\mu} \times \ddot{\vec{D}}_{\nu\mu}). \quad (4.9b)$$

Consider the second double sum in (4.9b) in which the summation indices are μ and ν. Clearly, the combined summation range of the ordered pair (μ, ν) will be a subset of the cartesian product set $S \times S$. Furthermore, this combined range is symmetric in the sense that (μ, ν) is an element of it if and only if (ν, μ) is also contained in it. By virtue of this symmetry, we interchange the indices μ and ν in the summand (only) of the second double sum in (4.9b). Rewriting then (4.9b) in factored form, we have

$$\sum_{\mu \in R_\lambda} \left[\sum_{\nu \in R_\mu} m_\nu (\vec{H}_{\lambda\mu} \times \ddot{\vec{D}}_{\mu\nu}) - \sum_{\nu \in R_\mu - \{\lambda\}} m_\nu (\vec{H}_{\lambda\nu} \times \ddot{\vec{D}}_{\mu\nu}) \right] \tag{4.9c}$$

Now, from elementary set considerations, we have (using $\cup$ to denote only disjoint unions)

$$R_\mu = S_{\mu\lambda} \cup R_{\mu\lambda}, \tag{4.9d}$$

$$R_\mu - \{\lambda\} = [R_\lambda - (S - S_{\mu\lambda})] \cup R_{\mu\lambda}, \tag{4.9e}$$

and

$$\ddot{\vec{D}}_{\mu\nu} = \ddot{\vec{D}}_{\mu\lambda} \quad \begin{cases} \text{whenever } \nu \in S_{\mu\lambda}, \\ \text{whenever } \nu \in [R_\lambda - (S - S_{\mu\lambda})], \end{cases} \tag{4.9f}$$

$$\vec{H}_{\lambda\nu} = \vec{H}_{\lambda\mu} \quad \begin{cases} \text{whenever } \nu \in R_{\mu\lambda}, \\ \text{whenever } \nu \in (S - S_{\mu\lambda}). \end{cases} \tag{4.9g}$$

where, in Eq. (4.9f), we have used the fact that $R_\lambda - (S - S_{\mu\lambda}) = S_{\mu\lambda} - \{\lambda\}$.

Decomposing the (inner) summation sets in (4.9c) according to (4.9d) and (4.9e), we see that the sums over $\nu \in R_{\mu\lambda}$ cancel because of the replacement made possible by Eq. (4.9g). Using next the replacement Eq. (4.9f) in the remaining sums, (4.9c) reduces to

$$\sum_{\mu \in R_\lambda} \left\{ \left[\sum_{\nu \in S_{\mu\lambda}} m_\nu \vec{H}_{\lambda\mu} - \sum_{\nu \in [R_\lambda - (S - S_{\mu\lambda})]} m_\nu \vec{H}_{\lambda\nu} \right] \times \ddot{\vec{D}}_{\mu\lambda} \right\} \tag{4.9h}$$

Finally, the second (inner) sum in (4.9h) can be written as the difference of a sum over R_λ and a sum over $S - S_{\mu\lambda}$; in the latter sum, replacement (4.9g) is valid and a further breakdown into sums over S and over $S_{\mu\lambda}$ will then allow calcellation with the first (inner) sum in (4.9h). Recalling the definitions of the barycentric vectors $\vec{D}$ (given at the end of the list of notation) and the fact that $\mu \neq \lambda$ whenever $\mu \in R_\lambda$, we collect the sums remaining in (4.9h) and obtain

$$\Sigma_{\mu\neq\lambda}\{[\Sigma_{\nu\neq\lambda}(-m_\nu)\vec{H}_{\lambda\nu} + m\vec{H}_{\lambda\mu}]\times \ddot{\vec{D}}_{\mu\lambda}\} = \Sigma_{\mu\neq\lambda}[(m\vec{D}_\lambda + m\vec{H}_{\lambda\mu})\times\ddot{\vec{D}}_{\mu\lambda}]$$

$$= m\Sigma_{\mu\neq\lambda}\vec{D}_{\lambda\mu}\times\ddot{\vec{D}}_{\mu\lambda} \qquad (4.9i)$$

and this establishes Eq. (4.9) previously stated.

Returning to Eq. (4.9), we compute the first term on its right-hand side, using identify (4.1) and the definitions fo the barycentric vectors $\vec{D}$ and the dyadic $\bar{\bar{X}}_\lambda$. One obtains

$$-\sum_{\mu\neq\lambda} m_\mu\vec{H}_{\lambda\mu}\times\ddot{\vec{D}}_{\lambda\mu} = -\sum_{\mu\neq\lambda} m_\mu\vec{D}_{\lambda\mu}\times\ddot{\vec{D}}_{\lambda\mu} - m_\lambda\vec{D}_\lambda\times\ddot{\vec{D}}_\lambda$$

$$= -\frac{d}{dt}(\bar{\bar{X}}_\lambda\cdot\vec{\omega}_\lambda)$$

$$= -\bar{\bar{X}}_\lambda\cdot\dot{\vec{\omega}}_\lambda - \vec{\omega}_\lambda\times\bar{\bar{X}}_\lambda\cdot\vec{\omega}_\lambda \qquad (4.10)$$

This last term has the same form as the left-hand side of the Euler equations (4.3) and suggests, therefore, the definition $\bar{\bar{\Phi}}^*_\lambda = \bar{\bar{\Phi}}_\lambda + \bar{\bar{X}}_\lambda$ previously given. Using this definition, we substitute Eq. (4.10) into Eq. (4.9), Eq. (4.9) into Eq. (4.8), Eq. (4.8) into Eq. (4.3) and obtain the first form of the dynamical equation

$$\bar{\bar{\Phi}}^*_\lambda\cdot\dot{\vec{\omega}}_\lambda + \vec{\omega}_\lambda\times\bar{\bar{\Phi}}^*_\lambda\cdot\vec{\omega}_\lambda = \vec{T}_\lambda + \sum_{j\in J_\lambda}\vec{T}^H_{\lambda j} + \vec{D}_\lambda\times\vec{F}_\lambda$$

$$+ \sum_{\mu=\lambda}\vec{D}_{\lambda\mu}\times(\vec{F}_\mu + m\ddot{\vec{D}}_{\mu\lambda}) \qquad (4.11a)$$

where

$$\ddot{\vec{D}}_{\mu\lambda} = \dot{\vec{\omega}}_{\mu} \times \vec{D}_{\mu\lambda} + \vec{\omega}_{\mu} \times (\vec{\omega}_{\mu} \times \vec{D}_{\mu\lambda}) \qquad (4.11b)$$

In the above, as in the starting equations, Eqs. (4.2) and (4.3), it is clear that the overdots denote time derivatives in an inertial frame. (Recall that $\dot{\vec{\omega}}_{\lambda}$ is the same whether the time derivative is w.r.t. an inertial frame or w.r.t. a frame fixed in body λ.)

4.4 GRAVITY-GRADIENT TORQUES AND MOMENTS OF GRAVITATIONAL FORCES ON THE ATM

Because the ATM vehicle consists of ten interconnected rigid bodies, the gravitational effects on its attitude come not only from the individual gravity-gradient torques acting on each part separately but also from the hinge-moments of the gravitational forces acting on each part. This situation arises because, for an arbitary deformation of the entire system, the so-called cancellation of gravitational pull by centrifugal effects occurs only for the composite center of mass of the entire system. The residual gravitational pull on each component part produces a moment comparable to the classical gravity-gradient torque and therefore needs to be evaluated.

Let γ be the Earth's gravitational constant as appears in the gravitational force equation

$$d\vec{F}^{G} = -\gamma \rho^{-2} \hat{\rho}\, dm$$

where

$\hat{\rho} = \vec{\rho}/\rho$ is the "local vertical" unit vector.

Now we separate from the total external torque $\vec{T}_{\lambda}$ on body λ the gravitational part:

$$\vec{T}_{\lambda} = \vec{T}^{G}_{\lambda} + \vec{T}'_{\lambda} ,$$

where

$$\vec{T}^G_\lambda = (3\gamma/\rho^3)\,(\hat{\rho}\times\bar{\bar{\Phi}}_\lambda\cdot\hat{\rho}) \tag{4.12}$$

is (to first order in the ratio of satellite dimensions to orbital radius ρ) the (differential) gravitational torque on body λ, while $\vec{T}'_\lambda$ is the sum of any other external torques on body λ.

Similarly, we separate from the total external force $\vec{F}_\lambda$ the gravitational part

$$\vec{F}_\lambda = \vec{F}^G_\lambda + \vec{F}'_\lambda$$

where

$$\vec{F}^G_\lambda = \gamma m_\lambda \rho_\lambda^{-3}\vec{\rho}_\lambda \approx -\gamma m_\lambda \rho^{-3}\,[\vec{\rho} + (\bar{\bar{1}} - 3\hat{\rho}\hat{\rho})\cdot(\vec{\rho}_\lambda - \vec{\rho})] \tag{4.13}$$

is (to second order) the gravitational force on body λ, while $\vec{F}'_\lambda$ is the sum of any other external forces on body λ.

On substituting $\vec{F}^G_\lambda + \vec{F}_\lambda$ for $\vec{F}_\lambda$ in Eq (4.11a), we obtain, by manipulations completely parallel to the derivation of Eq (4.9)

$$\vec{D}_\lambda\times\vec{F}^G_\lambda + \sum_{\mu\neq\lambda}\vec{D}_{\lambda\mu}\times\vec{F}^G_\mu = -\sum_{\mu\neq\lambda} m_\mu\vec{H}_{\lambda\mu}\times\bar{\bar{G}}.\vec{D}_{\lambda\mu} + m\sum_{\mu\neq\lambda}\vec{D}_{\lambda\mu}\times\bar{\bar{G}}.\vec{D}_{\mu\lambda} \tag{4.14}$$

where the linear operator $\bar{\bar{G}} = (\gamma/\rho^3)\,(\bar{\bar{1}} - 3\,\hat{\rho}\hat{\rho})$ here replaces the operator d^2/dt^2 which previously appeared in Eq. (4.9). The first sum on the right reduces to $(3\gamma/\rho^3)\,(\hat{\rho}\times\bar{\bar{X}}_\lambda.\hat{\rho})$ and thus combines with $\vec{T}^G_\lambda$ of Eq. (4.12) resulting in the gravity-gradient attitude equations for body λ:

$$\left.\begin{aligned}\bar{\bar{\Phi}}_\lambda{*}.\dot{\vec{\omega}}_\lambda + \vec{\omega}_\lambda\;\;\bar{\bar{\Phi}}_\lambda{*}.\vec{\omega}_\lambda &= (3\gamma/\rho^3)\,(\hat{\rho}\times\bar{\bar{\Phi}}_\lambda{*}.\hat{\rho}) + \vec{T}'_\lambda + \sum_{j\in J_\lambda}\vec{T}^H_{\lambda j}\\ &+ \vec{D}_\lambda\times\vec{F}'_\lambda + \sum_{\mu\neq\lambda}\vec{D}_{\lambda\mu}\times\left[\vec{F}'_\mu + m\ddot{\vec{D}}_{\mu\lambda} + m(\gamma/\rho^3)\,(\bar{\bar{1}} - 3\hat{\rho}\hat{\rho}).\vec{D}_{\mu\lambda}\right].\end{aligned}\right\} \tag{4.15}$$

4.5 COMPUTATION OF HINGE TORQUES AND FINAL FORM OF THE DYNAMICAL EQUATIONS

Referring to Fig. 4-1 and to the discussion at the end of subsection 4.2 dealing with assumptions of restricted rotational bending about a hinge, we could, for example, in a first iteration of the analysis, assume that each solar panel has only one degree of freedom relative to body 1, that body 9 and body 8 each have only two rotational degrees of freedom relative to body 10, and so on, in a manner consistent with specific information about the relative "stiffness" of the elastic behavior about various axes at each hinge.

The maximum number of degrees of rotational freedom for the entire system is 30. Let the actual number of degrees of freedom considered by n. Then $n' \equiv 30 - n$ is the number of locked modes. Let $\vec{p}_i$ $(i = 1, 2, \ldots, n')$ be a set of unit vectors "spanning" this set of locked modes. That is, at a two degree of freedom hingepoint (mathematically equivalent to a two-gimbal system) there would be one $\vec{p}_i$ orthogonal to the two gimbal axes, whereas at a single degree of freedom hinge (mathematically equivalent to a single gimbal) there would be two vectors $\vec{p}_i$ orthogonal to the single gimbal's axis and to each other. To account for the fact that a constraint torque shared by two adjacent bodies is positive for one and negative for the other, we introduce the numerical-valued symbol $\delta_{\lambda i}$ defined as follows:

$$\delta_{\lambda i} = \begin{cases} 0 \text{ if } \vec{p}_i \text{ is not defined for a hinge on body } \lambda \\ +1 \text{ if } T_i^c \vec{p}_i \text{ is a constraint torque } \underline{\text{on}} \text{ body } \lambda \\ -1 \text{ if } T_i^c \vec{p}_i \text{ is a constraint torque on a body adjacent to body } \lambda \end{cases}$$

where T_i^c is the projection of the appropriate constraint torque along $\vec{p}_i$.

In terms of the above, the hinge torque on body λ can be written

$$\sum_{j\in J_\lambda} \vec{T}^{H}_{\lambda j} = \sum_{j\in J_\lambda} \vec{T}^{SD}_{\lambda j} + \sum_{i=1}^{n'} \delta_{\lambda i}\, T^{c}_{i}\vec{p}_{i} \tag{4.16}$$

where $\vec{T}^{SD}_{\lambda j}$ is the spring-and-damper torque on body λ at hinge j.

We now substitute Eq. (4.16) and (4.11b) into Eq. (4.15), making use of the identity

$$m\,\vec{D}_{\lambda\mu} \times (\dot{\vec{\omega}}_{\mu} \times D_{\mu\lambda}) = -m(\vec{D}_{\mu\lambda}\vec{D}_{\lambda\mu} - \vec{D}_{\mu\lambda}\cdot D_{\lambda\mu}\,\bar{\bar{1}})\cdot\dot{\vec{\omega}}_{\mu}$$

$$\equiv -\,\bar{\bar{\Phi}}_{\lambda\mu}\cdot\dot{\vec{\omega}}_{\mu} \text{ (by definition; see list)}$$

and obtain the equations of motion (recall that $\bar{\bar{\Phi}}^{*}_{\lambda}$ is also written as $\bar{\bar{\Phi}}_{\lambda\lambda}$)

$$\sum_{\mu} \bar{\bar{\Phi}}_{\lambda\mu}\cdot\dot{\vec{\omega}}_{\mu} = \vec{E}_{\lambda} + \sum_{i=1}^{n'} \delta_{\lambda i}\, T^{c}_{i}\vec{p}_{i} \tag{4.17}$$

where

$$\vec{E}_{\lambda} \equiv (3\gamma/\rho^{3})(\hat{\rho} \times \bar{\bar{\Phi}}^{*}_{\lambda}\cdot\hat{\rho}) - \vec{\omega}_{\lambda}\times \bar{\bar{\Phi}}^{*}_{\lambda}\cdot\vec{\omega}_{\lambda} + \vec{T}'_{\lambda}$$

$$+ \sum_{j\in J_\lambda} \vec{T}^{SD}_{\lambda j} + \vec{D}_{\lambda} \times \vec{F}'_{\lambda}$$

$$+ \sum_{\mu\neq\lambda} \vec{D}_{\lambda\mu} \times \left[\vec{F}'_{\mu} + m\,\vec{\omega}_{\mu} \times (\vec{\omega}_{\mu} \times \vec{D}_{\mu\lambda}) + m(\gamma/\rho^{3})\,(\bar{\bar{1}} - 3\hat{\rho}\hat{\rho})\cdot\vec{D}_{\mu\lambda}\right]$$

By projecting the vector-dyadic equations (4.17) on the corresponding appropriately chosen orthonormal frame in body λ (see for example Fig 4-1), one obtains a set of matrix-scalar equations of the form

$$\sum_{\mu} \Phi_{\lambda\mu}\dot{\omega}_{\mu} = E_{\lambda} + P_{\lambda}T^{c} ,$$

where

$\Phi_{\lambda\lambda}$ is the 3×3 matrix of body-λ components of $\bar{\bar{\Phi}}_{\lambda}{}^{*}$,

$\dot{\omega}_{\mu}$ is the 3×1 matrix of body-μ components of $\dot{\vec{\omega}}_{\mu}$,

$\Phi_{\lambda\mu}\dot{\omega}_{\mu}$ (for $\mu \neq \lambda$) is the 3×1 matrix of body-λ components of the vector

$$m(\vec{D}_{\mu\lambda}\vec{D}_{\lambda\mu} - \vec{D}_{\mu\lambda} \cdot \vec{D}_{\lambda\mu}\bar{\bar{1}}) \cdot \dot{\vec{\omega}}_{\mu},$$

P_{λ} is the 3×n' matrix whose i-th column consists of the body-λ components of $\delta_{\lambda i}\vec{p}_{i}$,

T^{c} is the n'×1 matrix whose i-th element is T_{i}^{c} , and

E_{λ} is the 3×1 matrix of body-λ components of $\vec{E}_{\lambda}$ defined above in Eq. (4.17).

The entire set of equations (4.18) for all the $\lambda \epsilon S$, i.e. for λ = 1, 3, 2, ... 10 can be written together in matrix form as

$$\Phi\,\dot{\omega} = E + P\,T^{c} \tag{4.19}$$

where Φ, $\dot{\omega}$, E, P, and T^{c} are, respectively, 30×30, 30×1', 30×1, 30×n', and n'×1 matrices constructed in the obvious way from the matrix blocks appearing in Eq. (4.18); recall that n' represents the number of locked modes, i.e. n' = 30 - n, where n is the total number of degrees of freedom considered. As in the discussion previously given in LMSC-A842157 on pp. 6-13, 6-14, we observe again that each constraint condition is equivalent to requiring that the relative angular velocity $\vec{\omega}_{\lambda} - \vec{\omega}_{\mu}$ between two adjacent bodies λ and μ be orthogonal to the corresponding constraint torque axis (or axes) $\vec{p}_{i}$, i.e.,

$$0 = \vec{p}_{i} \cdot (\vec{\omega}_{\lambda} - \vec{\omega}_{\mu}) \quad \text{or in matrix form} \quad 0 = P^{T}\omega \tag{4.20}$$

where $(\;)^{T}$ denotes matrix transposition and where the 30×1 matrix ω is defined similarly to the matrix $\dot{\omega}$. Differentiating Eq. (4.20) we obtain

$$P^{T}\omega = -\dot{P}^{T}\omega \tag{4-21}$$

By eliminating $\dot{\omega}$ between Eqs. (4.19) and (4.21), we can solve for T^c

$$T^c = -(P^T\Phi^{-1}P)^{-1}(P^T\Phi^{-1}E + \dot{P}^T\omega) \tag{4.22}$$

and substituting Eq. (4.22) back into Eq. (4.19) we obtain

$$\Phi\dot{\omega} = E - P(P^T\Phi^{-1}P)^{-1}(P^T\Phi^{-1}E + \dot{P}^T\omega) \tag{4.23}$$

Alternatively, we can adjoin Eq. (4.21) to Eq. (4.19) to obtain the augmented matrix system

$$\begin{bmatrix} \Phi & P \\ P^T & O \end{bmatrix} \begin{bmatrix} \dot{\omega} \\ -T^c \end{bmatrix} = \begin{bmatrix} E \\ -P^T\dot{\omega} \end{bmatrix} \qquad (4.2\ \ )$$

We observe that the 30×30 matrix Φ is naturally partitioned into a 10×10 symmetric array of 3×3 matrices $\Phi_{\lambda\mu}$ as shown in Eq. (4.18). Also, from the definition of the dyadics $\overline{\overline{\Phi}}{}^*_\lambda \equiv \overline{\overline{\Phi}}_{\lambda\lambda}$ it is clear that the diagonal elements of this partition, i.e. the matrices $\Phi_{\lambda\lambda}$, are made up of constants. For the off-diagonal elements in the partition, i.e. the matrices $\Phi_{\lambda\mu}$, the entries will be time-varying. However, if one assumes that the relative rotational deflections between the bodies are small, each of the off-diagonal matrices $\Phi_{\lambda\mu}$ in the partition may be expressed as the sum of a constant matrix and of a small time-varying matrix. For example, consider the coupling matrix Φ_{18} between body 1 and body 8. Assume (see Fig. 4-1) that

$$\begin{bmatrix} \vec{e}_{22} \\ \vec{e}_{23} \\ \vec{e}_{24} \end{bmatrix} = \begin{bmatrix} 1 & \gamma & -\beta \\ -\gamma & 1 & \alpha \\ \beta & -\alpha & 1 \end{bmatrix} \begin{bmatrix} \vec{e}_1 \\ \vec{e}_2 \\ \vec{e}_3 \end{bmatrix}$$

represents the rotational deflection, given by small angles $\alpha(t)$, $\beta(t)$, $\gamma(t)$, of body 8 relative to body 1. Now for the dyadic $\overline{\overline{\Phi}}_{18}$ we have

$$\overline{\overline{\Phi}}_{18} = m(\vec{D}_{81}\vec{D}_{18} - \vec{D}_{81} \cdot \vec{D}_{18}\,\overline{\overline{1}})$$

$$= m\,\vec{D}_{18} \times (\vec{D}_{81} \times \quad)$$

Changing from the $\vec{D}_{\lambda\mu}$ notation to the $\vec{D}_{\lambda,j}$ notation used in Fig. 4-2, we have $\vec{D}_{18} = \vec{D}_{1,1}$ and $\vec{D}_{81} = \vec{D}_{8,8}$ and define:

$$\vec{D}_{1,1} = D_{1,1}^{1}\vec{e}_1 + D_{1,1}^{2}\vec{e}_2 + D_{1,1}^{3}\vec{e}_3 \ ,$$

and similarly

$$\vec{D}_{8,8} = D_{8,8}^{1}\vec{e}_{22} + D_{8,8}^{2}\vec{e}_{23} + D_{8,8}^{3}\vec{e}_{24} \ .$$

Then, corresponding to the dyadic $\overline{\overline{\Phi}}_{18}$ we have the matrix:

$$m\begin{bmatrix} O & -D_{1,1}^{3} & D_{1,1}^{2} \\ D_{1,1}^{3} & O & -D_{1,1}^{1} \\ -D_{1,1}^{2} & D_{1,1}^{1} & O \end{bmatrix}\begin{bmatrix} 1 & -\gamma & \beta \\ \gamma & 1 & -\alpha \\ -\beta & \alpha & 1 \end{bmatrix}\begin{bmatrix} O & -D_{8,8}^{3} & D_{8,8}^{2} \\ D_{8,8}^{3} & O & -D_{8,8}^{1} \\ -D_{8,8}^{2} & D_{8,8}^{1} & O \end{bmatrix} = \left[\Phi_{18}\right]_{ij}$$

The decomposition of the middle matrix as the sum of the identity plus a "small" skew-symmetric matrix shows that Φ_{18} may be expressed as the sum of a constant plus a small time-varying matrix. A similar result holds for the bordering matrices P in Eq. (4.2) since their entries consist of direction cosines. Hence, under the assumption that all relative rotational deflections are small, the entire augmented matrix on the left in Eq. (4.2) may be written as $A(I + \epsilon)$, where A is a constant matrix, $\epsilon(t)$ is a small time-varying matrix and I is the identity matrix of proper dimension. Its inverse can then be closely approximated by $(I - \epsilon)A^{-1}$.

Section 5
EXPERIMENT POINTING SYSTEM CABLING HYSTERESIS

Electrical cabling across the pivot axes of the vernier gimbal system adds to the spring rates contributed by the flexure pivots. This effect can be overcome by increasing the gain, and consequently the bandwidth, of the gimbal control loop. The increase in bandwidth permits more noise from the sensors to be transmitted to the spar, thus increasing the rms error.

In addition, there is a hysteresis in the torques induced by the cabling which results from plasticity in the insulation and slippage between layers of cabling. Tests on various configurations of cables have established the existence of this effect and its nature. The effect can be described approximately by spring rates K_w and K_h and a breakaway angle θ_h. A typical contour of torque on the cable versus the relative rotation between its ends is shown in Fig. 5-1.

Two conditions can exist. If θ_m is the maximum excursion of the gimbals and if θ_h is greater than θ_m, the breakaway condition cannot occur and the control behaves as if a spring rate of magnitude $(K_w + K_h)$ acts in parallel with the spring rate induced by the flexure pivots. With θ_h less than θ_m, breakaway is possible; both the cabling spring rate and a shifting position of zero torque are present. For the former condition, the undamped natural frequency ω_o must be made such that

$$\omega_o^2 \geq \frac{J_s E_s}{(K_w + K_h + K_f)\, \theta_m}$$

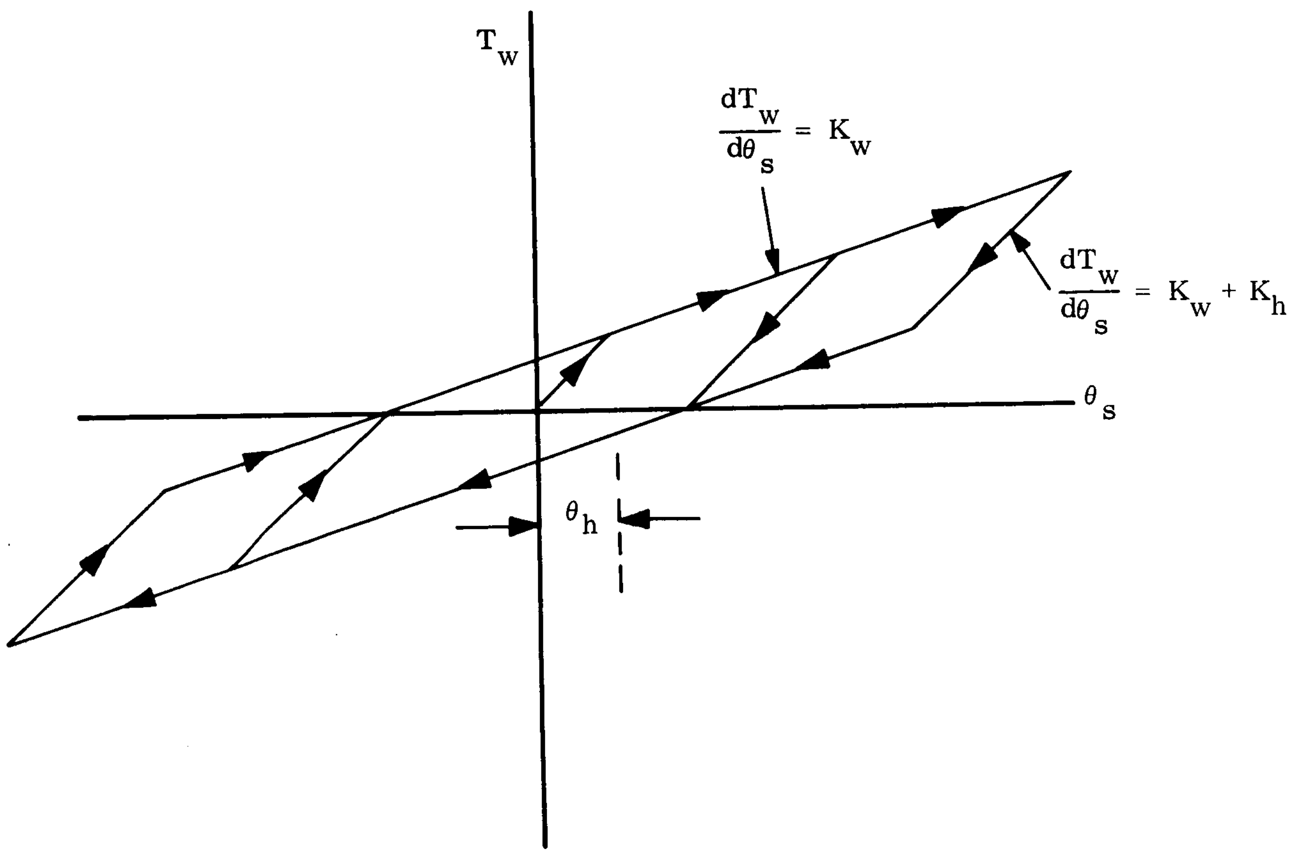

Fig. 5-1 Cabling Torque Hysteresis Contours

where

E_s = permissible steady state error at maximum excursion

J_s = moment of inertia of spar

K_f = spring rate of flexure pivots

For the latter condition,

$$\omega_o^2 \geq \frac{J_s E_s}{(K_w + K_f)\,\theta_m + K_h \theta_h}$$

From these results, it is concluded that hysteresis in the cabling does not degrade accuracy; however, the design must be made on the basis of the total spring rate of the cable $K_w + K_h$, and not on the basis of K_w alone.

Section 6
TOTAL ATM SIMULATOR

6.1 INTRODUCTION

The primary objective of this work is the definition of a Total ATM Simulator to be used as a tool to evaluate and optimize man's operation in the total integrated ATM control system and the onboard experiments. These spacecraft systems, and the astronauts' interface with them, are fully described in subsection 6.2.

It is critical to have an operational simulator on line as soon as possible so that a systems evaluation can take place before the flight hardware is completely fabricated. It was necessary then to survey facilities for both computer availability, the space and support functions, and any simulation hardware which might be applicable. Such facilities are outlined in subsection 6.4.

6.2 MISSION ANALYSIS

ATM System consists of a carrier vehicle to which is attached a gimballed spar containing optical equipment for performing various solar astronomy experiments from orbit. The carrier may be either the ascent stage of the Lunar Module (LM) or this vehicle docked by means of a multiple docking adapter (MDA) to an aggregation of other flight modules, principally the Command and Service Modules (CSM) and the S-IVB stage of the Saturn booster. This latter configuration is called the Cluster. See Fig. 6-1.

The carrier attitude is controlled by three, double-gimballed, orthogonally mounted control moment gyros (CMG's) and a valve/jet, mass expulsion, reaction control system (RCS). The RCS is located on the LM and is used for basic control of the carrier.

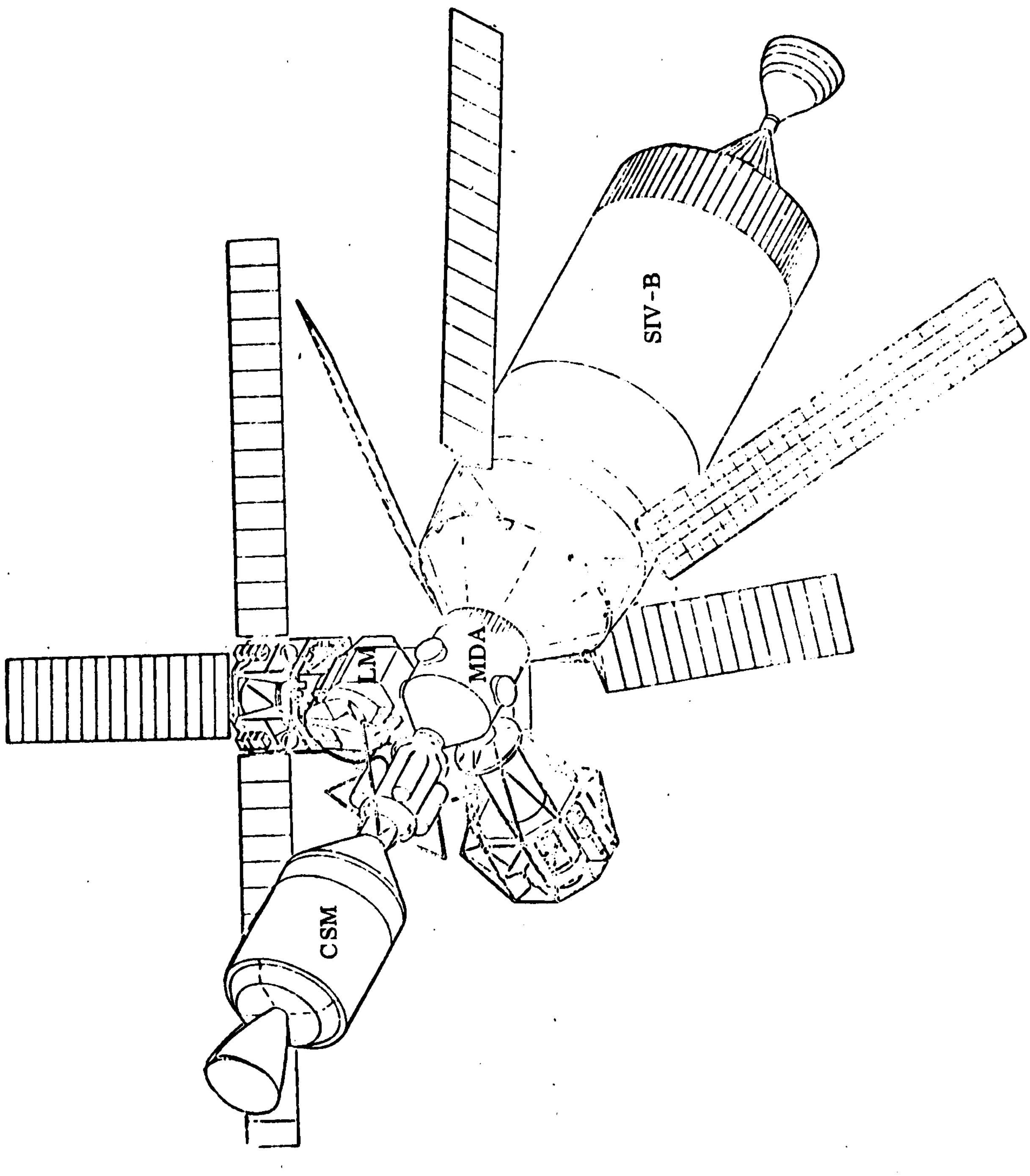

Fig. 6-1 Cluster Configuration

Operating within a deadband built into the jet reaction system is the secondary CMG system which is designed to absorb cyclic disturbances and provide low residual rates. The CMG's are located on the portion of the carrier designated as the Rack. Unloading or dumping of the momentum of the CMG's and certain mission requirements, such as stationkeeping and docking, are functions of the RCS. The momentum from cyclic and noncyclic disturbances accumulated by the CMG's may also be dumped by attitude maneuvers, which alter the gravitational torques acting on the vehicle. Gross vehicle orientations in pitch and yaw are referenced to a sun line established by a coarse sun sensor (CSS). The gross vehicle roll attitude is referenced to a Star Tracker (ST) that is trained on the star Canopus. The carrier control system is also provided with three, body-mounted, single-degree-of-freedom, rate integrating gyros for basic or inner-loop reference. Rate damping of the carrier motion is also derived from these gyros.

The Spar possesses its own attitude control system to permit the extremely fine pointing accuracy required by the telescope. In order that the Spar have maximum isolation from disturbance torques, it is articulated with respect to the Rack attached to the LM. The Spar is actuated by torque motors mounted between the gimbal system and the Rack. Two of the gimbal axes (pitch and yaw) are hinged on flexure pivots. The third axis (roll) is not controlled other than for being moved from one fixed orientation to another. The Spar is locked within the Rack during initial attitude acquisition of the entire vehicle, i.e., Cluster, CSM/LM/ATM, or free LM/ATM. When the entire vehicle has been brought to the proper sun-Canopus orientation, and the Rack is in the automatic attitude hold mode, the Spar-Rack locks of the mechanical cage are de-energized and fine pointing takes place. In the Spar's attitude control system, called either the Fine Pointing System (FPS) or Experiment Pointing System (EPS), pitch and yaw deviations from the sun line are sensed by a precision or fine sun sensor (FSS) capable of tracking the center of the sun. This sensor has manually controllable optical wedges in its field of view to permit offset pointing. Rate damping, on the pitch and yaw axes is provided by two precision rate integrating gyros mounted on the Spar. No independent automatic roll control system is provided to the Spar. Primary roll reference is obtained from the Canopus sensor on the Rack. However, the Spar does have a roll degree of freedom within the Rack. Spar roll is controlled manually by the astronauts and referenced by a precision roll angle pickoff between the Spar and Rack.

The overall ATM control system, showing all three torquing systems together with their controls, is presented in the functional block diagram, Fig. 6-2. One channel of the ATM/Carrier CMG Control Loop is shown in Fig. 6-3. Also, a schematic of one channel of the ATM/Spar Flex Gimbal Control Loop is shown in Fig. 6-4.

6.2.1 ATM Control System

6.2.1.1 ATM Control System Operational Sequences and Mission or Task Descriptions

Carrier Vehicle Attitude. At first the Spar will be rigidly locked to a neutral position within the Rack by means of a mechanical caging device. The mechanical cage will be maintained until the Rack, i.e., the carrier vehicle, has been oriented to the desired attitude, which consists of pointing roughly at the sun while maintaining a roll reference using the Star Canopus.

Gross orientations are performed by using manual signal transmitters to torque the three, uncaged, body-mounted, single-degree-of-freedom rate integrating gyros provided for carrier attitude reference. Signals from the gyros are applied through compensation and deadband circuits to the reaction jet valves and nozzles. The same gyro signals are processed to generate CMG control signals. Since the CMG control signals are applied directly to the CMG's while the reaction jet signals are passed through a deadband circuit before being applied to the reaction jet valve drive amplifiers, it is clear that the CMG's will act as a vernier moment generating system within the deadband of the RCS. When the CMG's are not capable of handling a particular disturbance, they will overload, that is, drive to their gimbal limits or drive to an orientation where their spin axes are parallel. When this occurs, the RCS is called into play.

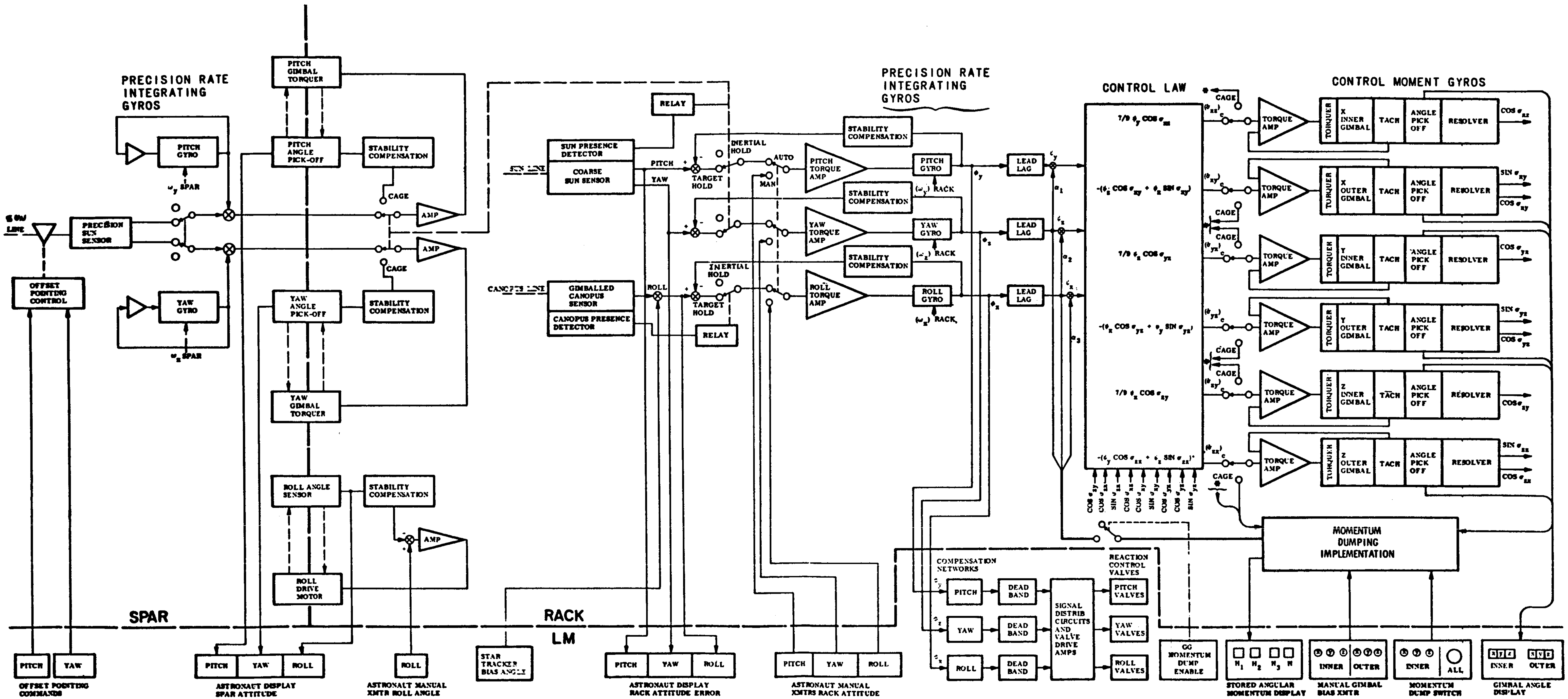

Fig. 6-2 ATM Control System

FOLDOUT FRAME 1

FOLDOUT FRAME 2

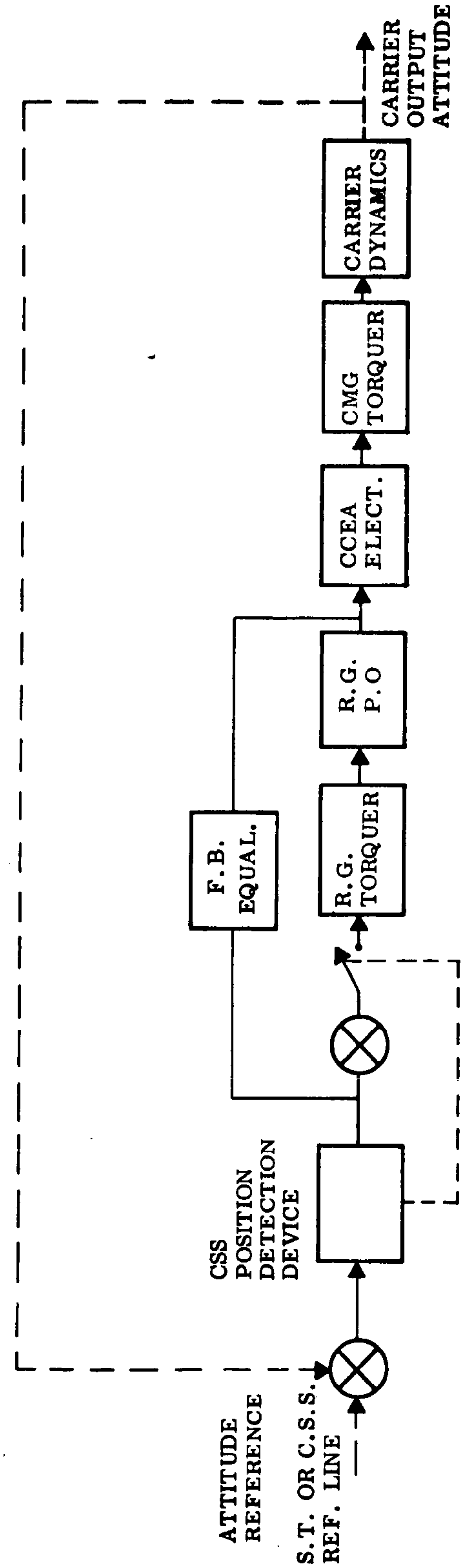

Fig. 6-3 ATM/Carrier CMG Control Loop (P, Y, R Axes)

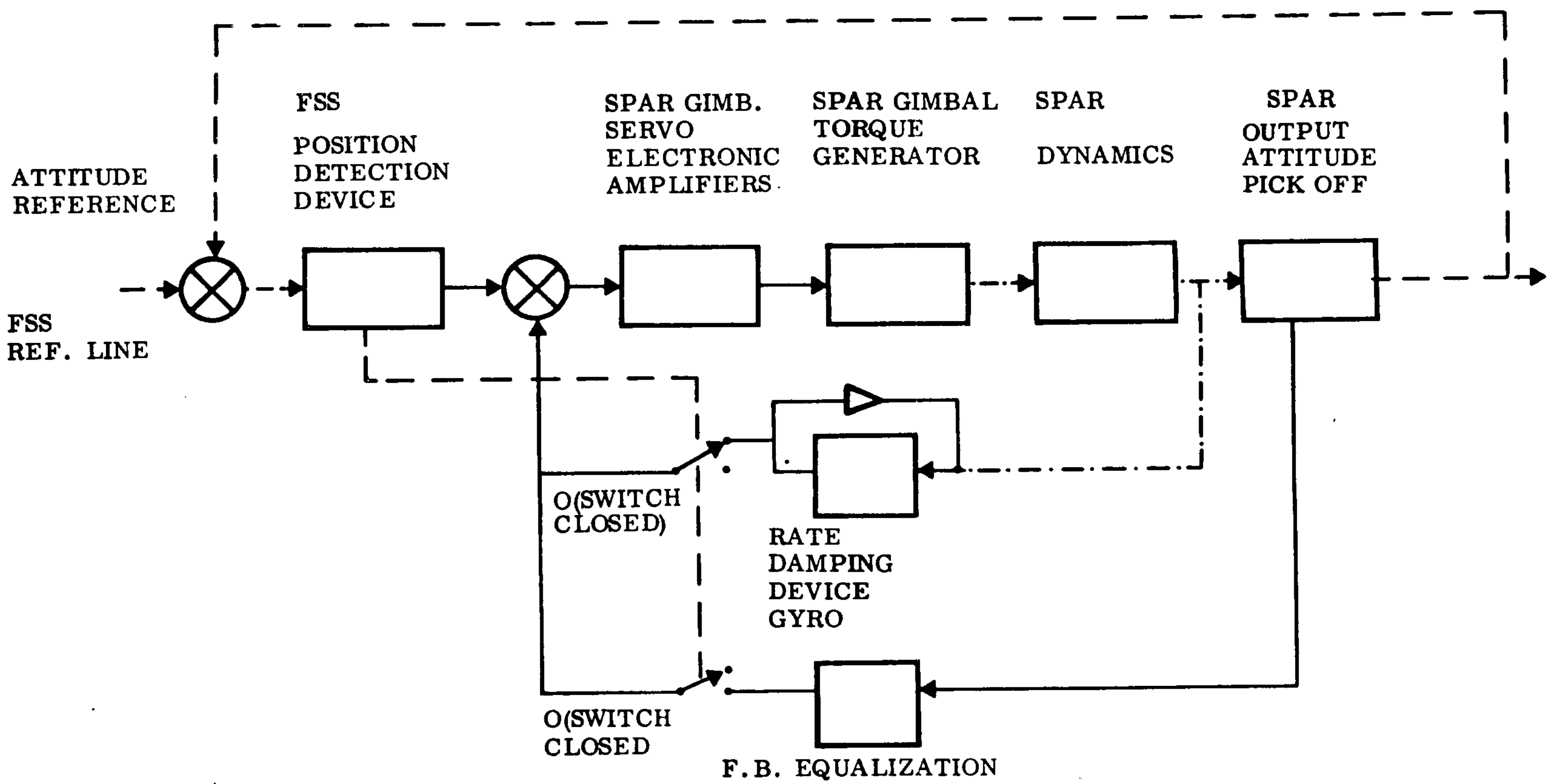

Fig. 6-4 ATM/Spar Flex Gimbal Control Loop (P and Y Axes)

Initial sun acquisition consists of manually driving the vehicle roll axis to rough alignment with the sun line. When the vehicle roll axis has been brought sufficiently near the sun line, the "sun presence detector" in the sun sensor will produce a signal used to actuate the MAN-AUTO relay to automatic. Signals proportional to angular deviation from the sun line, developed within the sun sensor, are then applied through the relay to torque the uncaged, vehicle attitude, reference gyros. This procedure slaves the pitch and yaw axes of the ATM carrier to the sun line.

During periods of occultation of the sun, the absence of a signal from the "sun presence detector" releases the relay, and attitude reference reverts to the gyros alone. The vehicle attitude reference gyros will hold the vehicle so that the sun, when next seen, is within the field of view of the acquisition sun sensor. Thus, the sun will be automatically reacquired each time the sun rises.

The proposed reference for roll about the sun line is a Canopus tracker mounted on the Rack. Figure 6-5 shows the geometry of the ATM in orbit when the LM/ATM is docked to the Cluster. The nominal flight mode is assumed to be one that keeps the longitudinal axis (x_2) of the Cluster in the orbit plane. This is required to minimize large unidirectional torques, which would act with this axis out of the orbit plane. The Cluster remains essentially fixed relative to the sun, with the CMG's absorbing and releasing the cyclic angular momentum accrued from the gravity-gradient torques acting in pitch.

The roll-sensing geometry of the ATM in orbit is shown in Fig. 6-6. To accommodate the flight mode, the tracker must be gimballed through ± 67 deg on one axis (the outer) and ± 15 deg on the other (the inner) to maintain a view of Canopus. The inclination of the orbit, i, and the regression of the line of nodes relative to the ecliptic establish the limits of travel of the outer gimbal angle α_s. Similarly the earth's revolution about the sun determine the limits of travel of the inner gimbal angle β_s.

The angle α_s is computed and used to bias the signal from one gimbal of the star tracker. The difference between this gimbal angle and the computed α_s is used as

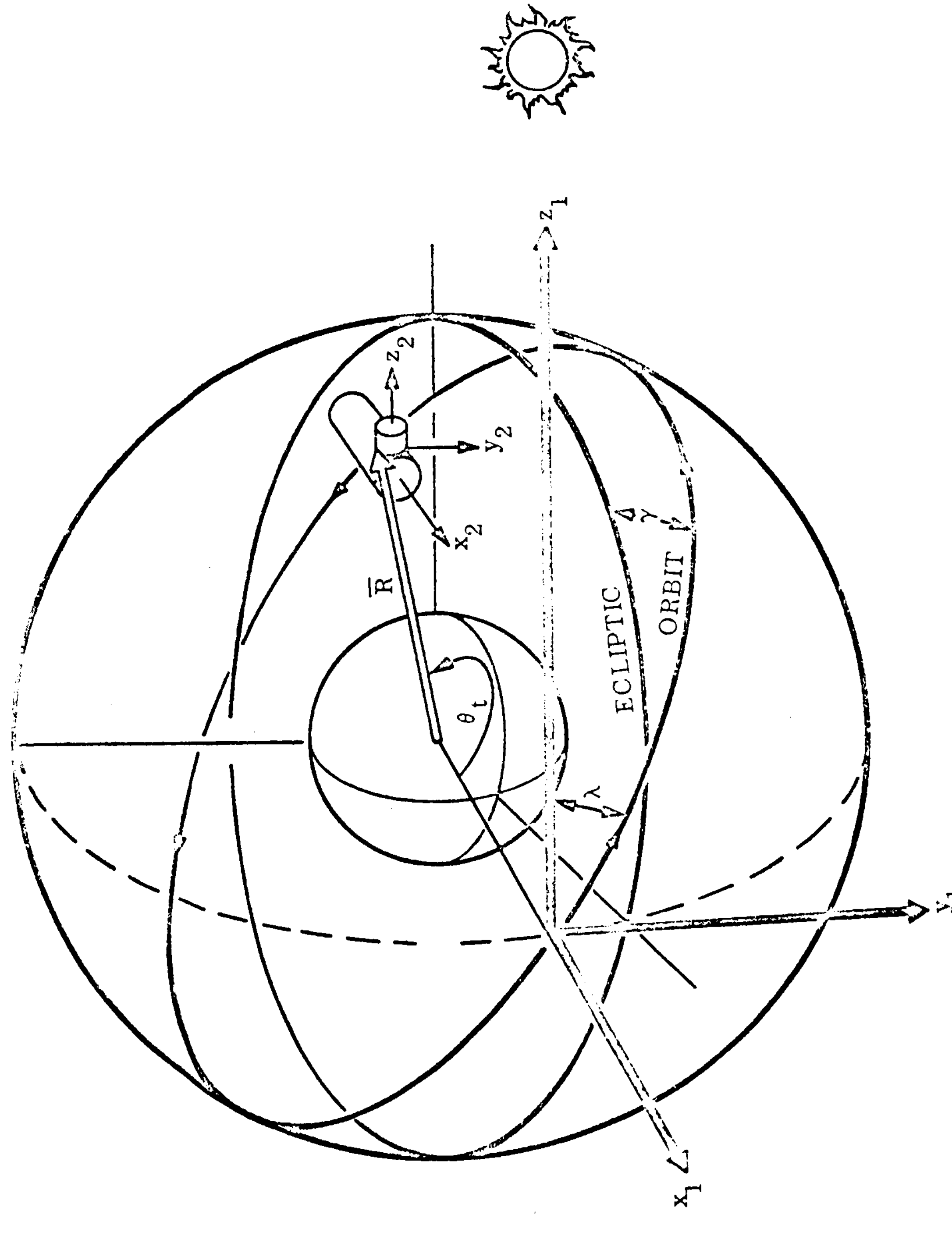

Fig. 6-5 Nominal ATM Flight Mode

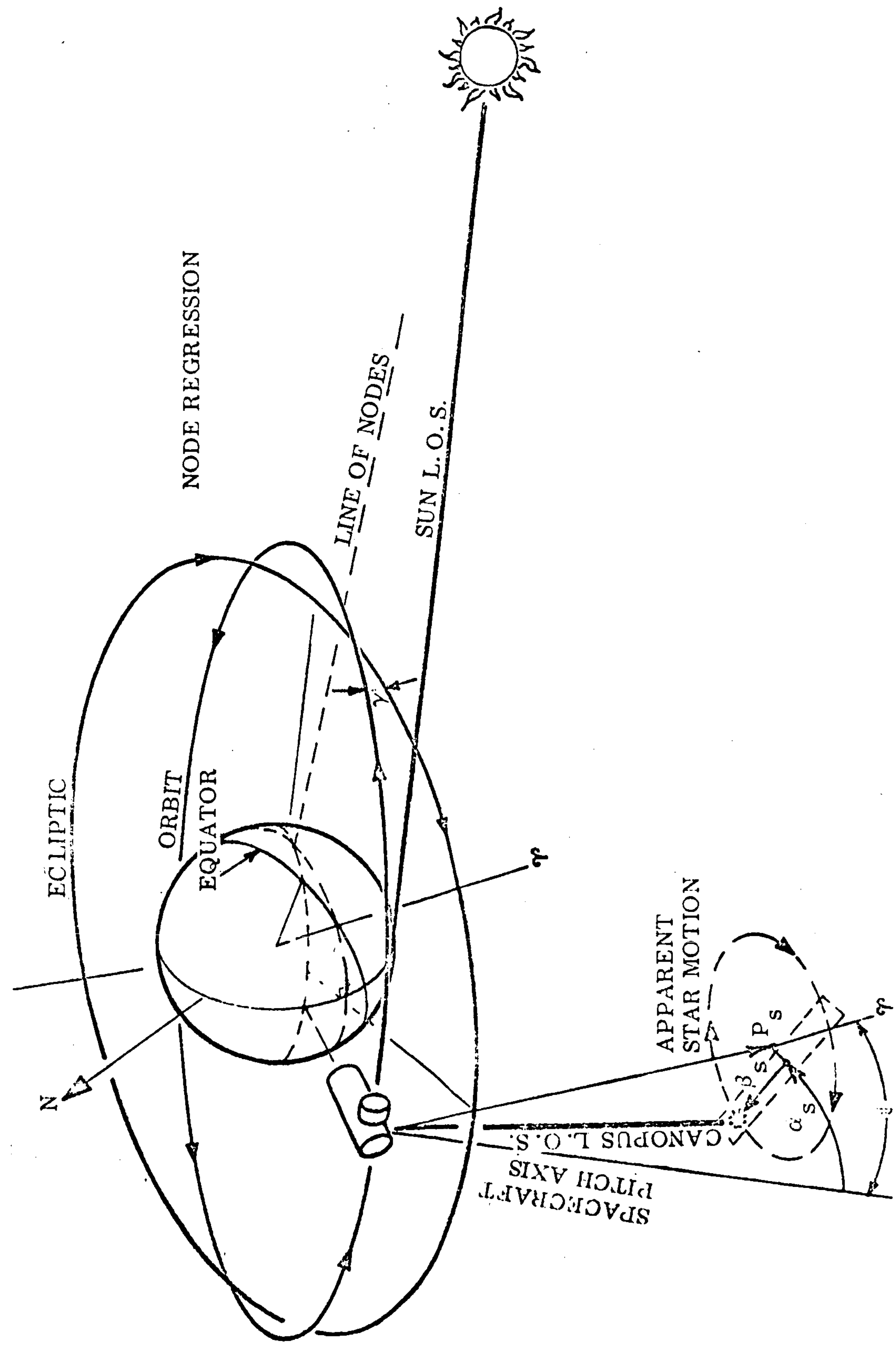

Fig. 6-6 Roll-Sensing Geometry

the roll reference for the Cluster control system. Since α_s varies with time, it must be updated periodically. The frequency of updating and the accuracy of its computation are not critical, however, since a slight deviation of the longitudinal axis from the orbit plane is tolerable.

The roll angle of the Spar is referenced to the Rack by a precision angle pickoff, as is the gimbal angle on the star tracker, which moves in the direction of α_s. The difference between the angles gives a precise measure of the Spar's roll angle relative to inertial space if only the time of the year is known. The precision of this measurement is limited by the accuracy of the angle pickoffs on the Spar and tracker gimbal; these pickoffs can conveniently be made less than 10 arc sec.

The line of sight to Canopus becomes occulted by the earth during a part of each orbit. A Canopus presence detector removes the signal from the star tracker, leaving the CMG's to maintain attitude on the basis of the roll-reference gyro, which is continuously torqued to the required orientation by the signal from the star tracker when Canopus is in view. To facilitate automatic reacquisition of Canopus after occultation, the Canopus presence detector should also actuate a lock to cage the tracker gimbals during the period of occultation.

The primary source of actuation of the carrier control system during ATM operation is the three CMG's. The reaction jets may be used for momentum dumping and as backup actuators if the CMG's fail. However, after the desired carrier vehicle orientation has been achieved and during normal ATM operations, the RCS should be inactive. When the LM/Rack is operated with the Cluster configuration oriented to point the Rack to the sun, large aerodynamic and gravity-gradient torques cause angular momentum to be accumulated by the CMG's. These are for the most part cyclic torques for which the average change in angular momentum is zero. One component of the gravity-gradient torque is not cyclic and certain deviations of the Cluster from a cylindrical torque. Also, magnetic torques may exist whose average value is not zero. Consequently, angular momentum is accumulated and must be dumped periodically. A method for dumping the accumulated angular momentum using the gradient of the gravity field itself in conjunction with the CMG's has been carefully studied. The gravity-gradient method can be implemented as either a manual or an automatic procedure and requires only small changes from the nominal flight mode for momentum control. These may be made when the spacecraft is on the dark side of the orbit and the ATM is not operating, or they may be made throughout the orbit with the Spar attitude control system correcting for the pointing errors they produce.

ATM Spar Fine Pointing System. As previously mentioned, the Spar possesses its own attitude control system to permit the extremely fine pointing accuracy required by the telescope. Pitch and yaw deviations from the sun line are sensed by a precision sun sensor capable of tracking the center of the sun. This sensor is provided with manually controllable optical wedges in its field of view to permit offset pointing.

Recall that the Spar is locked within the Rack during initial attitude acquisition of the entire vehicle. When it has been brought to the proper sun-Canopus orientation and the Rack is in the automatic attitude hold mode, the Spar-Rack locks are de-energized and fine pointing takes place. Signals from the precision sun sensor located on the Spar are fed to torque amplifiers, which drive pitch and yaw gimbal torquers. Moments are developed by the torquers, which are mounted on the gimbals holding the Spar to the Rack. Thus, the Spar is pointed in a vernier manner by being torqued against the inertia of the Rack. The resulting disturbances in the Rack are absorbed by the previously described CMG system. Rate damping is provided by two precision rate integrating gyros mounted on the Spar.

Ultimate pointing is achieved by means of the manually controllable optical wedges. The results are observed through a bore-sighted vidicon sun viewer.

Typical Control Procedures and Experiment Timelines. Typical control procedures and events are itemized in Table 6-1 for the normal (non-occulted) operation and Table 6-2 describes a set of events for a perturbed (occulted) operation, for the ATM control system mechanization shown in Fig. 6-2. The ATM/Carrier CMG control loop is shown in Fig. 6-3.

Table 6-1

NORMAL ATM CONTROL SYSTEM SEQUENCE

Control Function	Cause	Effect	Axes	Accuracy
(1) Control Mode Select	Manual selection	Selects rack gyro torquing source	P, Y, R	–
(2) Vehicle Gross Pointing	Manual commands Manual commands	Torques rack gyros Torques rack gyro	P, Y R	$<$ 20 deg (CSS FOV) $<$1 deg (ST ACQ FOV)
(3) Control Mode Switching	Manual event	Mode switch set to "Auto."	P, Y, R	–
(4) Vehicle Coarse Pointing	CSS acquisition	Switches to "track" mode and torques rack gyros	P, Y	$<$2.5 deg (FSS FOV)
(5) Vehicle Fine Pointing	ST acquisition	Switches to "track" mode and torques rack gyro	R	7.5 arc min (ST null)
(6) ATM fine Pointing	FSS acquisition	Switches to "track" mode and torques Spar gimbal torquers	P, Y	2.5 arc sec (FSS null)

Table 6-2

PERTURBED ATM CONTROL SYSTEM SEQUENCE

Solar Occultation (FSS assumed to lose sun signal first and CSS second):

(1) FSS Sun Sensor loses its input reference signal (sunlight).

(2) FSS resets to Acquisition mode and Spar flex gimbal loops now operated in Rate Control mode via rate gyros.

(3) CSS loses its input reference signals in its pitch and yaw axes.

(4) CSS Sun Presence Detector switches its relay to Inertial Hold mode.

(5) Precision pitch and yaw gyro control loops are switched from the CSS sunline and gyro caging feedback signal summing points to Inertial Hold mode.

(5a) Spar pitch and yaw servo control loop switched from FSS sunline reference and rate gyro signal summing points to Cage mode.

(6) Precision pitch and yaw gyros now operating in Attitude mode.

(6a) Spar pitch and yaw flex gimbal servos slaved to their respective gimbal attitude pickoff signals.

(7) Carrier pitch and yaw CMG control loops slaved to the precision pitch and yaw gyro gimbals, respectively.

(7a) Spar pitch and yaw gimbals driven to their "null" attitude angle.

Stellar Occultation:

(1) Star tracker (ST) loses its input reference signal (star light).

(2) ST Star Presence Detector switches its relay to Inertial Hold mode.

(3) Roll precision gyro control loop switched from Star Line and gyro caging feedback signal summing points to Inertial Hold mode.

(4) Precision roll gyro now operating in Attitude mode.

(5) ST gimbals now slaved to precision roll gyro gimbal.

(6) Carrier roll CMG control loop slaved to precision roll gyro gimbal.

The ATM Spar pitch and yaw fine pointing servomechanisms are attitude (position) servos and are each rate damped by mechanization of rate (electrically caged) precision gyros. The basic control loop is shown in Fig. 6-4.

Detailed timeline studies of the procedures to be followed by the astronauts during the first orbit and a subsequent representative experiment are given in Appendix A. The timeline of the dark-side activities is also included.

6.2.1.2 ATM Control System Analyses

The conceptual design and analysis of the control system for the ATM are presented in detail in Refs. 6-1 and 6-2. Only summaries of the major components are presented in this subsection. A brief discussion and rationale are given in a later section to explain those concepts and problem areas not included.

Dynamics of the ATM System. The complete ATM system consists of two bodies, the telescope and the carrier, and involves five interacting axes of control. To evaluate in detail the stability and accuracy of the ATM control system and to have a base upon which an overall ATM mission simulation can be made, the dynamics, kinematics, and feedback control laws for the entire system must be represented in a mathematical model. This model is derived in subsection 6 of Ref. 6-1 and includes the coupled equations of motion for the two bodies, the effects of three double-gimballed angular momentum vectors in one of the bodies, a description of gravitational torques and their variation with respect to vehicle attitude and orbital parameters, and a representation of a compliant structure connecting the two bodies. The notation and definitions are given in Table 6-3. The attitude reference frames, a mathematical flow chart (which contains the system's differential equation's of motion), and a summary of the torques acting on the system are given in Figs. 6-7, 6-8, and 6-9, respectively. The three ATM torquing control systems are shown in Fig. 6-2.

CMG Dynamics and Control Laws. The dynamics of the CMG's were derived in Section 5 of Ref. 6-1. It was convenient to adopt a vector and matrix notation to

Table 6-3

NOTATION AND DEFINITIONS

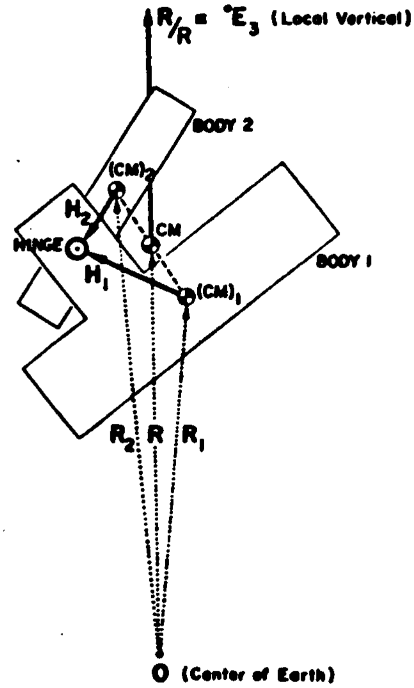

$(CM)_1$, $(CM)_2$, (CM)	:	center of mass of body 1,2 and composite center of mass
m_1, m_2	:	mass of body 1,2
$m = m_1 + m_2$	:	total mass (<u>Note</u>: m_1 includes masses of CMG's)
$\bar{m} = m_1 m_2/m$	:	reduced mass
$\vec{R}_1$, $\vec{R}_2$, $\vec{R}$	:	radius vector from Earth's center to $(CM)_1$, $(CM)_2$, (CM)
$\vec{H}_1$, $\vec{H}_2$	:	body-fixed hinge vector, from $(CM)_1$, $(CM)_2$ to hinge
$\vec{\omega}_1$, $\vec{\omega}_2$	:	angular velocity vector of body 1,2
Φ_1, Φ_2	:	inertia dyadic of body 1,2 about $(CM)_1$, $(CM)_2$
Φ_{11}, Φ_{12}, Φ_{21}, Φ_{22}	:	inertia-type dyadics defined by (I: identity dyadic): (a,b = 1,2) $\Phi_{ab} = \bar{m}[(\vec{H}_b \cdot \vec{H}_a)I - \vec{H}_b \vec{H}_a]$
Φ'_{11}, Φ'_{22}	:	"reduced inertia" dyadic for body 1,2 defined by: $\Phi'_{11} = \Phi_1 + \Phi_{11}$ and $\Phi'_{22} = \Phi_2 + \Phi_{22}$
Φ'_{12}, Φ'_{21}	:	"hinge-interaction" inertia dyadics defined by: $\Phi'_{12} = -\Phi_{12}$ and $\Phi'_{21} = -\Phi_{21}$
$\vec{F}^H$	:	reactive hinge force on body 1, transmitted through the hinge
$\vec{F}_1^G$, $\vec{F}_2^G$	:	resultant gravitational force on body 1,2
$\vec{F}_1$, $\vec{F}_2$	:	resultant of all <u>other</u> forces on body 1,2 (e.g., aero-dynamic, solar radiation pressure, etc.)
$\vec{T}^c$	:	reactive constraint torque on body 1, transmitted through the hinge; because the relative rotational motion between body 1 and 2 occurs through a two-axis gimbal, that motion has only two degrees of freedom, with the constraint torque axis along the common perpendicular to the gimbal axes
$\vec{T}^H$	:	reactive hinge torque on body 1, exclusive of $\vec{T}^c$, transmitted through the hinge and having components along the gimbal axes (e.g. torques arising from flexure pivots, gimbal motors for spar control, etc.)
$\vec{T}_1^{GG}$, $\vec{T}_2^{GG}$	:	gravity gradient torque on body 1,2
$\vec{T}_1$, $\vec{T}_2$	:	resultant of all <u>other</u> torques on body 1,2
$\vec{T}^{CMG}$	:	torque on body 1 produced by the Control Moment Gyros
R_1, R_2, R	:	magnitudes $\lvert\vec{R}_1\rvert$, $\lvert\vec{R}_2\rvert$, $\lvert\vec{R}\rvert$ of the radius vectors defined above
R_E	:	Earth radius
g	:	gravitational acceleration at surface of the Earth
Ω_0	:	mean orbital rate
ϵ	:	orbit eccentricity
θ_t	:	true anomaly

$G = gR_E^2/R^3 = \Omega_0^2 (1 - \epsilon^2)^{-3} (1 + \epsilon \cos \theta_t)^3$

ORTHONORMAL FRAMES, ROTATION MATRICES[1] & RELATED COMPONENTS

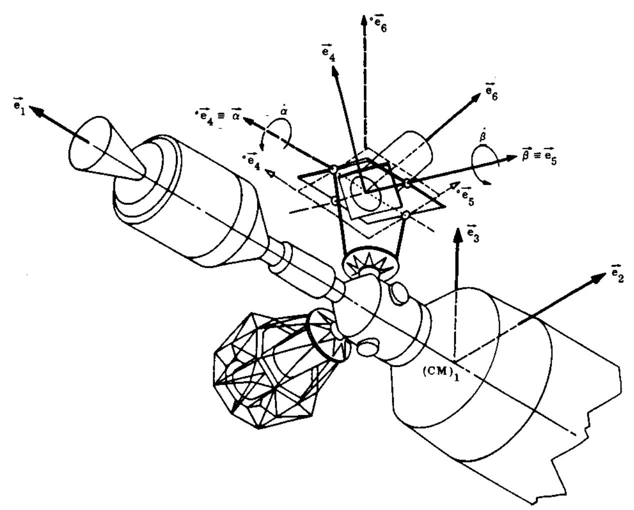

$[{}^{o}A_{ij}]$: Inertial Attitude matrix for body 1

$[A_{ij}]$: Attitude matrix for body 1 relative to Earth pointing Orbiting Reference Frame

$[G_{ij}]$: Gimbal orientation matrix (G_{ij}'s input constants) specifying nominal orientation of body 2 relative to body 1.

$[B_{ij}]$: Relative attitude matrix specifying orientation of body 2 relative to its nominal orientation.

$[C_{ij}] = [[BG]_{ij}]$: Relative attitude matrix specifying orientation of body 2 relative to body 1.

$[[CA]_{ij}]$: Attitude matrix for body 2 relative to Earth pointing Orbiting Reference Frame

$[[{}^{o}CA]_{ij}]$: Inertial Attitude matrix for body 2.

[1]NOTE: The various parametrizations and Euler angle factorizations used in the time-varying matrices above are given in Fig. 6-2

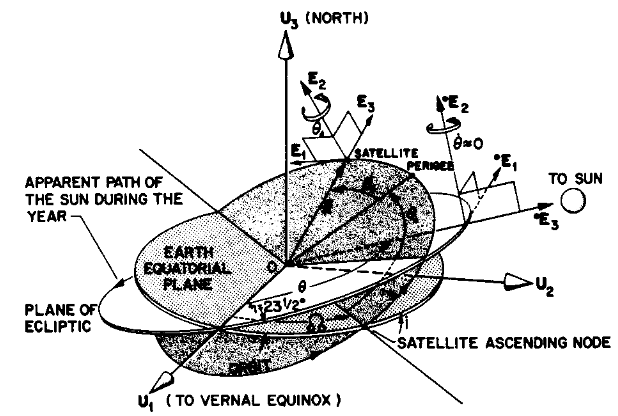

$\{e_1, e_2, e_3,\}$: Frame fixed in body 1

$\{e_4, e_5, e_6,\}$: Frame fixed in body 2

$\{{}^{o}e_4, {}^{o}e_5, {}^{o}e_6,\}$: Nominal alignment of $\{e_4, e_5, e_6,\}$, i.e. position of body 2 relative to body 1 for which gimbal angles at hinge are in their rest (zero) position.

Angular Velocity Vector Components

$\omega_1 = \omega_1 e_1 + \omega_2 e_2 + \omega_3 e_3$

$\omega_2 = \omega_4 e_4 + \omega_5 e_5 + \omega_6 e_6$

$$\begin{bmatrix} e_1 \\ e_2 \\ e_3 \end{bmatrix} = \begin{bmatrix} {}^{o}A_{11} & {}^{o}A_{12} & {}^{o}A_{13} \\ {}^{o}A_{21} & {}^{o}A_{22} & {}^{o}A_{23} \\ {}^{o}A_{31} & {}^{o}A_{32} & {}^{o}A_{33} \end{bmatrix} \begin{bmatrix} {}^{o}E_1 \\ {}^{o}E_2 \\ {}^{o}E_3 \end{bmatrix} = \begin{bmatrix} A_{11} & A_{12} & A_{13} \\ A_{21} & A_{22} & A_{23} \\ A_{31} & A_{32} & A_{33} \end{bmatrix} \begin{bmatrix} E_1 \\ E_2 \\ E_3 \end{bmatrix}$$

$$\begin{bmatrix} {}^{o}e_4 \\ {}^{o}e_5 \\ {}^{o}e_6 \end{bmatrix} = \begin{bmatrix} G_{11} & G_{12} & G_{13} \\ G_{21} & G_{22} & G_{23} \\ G_{31} & G_{32} & G_{33} \end{bmatrix} \begin{bmatrix} e_1 \\ e_2 \\ e_3 \end{bmatrix}$$

$$\begin{bmatrix} e_4 \\ e_5 \\ e_6 \end{bmatrix} = \begin{bmatrix} B_{11} & B_{12} & B_{13} \\ B_{21} & B_{22} & B_{23} \\ B_{31} & B_{32} & B_{33} \end{bmatrix} \begin{bmatrix} {}^{o}e_4 \\ {}^{o}e_5 \\ {}^{o}e_6 \end{bmatrix} = \begin{bmatrix} C_{11} & C_{12} & C_{13} \\ C_{21} & C_{22} & C_{23} \\ C_{31} & C_{32} & C_{33} \end{bmatrix} \begin{bmatrix} e_1 \\ e_2 \\ e_3 \end{bmatrix}$$

$$\begin{bmatrix} C_{11} & C_{12} & C_{13} \\ C_{21} & C_{22} & C_{23} \\ C_{31} & C_{32} & C_{33} \end{bmatrix} \stackrel{def}{\equiv} \begin{bmatrix} B_{11} & B_{12} & B_{13} \\ B_{21} & B_{22} & B_{23} \\ B_{31} & B_{32} & B_{33} \end{bmatrix} \begin{bmatrix} G_{11} & G_{12} & G_{13} \\ G_{21} & G_{22} & G_{23} \\ G_{31} & G_{32} & G_{33} \end{bmatrix}$$

$$\begin{bmatrix} e_4 \\ e_5 \\ e_6 \end{bmatrix} = \begin{bmatrix} [{}^{o}CA]_{11} & [{}^{o}CA]_{12} & [{}^{o}CA]_{13} \\ [{}^{o}CA]_{21} & [{}^{o}CA]_{22} & [{}^{o}CA]_{23} \\ [{}^{o}CA]_{31} & [{}^{o}CA]_{32} & [{}^{o}CA]_{33} \end{bmatrix} \begin{bmatrix} {}^{o}E_1 \\ {}^{o}E_2 \\ {}^{o}E_3 \end{bmatrix} = \begin{bmatrix} [CA]_{11} & [CA]_{12} & [CA]_{13} \\ [CA]_{21} & [CA]_{22} & [CA]_{23} \\ [CA]_{31} & [CA]_{32} & [CA]_{33} \end{bmatrix} \begin{bmatrix} E_1 \\ E_2 \\ E_3 \end{bmatrix}$$

$$\begin{bmatrix} [{}^{o}CA]_{11} & [{}^{o}CA]_{12} & [{}^{o}CA]_{13} \\ [{}^{o}CA]_{21} & [{}^{o}CA]_{22} & [{}^{o}CA]_{23} \\ [{}^{o}CA]_{31} & [{}^{o}CA]_{32} & [{}^{o}CA]_{33} \end{bmatrix} \stackrel{def}{\equiv} \begin{bmatrix} C_{11} & C_{12} & C_{13} \\ C_{21} & C_{22} & C_{23} \\ C_{31} & C_{32} & C_{33} \end{bmatrix} \begin{bmatrix} {}^{o}A_{11} & {}^{o}A_{12} & {}^{o}A_{13} \\ {}^{o}A_{21} & {}^{o}A_{22} & {}^{o}A_{23} \\ {}^{o}A_{31} & {}^{o}A_{32} & {}^{o}A_{33} \end{bmatrix}$$

$$\begin{bmatrix} [CA]_{11} & [CA]_{12} & [CA]_{13} \\ [CA]_{21} & [CA]_{22} & [CA]_{23} \\ [CA]_{31} & [CA]_{32} & [CA]_{33} \end{bmatrix} \stackrel{def}{\equiv} \begin{bmatrix} C_{11} & C_{12} & C_{13} \\ C_{21} & C_{22} & C_{23} \\ C_{31} & C_{32} & C_{33} \end{bmatrix} \begin{bmatrix} A_{11} & A_{12} & A_{13} \\ A_{21} & A_{22} & A_{23} \\ A_{31} & A_{32} & A_{33} \end{bmatrix}$$

$\{U_1, U_2, U_3,\}$: Geocentric inertial frame

$\{{}^{o}E_1, {}^{o}E_2, {}^{o}E_3,\}$: Sun pointing inertial reference frame

$\{E_1, E_2, E_3,\}$: Earth pointing Orbiting reference frame

(Angles related to orbit and sun position are described in Fig. 6-2)

MOMENTS AND PRODUCTS OF INERTIA

Inertias and Masses

Φ_1 : Central inertia dyadic of body 1

Φ_2 : Central inertia dyadic of body 2

m_1 : Mass of body 1

m_2 : Mass of body 2

$\bar{m}$: $(m_1 m_2)/(m_1 + m_2)$: reduced mass

Reduced Inertia Dyadics ($\mathbb{1}$: identity dyadic)

$\Phi'_{11} \stackrel{def}{\equiv} \Phi_1 + \bar{m} \; (H_1 \cdot H_1 \, \mathbb{1} - H_1 H_1)$

$\Phi'_{22} \stackrel{def}{\equiv} \Phi_2 + \bar{m} \; (H_2 \cdot H_2 \, \mathbb{1} - H_2 H_2)$

Hinge Interaction Inertia Dyadics

$\Phi'_{12} \stackrel{def}{\equiv} -\bar{m} \; (H_1 \cdot H_2 \, \mathbb{1} - H_1 H_2)$

$\Phi'_{21} \stackrel{def}{\equiv} -\bar{m} \; (H_2 \cdot H_1 \, \mathbb{1} - H_2 H_1)$

Components of Reduced Inertia Dyadics

$$\Phi'_{11} = [e_1 \; e_2 \; e_3] \begin{bmatrix} I_{11} & I_{12} & I_{13} \\ I_{21} & I_{22} & I_{23} \\ I_{31} & I_{32} & I_{33} \end{bmatrix} \begin{bmatrix} e_1 \\ e_2 \\ e_3 \end{bmatrix}$$

$$\Phi'_{22} = [e_4 \; e_5 \; e_6] \begin{bmatrix} I_{44} & I_{45} & I_{46} \\ I_{54} & I_{55} & I_{56} \\ I_{64} & I_{65} & I_{66} \end{bmatrix} \begin{bmatrix} e_4 \\ e_5 \\ e_6 \end{bmatrix}$$

Components of Hinge Interaction Inertia Dyadics

$$\Phi'_{12} = [e_1 \; e_2 \; e_3] \begin{bmatrix} I_{14} & I_{15} & I_{16} \\ I_{24} & I_{25} & I_{26} \\ I_{34} & I_{35} & I_{36} \end{bmatrix} \begin{bmatrix} e_4 \\ e_5 \\ e_6 \end{bmatrix}$$

$$\Phi'_{21} = [e_4 \; e_5 \; e_6] \begin{bmatrix} I_{41} & I_{42} & I_{43} \\ I_{51} & I_{52} & I_{53} \\ I_{61} & I_{62} & I_{63} \end{bmatrix} \begin{bmatrix} e_1 \\ e_2 \\ e_3 \end{bmatrix}$$

Hinge Vector Components $\quad H_1 = H_1 e_1 + H_2 e_2 + H_3 e_3 \quad H_2 = H_4 e_4 + H_5 e_5 + H_6 e_6$

hence:

$$\begin{bmatrix} I_{14} & I_{24} & I_{34} \\ I_{15} & I_{25} & I_{35} \\ I_{16} & I_{26} & I_{36} \end{bmatrix} = \begin{bmatrix} I_{41} & I_{42} & I_{43} \\ I_{51} & I_{52} & I_{53} \\ I_{61} & I_{62} & I_{63} \end{bmatrix} \stackrel{def}{\equiv} \bar{m} \begin{bmatrix} 0 & -H_6 & H_5 \\ H_6 & 0 & -H_4 \\ -H_5 & H_4 & 0 \end{bmatrix} \begin{bmatrix} C_{11} & C_{12} & C_{13} \\ C_{21} & C_{22} & C_{23} \\ C_{31} & C_{32} & C_{33} \end{bmatrix} \begin{bmatrix} 0 & -H_3 & H_2 \\ H_3 & 0 & -H_1 \\ -H_2 & H_1 & 0 \end{bmatrix}$$

Fig. 6-7 Attitude Reference Frames

FOLDOUT FRAME 1

FOLDOUT FRAME 2

PRECEDING PAGE BLANK NOT FILMED.

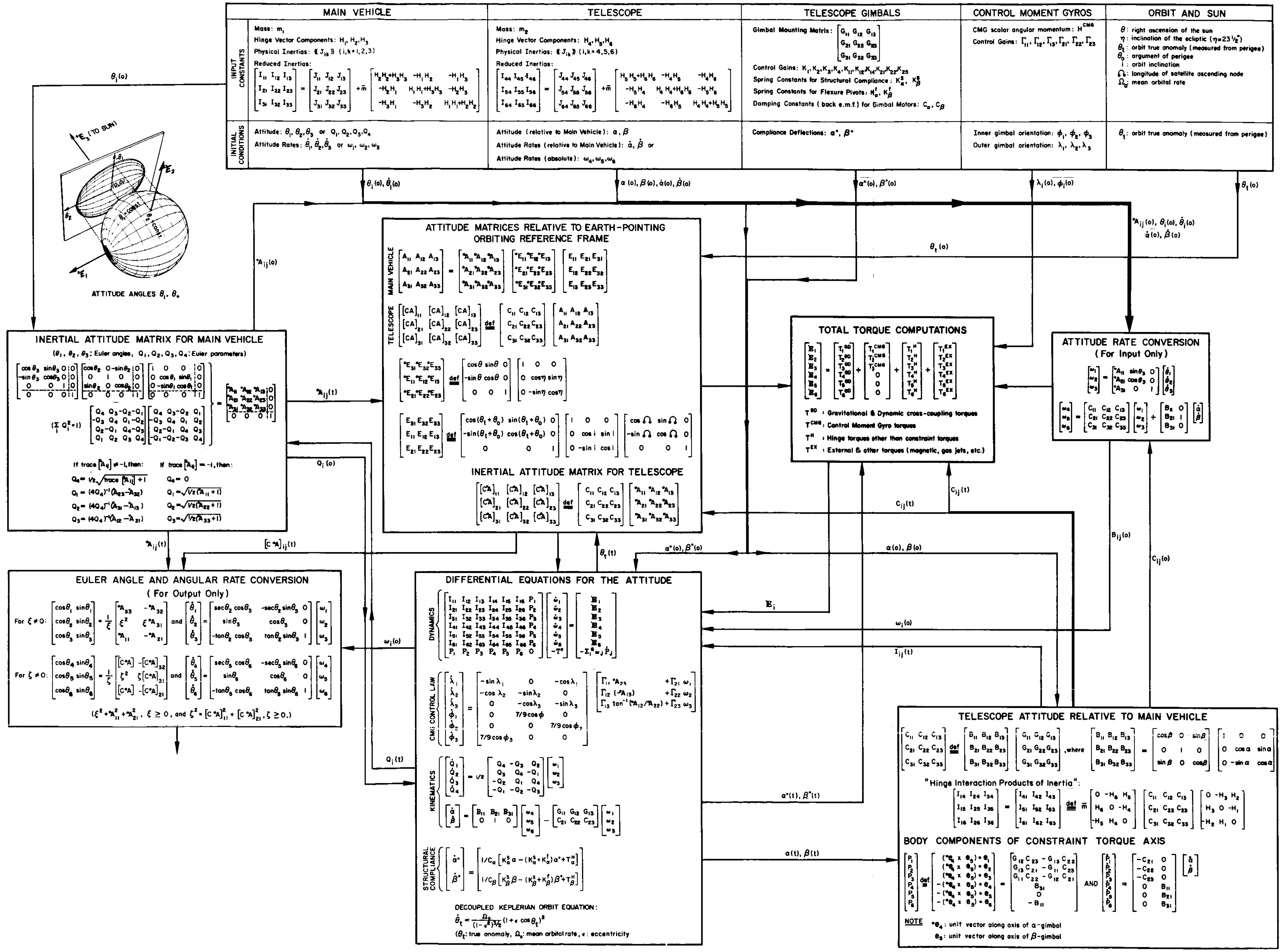

Fig. 6-8 Mathematical Flow Chart

FOLDOUT FRAME 1

FOLDOUT FRAME 2

PRECEDING PAGE BLANK NOT FILMED.

SUMMARY OF ALL MOMENTS AND TORQUES

(EXCLUDING CONSTRAINT TORQUES DUE TO TWO-AXIS GIMBALING AT THE HINGE)

$$\left(G \overset{\text{def}}{=} \frac{\Omega_0^2}{(1-\epsilon^2)^3} (1+\epsilon \cos\theta_t)^3 \right)$$

$$\begin{bmatrix} T_1^{GD} \\ T_2^{GD} \\ T_3^{GD} \\ T_4^{GD} \\ T_5^{GD} \\ T_6^{GD} \end{bmatrix} = \underbrace{\begin{bmatrix} 0 & \omega_3 & -\omega_2 & 0 & 0 & 0 \\ -\omega_3 & 0 & \omega_1 & 0 & 0 & 0 \\ \omega_2 & -\omega_1 & 0 & 0 & 0 & 0 \\ 0 & 0 & 0 & 0 & \omega_6 & -\omega_5 \\ 0 & 0 & 0 & -\omega_6 & 0 & \omega_4 \\ 0 & 0 & 0 & \omega_5 & -\omega_4 & 0 \end{bmatrix} \begin{bmatrix} I_{11} & I_{12} & I_{13} & 0 & 0 & 0 \\ I_{21} & I_{22} & I_{23} & 0 & 0 & 0 \\ I_{31} & I_{32} & I_{33} & 0 & 0 & 0 \\ 0 & 0 & 0 & I_{44} & I_{45} & I_{46} \\ 0 & 0 & 0 & I_{54} & I_{55} & I_{56} \\ 0 & 0 & 0 & I_{64} & I_{65} & I_{66} \end{bmatrix} \begin{bmatrix} \omega_1 \\ \omega_2 \\ \omega_3 \\ \omega_4 \\ \omega_5 \\ \omega_6 \end{bmatrix}}_{\text{GYROSCOPIC TORQUES}} + \underbrace{3G \begin{bmatrix} 0 & -A_{33} & A_{23} & 0 & 0 & 0 \\ A_{33} & 0 & -A_{13} & 0 & 0 & 0 \\ -A_{23} & A_{13} & 0 & 0 & 0 & 0 \\ 0 & 0 & 0 & 0 & -[CA]_{33} & [CA]_{23} \\ 0 & 0 & 0 & [CA]_{33} & 0 & -[CA]_{13} \\ 0 & 0 & 0 & -[CA]_{23} & [CA]_{13} & 0 \end{bmatrix} \begin{bmatrix} I_{11} & I_{12} & I_{13} & 0 & 0 & 0 \\ I_{21} & I_{22} & I_{23} & 0 & 0 & 0 \\ I_{31} & I_{32} & I_{33} & 0 & 0 & 0 \\ 0 & 0 & 0 & I_{44} & I_{45} & I_{46} \\ 0 & 0 & 0 & I_{54} & I_{55} & I_{56} \\ 0 & 0 & 0 & I_{64} & I_{65} & I_{66} \end{bmatrix} \begin{bmatrix} A_{13} \\ A_{23} \\ A_{33} \\ [CA]_{13} \\ [CA]_{23} \\ [CA]_{33} \end{bmatrix}}_{\text{GRAVITY-GRADIENT TORQUES}}$$

$$+ \bar{m} \begin{bmatrix} 0 & 0 & 0 & 0 & -H_3 & H_2 \\ 0 & 0 & 0 & H_3 & 0 & -H_1 \\ 0 & 0 & 0 & -H_2 & H_1 & 0 \\ 0 & -H_6 & H_5 & 0 & 0 & 0 \\ H_6 & 0 & -H_4 & 0 & 0 & 0 \\ -H_5 & H_4 & 0 & 0 & 0 & 0 \end{bmatrix} \left\{ \begin{bmatrix} C_{11} & C_{12} & C_{13} & 0 & 0 & 0 \\ C_{21} & C_{22} & C_{23} & 0 & 0 & 0 \\ C_{31} & C_{32} & C_{33} & 0 & 0 & 0 \\ 0 & 0 & 0 & C_{11} & C_{21} & C_{31} \\ 0 & 0 & 0 & C_{12} & C_{22} & C_{32} \\ 0 & 0 & 0 & C_{13} & C_{23} & C_{33} \end{bmatrix} \begin{bmatrix} 0 & -\omega_3 & \omega_2 & 0 & 0 & 0 \\ \omega_3 & 0 & -\omega_1 & 0 & 0 & 0 \\ -\omega_2 & \omega_1 & 0 & 0 & 0 & 0 \\ 0 & 0 & 0 & 0 & -\omega_6 & \omega_5 \\ 0 & 0 & 0 & \omega_6 & 0 & -\omega_4 \\ 0 & 0 & 0 & -\omega_5 & \omega_4 & 0 \end{bmatrix} \begin{bmatrix} 0 & -\omega_3 & \omega_2 & 0 & 0 & 0 \\ \omega_3 & 0 & -\omega_1 & 0 & 0 & 0 \\ -\omega_2 & \omega_1 & 0 & 0 & 0 & 0 \\ 0 & 0 & 0 & 0 & -\omega_6 & \omega_5 \\ 0 & 0 & 0 & \omega_6 & 0 & -\omega_4 \\ 0 & 0 & 0 & -\omega_5 & \omega_4 & 0 \end{bmatrix} \right.$$

$$\left. - 3G \begin{bmatrix} C_{11} & C_{12} & C_{13} & 0 & 0 & 0 \\ C_{21} & C_{22} & C_{23} & 0 & 0 & 0 \\ C_{31} & C_{32} & C_{33} & 0 & 0 & 0 \\ 0 & 0 & 0 & (A_{13}A_{13}-\frac{1}{3}) & A_{13}A_{23} & A_{13}A_{33} \\ 0 & 0 & 0 & A_{23}A_{13} & (A_{23}A_{23}-\frac{1}{3}) & A_{23}A_{33} \\ 0 & 0 & 0 & A_{33}A_{13} & A_{33}A_{23} & (A_{33}A_{33}-\frac{1}{3}) \end{bmatrix} \begin{bmatrix} (A_{13}A_{13}-\frac{1}{3}) & A_{13}A_{23} & A_{13}A_{33} & 0 & 0 & 0 \\ A_{23}A_{13} & (A_{23}A_{23}-\frac{1}{3}) & A_{23}A_{33} & 0 & 0 & 0 \\ A_{33}A_{13} & A_{33}A_{23} & (A_{33}A_{33}-\frac{1}{3}) & 0 & 0 & 0 \\ 0 & 0 & 0 & C_{12} & C_{21} & C_{31} \\ 0 & 0 & 0 & C_{12} & C_{22} & C_{32} \\ 0 & 0 & 0 & C_{13} & C_{23} & C_{33} \end{bmatrix} \right\} \begin{bmatrix} H_1 \\ H_2 \\ H_3 \\ H_4 \\ H_5 \\ H_6 \end{bmatrix}$$

HINGE-ACCELERATION TORQUES — MOMENTS OF GRAVITATIONAL FORCES INTERACTING THROUGH HINGE

$$\begin{bmatrix} T_1^{CMG} \\ T_2^{CMG} \\ T_3^{CMG} \end{bmatrix} = H^{CMG} \left\{ \begin{bmatrix} 0 & \cos\phi_1 \sin\lambda_1 & \sin\phi_1 \\ -\cos\phi_1 \sin\lambda_1 & 0 & -\cos\phi_1 \cos\lambda_1 \\ -\sin\phi_1 & \cos\phi_1\cos\lambda_1 & 0 \end{bmatrix} \begin{bmatrix} \omega_1 + \dot{\phi}_1 \sin\lambda_1 \\ \omega_2 + \dot{\lambda}_1 \\ \omega_3 + \dot{\phi}_1 \cos\lambda_1 \end{bmatrix} + \begin{bmatrix} 0 & -\sin\phi_2 & \cos\phi_2\cos\lambda_2 \\ \sin\phi_2 & 0 & \cos\phi_2 \sin\lambda_2 \\ -\cos\phi_2\cos\lambda_2 & -\cos\phi_2\sin\lambda_2 & 0 \end{bmatrix} \begin{bmatrix} \omega_1 + \dot{\phi}_2 \cos\lambda_2 \\ \omega_2 + \dot{\phi}_2 \sin\lambda_2 \\ \omega_3 + \dot{\lambda}_2 \end{bmatrix} + \begin{bmatrix} 0 & -\cos\phi_3\cos\lambda_3 & -\cos\phi_3\sin\lambda_3 \\ \cos\phi_3\cos\lambda_3 & 0 & -\sin\phi_3 \\ \cos\phi_3\sin\lambda_3 & \sin\phi_3 & 0 \end{bmatrix} \begin{bmatrix} \omega_1 + \dot{\lambda}_3 \\ \omega_2 + \dot{\phi}_3\cos\lambda_3 \\ \omega_3 + \dot{\phi}_3 \sin\lambda_3 \end{bmatrix} \right\}$$

$$\begin{bmatrix} T_1^H \\ T_2^H \\ T_3^H \\ T_4^H \\ T_5^H \\ T_6^H \end{bmatrix} = \begin{bmatrix} G_{11} & C_{21} \\ G_{12} & C_{22} \\ G_{13} & C_{23} \\ -B_{11} & 0 \\ -B_{21} & -1 \\ -B_{31} & 0 \end{bmatrix} \begin{bmatrix} K_\alpha^F \alpha^* + C_\alpha \dot{\alpha}^* - T_\alpha^H \\ K_\beta^F \beta^* + C_\beta \dot{\beta}^* - T_\beta^H \end{bmatrix}$$

where:

$$T_\alpha^H = \begin{cases} W_1 & \text{if } |W_1| \le K_3 \\ K_3 & \text{if } |W_1| > K_3 \end{cases} \qquad T_\beta^H = \begin{cases} W_2 & \text{if } |W_2| \le K_4 \\ K_4 & \text{if } |W_2| > K_4 \end{cases}, \quad \begin{bmatrix} W_1 \\ W_2 \end{bmatrix} = \begin{bmatrix} K_{11} & K_{12} \\ K_{21} & K_{22} \end{bmatrix} \begin{bmatrix} V_1 \\ V_2 \end{bmatrix} + \begin{bmatrix} K_{14}\omega_4 \\ K_{25}\omega_5 \end{bmatrix},$$

$$V_1 = \begin{cases} [C^oA]_{13} & \text{if } |[C^oA]_{13}| \le K_1 \\ K_1 & \text{if } |[C^oA]_{13}| > K_1 \end{cases} \qquad V_2 = \begin{cases} [C^oA]_{23} & \text{if } |[C^oA]_{23}| \le K_2 \\ K_2 & \text{if } |[C^oA]_{23}| > K_2 \end{cases}$$

NOTE: $\alpha^*(t)$ and $\beta^*(t)$ are obtained from the STRUCTURAL COMPLIANCE differential equations for $C_\alpha \neq 0$, $C_\beta \neq 0$. For the case that $C_\alpha = C_\beta = 0$, the differential equations are replaced by the algebraic equations:

$$\alpha^* = \frac{K_\alpha^S \alpha - T_\alpha^H}{K_\alpha^S + K_\alpha^F}, \quad \beta^* = \frac{K_\beta^S \beta - T_\beta^H}{K_\beta^S + K_\beta^F}.$$

When STRUCTURAL COMPLIANCE is not taken into account, the corresponding differential equations are omitted and $\alpha = \alpha^*$, $\beta = \beta^*$.

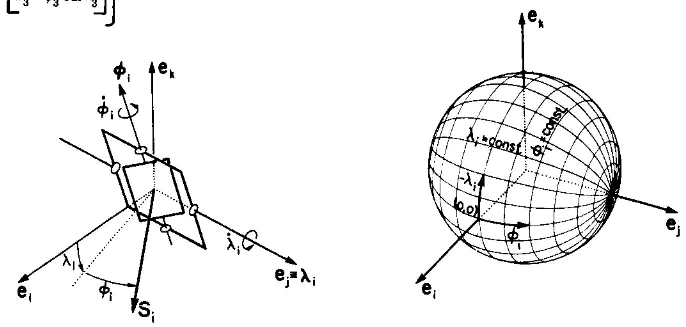

GIMBAL SYSTEM AND GIMBAL ANGLE NET SPANNED BY ROTOR AXIS $\vec{S}_i$ OF i-th CONTROL MOMENT GYRO
(i, j, k: cyclic permutation of 1, 2, 3)

$$\begin{bmatrix} T_1^{EX} \\ T_2^{EX} \\ T_3^{EX} \\ T_4^{EX} \\ T_5^{EX} \\ T_6^{EX} \end{bmatrix} = \underbrace{\frac{1}{(m_1+m_2)} \begin{bmatrix} 0 & -H_3 & H_2 & 0 & 0 & 0 \\ H_3 & 0 & -H_1 & 0 & 0 & 0 \\ -H_2 & H_1 & 0 & 0 & 0 & 0 \\ 0 & 0 & 0 & 0 & -H_6 & H_5 \\ 0 & 0 & 0 & H_6 & 0 & -H_4 \\ 0 & 0 & 0 & -H_5 & H_4 & 0 \end{bmatrix} \begin{bmatrix} -1 & 0 & 0 & C_{11} & C_{21} & C_{31} \\ 0 & -1 & 0 & C_{12} & C_{22} & C_{32} \\ 0 & 0 & -1 & C_{13} & C_{23} & C_{33} \\ C_{11} & C_{12} & C_{13} & -1 & 0 & 0 \\ C_{21} & C_{22} & C_{23} & 0 & -1 & 0 \\ C_{31} & C_{32} & C_{33} & 0 & 0 & -1 \end{bmatrix} \begin{bmatrix} m_2 F_1 \\ m_2 F_2 \\ m_2 F_3 \\ m_1 F_4 \\ m_1 F_5 \\ m_1 F_6 \end{bmatrix}}_{\text{MOMENTS OF EXTERNAL FORCES INTERACTING THROUGH HINGE (e.g., Solar, Aerodynamic)}} + \underbrace{\begin{bmatrix} T_1' \\ T_2' \\ T_3' \\ T_4' \\ T_5' \\ T_6' \end{bmatrix}}_{\text{EXTERNAL TORQUES (e.g., Solar, Magnetic)}} + \underbrace{\begin{bmatrix} T_1'' \\ T_2'' \\ T_3'' \\ T_4'' \\ T_5'' \\ T_6'' \end{bmatrix}}_{\text{OTHER TORQUES (e.g. Gas Jets, Moving Parts)}}$$

Fig. 6-9 Summary of Torques

FOLDOUT FRAME 1

FOLDOUT FRAME 2

PRECEDING PAGE BLANK NOT FILMED.

describe the CMG's even though not all the quantities involved are transformable vectors. The vectors and matrices involved are defined in Table 6-4. The dynamics of the CMG-actuated carrier can be described in terms of these quantities by a set of vector equations with the restriction that the equations are generally valid only in a reference frame fixed in the carrier. The angular momentum vecotrs as well as the angular velocities of the CMG's and carrier are, of course, vectors and may be transformed into any frame of reference.

The CMG's can be regarded as gimballed angular momentum vectors. Figure 6-10 illustrates the three vectors and the angles through which they rotate as a result of gimballing. Figure 6-11 shows a single CMG and the torques which act upon it. Two of the torques are produced by motors on the gimbal axes; the other, T_{11}, is produced by a reaction to the constraint imposed by the bearings on the outer gimbal. The equations of motion governing the CMG's and carrier are listed in Table 6-5. They are based on the assumptions that the angular momentum of all three CMG's are equal, that the carrier behaves as a rigid body, that the inertia of the Spar is negligible, and that the characteristics of all six torque motors on the CMG gimbal axes are the same. These equations may be represented by a vector block diagram, as shown in Fig. 6-12. Each line of flow in the diagram represents three quantities, and the blocks represent matrix transformations. Observe that the notation in these figures has been changed from that in subsection 5, of Ref. 6-1 in order to conform with the notation of subsection 6 of Ref. 6-1. The directions of the angular momentum vectors of the CMG's relative to the axes of the carrier are to be controlled as functions of errors, $\bar{\epsilon}$ derived from angle and rate sensors on the carrier.

The vector-matrix dynamic equation of motion for the carrier and CMG's is

$$\frac{K_t}{\mu R_M} (\bar{A}\bar{C}\bar{P} + \bar{B}\bar{C}\bar{Q})\bar{\epsilon} + \bar{\omega} \times \bar{H} = -\bar{J}\dot{\bar{\omega}} - \bar{\omega} \times \bar{J}\bar{\omega}. \tag{6.0}$$

Table 6-4
CMG NOTATION

$$\bar{T}_E = \begin{pmatrix} T_{31} \\ T_{12} \\ T_{23} \end{pmatrix} = \text{outer gimbal torques}$$

$$\bar{T}_I = \begin{pmatrix} T_{32} \\ T_{13} \\ T_{21} \end{pmatrix} = \text{inner gimbal torques}$$

$$\dot{\bar{\sigma}}_E = \begin{pmatrix} \dot{\lambda}_1 \\ \dot{\lambda}_2 \\ \dot{\lambda}_3 \end{pmatrix} = \text{outer gimbal rates}$$

$$\dot{\bar{\sigma}}_I = \begin{pmatrix} \dot{\phi}_1 \\ \dot{\phi}_2 \\ \dot{\phi}_3 \end{pmatrix} = \text{inner gimbal rates}$$

$$\bar{A} = \begin{pmatrix} 0 & \sin\lambda_1 & \cos\lambda_2 \\ \cos\lambda_3 & 0 & \sin\lambda_2 \\ \sin\lambda_3 & \cos\lambda_1 & 0 \end{pmatrix}$$

$$\bar{B} = \begin{pmatrix} 1 & -\cos\lambda_1\tan\phi_1 & \sin\lambda_2\tan\phi_2 \\ \sin\lambda_3\tan\phi_3 & 1 & -\cos\lambda_2\tan\phi_2 \\ -\cos\lambda_3\tan\phi_3 & \sin\lambda_1\tan\phi_1 & 1 \end{pmatrix}$$

$$\bar{C} = \begin{pmatrix} \cos\phi_3 & 0 & 0 \\ 0 & \cos\phi_1 & 0 \\ 0 & 0 & \cos\phi_2 \end{pmatrix}$$

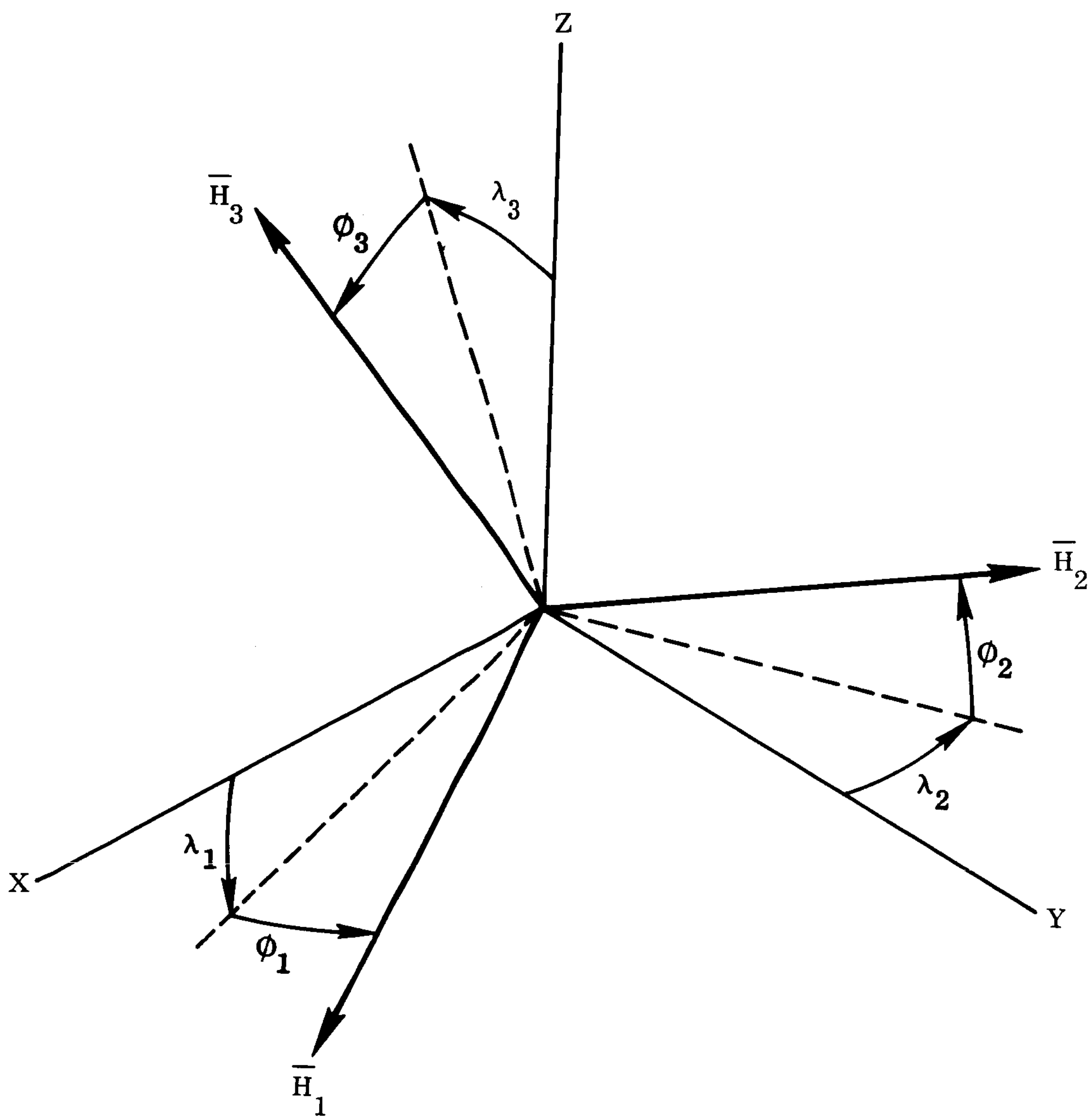

Fig. 6-10 CMG Angular Momentum

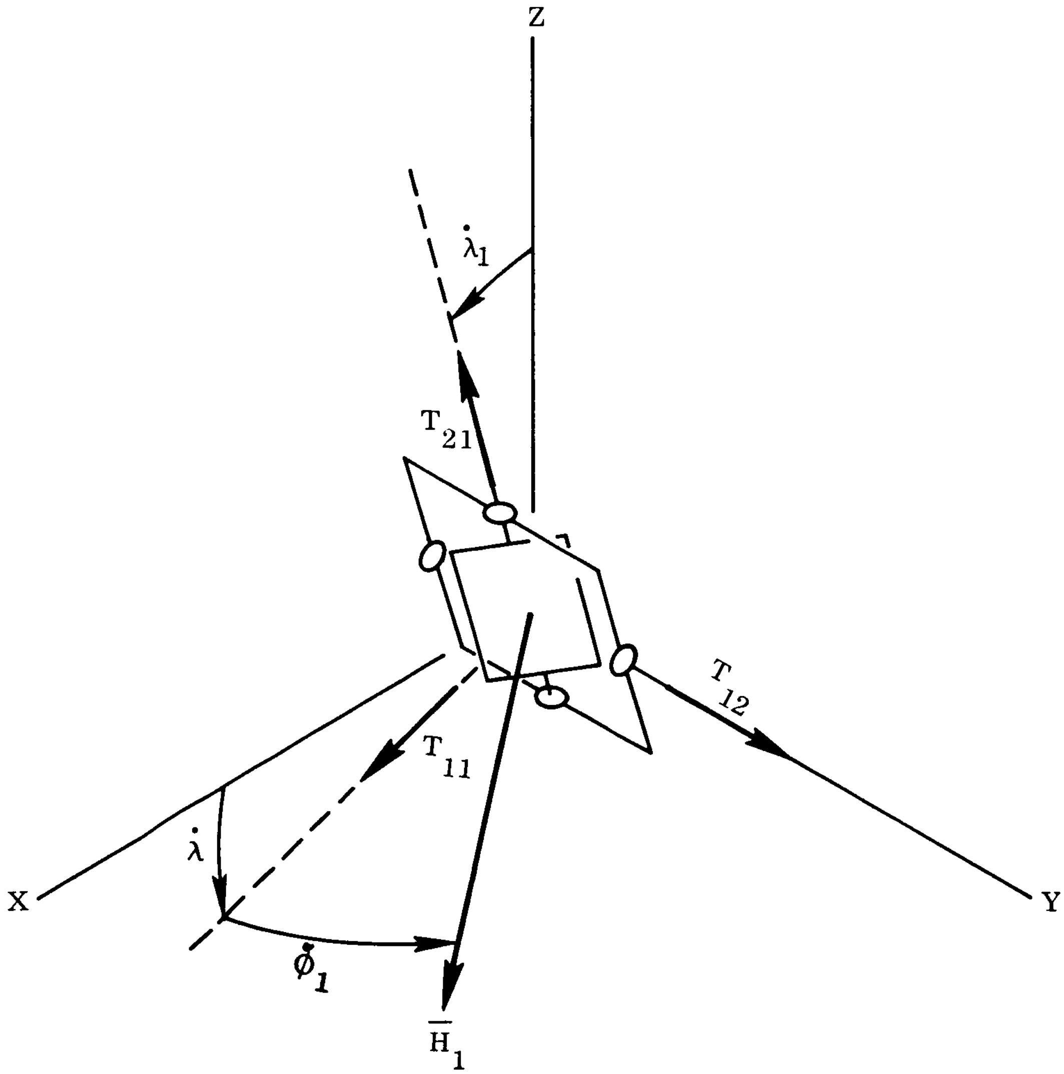

Fig. 6-11 CMG Torques

Table 6-5

CMG DYNAMICS

$$H_1 = H_2 = H_3$$

$$\bar{T}_E = H_3 \bar{C} (\mathring{\bar{\phi}} + \bar{A}' \bar{\omega})$$

$$\bar{T}_I = -H_3 \bar{C} (\mathring{\bar{\lambda}} + B' \bar{\omega})$$

$$\bar{T} = \bar{A} \bar{T}_I + \bar{B} \bar{T}_E = \dot{\bar{H}} + \bar{\omega} \times \bar{H} = -\bar{J} \dot{\bar{\omega}} - \bar{\omega} \times \bar{J} \bar{\omega}$$

$$\bar{H} = \bar{H}_1 + \bar{H}_2 + \bar{H}_3$$

$$\dot{\bar{H}} = H_3 (-\bar{A} \bar{C} \mathring{\bar{\lambda}} + \bar{B} \bar{C} \mathring{\bar{\phi}})$$

$$\bar{\omega} \times \bar{H} = H_3 (-\bar{A} \bar{C} \bar{B}' + \bar{B} \bar{C} \bar{A}') \omega$$

$$\bar{T}_E = \frac{K_T}{R_M} (\bar{E}_E - K_G \mathring{\bar{\lambda}})$$

$$\bar{T}_I = \frac{K_T}{R_M} (\bar{E}_I - K_G \mathring{\bar{\phi}})$$

$$T_{11} = -T_{12} \tan \phi_2 \qquad T_{22} = -T_{23} \tan \lambda_2 \qquad T_{33} = -T_{31} \tan \lambda_3$$

where:

$-\bar{T}$	=	torque on vehicle due to CMG's
$\bar{J}$	=	inertia tensor of vehicle
$\bar{A}', \bar{B}'$	=	transposed matrices
$\bar{E}_E$	=	outer gimbal motor excitations
$\bar{E}_I$	=	inner gimbal motor excitations
K_T	=	gimbal motor torque constant
K_G	=	gimbal motor back EMF constant
R_M	=	gimbal motor resistance
$\bar{\omega}$	=	vehicle angular rate
$(\dot{\bar{\ }})$	=	derivative in body axes

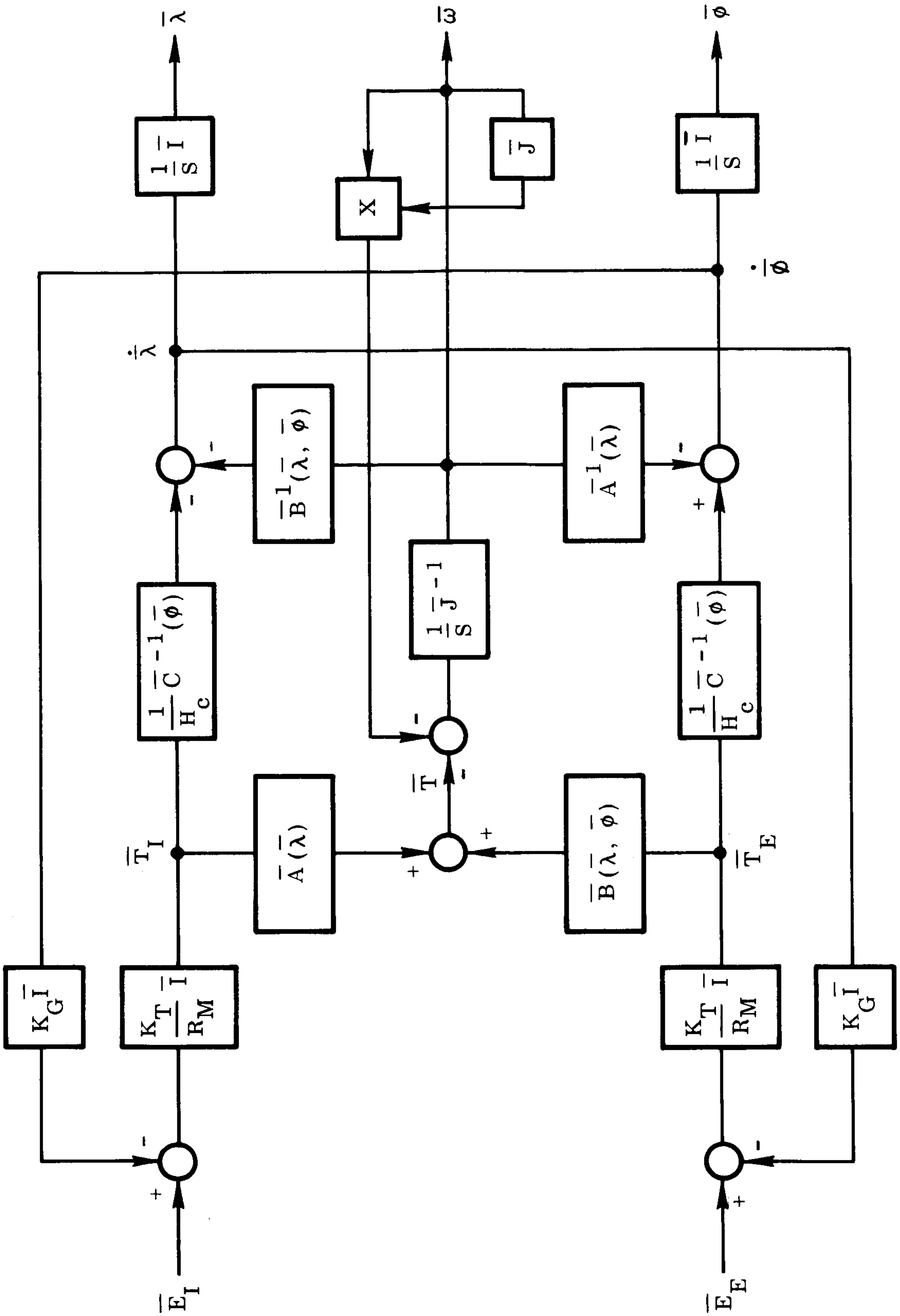

Fig. 6-12 CMG Dynamics (Vector Block Diagram)

This equation is represented in the vector block diagram of Fig. 6-13. The matrices $\overline{P}$ and $\overline{Q}$ transform the error signal into the voltages applied to drive the rate loops on the outer and inner gimbal axes, respectively. These transformations are known as the control law and cause the components of error to produce torques about the appropriate vehicle axes. As discussed in subsection 5 of Ref. 6-1, this particular control concept was chosen to remove the effects of nonlinearities in the gimbal motors and bearings and to permit the angular rates of the gimbals to be controlled directly. As suggested, this could be accomplished by placing a tachometer in each gimbal axis and feeding the signal derived from it back through an amplifier around the corresponding motors. With sufficiently high gain in the tachometer loops, Fig. 6-12 reduces to that in Fig. 6-13. A further simplification could be achieved if it is assumed the carrier deviates only a small amount from a reference attitude. The error is derived by summing the angular displacement, as measured by the sun and star sensors, with the angular rates, as measured by gyros mounted along mutually perpendicular axes in the carrier. The closed feedback loop in the vector-matrix block diagram for this condition is shown in Fig. 6-14.

Various control laws, that is, the selection of the matrices $\overline{P}$ and $\overline{Q}$, are discussed in subsection 5.2 of Ref. 6-1. In form, the simplest is the control law proposed by P. Kurzhals of the Langley Research Center which uses the transformations

$$\overline{P} = -\overline{A}' \quad \text{and} \quad \overline{Q} = \frac{7}{9}\,\overline{C}\,.$$

<u>Roll Axis Control of the ATM Carrier Vehicle.</u> The implementation and analysis of the roll axis control of the carrier vehicle is considered in subsection 5.5 of Ref. 6-1. A conceptual design of the control system is presented that accounts for normal operation, operation during occultation, automatic reacquisition, and operation during attitude perturbations.

The nominal flight mode of the Cluster during ATM operation is shown in Fig. 6-5 and was discussed in the preceding paragraphs. Figure 6-6 shows the geometry of the sun and star references relative to the nominal flight. This geometry is expanded

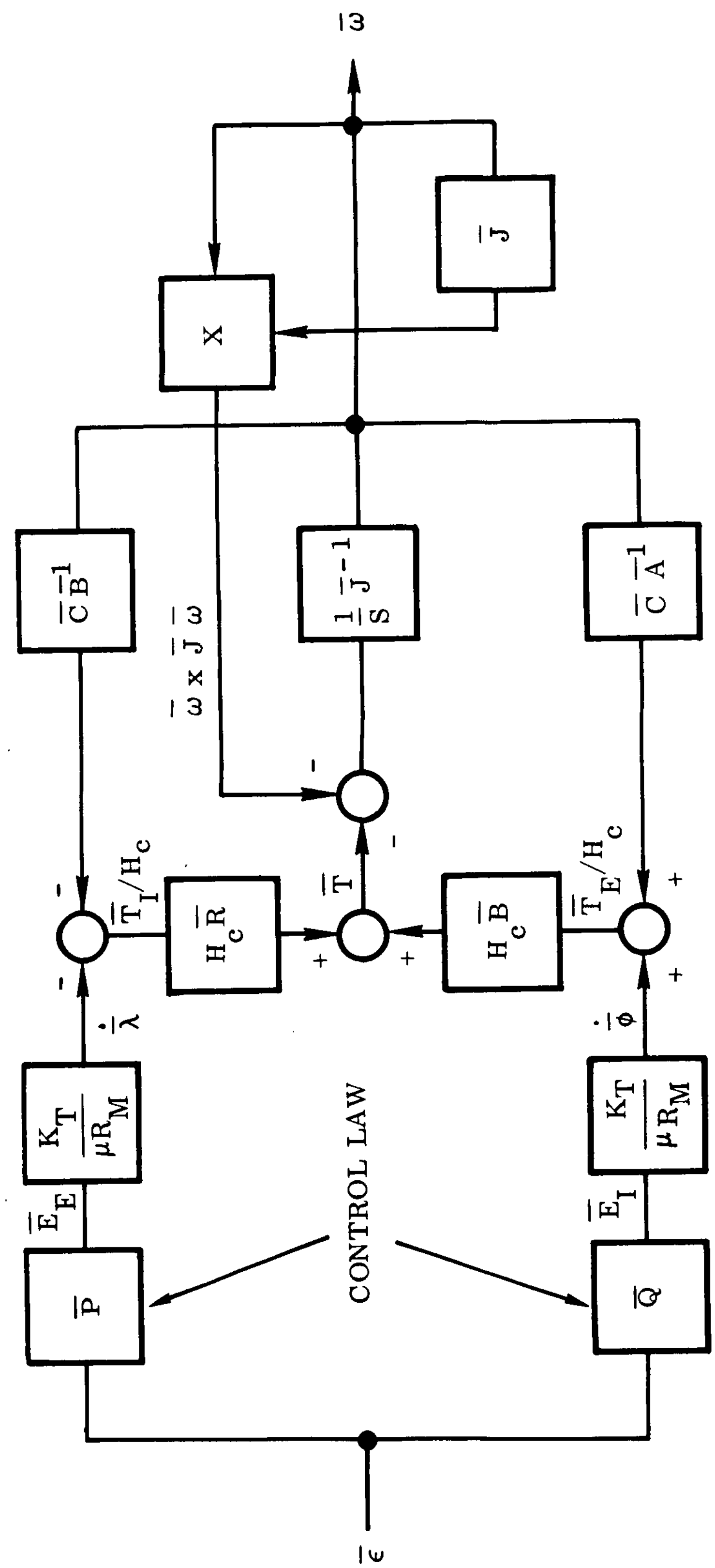

Fig. 6-13 CMG's With Gimbal Rate Feedback (Vector Block Diagram)

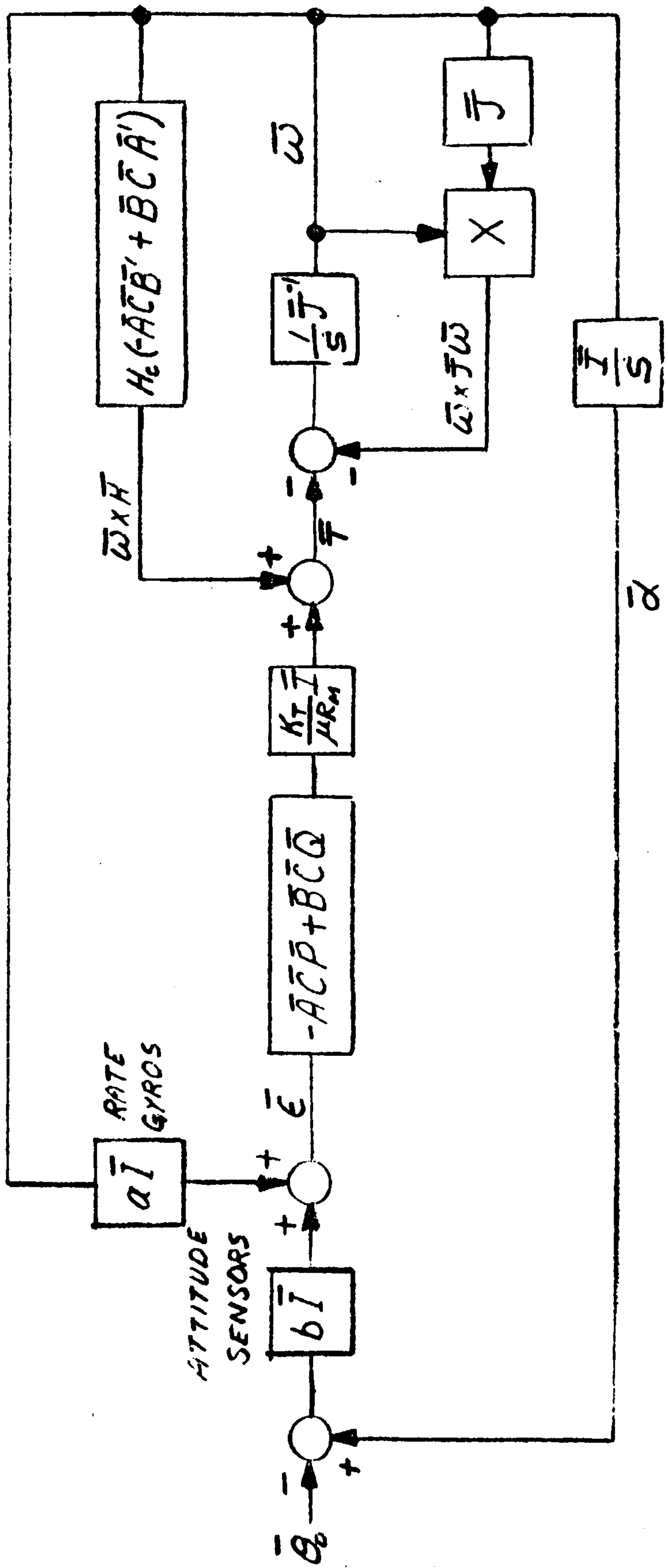

Fig. 6-14 Carrier CMG Control System for Small-Angle Attitude Changes

and shown in more detail in Figs. 6-15 and 6-16, which also contain the trigonometric relations between the geometric parameters.

The spacecraft is assumed to be in a circular orbit which is inclined at i = 28.5 deg to the equatorial plane and is at an altitude of 463 km. In this orbit, the location of the descending node as measured from the vernal equinox ♈ , i.e., the angle Ω regresses at a rate of 6.9 deg/day due to the earth's oblateness. This causes the nodes between the orbit plane and the ecliptic to regress and the inclination between these two planes to vary between 5 deg and 52 deg.

In Fig. 6-16, the direction of Canopus relative to the sun-referenced axes is shown. It is produced by rotating the y axis about the positive direction of the z_1 axis through the angle α_s and then the rotated x_1 axis through the angle β_s. If the two-axis star tracker is mounted on the Rack so that with its gimbal angles at zero the outer gimbal axis lies along the z_2 axis and the inner gimbal axis along the x_2 axis. Then, with the Cluster in its nominal attitude, the outer gimbal will be rotated through the angle α_s and the inner gimbal through the angle β_s when the star is being tracked. Using the trigonometric relations accompanying Figs. 6-15 and 6-16, the values of α_s and β_s can be computed in terms of invariant parameters and two functions of time, θ and Ω .

The variations of these are nearly uniform, θ at the rate of 1 rev/yr and Ω at the rate of 6.9 deg/day. The excursions of β_s are limited to the 15 deg that Canopus is off the south celestial pole; those of α_s may become as high as 67 deg – the angle to Canopus plus the maximum inclination of the orbit plane from the ecliptic. Figure 6-17 shows the variations of the gimbal angles over a period of 1 yr. The time of launch is selected to give the greatest variation in α_s , i.e., the most stringent condition for roll control. At its maximum, α_s varies by 4 deg/day. Therefore, maintaining the x_2 axis within 1 deg of the nominal flight mode requires a computation of α_s once every 12 hr.

The conditions under which Canopus is occulted are illustrated in Fig. 6-18. The inner sphere represents the earth; the outer sphere is the locus of all possible

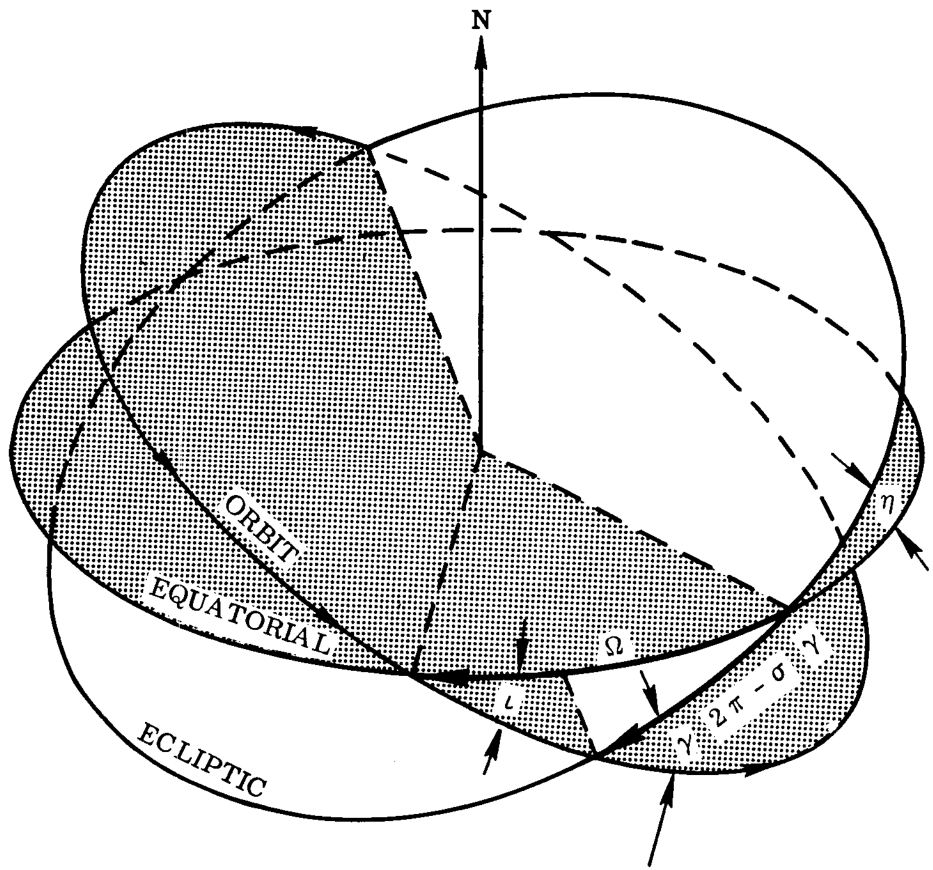

$$\cos\ \gamma = \cos\ i \cos\eta - \sin\ i \sin\eta\cos\Omega$$

$$\sin\sigma = \frac{\sin\ i\ \sin\Omega}{\sin\ \gamma}$$

$$\cos\ \sigma = \frac{\cos\ i\ \sin\eta + \sin\ i\cos\eta\cos\Omega}{\sin\gamma}$$

$$i = 28.5 \text{ deg} \qquad \eta = 23.5 \text{ deg}$$

Fig. 6-15 Orbit Geometry

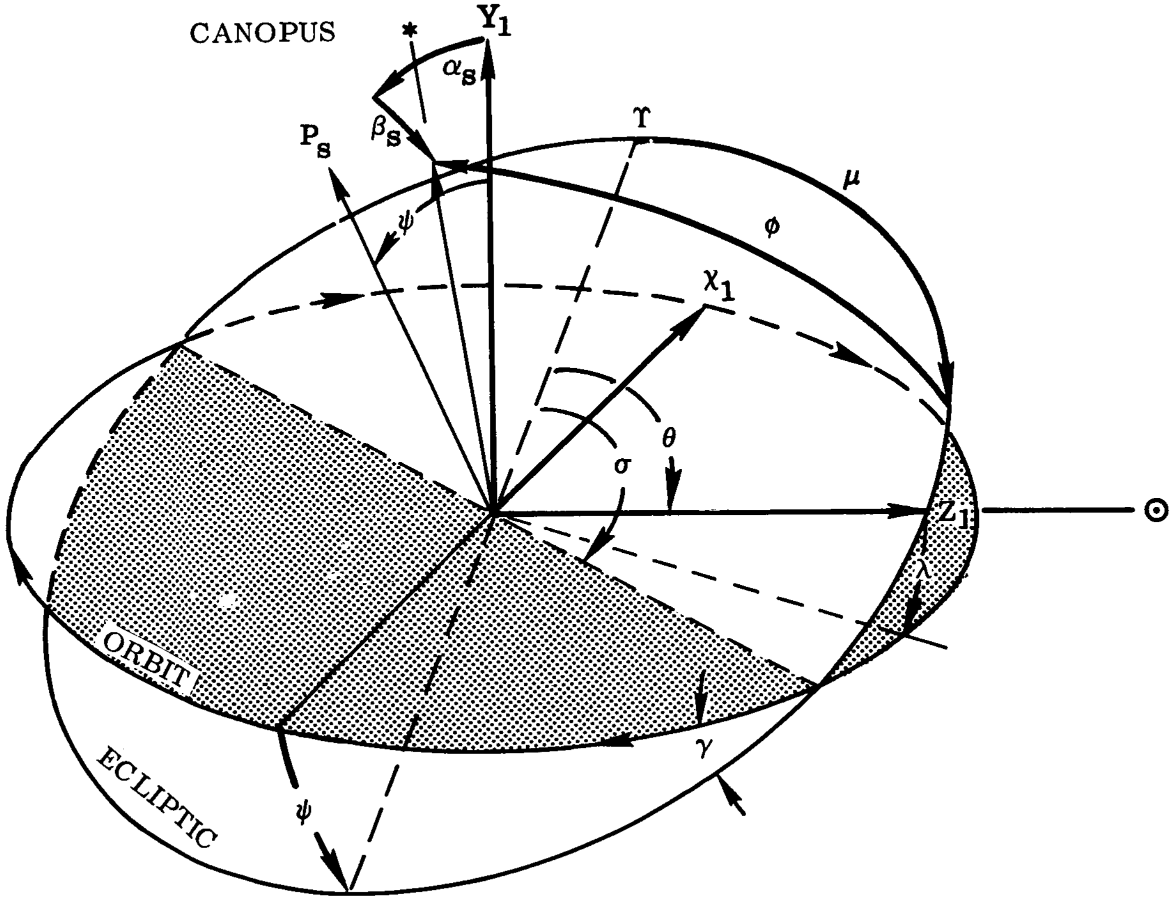

$$\sin\beta_s = \cos(\theta-\mu)\cos\phi$$

$$\cos(\psi-\alpha_s)\cos\beta_s = \sin\phi$$

$$\tan(\psi-\alpha_s)\tan\phi = \sin(\theta-\mu)$$

$$\tan\psi = \tan\gamma\cos(\sigma-\theta)$$

$$\sin\lambda = \sin\gamma\sin(\sigma-\theta)$$

$\mu = 96.3$ deg

$\phi = 75.05$ deg

$\gamma < 52$ deg

$-15 < \beta_s < 15$ deg

$-67 < \alpha_s < 67$ deg

Fig. 6-16 Star Tracking Geometry

locations of a satellite in a circular orbit. The segment of the outer sphere subtended by a cone directly opposite the line to Canopus is the locus of all points in orbit for which Canopus is occulted. The sine of the half angle of the cone is r_e/R, which, for an orbital altitude of 463 km, results in a cone half-angle of 84.2 deg. The fraction of time F during which the star is occulted can also be determined. A plot of F over a period of 1 yr is also shown in Fig. 6-17, along with variations in the angles of the star tracker's gimbals.

A block diagram for one method of implementing control of the carrier's roll axis is shown in Fig. 6-19. In normal operation, it is designed to control the spacecraft to its normal flight mode. It has provision for a manual override for use during star acquisition. When Canopus is occulted, the star tracker is switched out and roll is referenced to a gyro. The star tracker and gyro are interconnected in such a way that the tracker remains pointing at the star during occultation, even if the roll attitude is perturbed for dumping stored angular momentum.

In this implementation the angles between the vernal equinox, the descending node, and the sun line are determined initially and are set into a computer which calculates the desired value of α_s, the outer gimbal angle. These inputs are updated periodically as Ω and θ vary. They are shown as manual inputs to the computer but, since the variation of each is directly proportional to elapsed time, they may be driven from a clock to perform the updating continuously. The computed α_s is compared with the measured outer gimbal angle α_m. The difference constitutes an error signal which actuates the CMG's to produce the appropriate torques to reduce it to zero, thereby slaving the roll angle of the carrier to the computed value of α_s. The inner gimbal of the star tracker is not shown in the diagram and is used only to keep the star in the field of view. It may be driven either in an automatic tracking mode or be set at a fixed value and periodically updated as a function of time.

Initial acquisition is accomplished by locking the pitch and yaw axes to the sun, setting the tracker gimbals to the computed values of α_s and β_s, and rolling the vehicle under manual control until Canopus comes into the tracker's field. Release of the manual control at that time causes the tracker to lock on and the control system to go

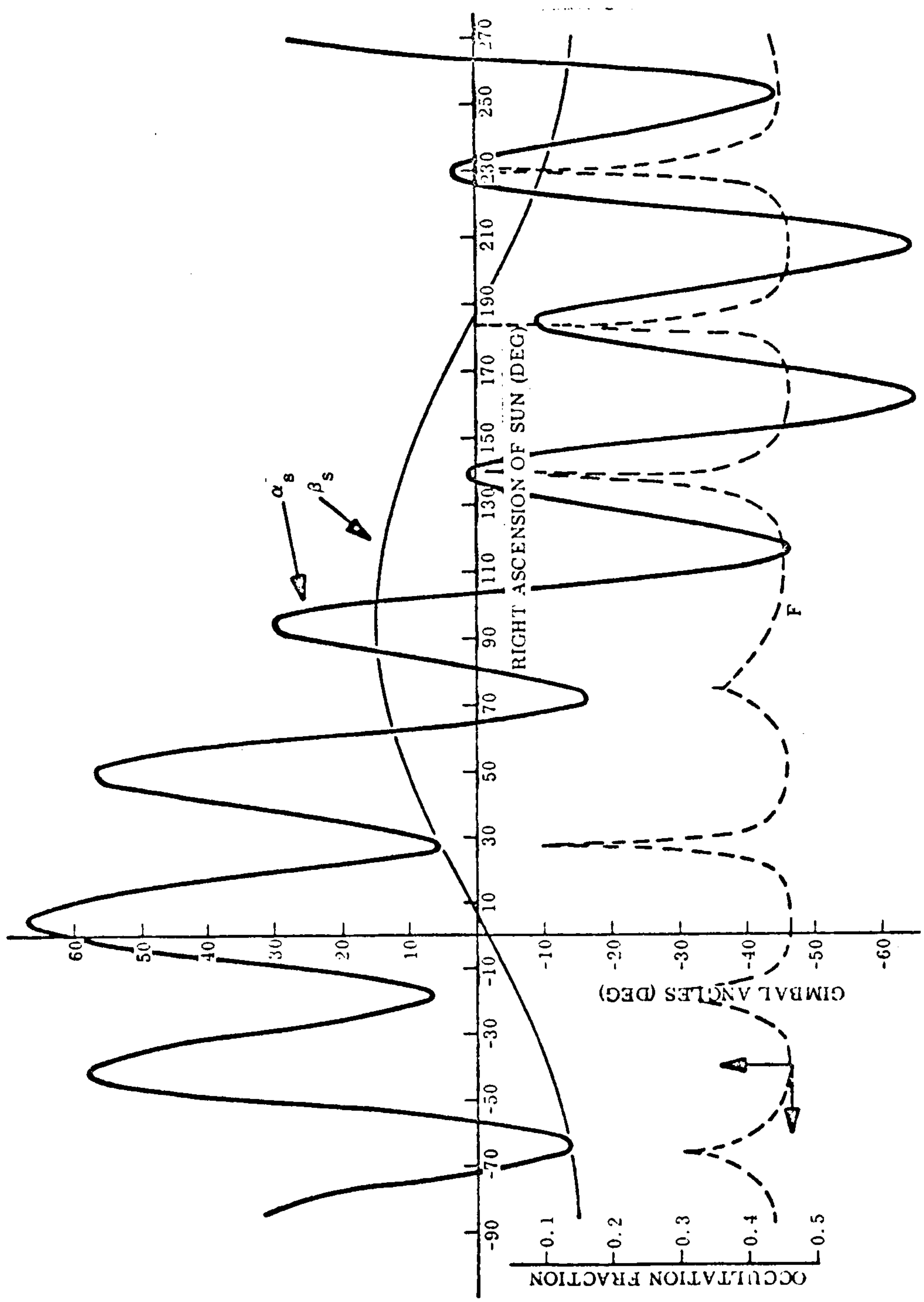

Fig. 6-17 Star Tracker Angles

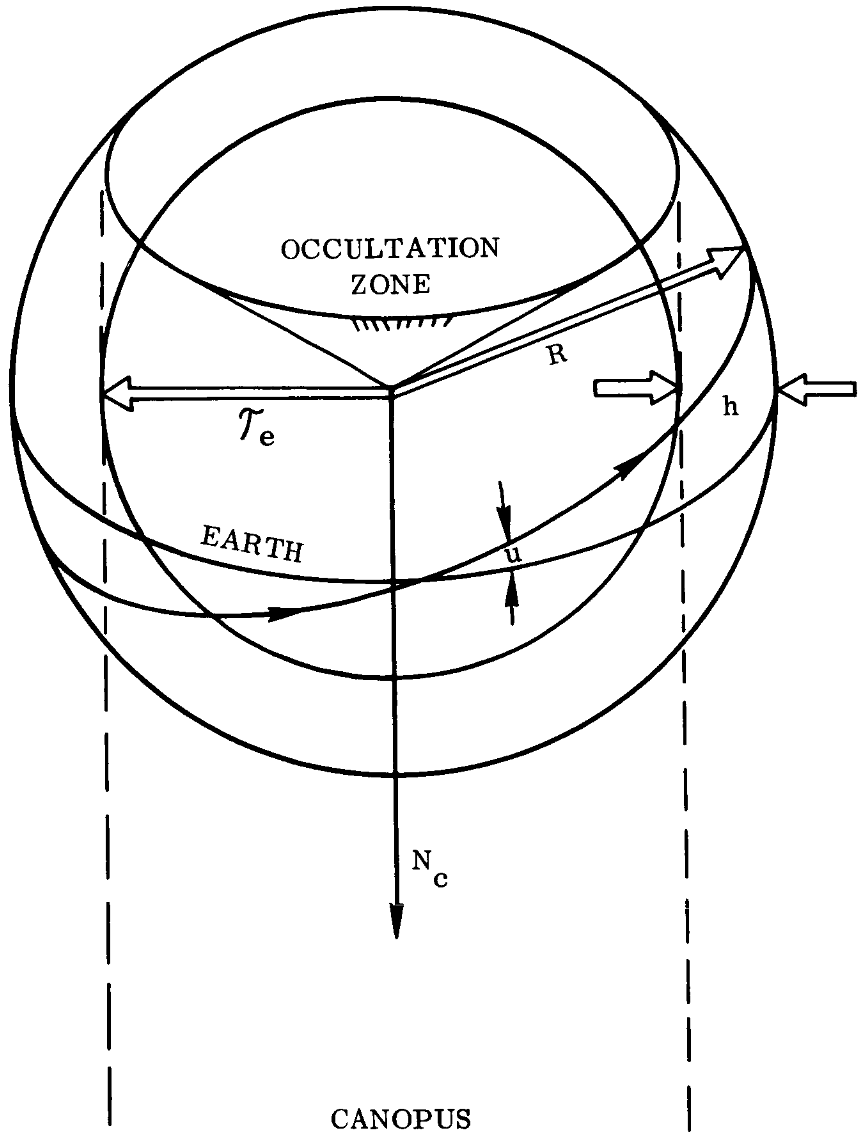

Fig. 6-18 Star Occultation Geometry

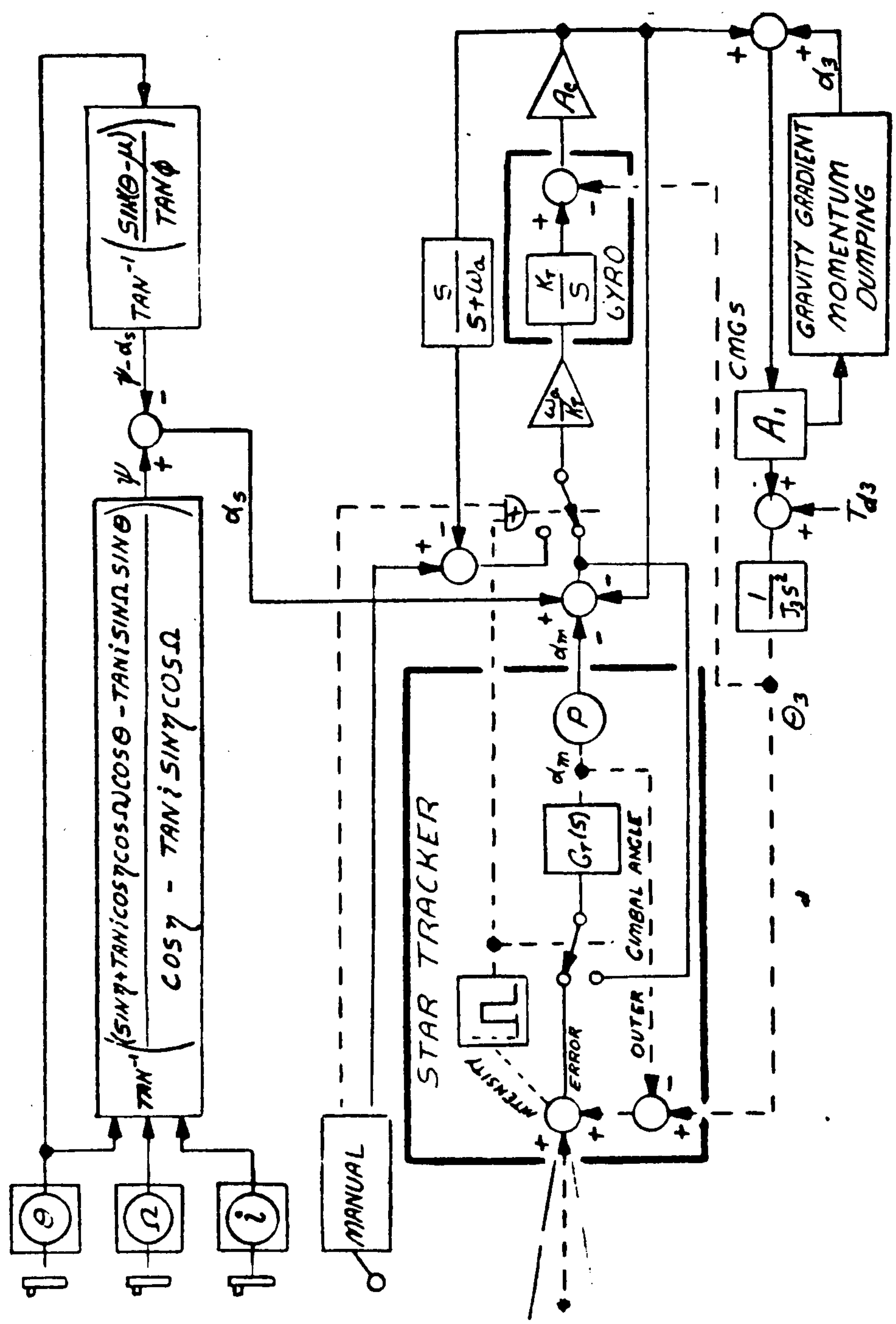

Fig. 6-19 Roll Axis Geometry

into its normal operating mode. Since the star tracker responds to the manual control faster than the vehicle, it is possible to generate a rapid search pattern about any attitude by manipulating the control back and forth.

Gravity Gradient Momentum Dumping. When the ATM is operated with the Cluster configuration oriented to point at the sun, large aerodynamic and gravity gradient torques exist on the configuration which cause angular momentum to be accumulated by the CMG's. These are for the most part cyclic torques for which the average stored momentum vanishes. One component of the gravity torque, however, is not cyclic and certain small deviations of the Cluster from a cylindrical geometry can result in unidirectional components of aerodynamic torque. In addition, magnetic torques may exist whose average value is not zero.

The principles of a method for using gravity torques to dump momentum accumulated in the CMG's were developed in Ref. 6-1. That analysis was extended in Ref. 6-2 for the purpose of generating details of the design of such a system and evaluating its performance. The system proposed can be implemented as an automatic adaptation of the control system and requires only small deviations from the nominal flight mode for momentum control. The method uses the CMG's to maneuver the vehicle during periods of solar occultation, i.e., dark-side passage, in such a way that the gravitational torques produced tend to reduce the accumulated angular momentum. The elements of an implementation of the method are shown in Fig. 6-20. The differential equation governing the accrual of angular momentum is

$$\mathring{\overline{H}}_1 - h(\theta_t)\Omega_o^2 \,\overline{E}\,\overline{F}(\overline{I} - \overline{\alpha}x)\overline{H}_1 = \overline{T}_d = \Omega_o^2 \,\overline{E}\overline{\delta} \tag{6.1}$$

The matrix $\overline{F}_1$, where $\overline{F}_1 = \overline{F}(\overline{I} - \overline{\alpha}x)$, represents the momentum control law to be implemented. By using the parametric substitutions indicated in Table 6-6, Eq. (6.1) was placed in a more tractable form. It becomes

$$\begin{aligned} \overline{H}'_1 &= \overline{u} \quad \text{during sun-side passage} \\ \overline{H}'_1 &= \overline{B}\overline{G}\overline{H}_1 + \overline{u} \quad \text{during dark-side passage.} \end{aligned} \tag{6.2}$$

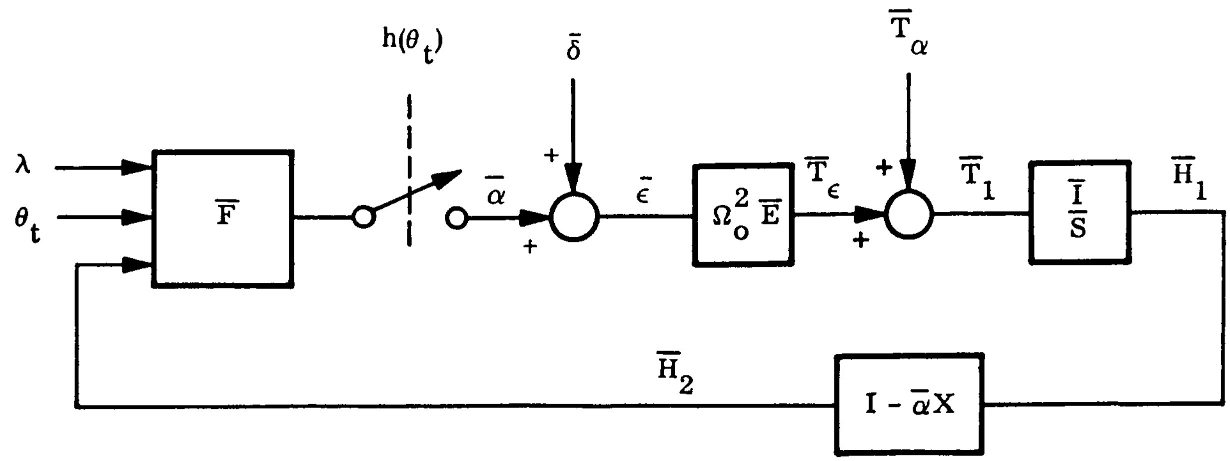

Ω_o = orbital angular rate

$\bar{H}_1$ = stored angular momentum in sun-referenced axes

$\bar{H}_2$ = stored angular momentum in geometric axes

$\bar{T}_1$ = summation of external torques

$\bar{T}_\epsilon$ = controlled gravity gradient torques

$\bar{T}_\alpha$ = disturbance torques

$\bar{\epsilon}$ = rotation of principal axes from sun-referenced axes

$\bar{\alpha}$ = rotation of geometric axes from sun-referenced axes

$\bar{\delta}$ = deviation of principal axes from geometric axes

λ = angle between sun line and orbit plane

θ_t = true anomaly from terminator

$\bar{F}$ = momentum dumping law matrix

$\bar{I}$ = identity matrix

$h(\theta_t)$ = $1/2\ [1 - \mathrm{sgn}(\sin\rho + \sin\theta_t)]$

$\pi + \rho$ = true anomaly at beginning of occultation

$$\bar{E} = \frac{3}{2}\begin{bmatrix} -2\sin^2\theta_t\cos 2\lambda & \sin 2\theta_t \sin\lambda & -\sin 2\theta_t \cos\lambda \\ -\sin 2\theta_t \sin\lambda & 2(\sin^2\theta_t\cos^2\lambda - \cos^2\theta_t) & \sin^2\theta_t \sin 2\lambda \\ \sin 2\theta_t \cos\lambda & -\sin^2\theta_t \sin 2\lambda & 2(\cos^2\theta_t - \sin^2\theta_t \sin^2\lambda) \end{bmatrix}\begin{bmatrix} J_2-J_3 & 0 & 0 \\ 0 & J_3-J_1 & 0 \\ 0 & 0 & J_1-J_2 \end{bmatrix}$$

Fig. 6-20 Gravity-Gradient Momentum Dumping

Table 6-6

PARAMETER SUBSTITUTIONS

$$\tau = 2\,\theta_t$$

$$\bar{H}_1' = d\bar{H}_1 / d\tau$$

$$\bar{G} = \frac{3\,\Omega_o}{4}\begin{pmatrix} J_2 - J_3 & 0 & 0 \\ 0 & J_3 - J_1 & 0 \\ 0 & 0 & J_1 - J_2 \end{pmatrix}\bar{F}_1$$

$$\bar{m} = \frac{\bar{T}_d}{2\Omega_o} = \begin{pmatrix} m_1(1 - \cos\tau) \\ m_2 \sin\tau \\ m_3 \sin\tau \end{pmatrix}$$

where

$$m_1 = -\frac{3\,\Omega_o}{4}(J_2 - J_3)\sin\lambda\cos\lambda$$

$$m_2 = -\frac{3\,\Omega_o}{4}(J_3 - J_1)\cos\lambda$$

$$m_3 = -\frac{3\,\Omega_o}{4}(J_1 - J_2)\sin\lambda$$

$$\bar{m} = \begin{pmatrix} m_1 \\ m_2 \\ m_3 \end{pmatrix}$$

$$\bar{B} = \begin{pmatrix} -\cos 2\lambda(1-\cos\tau) & \sin\lambda\sin\tau & -\cos\lambda\sin\tau \\ -\sin\lambda\sin\tau & -\sin^2\lambda-(1+\cos^2\lambda)\cos\tau & \sin\lambda\cos\lambda(1-\cos\tau) \\ \cos\lambda\sin\tau & -\sin\lambda\cos\lambda(1-\cos\tau) & \cos^2\lambda+(1+\sin^2\lambda)\cos\tau \end{pmatrix}$$

An iterative approach to the solution of Eq. (6.2) gave, as a first iteration, the result in Table 6-7 with the corresponding momentum control law shown in Table 6-8.

An alternate discrete mechanization was also presented in Ref. 6-2. It was based on the assumption that the disturbing torques have cyclic components which vary, approximately sinusoidally; thus their average values can be determined by taking the average of their maximum and minimum excursions. An implementation based upon this principle is shown in Fig. 6-21. Six registers are set at each sunrise to record the components of stored angular momentum. Three of the registers are permitted to increase as the corresponding component of momentum increases, but are not permitted to decrease. The other three are allowed to decrease, but not to increase. At sunset the inputs to the registers are disengaged. During the dark-side passage, the sum of the average values of the vector components stored in the registers are held and operated upon by a control law to maneuver the vehicle for momentum dumping.

The discrete mechanization was also discussed in Ref. 6-2 with regard to manual implementation — either as a backup mode or as the primary method of operation. During the sun-side passage, the astronaut notes the maximum excursions of the components of angular momentum as they are displayed on the control panel. A sliderule with three sliding elements can be devised, the front side to accept λ and the components of $\overline{H}_o$, and yield the four values of ϵ_2. The value of ϵ_1 can be taken as zero and $\overline{H}_o$ represents the averaged components of $\overline{H}_2$ as indicated in Fig. 6-21. $\overline{H}_2$ is recorded in the registers. The reverse side performs the same computations to give four values of ϵ_3. Then at the sunset terminator, the 2100-hr and 2400-hr meridians, and the 0300-hr meridian, the astronaut maneuvers the vehicle through the indicated rotations ϵ_2 and ϵ_3. The performance of this momentum dumping procedure will then be in accordance with the analysis given in Ref. 6-2.

The equipment required for the manual mode of momentum dumping would be the aforementioned sliderule and an orbit clock, provided the components of stored angular momentum are computed and displayed. Also λ must be provided by either ground-based communication or prior to flight by tabulated date carried aboard.

Table 6-7

FIRST ITERATION OF SOLUTION

$$\Delta \bar{H}_{11} = \bar{M}_1 \bar{H}_1(0) + \bar{N}_1$$

$$\bar{G} = \bar{G}^1 \operatorname{sgn}(\sin\ ) + \bar{G}^2 \operatorname{sgn}(\cos\ ) + G^3$$

$$G^1_{1j} = G^2_{1j} = G^3_{1j} = G^3_{1j} = 0$$

$$A^\kappa_{1j} = G^\kappa_{2j} \sin\lambda - G^\kappa_{3j} \cos\lambda$$

$$A^\kappa_{2j} = G^\kappa_{2j}(1 + \cos^2\lambda) + G^\kappa_{3j} \sin\lambda \cos\lambda$$

$$A^\kappa_{3j} = -G^\kappa_{2j} \sin\lambda\cos\lambda - G^\kappa_{3j}(1 + \sin^2\lambda)$$

$$\bar{M}_1 = \begin{pmatrix} 4A^1_{11} & 4A^1_{12} & 4A^1_{13} \\ -2\pi A^3_{11}\sin\lambda - 4A^2_{21} & 2\pi(A^1_{12} - A^3_{12})\sin\lambda - 4A^2_{22} & 2\pi(A^1_{13} - A_{13})\sin\lambda - 4A^2_{23} \\ -2\pi A^3_{11}\cos\lambda - 4A^2_{31} & 2\pi(A^1_{12} - A^3_{12})\cos\lambda - 4A^2_{32} & 2\pi(A^1_{13} - A^3_{13})\cos\lambda - 4A^2_{33} \end{pmatrix}$$

$$N_1 = \begin{pmatrix} \pi(4 + 4A^1_{11} - 2A^2_{11} - 3A^3_{11}) + 4A^2_{11} & -4A^1_{12} & -4A^1_{13} \\ (\pi^2 + 8)A^1_{11}\sin\lambda - 2\pi^2 A^3_{11}\sin\lambda - 4\pi A^2_{21} & (4A^2_{12} - 2\pi A^3_{12})\sin\lambda - A^2_{22} + \pi A^3_{22} & (4A^2_{12} - 2\pi A^3_{13})\sin\lambda - 4A^2_{23} + \pi A^3_{23} \\ (\pi^2 + 8)A^1_{11}\cos\lambda - 2\pi A^3_{11}\cos\lambda - 4\pi A^2_{31} & (4A^2_{12} - 2\pi A^3_{12})\cos\lambda - 4A^2_{32} + \pi A^3_{32} & (4A^2_{13} - 2\pi A^3_{13})\cos\lambda - 4A^2_{33} + \pi A^3_{33} \end{pmatrix}$$

Table 6-8

MOMENTUM CONTROL LAW

$$G = \begin{pmatrix} 0 & 0 & 0 \\ -\frac{a}{4}\sin\lambda \,\text{sgn}(\sin\tau) + \frac{d}{4}\sin\lambda & \frac{b}{\pi}\left[\frac{\pi}{8}(1 - 3\sin^2\lambda)\,\text{sgn}(\cos\tau) + \sin^2\lambda\right] & \frac{-c\sin\lambda\cos\lambda}{\pi}\left[\frac{3\pi}{8}\text{sgn}(\cos\tau) - d\right] \\ \frac{a}{4}\cos\lambda\,\text{sgn}(\sin\tau) - \frac{d}{4}\cos\lambda & \frac{b\sin\lambda\cos\lambda}{\pi}\left[\frac{3\pi}{8}\text{sgn}(\cos\tau) - 1\right] & \frac{-c}{\pi}\left[\frac{\pi}{8}(1 - 3\cos^2\lambda)\,\text{sgn}(\cos\tau) + \cos^2\lambda\right] \end{pmatrix}$$

where

$$d = \frac{2}{3}\left[1 \pm \sqrt{1 + \frac{3}{2}\left(1 + \frac{8}{\pi^2}\right) a^2}\,\right]$$

a , b , c are momentum control system gains.

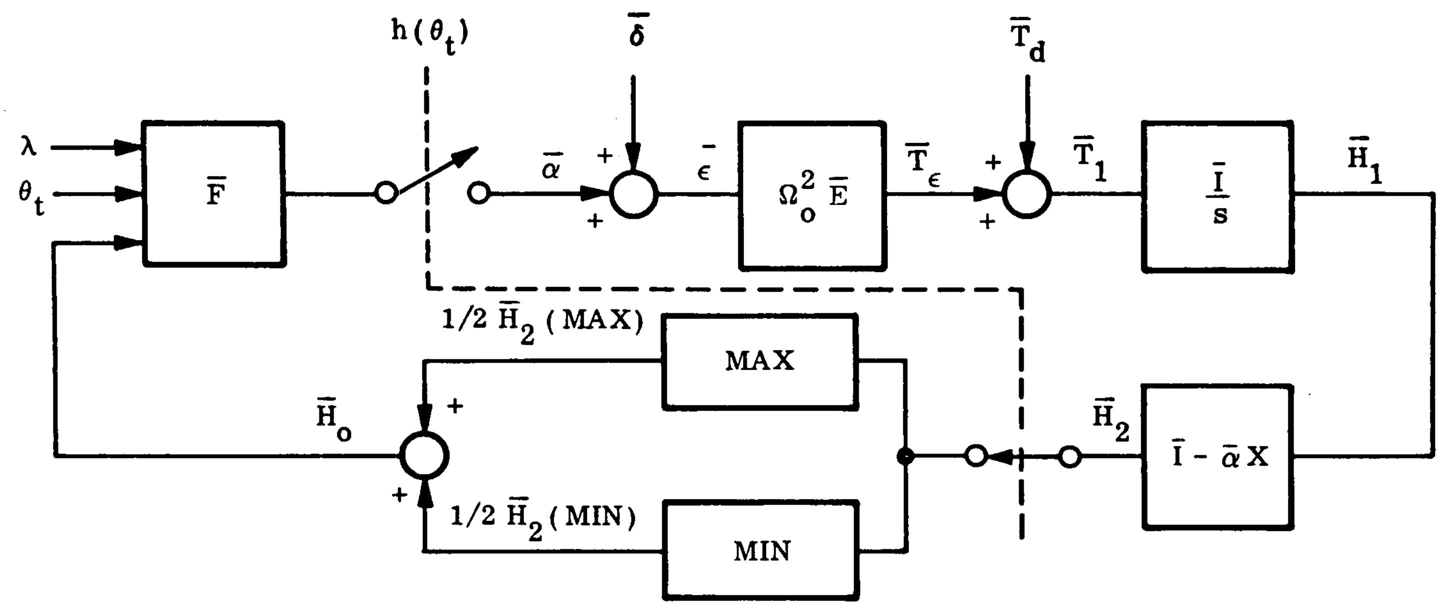

$\overline{H}_2$(MAX) = MAXIMUM OF EACH COMPONENT OF $\overline{H}_2$ FOR $0 < \theta_t < \pi$

$\overline{H}_2$(MIN) = MINIMUM OF EACH COMPONENT OF $\overline{H}_2$ FOR $0 < \theta_t < \pi$

Fig. 6-21 Gravity-Gradient Momentum Dumping – Discrete Implementation

ATM Spar Fine Pointing Control System. The Spar possesses its own attitude control system to permit the extremely fine pointing accuracy required by the telescope. The normal non-occulted operation of the fine pointing system was previously described in subsection 6.2.1.1. The mechanization of the pitch and yaw control loops was shown in Fig. 6-4.

The Apollo telescope is to be pointed at any location on the sun by the two-axis gimbal system capable of removing several degrees of offset in the attitude of the carrier vehicle. A third gimbal axis will cause the Spar, containing the optical equipment and the pitch and yaw gimbals, to rotate through 90 deg in either direction from its central position. This outermost gimbal is not controlled by a closed loop; it is to be used only to orient the roll axis of the telescope at a fixed rotation relative to the carrier. Rotation of the telescope about the line of sight must be maintained to within 10 arc min during the interval in time in each orbit period that solar astronomy experiments are conducted. This requirement is to be satisfied by controlling the roll of the carrier vehicle to this accuracy. The roll attitude is referenced to a star tracker on the Rack which tracks the star Canopus. The analysis and conceptual design of the roll reference control system and its proposed implementation were discussed in subsection 6.2.1.2.

During periods of sun occultation, the Spar gimbal torquers are electrically caged, with signals fed back from gimbal angle pickoffs to the corresponding torquer amplifier. Hence, a fine pointing mode acquisition is required each time the sun rises. This requirement presents no particular problem since the sun will be in the field of view of the precision sun sensor although not on null.

6.2.2 Simulation Rationale

6.2.2.1 Simulation Philosophies. Due to the complexity of the overall integrated ATM control system and its interaction with the two-body dynamics of the carrier vehicle and telescope, a total simulation that could faithfully represent every element is virtually impossible. One approach is to simplify the representation of the system in order to fit within the limitations of the simulation software and hardware. The most obvious and crucial limitation being the size of the computers, either analog and/or digital, which are available for the simulation. Rather than oversimplifying the representation of the ATM system, two alternate approaches suggest themselves:

- Task-Oriented Breakdown
- Control System Mode Breakdown

Task-Oriented Breakdown. From an operator's (astronaut's) standpoint this is possibly the most realistic division of the overall mission. In this approach, the orbit would be divided into sequential segments corresponding to a given task sequence or group of task sequences. The terminal state of the system, that is controls and dynamics, for one orbit segment would become the initial conditions for the next segment and so on through the overall mission. One obvious gross division of the orbit would be into a dark-side passage and a sun-side passage segment. Further segmentation of the sun-side passage could then be based on the tasks which specifically require the astronaut in the control loop. These tasks, defined and evaluated in Ref. 6-3, are as follows:

(1) Activation and alignment of the CMG's and experiment equipment
(2) Search and detection of solar activity, i.e., sunspots, flares, etc.
(3) Operation of the experiment equipment
(4) Manual dumping of the stored angular momentum in the CMG's
(5) Preparations for sunrise, e.g., sun-sensor activation

Observe that tasks (2) and (3) correspond to the sun-side passage and (4) and (5) to the dark-side passage. However, part of task (1), the activation and alignment of the CMG's and manual acquisition of roll reference of the carrier vehicle are activities unique to the first orbit. This suggests that the first orbit should be treated as a separate case. Possibly by means of relays in the software, the special requirements of the first orbit could be incorporated into the overall system simulation as needed.

Control System Mode Breakdown. One of the major drawbacks of the task oriented approach is the necessity in some of the task sequences for the simulation of several control modes at one time. This would thus require considerable software since all of the control system software would have to be held "on line" throughout the simulation. A study of the task sequences might, however, indicate that a group of specific tasks are performed while only one control mode is in operation. The drawback of this approach is that the specific tasks as isolated for the simulation of the given control mode might not be performed in the time sequence or in the midst of other tasks as they would occur in actual orbit. Therefore, this approach is less realistic to the astronaut. However, it has appeal from the standpoint of being able to concentrate on evaluating and optimizing each of the various control modes.

The control system mode approach would also lend itself to a study of stabilization and failure modes as was begun in Part II of Ref. 6-2. An initial summary of typical mechanizations for failure mode operation is shown in Tables 6-9 and 6-10. They indicate those alternates for which man-in-the-loop is required.

6.2.2.2 Control System Simulation.

System Equations. The overall ATM system, its dynamics and control, are presented in detail in Refs. 6-1 and 6-2 and are summarized in Section 6.2.1.2 of this report.

An overall flow diagram for the integrated ATM system is shown in Fig. 6-22.

Perturbations and/or Simulation Simplifications. Preliminary studies of various aspects of the ATM System have been made on greatly simplified models in order to establish general behavior and to make initial estimates of parameters. Among the topics examined thus far have been:

In Ref. 6-1:

- Gyro drift
- Sun sensor noise
- Mass center offset
- Structural compliance
- Errors due to carrier motion

In Ref. 6-2:

- Bending modes on the AAP Cluster

Table 6-9

ATM STABILIZATION AND CONTROL SYSTEM FAILURE MODE MECHANIZATION, RACK/CARRIER CMG CONTROL LOOP

Functional Requirement	Function Mechanization			Expected Performance
	Primary	1st Alternate	2nd Alternate	
Attitude Pointing Reference (pitch and yaw)	Coarse Sun Sensor			Baseline
		Gyros in attitude mode + manual torquing		Reduced
			Man-in-loop	Low
Attitude Pointing Reference (roll)	Star Tracker			Baseline
		Gyros in attitude mode + manual torquing		Reduced
			Man-in-loop	Low
Rate Damping	Gyros in rate mode			Baseline
		Redundant rate gyros		Baseline
			Error rate circuits	Reduced
Error Signal Conditioning, Amplification and Stabilization Circuitry, Torquing Signal Amplifier	CCEA			Baseline
		CCEA redundant circuitry		Baseline
			Man-in-loop	Low

Table 6-9 (Cont.)

Functional Requirement	Function Mechanization			Expected Performance
	Primary	1st Alternate	2nd Alternate	
Steering Control Law Computer	CCEA			Baseline
		CCEA redundant circuitry		Baseline
			Man-in-loop	Low
Carrier Torquing	CMG			Baseline
		Redundant CMG		Baseline
			–	Failed*

*Low performance could be attained through LM gas jets or alternate jets.

Table 6-10

ATM STABILIZATION AND CONTROL SYSTEM FAILURE MODE MECHANIZATION SPAR FLEX GIMBAL SERVO LOOP

Functional Requirement	Function Mechanization			Expected Performance
	Primary	1st Alternate	2nd Alternate	
Attitude Pointing Reference (pitch and yaw)	Fine Sun Sensor			Baseline
		Gyros in attitude mode + manual torquing		Reduced
			Man-in-loop	Low
Rate Damping	Gyros in rate mode			Baseline
		Redundant Rate Gyro		Baseline
			Error rate circuits	Reduced
Error Signal Conditioning Amplification and Stabilization Circuitry	CCEA			Baseline
		CCEA redundant circuitry		Baseline
			None	Failed
Gimbal Torquing	Torque motor			Baseline
		Redundant torque motor (active		Baseline
			None	Failed
Gimbal Angle Measurement	Gimbal pick-off	None	None	Failed*

*Caged mode only.

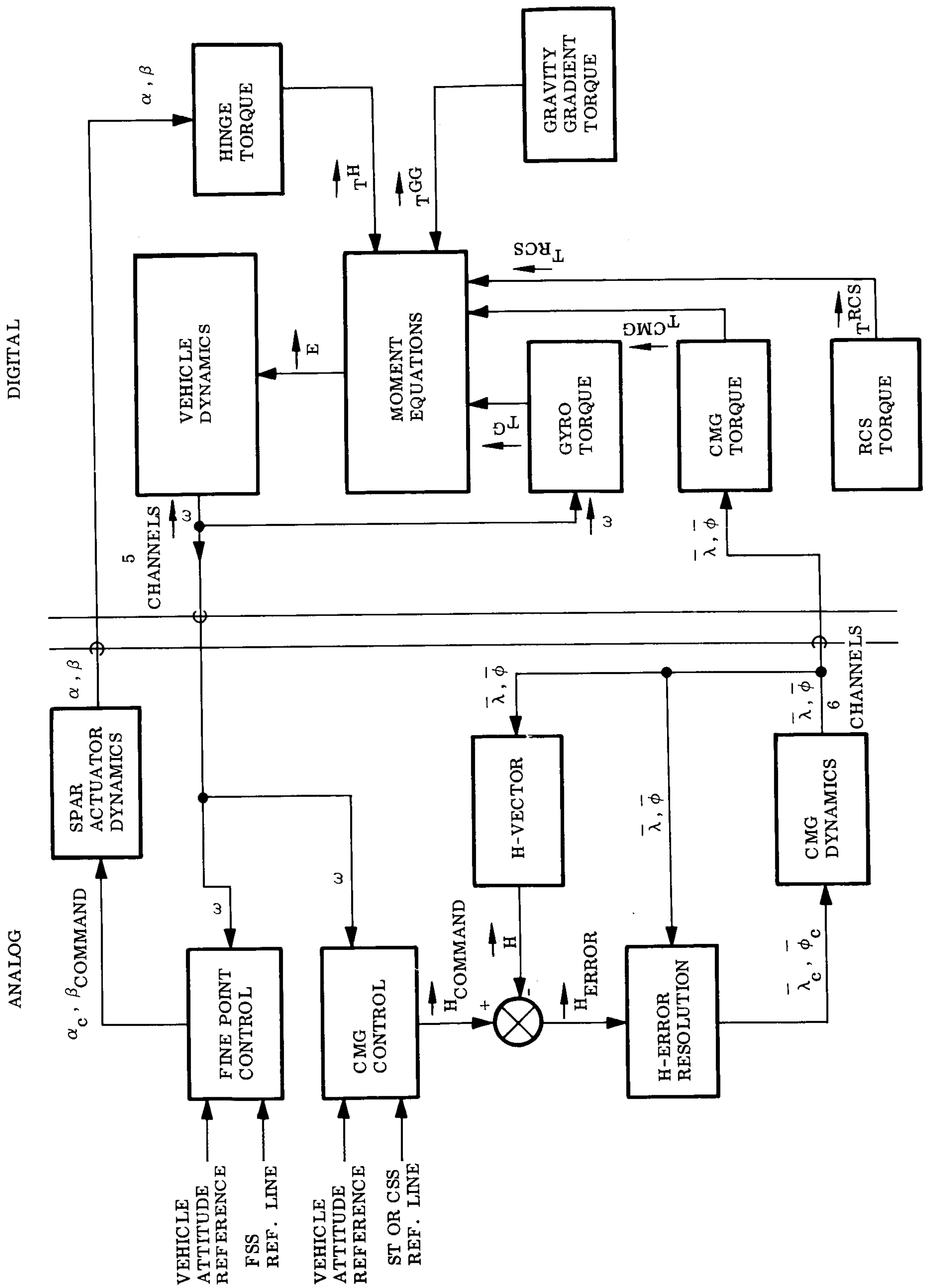

Fig. 6-22 Hybrid Flow Diagram

Along with these items, stability analyses have been conducted on the different control loops. The values of the parameters used are given in Tables 6-11 and 6-12. Since gross approximations were made to facilitate the ease with which these studies could be made, more elaborate studies are in progress or may be required. Provisions for the inclusion of any of the listed problem areas and other possible perturbations ought to be anticipated in any overall simulation. However, these simplified analyses can be of great value in making first approximations in the overall simulation. For example, it was concluded in Ref. 6-2 that the bending mode zeros very nearly coincide with their corresponding poles, indicating that the Cluster can be treated as essentially a rigid body. The root loci show that there are no unstable bending modes for in-plane motion. Likewise in Ref. 6-1, it was concluded that for the model chosen control of the error induced by offset of the Spar center of mass from the hinge pivot was realizable. Also for the same model that if the carrier does not deviate more than 0.2 deg from its nominal attitude, the induced pointing error cannot exceed 1 arc sec. Based on these conclusions, it would seem that two reasonable first approximations for the overall simulation would be to assume the carrier and telescope are each rigid bodies and to take the offset vector $\bar{H}_2$ as defined in Table 6-3 as identically zero. Thus, the components H_4, H_5, and H_6 in the equations shown in Fig. 6-8 would be zero. If necessary, assumptions on the structural compliance at the hinge pivot between carrier and telescope can also be made as was discussed in subsection 6.4 of Ref. 6-1.

6.3 SIMULATION REQUIREMENTS

6.3.1 General Considerations

The total ATM Simulation is to fulfill the following general requirements:

- To function as a tool to establish and evaluate design concepts
- To integrate flight hardware and software, and verify closed loop operation
- To evaluate the crew station (cabin) function, experiment operation, and vehicle control system with man-in-loop

Table 6-11

INERTIA PROPERTIES, MASSES, AND HINGE LOCATIONS

CARRIER

J_{11} = 819,147 kg-m^2
J_{22} = 4,412,603 kg-m^2
J_{33} = 4,383,947 kg-m^2
J_{12} = -191,285 kg-m^2
J_{13} = 45,809 kg-m^2
J_{23} = -15,172 kg-m^2

MASS (M_c): 52,026 kg

HINGE VECTOR:

H_1 = 106.3 m
H_2 = 11.8 m
H_3 = 237.1 m

SPAR

J_{44} = 954 kg-m^2
J_{55} = 2111 kg-m^2
J_{66} = 2309 kg-m^2
$J_{45} = J_{46} = J_{56} = 0$

MASS (M_s): 2000 kg

HINGE VECTOR:

$H_4 = H_5 = H_6 = 0$

Table 6-12

VALUES USED IN NUMERICAL ANALYSIS

Item	Values
CONTROL MOMENT GYROS	
Inner Gimbal Orientation (Initial)	$\varphi_1 = \varphi_2 = \varphi_3 = 0$
Outer Gimbal Orientation (Initial)	$\lambda_1 = \lambda_2 = \lambda_3 = 45$ deg
Angular Momentum	$H^{CMG} = 2720$ n-m-sec
Control Gains	
Position Gains	$\Gamma_{11} = \Gamma_{12} = \Gamma_{13} = 358$ rad/sec
Rate Gains	$\Gamma_{21} = \Gamma_{22} = \Gamma_{23} = 1140$
TELESCOPE	
Position Sensor Saturation	$\lvert K_1 \rvert = \lvert K_2 \rvert = 0.000267$ radian
Torquer Saturation	$\lvert K_3 \rvert = \lvert K_4 \rvert = 3.25$ N-m
Position Gains	$K_{12} = K_{21} = 12,200$ radian/sec
Rate Gains	$K_{14} = K_{25} = 14800$
Flexure Pivot Constants	$K_\alpha^f = K_\beta^f = 17.0$ N-m/radian
Back EMF Constants	$C_\alpha = C_\beta = 2.72$ N-m/sec

6.3.2 Simulation Philosophy

The total ATM Simulation must simulate the complete ATM vehicle dynamics, control system experiments, and the man-machine interfaces. The simulation should be set up to minimize the requirements for hardware; that is all possible subsystem simulations should be set up in the system software. Software would include vehicle dynamics, control systems, and experiments. By maximizing the use of software in the simulation, flexibility is maintained; i.e., changes in system characteristics and parameter perturbations may be easily inserted.

The man-machine interface must be of such a nature that the man's response and characteristics are representative of those which would be obtained under actual operating conditions. The interface must also have the same dynamic characteristics as that used in the actual vehicle. It would be advisable to use modular concepts in developing crew station hardware such that any system design changes are readily accommodated. The basic simulation with the man-in-loop must be capable of evaluating the system performance for the various modes of operation. Performance measures such as system and operator response times and accuracy, as well as classic control systems data such as phase plane plots, will be necessary.

Careful consideration should be given to the possibilities for automated data reduction to provide rapid assessment of the effects of proposed systems change. This is of particular importance in terms of the anticipated system development schedules and the limited time and tight schedules typically followed by the astronauts whose ability to operate the system will ultimately determine its adequacy.

6.3.3 Crew Station

The crew station for the total ATM Simulator must satisfy the man-machine interface requirements and be reliable, easy to maintain, and simple to reconfigure.

The interior section of the simulated cabin must provide an environment essentially equivalent to the ATM cabin. The basic size and environment must be such that the test subject will give realistic responses.

Areas of major concern are the displays and controls:

- Meters
- Switches
- Image Displays
- Hand Controller
- Digital Displays
- Indicator Lights

Environmental factors which will affect test subject response are:

- Light Level
- Acoustic Level
- Temperature
- Atmosphere Makeup

The meters must visually and dynamically be identical to the flight items; however, flight items are not required and in fact may not be adequate for simulation purposes. Meters should dynamically respond to simulated system disturbances in the same manner as they would under actual conditions.

Switches should feel and operate in a realistic manner. All switches should be properly labelled and positioned.

The hand controller must be mounted in the same relative position to the test subject and have identical dynamic characteristics to the real system. Damping, dead zones, and friction must be duplicated.

The image display must respond realistically to vehicle and pointing system maneuvers. The image must also reflect the spectrum being monitored. Spectrums being studied by the various experiments are white light, ultraviolet, extreme ultraviolet, x-ray, and hydrogen-alpha. The sun image must be slowly time varying to simulate the dynamic nature of the sun's thermal activity.

The cabin lighting must be at such a level that the test subject will be under actual operational environment. Cabin illumination should vary with changes in vehicle altitude due to the orientation of the windows with the sun.

6.3.4 Nature of Computations

The ATM vehicle dynamics, control systems, experiment simulation, and certain interfacing between peripheral simulation equipment will be simulated on a hybrid computer. The equations representing the vehicle dynamics and the control systems are presented in subsection 6.2 of this report. These equations must be programmed on a hybrid computer in a form that will allow real-time simulation. Additional software will be required to simulate instrument dynamics, and to form the logic interface between the crew station and the simulation equipment.

6.3.5 Data Accumulation and Reduction

It is important to consider the method whereby data is accumulated, stored, read out and reduced, when the simulator is first designed so that it is an integral part of the system rather than the usual appendage. Data should be accumulated in a manner and format compatible with computer data reduction techniques and also provide a number of immediate real time readouts at the simulation control and monitoring console.

With the exception of analog plots, all quantitative measurements are a period, a quantity figure or total, or a yes/no or go/no-go. These basic measurements are easily manipulated, recoded, printed out, and analyzed in digital form.

In many instances, when analyzing control systems, phase plane plots are extremely useful to abstract data from. Outputs from computer reduced data should be via the typewriter or a digital printer.

For certain applications, video tape recordings, either directly from the crew stating pointing display or from a camera set up to observe the test subject in the cabin environment, are extremely useful.

6.3.6 System Requirements (Experiment)

The major ATM experiment place make many varied demands on the system. Each experiment has its own requirements. The requirements may be categorized as pointing requirements and operational requirements. These major divisions might be subdivided as follows:

- Pointing Requirements
  - Pointing Reference
  - Pointing Accuracy
  - Pointing Stability
  - Jitter Rate
- Operational Requirements
  - Offset
  - Field of View
  - Spatial Resolution

The major solar ATM experiments have been compiled and their requirements listed in Table 6-13.

6.4 FACILITY, COMPUTER, AND EQUIPMENT SURVEY

6.4.1 General Considerations

A task requested by MSFC was to survey facilities in Huntsville and Sunnyvale which had computer capabilities sufficient for a total ATM Simulator. To be provided in conjunction with the facilities survey was a brief look at existing simulation equipment at the same locations which might be applicable for a simulation of this type.

6.4.2 Facility and Computer Survey

Three facilities were surveyed: Lockheed at Sunnyvale, Lockheed at Huntsville, and NASA/MSFC. All three facilities currently have a hybrid computer capability. Lockheed has its Alpha and Beta CDC-Comcor installations at Sunnyvale and its EAI 8900 installation at Huntsville. NASA-MSFC has an ASI 6050 and EAI 8900 installation at Huntsville. The following charts (Table 6-14) give a detailed summary of the available computation equipment, the location, and availability thereof.

All facilities surveyed had adequate space, air conditioning, electrical power, and man power to support the ATM Total Simulation. The simulation will require approximately 1,000 sq ft of floor space adjacent to the computer area and special power, lighting control, and acoustical control.

6.4.3 Simulation Equipment

The simulation equipment of particular interest is the type used for image generation. As equipment of this type is usually expensive and requires a long lead time to acquire, it seems highly desirable to acquire existing equipment if possible. What equipment is available, if any, could well influence the design of the simulation hardware for the Total ATM Simulator.

<u>6.4.3.1 ATM Fine Pointing Simulator.</u> The Biotechnology Department of Lockheed Missiles & Space Company in Sunnyvale has designed, built, and put into operation a simulator for the ATM fine-pointing task. This device was conceived of as an engineering type simulator as opposed to a trainer or mission simulator. It incorporates all important parameters which can be easily varied rather than one fixed configuration. With the exception of the hand controller (which is a LM Block I stick), the controls and displays are functionally represented; actual flight hardware is not used.

Table 6-13

SOLAR ATM

ATM EXPERIMENT	EXP NO.	EXPERIMENT FUNCTION	POINTING REQUIREMENTS					OPERATIONAL REQUIREMENTS		
			POINTING REFERENCE	POINTING ACCURACY	POINTING STABILITY	JITTER RATE	DISPLAYS	OFFSET	FIELD OF VIEW	SPATIAL RESOLUTION
HIGH ALTITUDE OBSERVATORY White Light Coronagraph	S052	Brightness, form, & polarization of the outer corona from 1.5 to 6.0 solar radii from sun's center.	Center of Sun	P = ±20 arc sec of sun center Y = same R = ±1 degree	P = ±2.5 arc sec Y = same R = ±0.5 arc min/min	P = ±5 arc sec/sec max Y = same R = ?	Electronic meter for pointing alignment	None	3° (6 solar radii) (May go to 5° or 10 solar radii)	2.5 arc sec
NAVAL RESEARCH LABORATORY U.V. Spectro-Heliograph	S053 "A"	Coronal spectroscopy	Selected active regions of the sun	P = ±1 arc min Y = same R = ±1 degree	P = ±2.5 arc sec Y = same R = ±7.5 arc min/ 15 min	P = 1 arc sec/sec Y = same R = to be determined	None	P = ±16 arc min. Y = same R = ±90 degrees	55 arc min.	1 arc sec
E.U.V. Spectrograph	"B"	Chromospheric spectroscopy	Sunspots & sun's limb	P = ±2.5 arc sec Y = same R = ±10 arc min	P = ±2.5 arc sec Y = same R = ±7.5 arc min/lt min	P = 1 arc sec/sec Y = same R = to be determined	Visible image in plane of slit. Auto holding signals when off limb	P = ±21 arc min. Y = same R = ±90°/±180°	Total F.O.V. is sun centered circle 42 arc min. diam.	2 arc sec x 10 arc sec
E.U.V. Telescope		To photograph entire solar disc in the EUV	Same	P = ±1 arc min Y = same R = N/A	P = ±2.5 arc sec Y = same R = ±7.5 arc min/15 min.	P = 1 arc sec/sec Y = same R = to be determined	Extreme U.V. image of total disc	P = ±16 arc min. Y = same R = N/A	40 arc min 48 x 48 Flare detector	2.5 arc sec
AMER. SCI. & ENG. INC. X-Ray Spectro-Radiometer	S054	Solar spectroscopy at soft X-ray wavelengths; 2 to 8 Å. Obtain soft X-ray images of quiet sun	Selected active regions on the sun	P = ±2 arc min Y = same R = N/A	P = ±2.5 arc sec Y = same R = ±10.0 arc min/60 sec	P, Y, R, Not applicable if stability is achieved.	X-ray image of total disc	P = ±16 arc min. Y = same R = N/A	40 arc min. 48 x 48 Flare detector	2.5 arc sec
HARVARD COLLEGE OBSERVATORY U.V. Spectro-Heliometer	S055 "A"	UV Spectroscopy of localized solar regions (300 to 1400 Å).	Same	P = ±30 arc sec Y = same R = N/A	P = ±2.5 arc sec Y = same R = To stay within above	P = ±1 arc sec/sec very satisfactory Y = same	None	P = ±17 arc min. Y = same R = none	5 arc sec square	5 arc sec square
U.V. Spectrometer	"B"	UV Spectroscopy of localized solar regions (1450 to 2250 Å).	Same plus sun's limb	P = ±30 arc sec Y = same R = ±1 degree	P = ±2.5 arc sec/15 min Y = same R = ±1° about expt. "B" axis/15 min per.	P = ±1 arc sec/sec Y = same R = N/A	Hydrogen-Alpha image in plane of slit	P = ±16 arc min. Y = same R = ±95° to ±130°	1.4 arc sec x 30 arc sec slit.	1.4 arc sec

FOLDOUT FRAME 2

FOLDOUT FRAME 1

Table 6-13 (Continued)

ATM EXPERIMENT	EXP NO.	EXPERIMENT FUNCTION	POINTING REQUIREMENTS					OPERATIONAL REQUIREMENTS		
			POINTING REFERENCE	POINTING ACCURACY	POINTING STABILITY	JITTER RATE	DISPLAYS	OFFSET	FIELD OF VIEW	SPATIAL RESOLUTION
Hydrogen-Alpha Telescope/ Camera	"C"	To record filter-grams of the sun in H-a.	Entire solar disc	P = ±1 arc min Y = same R = N/A	P = ±2.5 arc sec Y = same R = ±7.5 arc min/15 min	P = 10 arc sec/ sec Y = 10 arc sec/ sec R = N/A	H-Alpha image of total disc.	P = N/A Y = R =	40 arc min	2 arc sec
GODDARD SPACE FLIGHT CENTER X-Ray/E.U.V. Telescopes	S056	X-Ray EUV photo-graphy of selected solar regions	Selected active regions on the sun.	P = ±1 arc min Y = same R = ±20 arc min	P = ±2.5 arc sec Y = same R = ±7.5 arc min/100 sec	P = N/A is stability is achieved Y = same R = same	X-ray intensity indicator	P = ±16 arc min. Y = same R = N/A	40 arc min	5 arc sec on axis & est. 15 at edge of field.

FOLDOUT FRAME 1

FOLDOUT FRAME 2

This simulator, which includes a crew station, image generation equipment, simulation drive equipment, a simulation control and monitoring console, and an analog computer, is fully described in LMSC Report No. A842326.

6.4.3.2 Simulation Equipment at MSFC. A survey was made of the available equipment at the NASA/MSFC Astrionics Lab and the Computation Lab. Of the items examined the following were most applicable:

- Cockpit with a shrinking raster television display
- Cockpit with a large projection screen display
- Six-degree-of-freedom docking simulator
- Alternating action slide projectors with a TV output
- Three-axis flight table

A thorough study of these equipments indicated that none of the existing systems would be suitable for direct application to the total ATM Simulation.

Various subsystem and component parts could be utilized in developing the required simulation equipment, but this would require an extensive salvaging effort and it is questionable if this would lead to a cost effective program.

PRECEDING PAGE BLANK NOT FILMED.

Table 6-14

SUMMARY OF COMPUTER FACILITIES

LOCATION	DIGITAL	ANALOG (Complements given are for each)	INTERFACE (Complements given are for each)	AVAILABILITY	EXTERNAL EQUIPMENT INTERFACE
LOCKHEED Building 151 (Sunnyvale) (Hybrid Alpha)	CDC 3200 - 4 Data channel - 3 Tape drives - 2 Disk drives (10^6 - 24 bit words) - 1000 LPM printer - Card reader - Card punch - 32 K Core	2-EAI 231 R MARK V - 30 Integrators - 45 Summers - 73 Inverter - 48 Multiplier - 10 DFG - 5 Resolvers -170 Pots (150 servoed)	ASTRODATA INTRACOM - 40 D/AC channels - 24 A/DC channels - Precision int. gen. - Patchable logic system	One shift in use through 1967 – Two shifts open – One shift HAS/ADA usage possible and will extend through first quarter 1968	SCADS – (Simulation Cont. and Data System) Signal conditioning, provides necessary buffer and power conversion capability
LOCKHEED Building 181 (Sunnyvale) (Hybrid Beta)	CDC 6400 - 32K Core (60 bit words) - 40K Periph. (12 bit words) - 2 Tape drive (1. + $(10)^6$ - 60 bit words)	4-COMCOR CI 5000 - 60 Integrator - 60 Summers - 90 Multiplier - 3 Resolvers -400 Amplifiers - 22 DFG - 48 HODADS -176 Pots (144 servoed)	2-COMCOR INTRACOM - 40 D/AC channels - 32 A/DC channels	85% of 1.5 shift assigned to C3 through 1970 probable	None other than the two intracoms.
LOCKHEED Building 401 (Huntsville) (Hybrid EAI 8900)	EAI 8400 Fortran Compiler - 4 Tape drives - 32 Bit Word -600 LPM Printer Card Reader Card Punch Paper tape unit - 16 K Core Note: Expandable to 32 K within 60 days	EAI 8800 - 148 Integrators - 48 Summers - 70 Inverters - 24 Multipliers - 6 DFG (20 segments) - 172 Servo pots - 3 Resolvers Note: Expandable within 60 days to - 60 Integrator - 60 Summers - 90 Inverters - 48 Multipliers - 12 DFG (20 segments) - 290 Servo pots - 12 Resolvers	EAI 8900 - 16 D/AC channels - 16 A/DC channels Note: Expandable within 60 days to 32 channels	The HREC 8900 system is available for this simulation on a complete committment basis.	Interconnect through analogue and two sense liner to digital.

FOLDOUT FRAME 2

FOLDOUT FRAME 1

Table 6-14 (Continued)

LOCATION	DIGITAL	ANALOG (Complements given are for each)	INTERFACE (Complements given are for each)	AVAILABILITY	EXTERNAL EQUIPMENT INTERFACE
NASA/MSFC Computation Lab Huntsville (Hybrid ASI 6050)	ASI 6050 Machian Language - 2 Tape drive - 24 Bit word Punch paper tape unit Printer 16 K	2 Each EAI 231 RV - 50 Integrator - 75 Summers - 16 Inverters - 7 Multipliers - 16 DFG (20 segment) - 160 Pots - 3 Resolvers	Adage - 16 D/AC channels - 16 A/DC channels	Currently completely scheduled	
NASA/MSFC Computation Lab Huntsville (Hybrid EAI 8900)	EAI 8400 - 4 Tape drives - 32 bit word - 600 LPM Printer Card Reader Card Punch Fortran Compiler - 32 K Core	3 Each EAI 8800 - 60 Integrators - 60 Summers - 90 Inverters - 48 Multipliers - 12 DFG (10 segments) - 290 Servo pots - 12 Resolvers	EAI 8900 - 32 D/AC channels - 32 A/DC channels	Currently completely scheduled	Sense Lines Interface to digital Interconnect interface to Analogue

FOLDOUT FRAME 2

FOLDOUT FRAME 1

6.5 SIMULATOR CONCEPTUAL DESIGN

6.5.1 Description

The total ATM Simulator is to be used as a tool to evaluate and optimize mans' involvement in the total integrated ATM pointing control system. The three basic torque generating systems and their interactions to be simulated are the Reaction Control System (RCS), the Control Moment Gyros (CMG's), and the Spar Torques. The applications of, and the pilot's interface with, these systems are fully described in subsection 6.2.

The simulator must include the controls and displays, visual cues, control and display inter-reactions, and other such cues to the astronaut. These are utilized to perform the pointing, scanning, and orientation tasks required for the on-board ATM solar experiments, in addition to gross sun-Canopus acquisition, CMG momentum dumping, and the gross altitude orientation with the RCS.

Computational capability is required to model the vehicle and pointing dynamics, attitude control systems, and orbital parameters. Additional computations are also required to interface the simulation equipment dynamics with the simulated vehicle, experiment and orbifal conditions.

Image generation equipment is required to supply the dynamic visual displays for realistic solar experiment operation, Spar pointing, etc.

The design of all control stations, hardware requiring manual operation, and general facility will be based on generally accepted human engineering practices in the aerospace industry emphasizing safety.

6.5.2 Simulation Hardware

Due to the critical time scheduling involved, the final hardware design and image generation techniques will be dependent on equipment availability at the time of go-ahead.

Both procurement time and cost make the use of flight hardware prohibitive. With the exception of the hand controller, which might be one used for evaluation or be a reject, the instruments, controls, and other displays would be commercially available hardware items. Examples of such nonflight hardware which present to the astronaut the same visual and tactile inputs, are detailed in subsection 6.5.4.

This simulator is to be used as a design tool and therefore must be designed and fabricated in a manner which permits easy modifications, not only to the panel instruments, but also to the image generation equipment. See Fig. 6-23.

6.5.2.1 Simulation Control and Monitoring Console. This console will provide supervisory control and monitoring for the simulation facility. Prime functions include remote control of the computer, remote monitoring of the test subject, readouts of only those crew station parameters relevant to the particular functions being evaluated, simulation equipment and systems status, control function for associated equipment, real-time perturbation insertion, and the central communications link for the simulation facility.

To provide the necessary flexibility for system development, the console will have a patching and signal distribution network built in with the required interface electronics. It will, therefore, be possible to display any one of the many parameter signals in the simulation system.

All panels will be modular in concept for versatility and maintenance reasons. Hardware will be chosen for reliability, availability, cost and will be organized using the highest standards of human engineering practice.

Some of the major control functions are:

- Main power to switch on all simulation equipment
- Experiment start switch which initiates computer operation and cues the pilot to begin the task
- Controls to present real time perturbations to the pilot

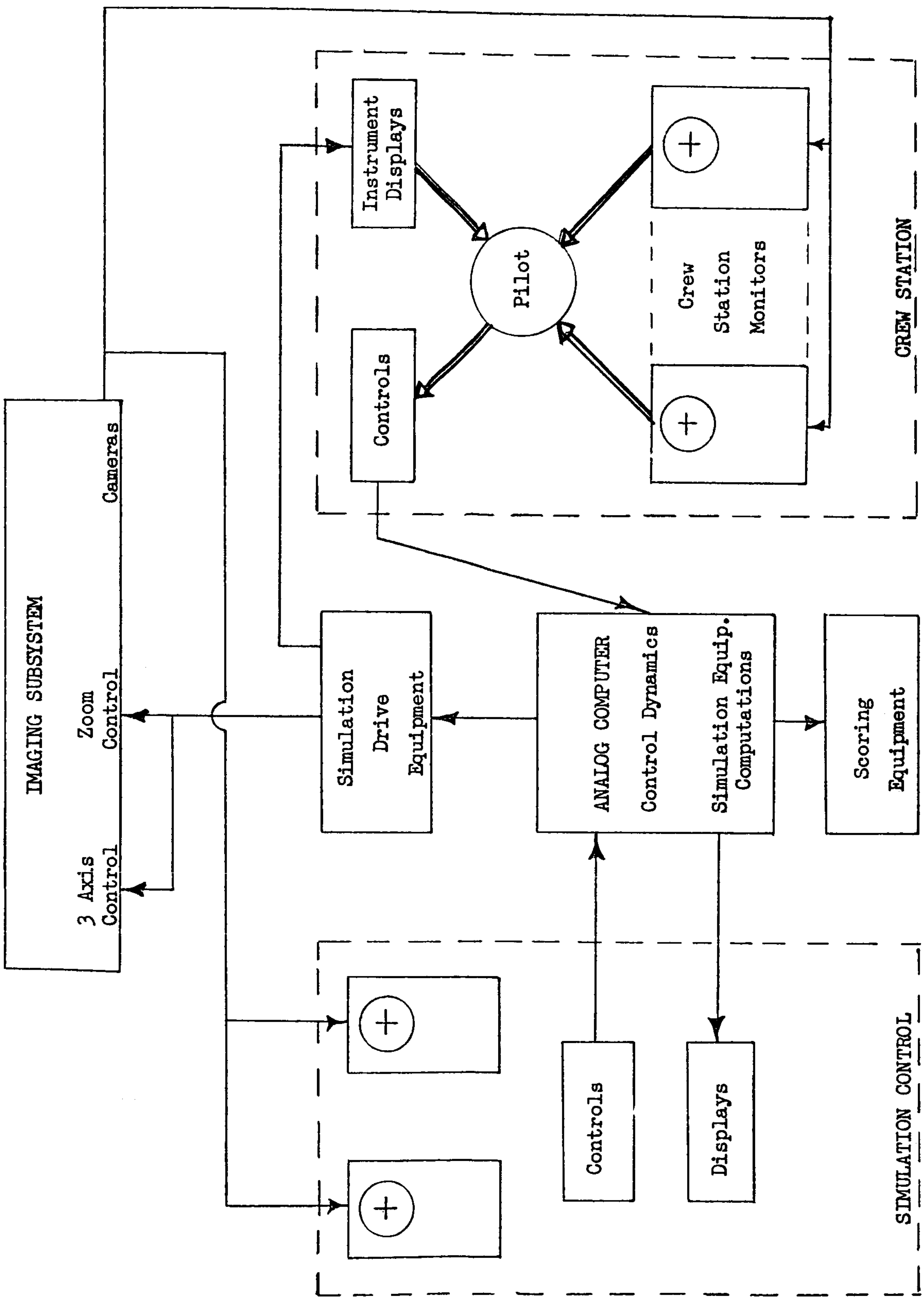

Fig. 6-23 Simulation Hardware

- Switching to automatically alter computer configurations for various phases of the experiment
- Control of data accumulation

Visual and instrument displays include:

- Two video displays to monitor the normal and magnified experiment images
- Spar attitude instrumentation
- Instrumentation to monitor CMG disposition
- Video and instrument monitoring of test subject and crew station controls to assist in acquiring "man-in-the-loop" data

6.5.2.2 Image Generation Equipment. The equipment in this subsystem is shown in Fig. 6-24. The design is intended to provide maximum flexibility of image format. A remote-controlled slide projector may be used to present a variety of photographs taken in different spectral bands, or a film strip projector for presentation of a dynamically changing target image. High image resolution will be obtained by using the fewest possible number of electro-optical elements.

The projector subsystem, as previously mentioned, will be remotely controlled through interface electronics with the computer.

Pitch and yaw motions will be generated by two-axis servo-driven optics. A more detailed study is required to determine the desirability of two single axis versus double gimballed control, and mirror versus prism optics.

The lens imaging and roll subsystem contains the collimating optics required for imaging compatibility with zoom optics. Beam splitting is required for normal and magnified image generation. Roll motions are obtained by a servo driven prism device.

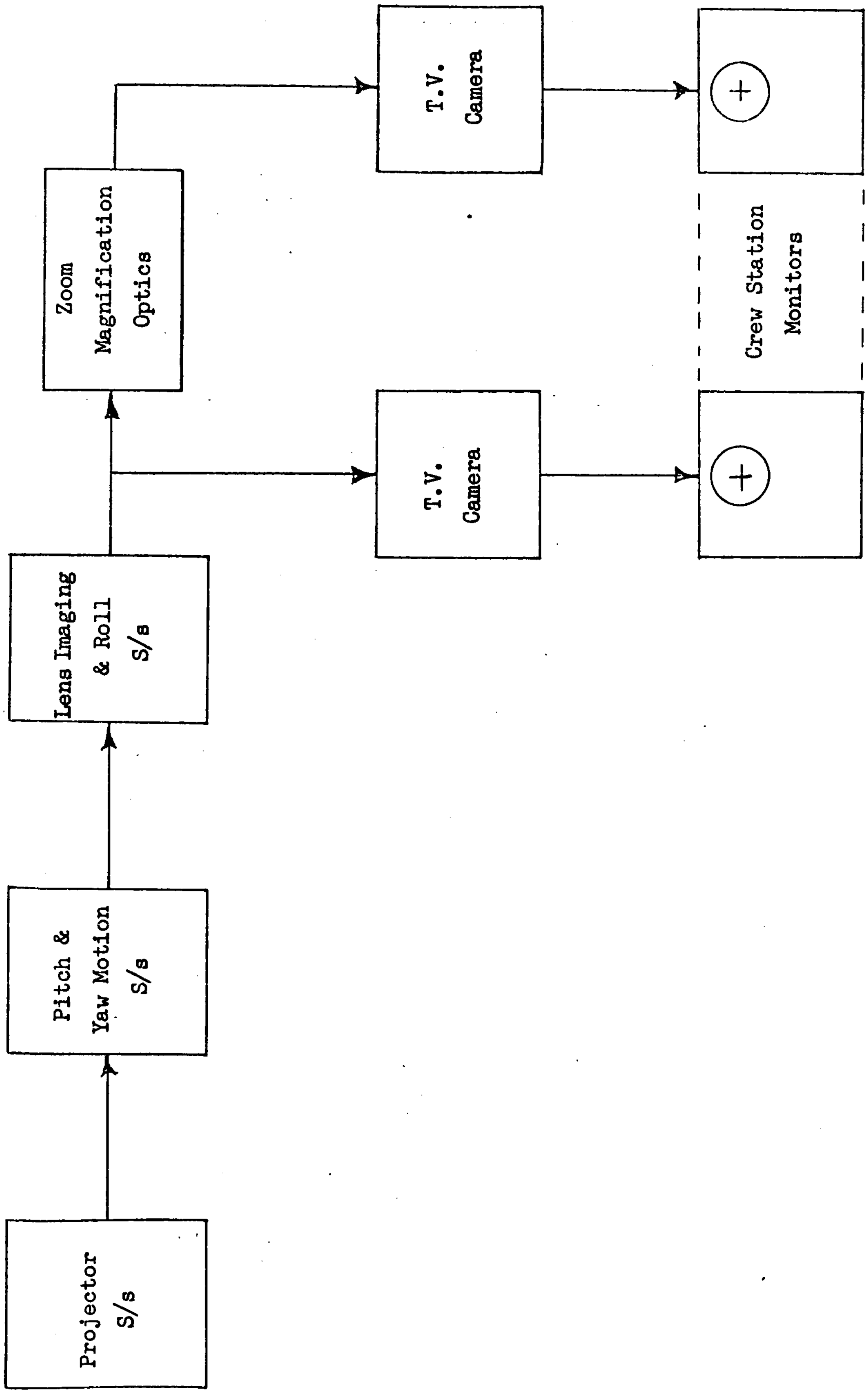

Fig. 6-24 Image Generation Subsystem

Image magnification is obtained by a servo-driven zoom lens. Control signals for the zoom and three axis servos originate in the computer as a function of the pointing control dynamics and simulation equipment computations.

The TV cameras and monitors are of wide bandwidth using 1029 line scan and capable of high-image resolution. Although this is far in excess of the flight video equipment, it is not significantly more expensive in a nonflight version. Initially, the operation may require degradation to match the flight system, but after data and photos are returned from the first AAP/ATM flight the higher resolution may be required to utilize the images brought back for simulation in bands other than H α.

6.5.2.3 Simulation Drive Equipment. This equipment represents the power interface between the control signals and related drive mechnisms. A large assortment of signal conditioning and power amplification electronics is required to provide the necessary interfaces for system compatibility. The electronics will be packaged in modular form and located with respect to associated equipment in such a way as to simplify the system cabling and switching requirements.

Signal conditioning electronics will consist of a variety of ac and dc low-level modulators, and demodulators for the conversion of crew station and computer control and instrument signals to the proper form and level.

Power amplifiers are required for servo drive functions and relay control boxes will simplify a number of control switching operations; the projection subsystem being one example.

6.5.2.4 Cabling and Patching System. This system is often overlooked in the preliminary stages of planning and results in a hardware system with a maze of wiring and inadequate flexibility for system change.

The simulation may be broken down into four major equipment groups. The crew station and simulation drive equipment located in one area, the computer in a second area, and the simulation control console in a third; see Fig. 6-25. Patch panels at

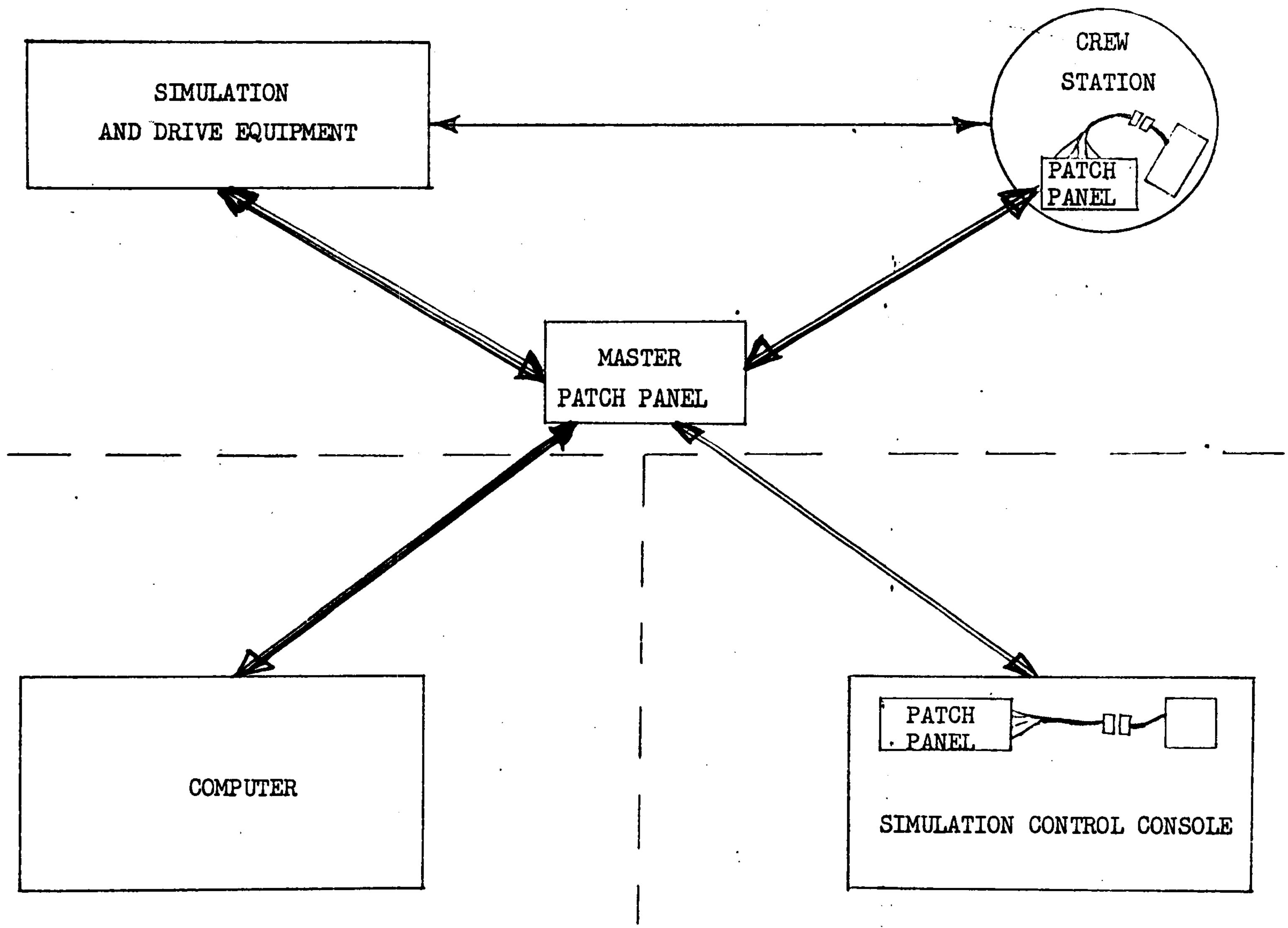

Fig. 6-25 Cabling and Patch Panel System

the crew station and simulation control and monitoring console facilitate the interchange of experiment panels on a day-to-day basis if so desired.

A master patch panel, semiautomatic in nature and using digital processing, can be programmed for a large number of possible interconnections. Due to the complexity of system interface, this technique will allow rapid transition from one group of experiments to the next.

A number of sizes of standard connectors will be used throughout for intermediate equipment connections. This is consistent with the modular philosophy adopted for the simulation. For example, by providing each experiment panel in the crew station with a connector terminated cable, the panel may be rapidly replaced with another without having to disturb the patch panel connections. Male-female connector pin relationships will be standardized for all equipment to prevent confusion and insure reliability.

6.5.2.5 Data Accumulation. The data accumulation and reduction equipment must be considered in the initial design so that it is an integral part of the system. Data will be accumulated in a manner and format compatible with the computer program and language. This data will be stored for later off-line computer processing (data reduction). There will be sufficient data conversion capacity for some real-time data monitoring at the simulation control and monitoring console.

The simulation control console will contain both analog and digital displays for data presentation in addition to a digital printer or computer control typewriter.

Both video and voice recording equipment will be utilized to monitor the performance of the test subject. This equipment will be compatible with the other television equipment used in the image generation hardware and will be remotely controlled at the option of the test controller.

All data, whether analog or digital, represents a quantity, a period, or a yes/no. When considered in conjunction with sequence, run number, time of day and other like information any parameter or group of functions may be presented or analyzed. When considered as having to handle only three basic types of quantities, computerized or automatic data reduction becomes a simple matter.

6.5.2.6 Simulation Facility Communication. A number of personnel necessary to run the simulation and the physical separation of the groups of equipment require that a network form of communications system be installed. Headsets (interchangeable with handsets) will be used and the system will be capable of talk, listen, and talk-listen operation. Three or four nets will probably be employed.

The system will incorporate capability for the simulation of ground/LM and LM/CM/SIVB communications.

6.5.3 Software

6.5.3.1 General Considerations. The software portion of the total ATM Simulator is divided into two general categories. The first is the simulation of the vehicle dynamics and the control systems. This includes such areas as CMG Control System, Fine Pointing Control System, H-Vector Control law and vehicle dynamics including gravity gradient and orbital parameters. The second category is that required to interface the various pieces of simulation equipment with the computer and the crew station. The software development program is centered around hybrid computation. It is felt that to simulate a complex dynamic system of this nature and form the hardware interface, a hybrid computer will be invaluable.

6.5.3.2 Hybrid Philosophy. The development of a hybrid simulation requires an understanding of the basic limitations and advantages of both the digital and analog computer. This discussion will be divided into two related topics:

- Division of the simulation
- Perturbations and changes

The division of the problem between the analog and digital portions of the hybrid computer is a critical point in the development of a hybrid simulation. This breakdown of the simulation is a function of several variables and must be formed through tradeoffs. Some general considerations for analog and digital tradeoffs are categorized below. The analog computer should contain:

- High-frequency terms
- Closed loop equations such as transfer functions and control loops
- Variables requiring hardware interface

The digital computer should contain:

- Open-loop equations such as trajectories and coordinate system transformations
- Variables requiring high accuracy and repeatability
- Complex logic and data storage
- Multivariant function generation
- Variables with a wide dynamic range requiring floating point arithmetic

The analog computer inherently performs specific functions better than the digital computer when we are considering real time simulation. High-frequency modules can ordinarily be handled better on the analog computer due to its continuous mode of operations. Closed-loop transfer functions such as filter, control loops and servo mechanisms are easily simulated on the analog side because of the continuous integration mode utilized by the analog. Interfacing with external hardware is easily accomplished on the analog computer. Analog signals may be scaled and used as direct inputs to the simulation. Digital signals must be converted to analog, but they may be handled by the analog on a continuous basis.

The digital computer compliments the analog by performing those functions which the analog cannot readily handle. The open loop evaluations may be very accurately handled on the digital computer since the digital system does not suffer from the drift inherent to analog computations. The digital computer has the ability to be highly accurate and repeatable when required. Complex data storage and the generation of complex functions through table lookup techniques and curve fitting are readily handled on the digital computer with existing software. By the use of floating point arithmetic, variables with a wide dynamic range may be accurately handled over several orders of magnitude.

The methods of program modification can be applied on line in a real-time simulation.

The normal methods for inserting data into the digital computer such as cardreader, typewriter, or magnetic tape unit are not fast enough for real time simulation or cannot be used on lines during a simulation run. However, there are two DAC's with an input from a hand turned pot or a thumbwheel dial with output transmitted through logic lines to the digital computer.

The hand turned potentiometer can be used to change parameters in a continuous fashion causing all values between the old number and the new number to be inserted while the change is occurring.

The thumbwheel dial can be used to insert data into the digital computer without using analog hardware. All necessary hardware is contained on the EAI 8900 logic panel.

A decimal number can be hand set using a four-digit thumbwheel dial. Each digit from the thumbwheel dial sets four flip-flops to represent the number in binary coded decimal (BCD) form. The four-digit number requires 16 flip-flops for representation in BCD. A 16-bit logic word is constructed using the state of the flip-flop outputs. The digital computer inputs the logic word using the 16 logic lines available with the hybrid interface hardware. The moment of input can be controlled by manually activating an interrupt signal to the digital computer. The name of the parameters can be specified by assigning each one to a different interrupt line.

The BCD logic word in memory will be converted to binary and then to decimal form using an assembly language subroutine.

Analog methods for inserting changes include:

- Potentiometers
- Manual function switches
- Comparator relays

Analog constants can be changed using hand-turned potentiometers.

Configuration changes can be accomplished using manual switches and comparator relays.

The comparator relays are used when switching conditions are predetermined. Manual function switches are used when the configuration changes are made on-line during a run.

Insertion of perturbations and changes will be easier to implement using the analog computer. However, the digital thumbwheel methods will have a slightly greater accuracy.

6.5.3.3 Hybrid Breakdown of the Total ATM Simulation. The breakdown of the simulation follows the criteria discussed in subsection 6.5.3.2. As previously stated, tradeoffs are required for development of a real-time hybrid simulation. A dominating factor is the amount and distribution of the computing equipment available. There may often be cases where a tradeoff will be required to decide which module must go where because there is not room for both. The computer software is divided into two distinct areas:

- Vehicle controls and dynamics
- Hardware interface

The equations representing the simplified vehicle dynamics and controls are developed in subsection 2 of this report. The hybrid break down of the controls and dynamics is exhibited in Fig. 6-26. The breakdown is as follows:

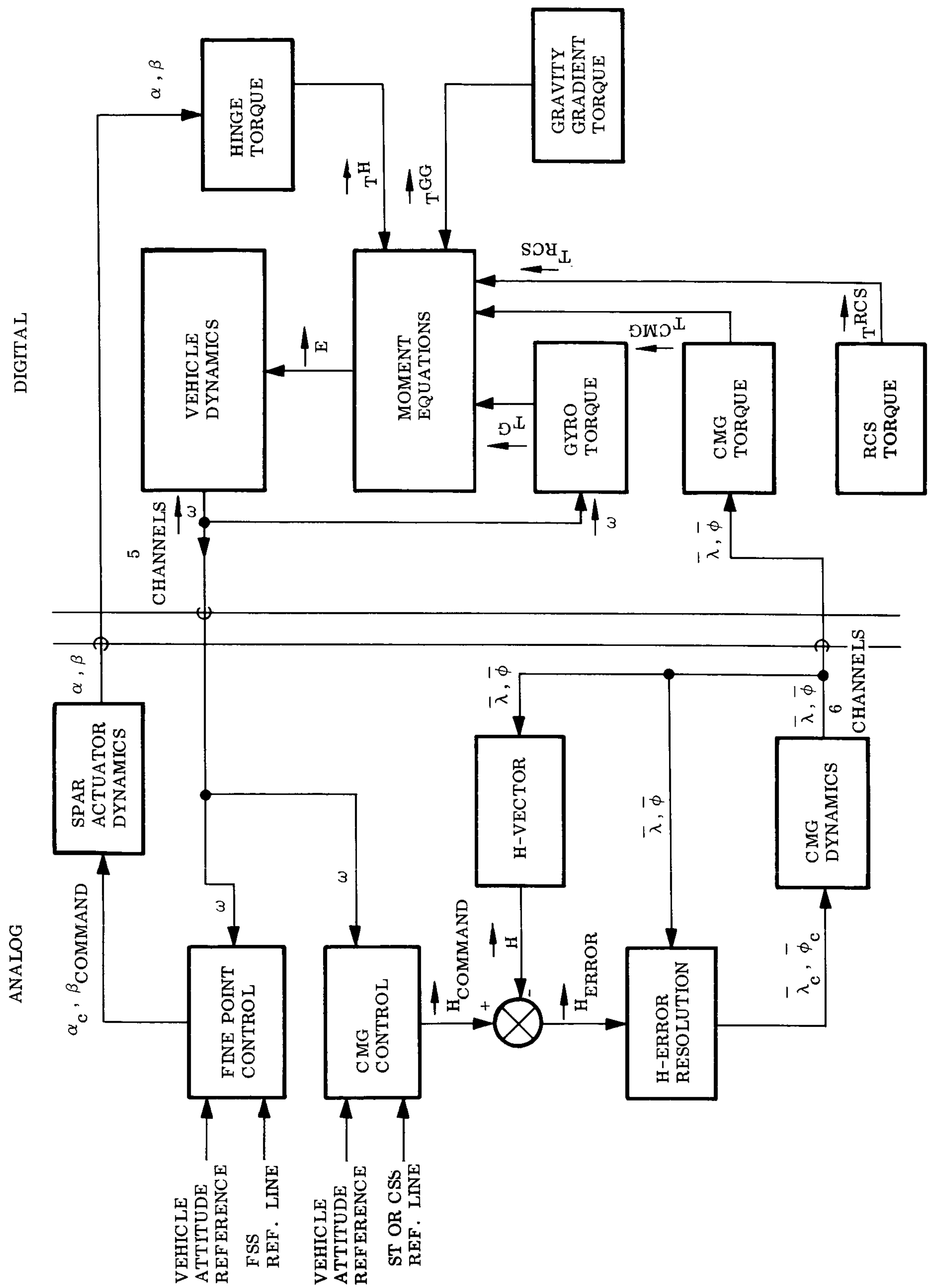

Fig. 6-26 Hybrid Flow Diagram

Digital

- Vehicle dynamics
- Moment equations
- Torque equations

Analog

- CMG control equations
- Fine pointing control equations
- H-vector control law
- CMG dynamics
- Spar actuator dynamics

The moment equations and torque calculations were placed on the digital side of the hybrid simulation because the inherent arithmetic accuracy. To avoid the drift that would build up on the analog, the vehicle dynamics were placed on the digital computer.

The control equations, control law, and actuator dynamics (CMG and Spare) were placed on the analog side of the simulation. This choice was made because of closed loop nature of CMG and actuator dynamics and the possible frequency of control perturbations. It was also felt that external perturbations were more likely in the control section.

The hardware interface software is that software required to interface the computer with the crew station, control console, and simulation equipment as well as perform logic functions required to allow simplification of the hardware. The interface software will be distributed as required between the digital and analog computer.

A software module will be developed for the collection and off-line reduction of simulation data.

6.5.3.4 Estimate of Hybrid Size. The complete simulation can be fitted onto an EAI 8900 hybrid computer or its equivalent. An EAI 8900 consists of the following equipment:

Analog 8800

Pots	-	290
Summers	-	60
Integrator	-	60
Multiplier	-	48
DFGS	-	10
Resolvers	-	6

Digital 8400

32K memory core

Interface

32 DAC

32 ADC

The software modules for the simulation were estimated as follows:

Module	Digital Core	Analog Components
Vehicle dynamics	6K	---
Moment equations	5K	---
Torque equations (Gyro, hinge, gravity gradient, CMG, RCS)	12K	---
On-line data acquisition	4K	---
Hybrid sepercronization routine and executive routine	4K	---
Control equations (CMG)	---	25 Pots 12 Summers 7 Integrators
Fine pointing control	---	12 Pots 6 Summers 4 Integrators
H-vector control law	---	30 Pots 16 Summers 9 Integrators 25 Multipliers 6 Resolvers

Module	Digital Core	Analog Components
CMG dynamics	---	30 Pots
		6 Summers
		6 Integrators
Spare dynamic	---	15 Pots
		6 Summers
		6 Integrators

The total equipment estimate indicates that a computer with approximately 32K core and an analog complement consisting of at least:

120 Pots
46 Summers
35 Integrators
25 Multipliers
6 Resolvers

could be used for a first cut at the simulation. A complete analog equivalent to the EAI 8800 is recommended in order to allow portions of the problem currently allocated to be digital to be placed on the analog if required to obtain real time operation.

6.5.4 Simulated Cabin

6.5.4.1 General Considerations. The ATM control and display consoles are to be installed in a simulated Lunar Module (LM) cabin. Requirements for the simulated LM cabin configuration for the ATM mission are defined herein. This report is concerned only with a preliminary description since the console designs are incomplete. However, it will serve to inform interested parties of the general plan proposed by the LMSC designers. All discussion herein is based upon the LM-4. Interior arrangement shown in Grumman document LDW 340-54050 was the principal reference used to identify affected areas of the LM. The drawing numbers used to designate the console assemblies are issued by Marshall Space Flight Center.

6.5.4.2 Structure. The simulator cabin must appear to duplicate the ATM physical environment which may affect the human operator.

The interior of the cabin must be enclosed with the same basic volume and dimensions of the ATM cabin. The controls and displays must be simulated in detail (see Fig. 6-27) since these are the items which most directly affect the test subjects performance. The physical detail of the rest of the cabin is not required. Other cabin requirements are: realistic lighting for complete mission, life support system so that suits may be utilized, and cabin ventilation when life support system is not in use.

The external portion of the ATM simulator should be open to allow unrestricted access to the equipment. The major requirement that the external portion of the simulator must satisfy is that of maintainability. The design should at all times strive to allow maximum access to the simulation equipment. There is no reason for the simulator to externally resemble the ATM vehicle.

<u>6.5.4.3 Controls and Displays.</u> As stated in paragraph 6.5.4.2, the control and display consoles of the ATM must be simulated in detail. The interface between the test subject and the vehicle control system is the control and display console, therefore this console must look, feel, and dynamically respond the same as the system being simulated.

While the controls and displays must on the surface be identical to those actually used on the ATM, it is undesirable in certain cases to use the identical items. The major criteria affecting the selection of components for the simulation are: Reliability, Cost, Availability, Required Interface, and Authenticity of Simulation. Tradeoff studies are required to determine if there are substitutes which are preferable to flight hardware.

LMSC performed a preliminary survey of the components required to build an ATM Simulator (Document No. LMSC/HREC A784609).

<u>Simulation Components.</u> Charts follow that contain information concerning the use of flight components for the first ATM simulator. The first simulator is considered as

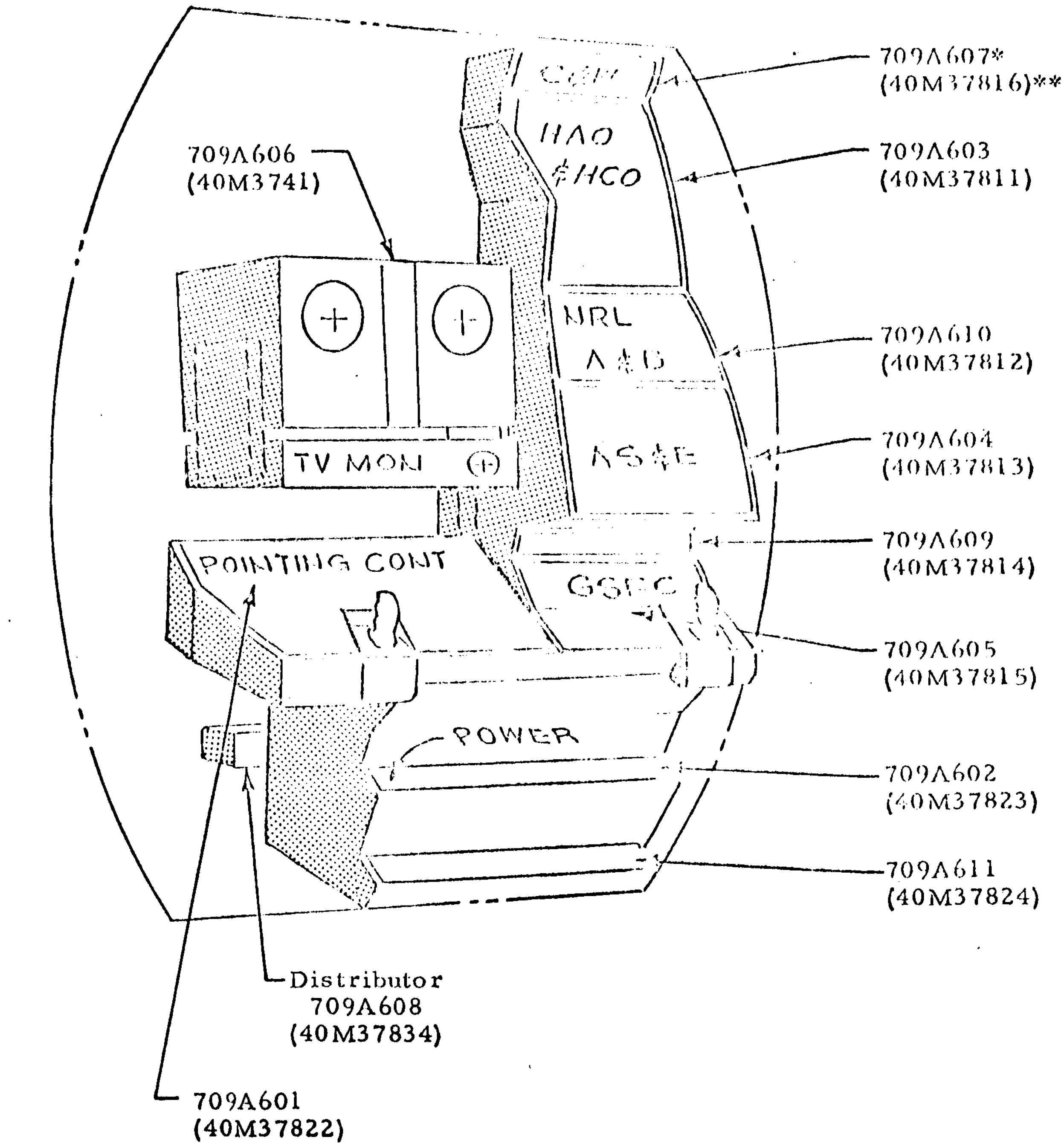

*MSFC Reference Designation
**MSFC Drawing No.

Fig. 6-27 ATM Control and Display Console Unit 709 (40M37800) being used for evaluation of the manned system. Comments on candidate hardware for the simulator, vendors, cost and tradeoffs are offered for each component. Where information is obviously omitted, it was not available at this time.

Three panels were chosen as representative examples; Naval Research Laboratory Experiment Panel No. 709A606, Power Monitor Panel No. 709A605, and American Science & Engineering Experiment Panel No. 709A503. Panel components are listed in Tables 6-15 through 6-17.

Each subsystem is contained on a single panel, with a few exceptions. The panel designator is shown by the subsystem name. Headings are used as follows:

- Required Components - The most common name of the control or indicator as used on the panel.
- Designator - The designator as assigned by LMSC to the component. The full designator would include that of the panel on which the component is mounted, e.g., 709A603S1; the full designator is used only when the component is not on the primary panel for its subsystem.
- Description - Brief information on essential distinctions of the component.
- Function - A description of the component's function in the subsystem.
- Part Number - The MSFC number (40 M XXXX) by which the flight component may be ordered.
- Weight - Weight of the component only, excluding any mounting hardware not on the part drawing.
- Continuous Power - Power dissipated by the part in normal operation in the panel, excluding EL lighting and transients. Picture taking shall be considered a transient.
- Flight Hardware Applicable - A simple yes or no to indicate whether the flight component is considered satisfactory for the simulator. "Later" is entered if the flight component is expected to be available later than 1 December 1967.
- Date Available - Best estimate of when first flight hardware will be available from the vendor.

- ROM Cost - Rough-order-of-magnitude unit cost of the flight component on common components, e.g., switches, cost will be in the notes.
- Remarks - To clarify any significant information not in the format. Especially significant are transient power, anticipated major change in the specified part, or reference to a document or appendix giving special information on simulator parts.

Information is presented concerning the advisability of using flight components for the first simulator. The first simulator is considered as being used for evaluating the manned system. Helpful comments on candidate hardware for the simulator, vendors, prices, and tradeoffs are offered for each component. Rough-order-of-magnitude (ROM) cost is repeated here from Section 2 to facilitate evaluation of components. Where information is obviously omitted, it was not available when this report was printed.

Repetitive information on flight qualified components is referenced to the following notes:

Note 1: The dual vertical meter will be available in December 1967. ROM cost is $6,000.

Note 2: The component indicator light will be available in October 1967. ROM cost is unknown.

Note 3: The exposures remaining counter will be available after January 1968. ROM cost is unknown.

Note 4: The rotary switches will be available in November 1967. ROM cost is $2500.

Note 5: The flag indicators will be available in November 1967. ROM cost is $900.

Note 6: The toggle switches will be available in November 1967. ROM cost is $200.

Component Tradeoffs. The following rational was used for the choice of the components for the simulated controls and displays.

- Counter Exposures Remaining - The flight model would be satisfactory for the simulator, but will be available too late for the first simulator, since the RFQ will not be released until about mid-August. The flight model will probably be too costly; also ROM cost is unknown.

Table 6-15

NAVAL RESEARCH LABORATORY EXPERIMENT PANEL NO. 709A606

REQUIRED COMPONENTS	DESIGNATOR	DESCRIPTION	FUNCTION	PART NO.	WEIGHT (LBS.)	CONTINUOUS POWER (WATTS)	FLIGHT HARDWARE APPLICABLE	DATE AVAILABLE	R.O.M. COST	REMARKS
NRL Shutdown Switch	S7	Ma-Ma	Terminates any sequence in progress, closes the camera shutter, closes the aperture door, recycles the instrument to starting conditions and turns off instrument power to both experiments A and B.		0.17	0	Yes	Note 6	Note 6	
Sequence Mode Switch	S5	Mo-Ma-Mo	Spect position initiates an automatic sequence of six exposures. After each exposure the grating position is changed. Time position initiates an automatic sequence of three exposures. All three exposures are taken at a manually selected grating position.		0.17	0	Yes	Note 6	Note 6	
Sequence Mode Flag	DS4	S - (B.P.) - T	S indicates that spectral sequence is in operation. T indicates that time sequence is in operation.	40M37768-23	0.09	0.041	Yes	Note 5	Note 5	
Exposure Switch	S4	Mo-Ma-Mo	Short command initiates a shorter exposure time. Norm command initiates a normal exposure time. Long command initiates a longer exposure time.		0.17	0	Yes	Note 6	Note 6	
Expo Flag	DS3	S - (Gray) - L	S indicates short exposure is being used. Gray indicates normal exposure is being used. L indicates long exposure is being used.	40M37768-27	0.09	0.41	Yes	Note 5	Note 5	
Grating Position Switch	S2	Mo-Ma-Mo	Selects which of the two gratings is in use.	40M37768-1	0.17	0	Yes	Note 6	Note 6	
Grating Position Flag	DS1	1 - (Red) - 2	Indicates which of the two gratings is in use.		0.09	0.041	Yes	Note 5	Note 5	
Manual Shutter Control	S3	Ma-Mo	Open position opens the camera shutter. Close position closes the camera shutter and cycles the film automatically in preparation for a new exposure.		0.17	0	Yes	Note 6	Note 6	
Shutter Position Flag	DS2	O - (Red) - (Gray)	O indicates the shutter is open whether manually or automatically. (Red) indicates failure. (Gray) indicates the shutter is closed.		0.09	0.041	Yes	Note 5	Note 5	
NRL Aperture Flag	DS13	(Gray) - (Red) - (b.P.)	Gray indicates aperture open. Red indicates a failure. Barber Pole indicates aperture closed.	40M37768-11	0.09	0.041	Yes	Note 5	Note 5	
Flare Mode Switch	S8	Mo-Ma-Mo	Initiates an automatic sequence of exposures optimized for flare conditions. Specific sequence is not yet defined.		0.17	0	Yes	Note 6	Note 6	

FOLDOUT FRAME 1

FOLDOUT FRAME 2

PRECEDING PAGE BLANK NOT FILMED.

Table 6-15 (Cont.)

REQUIRED COMPONENTS	DESIGNATOR	DESCRIPTION	FUNCTION	PART NO.	WEIGHT (LBS.)	CONTINUOUS POWER (WATTS)	FLIGHT HARDWARE APPLICABLE	DATE AVAILABLE	R.O.M. COST	REMARKS
Flare Mode Flag	DS14	R-NR-OP	R indicates experiment is ready for flare mode operation. NR indicates experiment is not ready for flare mode operation. OP indicates experiment is operating in the flare mode.	40M37768-7	0.09	0.041	Yes	Note 5	Note 5	
Exposure Remain Reset Switch	S1	Mo-Ma	Resets film counter to maximum film remaining indicator.		0.17	0	Yes	Note 6	Note 6	
Exposure Re-maining Counter	M1		Indicates the number of exposures available in the camera for taking pictures.			0	No	Note 3	Note 3	1. watts while operating
Internal Aperture Door Flag	DS11	(Gray) - (Red) - (B.P.)	Gray indicates internal aperture door is open. Red indicates a failure. Barber Pole indicates internal aperture door is closed.	40M37768-11	0.09	0.041	Yes	Note 5	Note 5	
External Aperture Door Flag	DS12	(Gray) - (Red) - (B.P.)	Gray indicates external aperture door is open. Red indicates a failure. Barber Pole indicates external aperture door is closed.	40M37768-11	0.09	0.041	Yes	Note 5	Note 5	
Experiment Power Switch	S6	Ma-Mo-Ma	ON turns power on to the instrument and, after a short delay, opens both the instrument aperture door and the thermal shield door. OFF turns power off to the experiment and closes both the instrument aperture door and the thermal shield door.							
Experiment Ready Flag	DS5	R-NR-OP	R indicates experiment is ready for operation. NR indicates experiment is not ready for operation. OP indicates experiment is operating.	40M37768-7	0.09	0.041	Yes	Note 5	Note 5	
Experiment Ready Flag	DS15	R-NR-OP	R indicates experiment B is ready for normal or flare mode operation.	40M37768-7	0.09	0.041	Yes	Note 5	Note 5	
Flare Model Switch	S11	Mo-Ma-Mo	ON initiates an automatic sequence of exposures optimized for flare conditions. (Sequence is not yet defined.) OFF is the normal position of the switch and implies the experiment will perform in the normal mode. STBY provides low power to flare mode compo-nents to keep them prepared to be initiated.		0.09	0.041	Yes	Note 5	Note 5	
Flare Mode Flag	DS19	R-NR-OP	R indicates experiment B is ready for flare mode operation. NR indicates experiment B is not ready for flare mode operation. OP indicates experiment B is operating in the flare mode.	40M37768-7	0.09	0.041	Yes	Note 5	Note 5	

FOLDOUT FRAME 1

FOLDOUT FRAME 2

Table 6-15 (Cont.)

REQUIRED COMPONENTS	DESIGNATOR	DESCRIPTION	FUNCTION	PART NO.	WEIGHT (LBS.)	CONTINUOUS POWER (WATTS)	FLIGHT HARDWARE APPLICABLE	DATE AVAILABLE	R.O.M. COST	REMARKS
Internal Aperture Door Flag	DS17	(Gray) - (Red) - (B.P.)	Gray indicates internal aperture door is open. Red indicates internal aperture door is closed. Barber Pole indicates internal aperture door is closed.	40M37768-11	0.09	0.041	Yes	Note 5	Note 5	
External Aperture Door Flag	DS18	(Gray) - (Red) - (B.P.)	Gray indicates external aperture door is open. Red indicates a failure. Barber Pole indicates external aperture door is closed.	40M37768-11	0.09	0.014	Yes	Note 5	Note 5	
Exposures Re-maining Counter	M2		Electromechanical counter which displays the num-ber of unexposed pictures remaining in the camera.				No	Note 3	Note 3	
Exposures Re-maining Counter Reset	S9	Mo-Ma	Reset is performed by the astronaut only after a new film magazine has been installed in the camera.		0.17	0	Yes	Note 6	Note 6	
Experiment Power Switch	S17	Ma-Mo-Ma	ON turns power on to the instrument and after a short delay, opens both the instruments aperture door and the thermal shield door. OFF turns power off to the experiment and closes both the instruments aperture door and the thermal shield door.		0.17	0	Yes	Note 6	Note 6	
Sequence Mode Flag	DS10	SP - (Red) - OFS	Indicates which sequence mode is in operation.		0.09	0.041	Yes	Note 5	Note 5	
Sequence Start Switch	S16	Mo-Ma-Mo	Spect initiates an automatic sequence of eight exposures. After each exposure the grating posi-tion is changed. Auto initiates a set of spectral sequences to be taken at different positions near the limb. The positions are pre-programmed and offset pointing is done automatically.		0.17	0	Yes	Note 6	Note 6	
Grating Position Flag	DS6	1-(B.P.)-2	Indicates position of the grating, position 1 or 2.		0.09	0.041	Yes	Note 5	Note 5	
Manual Grating Position Switch	S10		Changes grating position.		0.17	0	Yes	Note 6	Note 6	
Manual Shutter Flag	DS9	O - (B.P.) - (Gray)	O indicates shutter is open. Barber Pole indicates a failure. Gray indicates shutter is closed. This is the normal position of the shutter.		0.09	0.041	Yes	Note 5	Note 5	
Manual Shutter Switch	S15	Mo-Ma-Mo	Open - opens the shutter and begins the exposure. Close - closes the shutter and ends the exposure. Recycles the film automatically in preparation for a new exposure.		0.17	0	Yes	Note 6	Note 6	

Table 6-15 (Cont.)

REQUIRED COMPONENTS	DESIGNATOR	DESCRIPTION	FUNCTION	PART NO.	WEIGHT (LBS.)	CONTINUOUS POWER (WATTS)	FLIGHT HARDWARE APPLICABLE	DATE AVAILABLE	R.O.M. COST	REMARKS
Sequence Hold Flag	DS20				0.09	0.041	Yes	Note 5	Note 5	
Sequence Hold Switch	S18	Mo-Ma-Mo	ON command stops the camera sequence during operation. OFF command resumes camera operation.							
Slit Position Flag	DS8	(Gray) - (B.P.) - in	Gray indicates slit is out. This is the normal position of the slit. Barber Pole indicates a failure. In indicates short slit is in position.		0.09	0.041	Yes	Note 5	Note 5	
Short Slit Switch	S14	Mo-Ma-Mo	Shortens the entrance slit to the experiment.		0.17	0	Yes	Note 6	Note 6	
Limb Flag	DS16				0.09	0.041	Yes	Note 5	Note 5	
Limb Scanning Switch	S12	Mo-Ma	ON command initiates limb scanning.		0.17	0	Yes	Note 6	Note 6	
Manual Off Set Stepping Switch	S13		Causes painting control to move primary mirror 2 seconds of arc in a radial direction away from the sun center. Used only when solar edge control or mirror control commands have been executed.		0.17	0	Yes	Note 6	Note 6	

Table 6-16

POWER MONITOR PANEL NO. 709A605

REQUIRED COMPONENTS	DESIGNATOR	DESCRIPTION	FUNCTION	PART NO.	WEIGHT (LBS.)	CONTINUOUS POWER (WATTS)	FLIGHT HARDWARE APPLICABLE	DATE AVAILABLE	R.O.M. COST	REMARKS
Readout Select Switch	S-3	7 Position Rotary Switch	This seven Position Rotary Switch (OFF-Read Volt Bus 1 - Read Volt Bus 2 - Read Volt L.R. 1-12 - Read Volt L.R. 13-24 - Read Battery 1-12 - Read Battery 13-24) selects what is going to be monitored on the power panel meters, M8 and M9.		0.85	0	Yes	Note 6	Note 6	
Battery Readout Select or Switch	S-4	12 Position Switch	This Twelve Position Rotary Switch (1-13, 2-14, 3-15, 4-16, 5-17, 6-18, 7-19, 8-20, 9-21, 10-22, 11-23, 12-24) is used to select a specific load regulator, battery or bus to be monitored when the Readout Select Switch (S-29) is in the desired position.		0.85	0	Yes	Note 6	Note 6	
Temperature and Volt Meters	M1-1		This Dual Meter serves two functions. The temperature meter M8-1 is used only when the Readout Select switch (S-29) is in either of the Read Battery positions. This part of the meter reads only the temperature of the individual battery selected. The volt meter side of the dual meter M8-2 displays the voltage of the desired battery, bus, or load regulator as selected by the selector switches, 5294530.		1.15	1.05	No	Note 1	Note 1	
Ammeter	M2-1		This Ammeter is half of a dual meter M9-1, and is used only for reading the output current of any of the batteries. During all other readings the input to this meter is grounded. The other half of this meter has not yet been defined.		1.15	1.05	No	Note 1	Note 1	

Table 6-17

AMERICAN SCIENCE AND ENGINEERING EXPERIMENT PANEL NO. 709A603

REQUIRED COMPONENTS	DESIGNATOR	DESCRIPTION	FUNCTION	PART NO.	WEIGHT (LBS.)	CONTINUOUS POWER (WATTS)	FLIGHT HARDWARE APPLICABLE	DATE AVAILABLE	R.O.M. COST	REMARKS
X-Ray Scope	709A602* A4M1		Allows visual display of the X-ray and is used to align the telescope axis on the X-ray activity by centering the displayed image.		7	12	Later	Feb 1968		Wattage includes values for entire A3, A4 and A5.
Brightness Control	709A602 A4R1		Provides control of background brightness on the X-ray scope.		–	–	N/A	N/A	N/A	
Focus Dial	709A602 A4R2		The focus dial provides control of the focus of the X-ray scope.		–	–	N/A	N/A		
X-Ray Alert Flag	790A602* DS1	(Red) - (Gray)	Indicates when the X-ray activity detected by the PM Detector equals or exceeds the Discriminator Level setting.		0.09	0.041	Yes	Note 5	Note 5	
Exposure Count	A1		Presents a numerical readout proportional to the X-ray activity detected and amplified in the PM Detector Subassembly.			1.5	Later	Feb 1968		Wattage includes entire A1.
Intensity Count	A2		Presents a numerical readout of X-ray counts detected in the Image Dissector Subassembly. This readout is back-up for the Exposure Count. The readout between the two is not correlated. A chart relating the two readings will be provided.			1.5	Later	Feb 1968		Wattage includes entire A2.
Aperture Flag	DS11		Indicates whether canister cover is open or closed.	40M37768-11	0.09	0.041	Yes	Note 5	Note 5	
Aperture Switch	S13	Mo-Ma-Mo	Opens or closes canister cover.		0.17	0	Yes	Note 6	Note 6	
Grating Indicator Flag	DS12	IN - (Red) - OUT	Indicates whether the transmission grating is in or out.	40M37768-13	0.09	0.041	Yes	Note 5	Note 5	
Grating Switch	S14	Mo-Ma-Mo	Operates the grating into the in or out position.		0.17	0	Yes	Note 6	Note 6	
Discriminator Level Switch	S1	5 Position 1 Pole 1 Deck	Provides control of the triggering level of the X-ray alarm and the camera operation in five discrete steps. Panel nomenclature corresponds to the minimum number of X-ray counts which will trigger the X-ray alarm or initiate a picture sequence if in the automatic mode.		0.85	0	Yes	Note 4	Note 4	

*X-Ray Scope and X-Ray Alert Flag are on the TV Monitor Assembly

FOLDOUT FRAME 1

FOLDOUT FRAME 2

PRECEDING PAGE BLANK NOT FILMED.

Table 6-17 (Cont.)

REQUIRED COMPONENTS	DESIGNATOR	DESCRIPTION	FUNCTION	PART NO.	WEIGHT (LBS.)	CONTINUOUS POWER (WATTS)	FLIGHT HARDWARE APPLICABLE	DATE AVAILABLE	R.O.M. COST	REMARKS
Picture Rate Selector	S2	4 Position 2 Pole 2 Deck	Program permits picture taking at a preprogrammed rate for a specific time. In the automatic mode a picture sequence will be taken at high rate for four minutes and then continue at low rate until stopped manually or stopped by the X-ray counts falling below the Discriminator Level setting. In manual mode (Picture Sequencer Start) a picture sequence will be taken at the high rate for four minutes and then continue at the low rate for approximately nine minutes, for a total operating time of approximately 13 minutes.		0.85	0	Yes	Note 4	Note 4	
			High permits picture taking at approximately 0.1-second intervals between exposures. In automatic operation this sequence is continuous until stopped manually or by the X-ray count falling below the Discriminator Level setting. In manual operation, this sequence stops after approximately 13 minutes.		–	0	Yes			
			Low permits picture taking with approximately 12 seconds between exposures. Otherwise, operation is the same as in the Picture Rate High Position.		–	0	Yes			
			Single permits a single sequence of pictures to be taken. The number of pictures depends on the Exposure setting. A minimum of four and a maximum of eight pictures are taken in a single sequence.		–	0	Yes			
Threshold, Coarse	A4 S1	7 Position Pole Deck	Provides intensity modulation control of the X-ray scope, in seven discrete steps, when an image is produced. Panel nomenclature corresponds to the minimum number of counts that provide optimum image tensity for each switch position. Position is determined by the reading on the Intensity Count indicator or by observing the image on the X-ray scope.		0.85	0	Later	Feb 1968		
Threshold, Fine	A4 R1	Potentiometer	When turned fully counterclockwise, attenuates the intensity modulation signal 3:1. During normal quiescent operation (no solar flare activity) the Fine Control should be fully clockwise. This circuitry permits a threshold setting at any count between any two adjacent coarse positions.		–	–	Later	Feb 1968		
Power Switch	S8	Mo-Ma-Mo	Activates and deactivates power to experiment.		0.17	0	Yes	Note 6	Note 6	
Ready Flag	DS6	R-NR-OP	Indicates whether experiment is ready for operation or operating.	40M37768-7	0.09	0.041	Yes	Note 5	Note 5	

FOLDOUT FRAME 1

FOLDOUT FRAME 2

PRECEDING PAGE BLANK NOT FILMED.

Table 6-17 (Cont.)

REQUIRED COMPONENTS	DESIGNATOR	DESCRIPTION	FUNCTION	PART NO.	WEIGHT (LBS.)	CONTINUOUS POWER (WATTS)	FLIGHT HARDWARE APPLICABLE	DATE AVAILABLE	R.O.M. COST	REMARKS
Auto Picture Sequence On - Off	S11	Mo-Ma-Mo	Enables the camera control circuitry so that a picture sequence will be initiated automatically if the X-ray activity exceeds the Discriminator Level setting. This picture sequence stops automatically if the X-ray activity falls below the Discriminator Level setting or when the Picture Sequence Off is activated. Off terminates any picture sequence.		0.17	0	Yes	Note 6	Note 6	
Picture Manual Sequence On - Off	S12	Mo-Ma-Mo	Manually initiates a picture sequence independent of the level of X-ray activity. Off terminates a picture sequence when operating in manual mode.		0.17	0	Yes	Note 6	Note 6	
Picture Sequence Auto	DS9		Indicates On when in the automatic picture sequence mode.		0.09	0.041	Yes	Note 5	Note 5	
Picture Sequence Start	DS10		Indicates On when in the manual picture sequence mode.		0.09	0.041	Yes	Note 5	Note 5	
Intensity Normal Switch	S18	Ma-Ma	Switches the output of the normally used intensity counter and associated D/A converter to the X-ray scope.		0.17	0	Yes	Note 6	Note 6	
Intensity Alternate	S18	Ma-Ma	Switches the output of the alternate intensity counter and D/A converter to the X-ray scope and disconnects the output of the normally used counter and associated converter.		–	–	Yes	Note 6	Note 6	
Filter Position	DS13	1 - (Gray) - 2	Indicates whether Filter 1 or 2 is positioned in front of the camera.	40M37768-1	0.09	0.041	Yes	Note 5	Note 5	
Filter Position	DS14	3 - (Gray) - 4	Indicates whether Filter 3 or 4 is positioned in front of the camera.	40M37768-3	0.09	0.041	Yes	Note 5	Note 5	
Filter Position	DS15	5 - (Gray) - 6	Indicates whether Filter 5 or 6 is positioned in front of the camera.	40M37768-5	0.09	0.041	Yes	Note 5	Note 5	
Filter Select	S15	Mo-Ma-Mo	Positions Filter 1 or 2 in front of the camera when activated.		0.17	0	Yes	Note 6	Note 6	
Filter Select	S16	Mo-Ma-Mo	When activated positions Filter 3 or 4 in front of the camera.		0.17	0	Yes		Note 6	
Filter Select	S17	Mo-Ma-Mo	When activated positions Filter 5 or 6 in front of the camera.		0.17	0	Yes		Note 6	
Power Supply Spare	DS4	(Gray) - (Red) - B	Indicates that power supply B, a spare, has been switched in. Power supply A will be used under normal conditions. The power supplies are switched from keyboard commands.	40M37768-11	0.09	0.041	Yes		Note 5	

FOLDOUT FRAME 1

FOLDOUT FRAME 2

PRECEDING PAGE BLANK NOT FILMED.

Table 6-17 (Cont.)

REQUIRED COMPONENTS	DESIGNATOR	DESCRIPTION	FUNCTION	PART NO.	WEIGHT (LBS.)	CONTINUOUS POWER (WATTS)	FLIGHT HARDWARE APPLICABLE	DATE AVAILABLE	R.O.M. COST	REMARKS
Shutter Fly	DS5	O - (B.P.) - (Gray)	Indicates when the X-ray shutter in the camera is open.		0.09	0.041	Yes		Note 5	
Replaced Deflection Amplifier X or Y	DS3	X - (B.P.) - Y	X indicates that the spare deflection amplifier has been used to replace the X deflection amplifier. Y indicates that the spare deflection amplifier has been used to replace the Y deflection amplifier. X and Y replace commands and Spare Deflection Amplifier Off command are activated from the keyboard.	40M37768-13	0.09	0.041	Yes		Note 5	
Exposures Remaining Counter Reset	S9	Mo-Ma	Resets the Exposures Remaining counter. Reset is performed by the astronaut only after a new film magazine has been installed in the camera.		0.17	0	Later	June 1968	Note 6	
Exposures Remaining Counter	M1		Electromechanical counter which displays the number of unexposed pictures remaining in the camera.			0			Note 3	Power =1.6 when operating - 0 otherwise.
Exposure Range Selector	S3	6 Position 3 Poles 3 Decks	Auto selects the proper exposure sequence based on the continuous exposure times for the measured X-ray activity detected by the PM detector. Position 256 selects a sequence of eight exposure times. They are: 1/64, 1/16, 1/4, 16, 64 and 256 seconds. In each consecutive position from 256 through 1, the longest exposure time is eliminated and one less picture is taken. Position 1 has four exposure times: 1/64, 1/16, 1/4 and 1 second. The position number thus indicates the longest exposure time used.		0.85	0			Note 4	

FOLDOUT FRAME 1

FOLDOUT FRAME 2

The following is a reasonable substitute for the simulator:

Example: 709A603M6 — Contact: Veeder-Root
Magnetic Counter — Hartford, Conn.
ME 896130-001

They are available for about $200 each, but require mechanical (lever) reset procedure instead of electrical pushbutton. They will also lack the automatic "film inhibit" feature.

An alternate is:

Whittaker — Contact: Roy A. Steckmesser
816 Esslinger Road, S.E.
Huntsville, Alabama 35801
Phone (205) 881-1750

This will have the film inhibit feature and electrical reset, but will be very large.

A.W. Haydon Company — Contact: Arthur W. Bennett
Model K19502 — 232 N. Elm Street
Waterbury, Conn.
Phone (203) 756-4481

See the appendix for alternate vendors.

- <u>Rotary Switch</u> - Flight hardware models are quite expensive and should be replaced by either quality models or some other which has the same "feel." The strict hermetic seal of the flight hardware is a primary reason for its high price. If a discarded flight model is found available, its life would probably be long enough. Note that if a disassembled unsealed model is purchased, it could be ordered in one configuration (four decks, all 12 positions) and internally modified electrically and mechanically as required.

  Example: 709A603S34
  ROM Cost: $2,500.00

- <u>Flag Indicator</u> - The indicator flag used for flight uses a very high impedance input to power the wheel on which the flag is emblazoned. Since extremely low holding power is less important for the simulator, a lower impedance model would be satisfactory.

Example: 709A603DS21

ROM Cost: $900.00

Local Rep: R.F. (Slim) Johansson
Kemp Instruments
Governors Drive
Huntsville, Alabama
Phone: 837-4304

- Toggle Switch - The electrical circuit of the toggle switch to be used on the simulator will be determined by the simulator requirements; therefore, it will likely be different from the flight console requirements.

  Example: 709A605S

  ROM Cost: $200.00

- X-ray Scope - The X-ray scope (709A603A3M5) assembly is a special AS&E-supplied device. A non-qualified unit identical to the flight model should prove satisfactory.

- Intensity Modulation Assembly - This AS&E-supplied unit (709A603A4) may be replaceable by a rotary switch and potentiometer with all the functions done by computer instead of panel hardware.

- Intensity Counter - The AS&E-supplied assembly (709A603A2) will probably be replaced by a simple EL display unit driven by the computer.

- Exposure Counter - This AS&E-supplied assembly (709A603A) will probably be replaced by a simple EL display unit driven by the computer.

- NRL A TV Cain - This potentiometer (709A602A3R1) should be replaced by a nonqualified one.

- PC Digital Display - The displays (709A60DS10-11, and -12) should be replaced by a simple EL digital display panel driven directly by the computer. The flight hardware includes a BCD converter and is unsuitable due to cost. Its sophistication is unnecessary for simulation.

  Source: Lear Seigler

  ROM Cost: $20,000

6.5.5 Facility

The Total ATM Simulator will require an extensive facility. This facility will consist of the necessary computer support equipment (air conditioning, acoustic screening, and electric power) and the associated space required to set up the computer, crew station, and the simulation equipment (image generation equipment, power interface, simulation drive equipment).

The computation facility must be able to support adequate air conditioning, humidity control, and power to maintain a hybrid computer with a digital compliment consisting of a 32K core, tape driver, card reader, and other peripheral equipment. The hybrid interface and an analog computer contain the following basic elements: 120 Integrator, 120 Summers, 500 Pots, 60 Multipliers, and 12 Resolvers.

In addition to being able to support the computer requirements, there must be adequate facility adjoining the computer facility to contain and support the crew station, special simulation equipment and the operating personnel. Approximately 1,000 sq ft of floor space is required adjacent to the computer facility to handle the crew station, simulation control console, and special simulation equipment. The facility should be divided into three basic areas: crew station (simulated cabin) area, simulation control and monitoring area, and the simulation equipment area. Each of these areas should be light level and acoustically isolated. Each area should have individual light intensity control. There should be a one-way glass partition between the simulation control and monitoring area and the crew station area.

Figure 6-28 shows a tentative configuration for the Total ATM Simulator facility.

6.6 RECOMMENDATIONS

6.6.1 Benefits of Simulation

The need for an ATM Simulator is verified by the ATM Fine Pointing Simulation Study performed by LMSC. This study is reported in LMSC Report A-842326. In brief, the

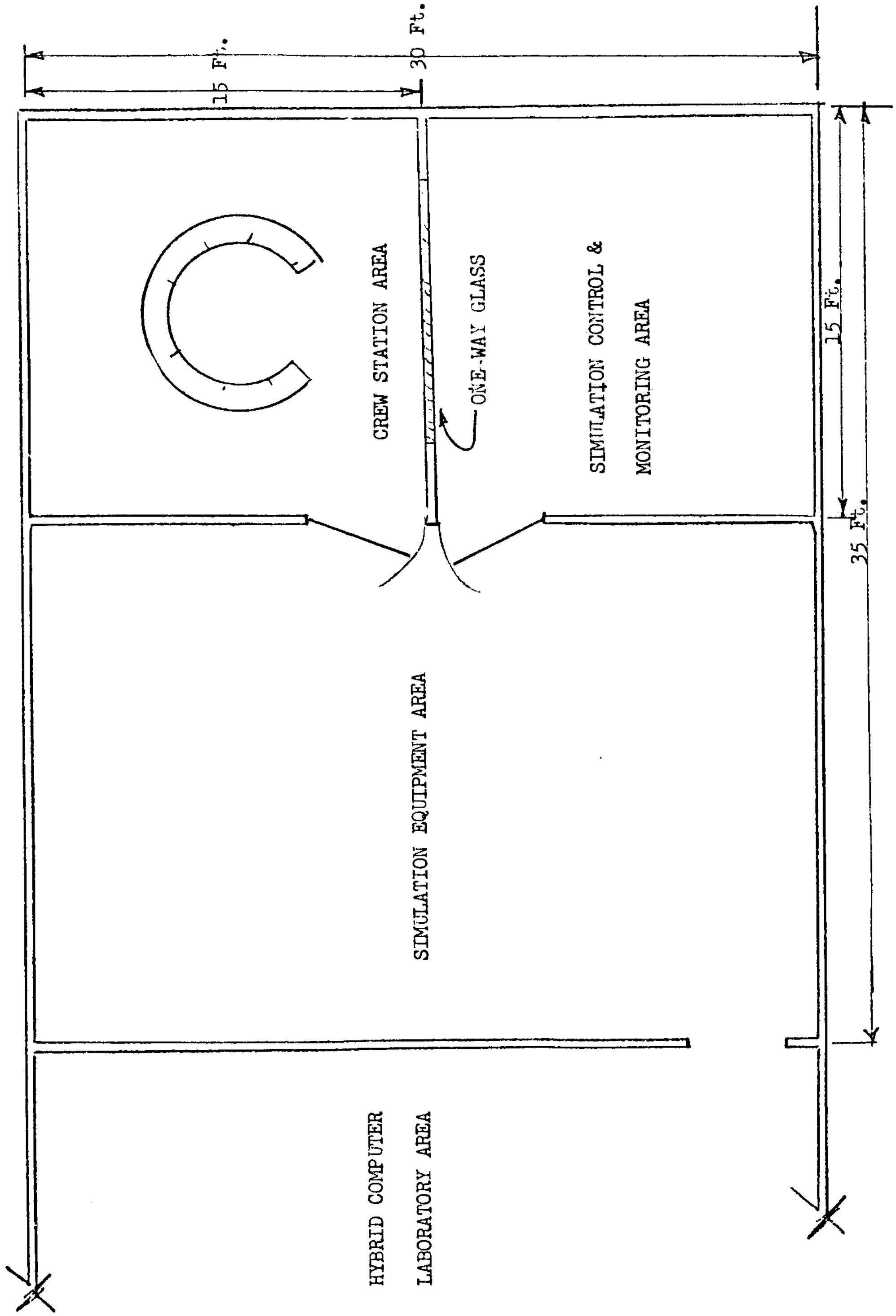

Fig. 6-28 Total ATM Simulation Facility

value of an ATM Simulation lies in the ability of the simulation operator and the system designer to evaluate the system (man-in-loop). Also, it allows the astronauts to operate the system and make recommendations during the design phase. In fact, it may be that the astronauts will not accept the system till it has been proven during simulation.

6.6.2 Schedule Requirements

For the ATM Simulation to be of value in the development phase, it must be operational before the hardware is procured. The simulation must obviously be operational as soon as possible. The simulation should be set up as rapidly as possible in a simplified manner and then expanded to encompass the required detail. The first cut at a simplified simulation must be operational by late 1967. The complete simulation must be ready by mid-1968. If these basic milestones are not met, the simulation will not be able to evaluate or prove system feasibility in time to meet mission dead lines.

6.6.3 Simulation Implementation

To implement the ATM Simulation and meet the required schedule, the organization chosen must have:

- ATM system experience
- ATM pointing system background
- Experience in man-in-loop simulation
- Existing simulation equipment that will satisfy the first cut requirement
- Hybrid computer that can be made available on a long-term basis immediately

If these criteria are not met, the schedule delays will be such that the simulator will not be available in time to serve a useful function and may thus jeopardize the Solar ATM Mission.

6.7 REFERENCES

6-1. Lockheed Missiles & Space Company, Conceptual Design and Analysis of the Control System for Apollo Telescope Mount, by Dale Ingwerson, et. al., LMSC-A842157, Sunnyvale, Calif., 17 Mar 1967

6-2. -----, Final Report for ATM and Cluster Systems Analyses, Augmentation Task Nos. 1 and 19, LMSC-A842251, Sunnyvale, Calif., 7 Jul 1967

6-3. -----, Final Report for Man-Machine Engineering and Docking Aids, Augmentation Task No. 6, LMSC-A842254, Sunnyvale, Calif., 26 Jun 1967

Uncited References

1. LMSC-A842157
2. LMSC-A842251
3. LMSC/HREL A784609
4. LMSC/HREC A784461
5. QA Gruman Low 34-054050
6. LMSC-A842254

Appendix A

TIME-LINES OF THE FIRST ORBIT, A REPRESENTATIVE EXPERIMENT PROCEDURE, AND A SUMMARY OF DARK-SIDE ACTIVITIES

TASK/EQUIPMENT ANALYSIS	Experimenter: MSFC	Experiment Number:	Experiment Title: ATM-PCS	Designator Code Number: 709A600A8, 9, 10, 11

FUNC.	NO.	CREW TASK/EVENT	ASTRONAUT ACTIVITY (%)	EQUIP-MENT INTERFACE	VISUAL FEEDBACK	DISPLAY	CONTROL	NOTES	EST TIME	CUM TIME
ACTIVATION AND ALIGNMENT	1	Verify Switch Position Monitor Selector Switch	B-100	A8	Switch in off position. No digital read-out.	M6	S8			
		Gyro Selector Switches			Vertical switch position. No digital read-out		S5, 6, 7			
	2	Verify Flag Status	B-100	A8	Flags show grey	DS10, 11 12				
		Star Present Flag			Flag shows grey	DS7				
		Acquisition Sensor Flag			Flag shows grey	DS8				
		Fine Sensor Flag			Flag shows grey	DS9				
	3	Verify Switch Position	B-100	A9						
		Configuration Mode Sub Mode			Switches in neutral position		S1, S2 S3, 4, 5 S6-S11			
		Computer Selector Switches Test Switch Insert Read/Erase Inhibit Switch			"A", 0, 0, 0. Locked in "OFF" Switch pos neutral		S16 S17 S18 S19			
	4	Verify Flag Status Configuration Mode Sub Mode Computer Confirm Ground Command System	B-100	A9	Flags show configuration Flag shows inhibit	DS1-2 DS3-6 DS7-12 DS13-14 DS15				

REVISIONS

SYM	DESCRIPTION	DATE	APPROVAL
3	Utilizes updated material	5-12-67	

PREPARED BY

LOCKHEED MISSILES & SPACE COMPANY

SUNNYVALE, CALIFORNIA

DATE PREPARED 5-12-67	SUBMITTED
PREPARED BY: C.V.J./G.T.B.	APPROVED
CHECKED BY	DIRECTOR

GEORGE C. MARSHALL SPACE FLIGHT CENTER

NATIONAL AERONAUTICS AND SPACE ADMINISTRATION

HUNTSVILLE, ALABAMA

DWG SIZE

SHEET 1 OF 6

FOLDOUT FRAME 1

FOLDOUT FRAME 2

PRECEDING PAGE BLANK NOT FILMED.

TASK/EQUIPMENT ANALYSIS	Experimenter: MSFC	Experiment Number:	Experiment Title: ATM-PCS	Designator Code Number: 709A600A8, 9, 10, 11

FUNC.	NO.	CREW TASK/EVENT	ASTRONAUT ACTIVITY (%)	EQUIP-MENT INTERFACE	VISUAL FEEDBACK	DISPLAY	CONTROL	NOTES	EST TIME	CUM TIME
ACTIVATION AND ALIGNMENT	5	Verify Switch Position Camera Selector Switches Camera Power Switches Monitor Power Switches TV Zoom Switches Sync. Gen. Switch	B-100	A10	Switch pos at ATM locked in Off Sw pos neu Sw pos neu Neu. pos		S3, S4 S5-9 S10-S11 S12-S13 S14			
	6	Verify Switches Positions Switch? External Door Switch	B-100	A11	In Off pos Lock in closed pos		S1			
	7	Verify Flag Status	B-100	A11	Flag shows "C"	DS1				
	8	Verify Switch Positions Power Monitoring	B-100	709A600A1	Sw pos		S1-S8			
	9	Verify Flag Status & Meters	B-100	709A600A1	Flags & analog meters	M1-M2 DS1-DS6				
	10	Select Flight Configuration	B-100	A9	Configuration flag shows	DS1 or 2	S-1, or 2	Flight configuration to be consistent with mission requirements.		
	11	Alert Astronauts that ATM is Ready for Acquisition Mode.	A-100	7 ?				This alert is given by Astronaut A in the CSM following gross positioning of the Cluster by RCS.		
	12	(Deploy Solar Arrays)	B-100	709A600A1	Flag shows extended-locked	DS8	S10	The Solar Array must supply a sufficient amount of power at the beginning of this mission to meet the total power load requirement. Solar panels will provide power when pointed within a few degrees of the sun.		
	13	Select ATM System Power "ON" Code Insert Coded-Signal into Computer Verify Signal Configuration Select Computer "read"	B-100	A9	Sw pos Flag shows confirm	 DS13, 14	S12-15 S17 S18	This follows the gross positioning of the Cluster/ATM. The Cluster is in a coarse inertial hold until ATM pointing control subsystem is fully activated.		

REVISIONS

SYM	DESCRIPTION	DATE	APPROVAL
3	Utilizes updated material	5-12-67	

PREPARED BY

LOCKHEED MISSILES & SPACE COMPANY

SUNNYVALE, CALIFORNIA

DATE PREPARED 5-12-67

PREPARED BY: C. V. J. /G. T. B.

CHECKED BY

SUBMITTED

APPROVED

DIRECTOR

GEORGE C. MARSHALL SPACE FLIGHT CENTER

NATIONAL AERONAUTICS AND SPACE ADMINISTRATION

HUNTSVILLE, ALABAMA

DWG SIZE

SHEET 2 OF 6

TASK/EQUIPMENT ANALYSIS	Experimenter: MSFC	Experiment Number:	Experiment Title: ATM-PCS	Designator Code Number: 709A600A8, 9, 10, 11

FUNC.	NO.	CREW TASK/EVENT	ASTRONAUT ACTIVITY (%)	EQUIP-MENT INTERFACE	VISUAL FEEDBACK	DISPLAY	CONTROL	NOTES	EST TIME	CUM TIME
ACTIVATION AND ALIGNMENT	14	Verify Power Status of Power Modules 1 Through 24	B-100	709A600A1	Readings on analog meters within tolerance	709A600A1 M1, M2	709A600A1 S1, S2	The Selector Switch allows for individual power modules capability and is on a time-shared basis between batteries. Temperature, voltage and current are monitored in this way.		
	15	Select TEST Mode	B-100	A9	Flag shows "Test"	DS6	S5	This mode must be used to verify ATM subsystem operation prior to entering experiment pointing mode.		
	16	Select Roll, Pitch and Yaw Switches	B-100	A9	Sw Pos		S5-S7			
	17	Select Spar Gimbal Operation Code	B-100	A9	Sw Pos		S12-S15			
		Insert Coded Signal into Computer					S17			
		Verify Signal Configuration			Flag shows confirm	DS13-14				
		Select Computer "Read"			Digital Disp. Change		S18			
	18	Verify Spar Gimbals Operation	B-100	A8	Digital Readout					
	19	Verify Sun Sensor Operation	B-100							
		Acquisition Sensor		A8	Flag shows "sunpresent"	DS8				
		Fine Sensor		A8	Flag shows "sunpresent"	DS9				
	20	Select Hand Control Switch	B-100	A8	Flag shows submode	DS9	S8			
		Operate Hand Controller (Verify Hand Controller Operation)					H1			
					Flag shows different face for each of four quadrants	DS14				
	21	Verify External Door Operation	B-100	A11	Flag shows "O" & "C"	DS1	S2			
		Select Switch to Open								
		Select Switch to Closed								
	22	Verify Operation of Hα TV System	B-100	A10	CRT Image	M1				
		Select ATM Hα "On" camera select Switch			Sw Pos		S3			
		Select Power "On" to Hα "Camera"			Sw Pos		S6			
		Select Power "On" to No. 1 Monitor			Sw Pos		S10			
					Raster					

REVISIONS

SYM	DESCRIPTION	DATE	APPROVAL
3	Utilizes updated material	5-12-67	

PREPARED BY

LOCKHEED MISSILES & SPACE COMPANY

SUNNYVALE, CALIFORNIA

DATE PREPARED 5-12-67	SUBMITTED
PREPARED BY: C.V.J./G.T.B.	APPROVED
CHECKED BY	DIRECTOR

GEORGE C. MARSHALL SPACE FLIGHT CENTER

NATIONAL AERONAUTICS AND SPACE ADMINISTRATION

HUNTSVILLE, ALABAMA

DWG SIZE

SHEET 3 OF 6

PRECEDING PAGE BLANK NOT FILMED.

TASK/EQUIPMENT ANALYSIS	Experimenter: MSFC	Experiment Number:	Experiment Title: ATM-PCS	Designator Code Number: 709A600A8, 9, 10, 11

FUNC.	NO.	CREW TASK/EVENT	ASTRONAUT ACTIVITY (%)	EQUIP-MENT INTERFACE	VISUAL FEEDBACK	DISPLAY	CONTROL	NOTES	EST TIME	CUM TIME
ACTIVATION AND ALIGNMENT	22	(Continued)								
		Select Crosshairs for "On" and Adjust Intensity			Image change	M1	R3			
		Adjust Brightness			Image change	M1	R4			
		Adjust Vertical & Horizontal Crosshairs			Hairs shift	M1	R1, R2			
		Select Power "Off" to No. 1 Monitor			Sw Pos	M1	S10			
		Select Power "Off" to Camera			Sw Pos		S6			
	23	Repeat Step 22 for No. 2 Monitor	B-100	A10		M2				
	24	Verify Operation of Test & Confirmation Circuits by Selecting to "Test"	B-100	A9	Flags show "Confirm"	DS14	S16			
	25	Inform Ground Control of ATM Status	C-100	7xx?				Vehicle communications system is used. (It is assumed that ATM is "GO" at this point.)		
	26	Receive Permission From Ground Control to Proceed with ATM Subsystem Activation	C-100	7xx?						
	27	Activate CMG Subsystem	B-100	A9						
		Select Stop-Start/Standby Code			Flag shows S-S	DS6	S5	This step must be undertaken regardless of a vehicle launch with or without CMG's spinning. The Cluster gross pointing will enable the solar arrays to provide power to batteries prior to CMG spin-up. The CMG's will be brought up to full speed while caged in a zero momentum position.		
		Insert Coded Signal Into Computer & Verify Signal Confirmation.			Sw Pos	DS13-14	S12–S15			
		Select Computer "read"			Digital Display Change		S18			
	28	Verify that CMG's are in Acceleration	B-100	A8				As gross solar orientation has been accomplished, this spin-up period will not involve further manual orientation.		
		Select to read speed for each of 3 axes			Analog meter reading	M6	S4			
	29	Perform Housekeeping tasks and Monitor CMG's, undertake experiment visual activation checks.	B-100 C-100					While CMG's are spinning up the astronauts require a minimum of vigilance in performing CMG monitor activities. Power drain due to CMG run-up will preclude experiments operational checks.		

REVISIONS

SYM	DESCRIPTION	DATE	APPROVAL
3	Utilizes updated material	5-12-67	

PREPARED BY

LOCKHEED MISSILES & SPACE COMPANY

SUNNYVALE, CALIFORNIA

DATE PREPARED 5-12-67

PREPARED BY: C. V. J. /G. T. B.

CHECKED BY

SUBMITTED

APPROVED

DIRECTOR

GEORGE C. MARSHALL SPACE FLIGHT CENTER

NATIONAL AERONAUTICS AND SPACE ADMINISTRATION

HUNTSVILLE, ALABAMA

DWG SIZE

SHEET 4 OF 6

PRECEDING PAGE BLANK NOT FILMED.

TASK/EQUIPMENT ANALYSIS	Experimenter: MSFC	Experiment Number:	Experiment Title: ATM-PCS	Designator Code Number: 709A600A8, 9, 10, 11

FUNC.	NO.	CREW TASK/EVENT	ASTRONAUT ACTIVITY (%)	EQUIP-MENT INTERFACE	VISUAL FEEDBACK	DISPLAY	CONTROL	NOTES	EST TIME	CUM TIME
ACTIVATION AND ALIGNMENT	30	(Verify that CMG's have attained maximum operational speed.)	B-100	A8	Flag shows	DS13				
	31	Alert Crew Members that Fine Pointing Maneuvers are starting	C-100	7xx?				Crew Movement must be reduced to a minimum. Crew Members will secure "seat" harness etc.		
	32	Select Monitor/Acquisition Mode Verify Mode Undertaken		A9	Flag shows Mode M&A	DS3	S3	Flag will only show mode letter after spar/rack lock has been activated.		
	33	Select External Door Switch to "Open"	B-100	A11	Sw Pos		S2			
	34	Verify the Door is "Open"	B-100	A11						
	35	Activate Hα Telescope Select ATM Hα Camera Select Power "On" to "Camera" Select Power "On" to No. 1 Monitor	B-100	A10	Sw Pos Sw Pos Sw Pos Sw Pos Raster	M1	S3 S3 S6 S10			
		Adjust Crosshairs Intensity			Image Change	M1	R3	This thumbwheel switch should also control intensity		
		Adjust Brightness & Contrast			Image Change	M1	R4, R5			
		Adjust Vertical & Horizontal Crosshairs Shift			Hairs Shift	M1	R1, R2			
	36	Select Hand Control Submode	B-100	A9	Flag shows mode entered		S8			
	37	Select Roll Ref Switch	B-100	A8	Sw Pos		S5			
	38	Astronaut Rolls Cluster by Operating Hand Controller	B-100	A8	Digital read-out	M3	H1	This operation makes use of visible star patterns, or LM or CSM inertial displays. Canopus must come within the freedom of the star tracker gimbals (±70° in roll)		
	39	Reset Hand Control Submode Switch	B-100	A9	Flag shows reset	DS9	S8			
	40	Select Star Tracker Switch	B-100	A9	Flag shows Mode	DS7	S6			

REVISIONS

SYM	DESCRIPTION	DATE	APPROVAL
3	Utilizes updated material	5-12-67	

PREPARED BY

LOCKHEED MISSILES & SPACE COMPANY

SUNNYVALE, CALIFORNIA

DATE PREPARED 5-12-67
PREPARED BY: C. V. J./G. T. B.
CHECKED BY
SUBMITTED
APPROVED
DIRECTOR

GEORGE C. MARSHALL SPACE FLIGHT CENTER
NATIONAL AERONAUTICS AND SPACE ADMINISTRATION
HUNTSVILLE, ALABAMA

DWG SIZE

SHEET 5 OF 6

FOLDOUT FRAME 1

FOLDOUT FRAME 2

PRECEDING PAGE BLANK NOT FILMED.

TASK/EQUIPMENT ANALYSIS	Experimenter: MSFC	Experiment Number:	Experiment Title: ATM-PCS	Designator Code Number: 709A600A8, 9, 10, 11

FUNC.	NO.	CREW TASK/EVENT	ASTRONAUT ACTIVITY (%)	EQUIPMENT INTERFACE	VISUAL FEEDBACK	DISPLAY	CONTROL	NOTES	EST TIME	CUM TIME
ACTIVATION AND ALIGNMENT	40	(Continued)								
		Select Search Submode Code Insert Coded Signal Into Computer	B-100	A9	Sw Pos		S12-S15 S17			
		Verify Signal Confirmation			Flag shows confirm	DS13-14				
		Select Computer "read"			Digital Disp. Change		S18			
	41	Select Outer Star Tracker Switch Pos.	B-100	A8	Sw Pos		S6			
	42	Select Inner Star Tracker Switch Pos.	B-100	A8	Sw Pos		S7			
	43	Select Hand Control Submode Switch	B-100	A9	Flag shows mode	DS9	S8			
	44	Slew Tracker by Operating the Hand Controller	B-100	A8	Digital Readout	M4	H1			
	45	Verify Star Presence	B-100	A8	Flag shows Canopus acquisition	DS7				
	46	Reset Hand Control Submode Switch	B-100	A9	Flag shows Reset	DS9	S8			
	47	Select Track Submode Code Insert coded signal into computer	B-100	A9	Sw Pos		S12-S15 S17			
		Verify signal confirmation			Flag shows confirm	DS13-14				
		Select Computer "read"					S18			
	48	Verify Star Tracker Locked on Canopus	B-100	A8	Flag shows lock-on	DS7				
	49	Select Ground Command System Enable Switch	B-100	A9	Flag shows ENA	DS15	S19			
	50	Select Orbital Plane Update Submode	B-100	A9	Flag shows	DS8	S7	Cluster is automatically oriented to angle (?) received from Ground Communication system.		
	51	(Verify Completion of Orbital Alignment mode)	B-100	A8?						
		ATM-PCS is ready to enter the Experiment Pointing Mode								

REVISIONS

SYM	DESCRIPTION	DATE	APPROVAL
3	Utilizes updated material	5-12-67	

PREPARED BY
LOCKHEED MISSILES & SPACE COMPANY
SUNNYVALE, CALIFORNIA

DATE PREPARED 5-12-67
PREPARED BY: C.V.J./G.T.B.
CHECKED BY
SUBMITTED
APPROVED
DIRECTOR

GEORGE C. MARSHALL SPACE FLIGHT CENTER
NATIONAL AERONAUTICS AND SPACE ADMINISTRATION
HUNTSVILLE, ALABAMA

DWG SIZE

SHEET 6 OF 6

PRECEDING PAGE BLANK NOT FILMED.

TASK/EQUIPMENT ANALYSIS	Experimenter: HIGH ALTITUDE OBSERVATORY	Experiment Number: S052	Experiment Title: WHITE LIGHT CORONAGRAPH	Designator Code Number: 709A600A2

FUNC.	NO.	CREW TASK/EVENT	ASTRONAUT ACTIVITY (%)	EQUIP-MENT INTERFACE	VISUAL FEEDBACK	DISPLAY	CONTROL	NOTES	EST TIME	CUM TIME
ACTIVATION AND ALIGNMENT	1	Confirm ATM Spar is Sun centered to within ±5 min.	B-100	709A600A10	Sun image centered	709 A600A10 M1	709 A600A10 S3 & S6 S10	Astronaut may choose 709A600A10M2		
	2	Activate Power to Standby	B-100	A2	Locked in "Standby"		S5	Activates temperature monitor circuits. No warm-up time required		
	3	Astronaut voice report of event #2 starting time	B-100	709A600A				Tape recorded using Vehicle Comm & Recording Sys.		
	4	Verify Experiment Status	B-100	A2						
		Sequence Flag			Flag reads "Stop"	DS3	S6			
		External Shutter Flag			Flag reads "Closed"	DS1	S3			
		Internal Shutter Flag			Flag reads "Closed	DS2	S4			
		Frames Remaining Monitor			Adequate No. Shown	M1	S1	Required Frames Remaining for: 1 min. Patrol Mode – 12 16 min. Patrol Mode – 192 Fast Scan – 384 plus 20% of full camera		
	5	Check Temperature Monitor	B-100	709A600A				70° ±5°		
	6	Activate Power to Operate	B-100	A2	Locked in "Power Operate"		S5	Activates experiment circuits. No warm-up time required.		
	7	Astronaut voice report of event #6 starting time	B-100	709A600A				Tape recorded using Vehicle Comm. & Recording Sys.		
	8	Open External Shutter	B-100	A2	Flag reads "Open"	DS1	S3	Closes automatically when over 5 arc min. off sun center.		
	9	Astronaut Voice report of event #8 start time	B-100	709A600A				Tape Recorded using Vehicle Comm. & Recording Sys.		
	10	Set Alignment System for HAO operation	B-100	709A600A5	Locked in "HAO"		709A600A5 S28	Secures time-shared HAO/HCO alignment controls & monitor for use with Coronagraph		
	11	Select Coronagraph Pointing Error Mode	B-100	709A600A5	Locked in "Pointing"		709A600A5 S29	Sets HAO/HCO alignment system to control & monitor pointing of Coronagraph Camera		

REVISIONS

SYM	DESCRIPTION	DATE	APPROVAL
3	Utilizes updated material	5-2-67	

PREPARED BY

LOCKHEED MISSILES & SPACE COMPANY

SUNNYVALE, CALIFORNIA

DATE PREPARED 5-2-67	SUBMITTED
PREPARED BY: R. Hacker	APPROVED
CHECKED BY	DIRECTOR

GEORGE C. MARSHALL SPACE FLIGHT CENTER

NATIONAL AERONAUTICS AND SPACE ADMINISTRATION

HUNTSVILLE, ALABAMA

DWG SIZE

SHEET 1 OF 5

FOLDOUT FRAME 1

FOLDOUT FRAME 2

TASK/EQUIPMENT ANALYSIS	Experimenter: HIGH ALTITUDE OBSERVATORY	Experiment Number: S052	Experiment Title: WHITE LIGHT CORONAGRAPH	Designator Code Number: 709A600A2

FUNC.	NO.	CREW TASK/EVENT	ASTRONAUT ACTIVITY (%)	EQUIP-MENT INTERFACE	VISUAL FEEDBACK	DISPLAY	CONTROL	NOTES	EST TIME	CUM TIME
ACTIVATION AND ALIGNMENT	12	Astronaut Voice report of event #11 Start Time	B-100	709A600A				Tape recorded using Vehicle Comm. & Recording Sys.		
	13	Check & Null Coronagraph Pointing Error to within ±20 arc sec Pitch Control Yaw Control	B-100	709A600A5	Meters read 0 ±20 sec	709A600A5 M3-1 M3-2	709A600A5 S26 S27	Used to align the axis of experiment.		
	14	Open Internal Shutter	B-100	A2	Flag Reads "Open"	DS2	S4	Opens after there have been no excursions in pointing >±20 arc sec for one minute. Closes when error exceeds ±20 arc sec.		
	15	Astronaut Voice report of event #14 start time.	B-100	709A600A				Tape recorded using Vehicle Comm. & Recording Sys.		
	16	Select Occulting Disc Position Error Mode	B-100	709A600A5	Locked in "Disc"		709A600A5 S29	Sets HAO/ HCO alignment system to control & monitor position of internal occulting disc		
	17	Astronaut Voice report of event #16 start time	B-100	709A600A				Tape recorded using Vehicle Comm & Recording Sys.		
	18	Check & Null Occulting Disc Position Error to within ±10 arc sec Pitch Control Yaw Control	B-100	709A600A5	Meters read 0 ±10 sec	M3-1 M3-2	709A600A5 S26 S27	Aligns internal occulting discs		
	19	Reconfirm Coronagraph Pointing Repeat events 11 & 13	B-100							
	20	Reconfirm Occulting Disc Position Repeat steps 16 & 18	B-100							

REVISIONS

SYM	DESCRIPTION	DATE	APPROVAL
3	Utilizes updated material	5-2-67	

PREPARED BY

LOCKHEED MISSILES & SPACE COMPANY

SUNNYVALE, CALIFORNIA

DATE PREPARED 5-2-67

PREPARED BY: R. Hacker

CHECKED BY

SUBMITTED

APPROVED

DIRECTOR

GEORGE C. MARSHALL SPACE FLIGHT CENTER

NATIONAL AERONAUTICS AND SPACE ADMINISTRATION

HUNTSVILLE, ALABAMA

DWG SIZE

SHEET 2 OF 5

PRECEDING PAGE BLANK NOT FILMED.

TASK/EQUIPMENT ANALYSIS	Experimenter: HIGH ALTITUDE OBSERVATORY	Experiment Number: S052	Experiment Title: WHITE LIGHT CORONAGRAPH	Designator Code Number: 709A600A2

FUNC.	NO.	CREW TASK/EVENT	ASTRONAUT ACTIVITY (%)	EQUIP-MENT INTERFACE	VISUAL FEEDBACK	DISPLAY	CONTROL	NOTES	EST TIME	CUM TIME
OPERATION	1	Select First Camera Operation Mode	B-100	A2	Locked in Selected Mode		S2	Available Modes: Patrol – 1 min (12 pictures) Patrol – 16 min (192 pictures) Fast Scan – (384 pictures)		
	2	Astronaut voice report of event #1 start time	B-100	709A600A				Tape recorded using Vehicle Comm. & Recording Sys.		
	3	Reconfirm Coronagraph Pointing Repeat events 11 & 13 of Activation & Alignment	B-100							
	4	Reconfirm Occulting Disc Position Repeat events 16 & 18 of Activation & Alignment	B-100							
	5	Activate Camera Operation Mode	B-100	A2	Flag reads "Op"	DS3	S6	Operation normally continues for selected 1 or 16 min. period. Stops if sun-centering is lost or shutter closes. Fast scan stops when 80% of film is expended.		
	6	Astronaut voice Report event #5	B-100	709A600A				Specify mode and start time		
	7	Monitor Coronagraph Pointing & Occulting Disc Position Repeat events 11 & 13 and 16 & 18 of Activation & Alignment	B-100					Frequency of monitoring will be contingent on system stability		
	8	Check camera mode completion Sequence Flag Frames Remaining Monitor	B-100	A2	Flag reads "Stop"	DS3 M1		Check after selected 1 or 16 min period elapses. Should be reduction of 12, 192 or 384 frames depending on mode selected		
	9	Astronaut voice report of event #8	B-100	709A600A				Tape recorded using Vehicle Comm & Recording Sys.		
	10	Select next camera operation mode	B-100	A2	Locked in Selected Mode		S2	Fast scan can be started when 16 min. Patrol Mode is still operational. Patrol Mode will stop & complete Fast Scan will begin when S6 is actuated.		
	11	Astronaut voice report of event #10	B-100	709A600A				Specify mode & start time		
	12	Check number of remaining frames	B-100	A2	Adequate No.	M1	S1	Required: 1 min Patrol Mode – 12 16 min Patrol mode – 192 Fast scan – 384 plus 20% of full camera		

REVISIONS

SYM	DESCRIPTION	DATE	APPROVAL
3	Utilizes updated material	5-2-67	

PREPARED BY
LOCKHEED MISSILES & SPACE COMPANY
SUNNYVALE, CALIFORNIA

DATE PREPARED 5-2-67
PREPARED BY: R. Hacker
CHECKED BY
SUBMITTED
APPROVED
DIRECTOR

GEORGE C. MARSHALL SPACE FLIGHT CENTER
NATIONAL AERONAUTICS AND SPACE ADMINISTRATION
HUNTSVILLE, ALABAMA

DWG SIZE

SHEET 3 OF 5

FOLDOUT FRAME 1 FOLDOUT FRAME 2

PRECEDING PAGE BLANK NOT FILMED.

TASK/EQUIPMENT ANALYSIS	Experimenter: HIGH ALTITUDE OBSERVATORY	Experiment Number: S052	Experiment Title: WHITE LIGHT CORONAGRAPH	Designator Code Number: 709A600A2

FUNC.	NO.	CREW TASK/EVENT	ASTRONAUT ACTIVITY (%)	EQUIP-MENT INTERFACE	VISUAL FEEDBACK	DISPLAY	CONTROL	NOTES	EST TIME	CUM TIME
OPERATION	13	Complete Camera Mode Procedure Repeat events 3 through 9	B-100					Report any interruption of procedure.		
	14	Implement subsequent camera mode Repeat events 10 through 12 and 3 through 9	B-100							
	15	Check number of remaining frames	B-100	A2	Adequate No. shown	M1	S1	Install new camera when indicated number of remaining frames is not adequate for desired mode.		
	16	Astronaut voice report of event #15	B-100	709A600A						

REVISIONS			
SYM	DESCRIPTION	DATE	APPROVAL
3	Utilizes updated material	5-2-67	

PREPARED BY

LOCKHEED MISSILES & SPACE COMPANY

SUNNYVALE, CALIFORNIA

DATE PREPARED 5-2-67	SUBMITTED
PREPARED BY: R. Hacker	APPROVED
CHECKED BY	DIRECTOR

GEORGE C. MARSHALL SPACE FLIGHT CENTER

NATIONAL AERONAUTICS AND SPACE ADMINISTRATION

HUNTSVILLE, ALABAMA

DWG SIZE

SHEET 4 OF 5

PRECEDING PAGE BLANK NOT FILMED.

TASK/EQUIPMENT ANALYSIS	Experimenter: HIGH ALTITUDE OBSERVATORY	Experiment Number: S052	Experiment Title: WHITE LIGHT CORONAGRAPH	Designator Code Number: 709A600A2

FUNC.	NO.	CREW TASK/EVENT	ASTRONAUT ACTIVITY (%)	EQUIP-MENT INTERFACE	VISUAL FEEDBACK	DISPLAY	CONTROL	NOTES	EST TIME	CUM TIME
DEACTIVATION	1	Check Camera Mode Completion	B-100	A2	Flag reads "Stop"	DS3		Camera operation can be stopped before mode completion by closing shutter or moving Power toggle from operate position. Mode sequence must be restarted when operational conditions are restored.		
	2	Close Internal Shutter	B-100	A2	Flag reads "Closed"	DS2	S4			
	3	Astronaut voice report of event #2	B-100	709A600A				Tape recorded using Vehicle Comm & Recording Sys.		
	4	Close External Shutter	B-100	A2	Flag reads "Closed"	DS1	S3			
	5	Astronaut voice report of event #4	B-100		709A600A			Tape recorded using Vehicle Comm & Recording Sys		
	6	Check remaining film. If number is less than required, change cameras	B-100	A2	No. remaining	M1		Required: 1 min Patrol Mode – 12 16 min. Patrol Mode – 192 Fast Scan – 384 plus 20% of full camera		
	7	Astronaut voice report of event #6	B-100	709A600A				Report film remaining		
	8	Turn off Power	B-100	A2	Locked in "Off"		S5	Complete shutdown required for camera removal		
	9	Astronaut voice report of event #8	B-100	709A600A				Tape recorded using Vehicle Comm & Recording Sys		
	10	Remove spent camera						To be supplied		
	11	Install new camera						To be supplied		
	12	Activate Power to Operate	B-100	A2	Locked in "Operate"		S5	Activates experiment circuits. No warm-up required.		
	13	Astronaut voice report of event #12	B-100	709A600A						
	14	Reset Frames Remaining Monitor	B-100	A2	Indicates full camera values	M1	S1			
	15	Reset Power to Standby or Off	B-100	A2	Locked in "Standby" or "Off"		S5	Reset to "Standby" if experiment reactivation is imminent. Reset to "Off" if astronaut is leaving experiment area or complete shutdown is required.		
	16	Astronaut voice report of event #15	B-100	709A600A				Tape recorded using Vehicle Comm & Recording Sys.		

REVISIONS

SYM	DESCRIPTION	DATE	APPROVAL
3	Utilizes updated material	5-2-67	

PREPARED BY
LOCKHEED MISSILES & SPACE COMPANY
SUNNYVALE, CALIFORNIA

DATE PREPARED 5-2-67	SUBMITTED	
PREPARED BY: R. Hacker	APPROVED	
CHECKED BY	DIRECTOR	

GEORGE C. MARSHALL SPACE FLIGHT CENTER
NATIONAL AERONAUTICS AND SPACE ADMINISTRATION
HUNTSVILLE, ALABAMA

DWG SIZE

SHEET 5 OF 5

FOLDOUT FRAME 1

FOLDOUT FRAME 2

PRECEDING PAGE BLANK NOT FILMED.

DARK-SIDE ACTIVITIES

No.	Crew Task/Event	Astronaut Activity (%)	Equipment Interface	Display	Control	Notes
1	Deactivate Experiments (Standby/Deactivate)	B-100	A2	Standby	S5	S052
		B-100	A3	Deact	S7	S053
		B-100	A4	Deact	S8	S054
		B-100	A5	Standby	S14-15	S055
		B-100	A6	Deact	S11	
2	Record Comments on Expmt	B-100				Vehicle Communications and Recording System
3	Momentum Dump (Manual)	B-100	Not designated at this time			See LMSC-A842251
	(a) Receive λ value					
	(b) Calculate H_e Averages					
	(c) Calculate $\epsilon_2^1 \ldots \epsilon_2^4$ and $\epsilon_3^1 \ldots \epsilon_3^4$					Implemented at four different times during dark period
	(d) Input Values of ϵ_2^1, ϵ_3^1					
	(e) Input Values of ϵ_2^2, ϵ_3^2					
	(f) Input Values of ϵ_2^3, ϵ_3^3					
	(g) Input Values of ϵ_2^4, ϵ_3^4					
	(h) Record Final $\overline{H}$ Values					
4	Verify CSS Sun Acquisition	B-100				See LMSC-A842254
5	Activate and Align Next	B-100				See LMSC-A842254
6	Verify ATM-PCS Activation and Operation	B-100				See LMSC-A842254